Cryptography with Chaos

George Makris , Ioannis Antoniou

Mathematics Department, Aristotle University, 54124, Thessaloniki, Greece
E-mail: geormak@hotmail.com
Mathematics Department, Aristotle University, 54124, Thessaloniki, Greece
E-mail: iantonio@math.auth.gr

Abstract: We implement Cryptography with Chaos following and extending the original program of Shannon with 3 selected Torus Automorphisms, namely the Baker Map, the Horseshoe Map and the Cat Map. The corresponding algorithms and the software (chaos_cryptography) were developed and applied to the encryption of picture as well as text in real time. The maps and algorithms may be combined as desired, creating keys as complicated as desired. Decryption requires the reverse application of the algorithms.

Keywords: Cryptography, Chaos, image encryption, text encryption, Cryptography with Chaos.

1. Chaotic Maps in Cryptography

Chaotic maps are simple unstable dynamical systems with high sensitivity to initial conditions [Devaney 1992]. Small deviations in the initial conditions (due to approximations or numerical calculations) lead to large deviations of the corresponding orbits, rendering the long-term forecast for the chaotic systems intractable [Lighthill 1986]. This deterministic in principle, but not determinable in practice dynamical behavior is a local mechanism for entropy production. In fact Chaotic systems are distinguished as Entropy producing deterministic systems. In practice the required information for predictions after a (small) number of steps, called horizon of predictability, exceeds the available memory and the computation time grows superexponentially. [Prigogine 1980, Strogatz 1994, Katok, ea 1995, Lasota, ea 1994, Meyers 2009].

Shannon in his classic 1949 first mathematical paper on Cryptography proposed chaotic maps as models - mechanisms for symmetric key encryption, before the development of Chaos Theory. This remarkable intuition was based on the use of the Baker's map by Hopf in 1934 as a simple deterministic mixing model with statistical regularity. The Baker's Map is defined below and the mixing character is presented in figure 1:

$$B:[0,1)\times[0,1)\to[0,1)\times[0,1):\begin{pmatrix}x\\y\end{pmatrix}\to\begin{cases}\begin{pmatrix}2x\\\dfrac{y}{2}\end{pmatrix} & x\in\left[0,\dfrac{1}{2}\right)\\[2ex]\begin{pmatrix}2x-1\\\dfrac{y+1}{2}\end{pmatrix} & x\in\left[\dfrac{1}{2},1\right)\end{cases}$$

The reverse transformation:

$$B^{-1}:[0,1)\times[0,1)\to[0,1)\times[0,1):\begin{pmatrix}x\\y\end{pmatrix}\to\begin{pmatrix}\frac{1}{2}&0\\0&2\end{pmatrix}\begin{pmatrix}x\\y\end{pmatrix}\mod 1=\begin{cases}\begin{pmatrix}\frac{x}{2}\\2y\end{pmatrix}&y\in\left[0,\frac{1}{2}\right)\\\begin{pmatrix}\frac{x+1}{2}\\2y-1\end{pmatrix}&y\in\left[\frac{1}{2},1\right)\end{cases}$$
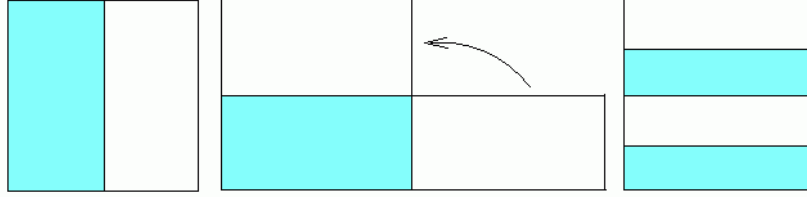

Fig. 1: Baker Map

The Entropy production theory of Chaotic maps was developed later by Kolmogorov and his group [Arnold, Avez 1968, Katok, ea 1995, Lasota, ea 1994]. Baker's map is the simplest example of chaotic automorphisms with constant Entropy production equal to one bit at every step and has served as toy model for understanding the problem of Irreversibility in Statistical Mechanics [Prigogine 1980]. Shannon observed that using chaotic maps, encryption is achieved via successive mixing of the initial information which is "spread" all over the available state space. In this way it is becoming exponentially hard to recover the initial message without knowing the reverse transformation.

A variation of the transformation of Baker Map is the Horseshoe Map [Smale 1967, Smale 1998], with the same Entropy production defined below and the mixing character presented in figure 2:

$$H:[0,1)\times[0,1)\to[0,1)\times[0,1):$$

$$H(x,y)=\begin{cases}\left(2x,\frac{y}{2}\right)&x\in\left[0,\frac{1}{2}\right)\\\left(2-2x,\frac{2-y}{2}\right)&x\in\left[\frac{1}{2},1\right)\end{cases}$$

The reverse transformation:

$$H^{-1}(x,y)=\begin{cases}\left(\frac{x}{2},2y\right)&y\in\left[0,\frac{1}{2}\right)\\\left(\frac{2-x}{2},2(1-y)\right)&y\in\left[\frac{1}{2},1\right)\end{cases}$$
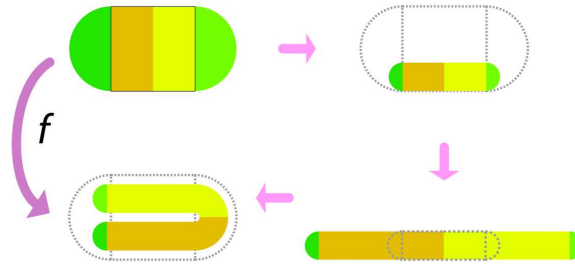
Fig. 2: HorseShoe Map

Both Baker's Map and the Horseshoe Map belong to the general class of torus automorphisms. The well known Cat Map introduced by Arnold in 1968 which is a torus automorphism a much stronger mix than two previous ones. The Cat Map is defined below and the mixing character is presented in figure 3:

$$\begin{bmatrix} x' \\ y' \end{bmatrix} = A \begin{bmatrix} x \\ y \end{bmatrix} (\mathrm{mod}\, N) = \begin{bmatrix} 1 & p \\ q & pq+1 \end{bmatrix} \begin{bmatrix} x \\ y \end{bmatrix} (\mathrm{mod}\, N)$$
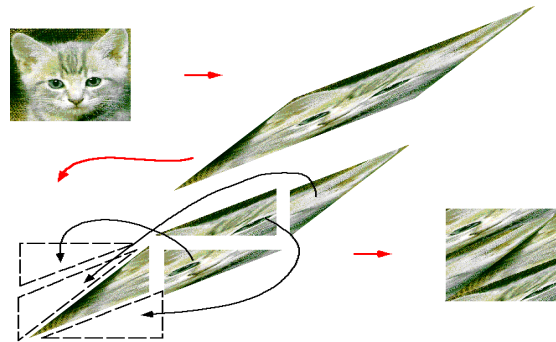

Fig. 3: Cat Map

The numerical analysis of the Cat Map shows interesting periodicity in the state space discretization [Vivaldi 1989]. Although the Cat Map and the torus automorphisms admit analytical solution, computability does not increase significantly. [Akritas, ea 2001]. Statistical estimates for the transformation of Baker Map and the Cat Map are possible through the spectral analysis [Antoniou and Tasaki 1992, Antoniou, ea 1997, Antoniou and Tasaki 1993].

From Pesin's 1977 Formula, the entropy of the Cat Map is: $\log_2 \dfrac{3+\sqrt{5}}{2}$; $1,39$,

ie. larger than the entropy of the Baker's map.

Following Shannon's idea, encryption is achieved by entropy producing (chaotic) maps like the torus automorphisms, via successive mixing of the initial information which is "spread" all over the available state space. In this way it is becoming exponentially hard to recover the initial message without knowing the reverse

transformation. However all results until now are restricted to the encryption of pictures. For review of relevant work we refer to Guan 2005 and Xiao 2009. We shall show how encryption of texts can also be achieved with chaotic maps.

2. Text Encryption and Decryption by Torus Automorphisms

The text Cryptography by Torus Automorphisms involves 3 steps:

Step 1: Place the text in a 2-dimensional table so that each array element is a character.

Step 2: Apply the selected transformations on the table for a number of steps specified by the key.

Step 3: convert the modified table from step 2 in the text.

The decryption process is equally simple for anyone who holds the key. Simply follow the steps backwards and use inverse transformations to the same number of steps.

We propose 2 algorithms for the implementation of the text cryptography:

Algorithm 1:

Step 1: Count all characters of text including line breaks ($=N_1$)

Step 2: If N_1 is not a perfect square of an integer, then find the smallest integer M $> N_1$ so that M is a perfect square. If the N_1 is a perfect square integer number then set M=N_1.

Step 3: Set $N = \sqrt{M}$

Step 4: Create a character table (NxN) and place the characters of the text inside the table, putting also the special characters newline (enter) in a position in the table.

Step 5: If there are empty cells at the end of the table place the spaces in these (cells).

So we create a NxN table of characters with the properties:

1) The number of rows and columns of the table depends on the length of the text only.

2) The number of lines of characters changes during the encryption because all the special characters like "enter" are involved in encryption.

Example:

Cryptography with chaos
George Makris, Ioannis Antoniou
Thessaloniki 54124
Greece.

The above text has 82 characters. We need a 10x10 table to fit the text in table (100 is the minimal encoding length)

C	r	y	p	t	o	g	r	a	p
h	y		w	i	t	h		c	h
a	o	s	\n	G	e	o	r	g	e
	M	a	k	r	i	s	,		I
o	a	n	n	i	s		A	n	t
o	n	i	o	u	\n	T	h	e	s
s	a	l	o	n	i	k	i		5
4	1	2	4	\n	G	r	e	e	c
e	.								
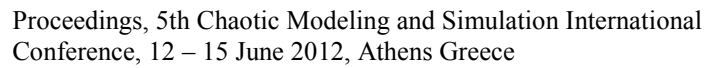
Algorithm 2:
Step 1: Count the number of lines (NL) of the text.
Step 2: Count the number of letters of each line.
Step 3: Find the M1 = max {the number of letters of each line}.
Step 4: Set N = max {NL, M1}
Step 5: Create a character table (NxN)
Step 6: Place each character in text in the table so that it corresponds to each line of text in the corresponding row of the table. Put the special character space (' ') in all the blank cells.
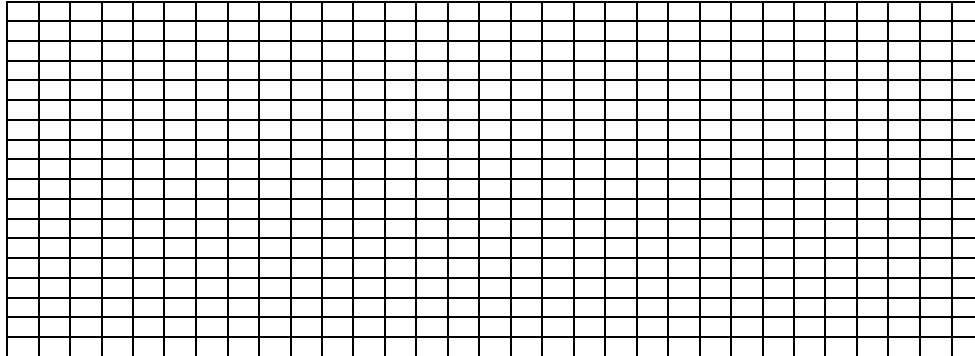
So we create a NxN table of characters with the properties:
1) The number of rows and columns of the table defined by the structure and the length of the text.
2) The number of lines of characters does not change in encryption because gaps were placed on each line so that all lines have the same number of characters.
For the same example we have:

Cryptography with chaos	→	23 characters
George Makris, Ioannis Antoniou	→	31 characters
Thessaloniki 54124	→	18 characters
Greece.	→	07 characters

Lines NL = 4
M1=max{23,31,18,07}=31
N=max{4,31}=31

C	r	y	p	t	o	g	r	a	p	h	y		w	i	t	h		c	h	a	o	s								
G	e	o	r	g	e		M	a	k	r	i	s	,		I	o	a	n	n	i	s		A	n	t	o	n	i	o	u
T	h	e	s	s	a	l	o	n	i	k	i		5	4	1	2	4													
G	r	e	e	c	e	.																								

Examples of text and image encryption are presented in the appendices

3. Software Development for the implementation of "Cryptography with Chaos"

The software for the algorithms was developed with Java, as this language is independent of the operating system and platform. Moreover the Java programs run on Windows, Linux, Unix and Macindosh, mobile phones, Ipads, Playstations and other game consoles without any modification like compilation or changing the source code for each different operating system.

The software developed (chaos_cryptography) has a graphical user interface and is very simple and user friendly (figure 4).

The user may encrypt / decrypt images and texts. The user may use any of the above chaotic maps with one or the other algorithm or any combination for more difficult deciphering.

Window dialogs alert the user in case of any errors in the procedure.

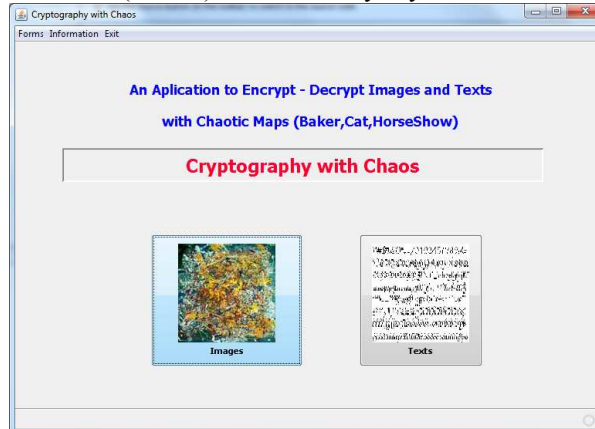The developed libraries (classes) can be used by any other software and application

Fig. 4: chaos_cryptography application (main window)

4. Concluding Remarks

Shannon Cryptography indices for chaos cryptography are summarized in the table below.

Shannon Cryptography indices	Cryptography with Chaos
Required degree of cryptographic security	High
Key Length	Small The key is the selected transformations and the number of iterations that apply each transformation.
Practical implementation of the encryption / decryption	Depends on the size of the text. Generally, permutation is a faster method than the replacement.
Growth of the encrypted text	involves only "spaces"
Error Propagation	In case of even one Error text is practically impossible. Correct key application is required

The key length includes the map definition, the number of iterations and the parameters of the specific map. The proposed encryption algorithms are "MonoBlock" ciphers based on permutations, however they are neither steams nor block ciphers. The Key is very small and does not depend on the size of text to be encrypted (block).

For example, the specific key for encryption algorithm (Baker, Cat, Horseshoe) has a size 4 (Table 2x2). In classical permutation algorithms to encrypt a text with N characters (MonoBlock, size of the block = N) a key size N is required which is the size of the Block.

The innovations of this work are summarized as follows:

a) The extension of Chaos Cryptography to texts.

b) The construction of examples of a new class on ciphers, namely the Mono–Block Ciphers as a third class beyond the Block Ciphers and the Stream Ciphers.

c) The key is completely independent from the length of the block that is encrypted and it is very small compared to the key of the classic permutation algorithms which is equal to the length of the block.

d) in the developed algorithms the key cannot operate if some small part of the document is lost.

Chaos Cryptography has only the disadvantage of all systems of symmetric cryptography, namely the safe transport of the key.

In this paper three of the most famous chaotic maps were investigated. The proposed algorithms can be adapted to other chaotic maps.

References

1. Akritas P., Antoniou I., Pronko G. 2001, "On the Torus Automorphisms: Analytic Solution, Computability and Quantization", Chaos, Solitons and Fractals 12, 2805-2814
2. Antoniou I., Tasaki S.1992, Generalized spectral decomposition of the ß-adic baker's transformation and intrinsic irreversibility, Physica A 190, 303-329.
3. Antoniou I., Bi Qiao, Suchanecki Z. 1997, "Generalized Spectral Decomposition and Intrinsic Irreversibility of the Arnold Cat Map", Chaos Solitons and Fractals 8, 77 – 90
4. Antoniou I., Tasaki S. 1993, Generalized spectral decomposition of mixing dynamical systems, Int. J. Quantum Chemistry 46, 425-474.
5. Arnold, V. I. and Avez, A. 1968, Ergodic Problems of Classical Mechanics Benjamin, New York
6. R. Devaney 1992, A First Course in Chaotic Dynamical Systems, Perseus Books.
7. Guan Z. H., Huang F., and Guan W. 2005. Chaos-based image encryption algorithm. Physics Letters A, Vol. 346, Issues 1-3, pp 153-157.
8. Hopf E. (1934), On Causality, Statistics and Probability, J. Math. and Phys. 13, 51-102.
9. Katok A., Hasselblatt B. 1995, Introduction to the Modern Theory of Dynamical Systems, Cambridge University Press, Cambridge, UK
10. Lasota A. and Mackey M. 1994, Chaos, Fractals, and Noise, Springer-Verlag New York.
11. Lighthill J. 1986, The recently recognized failure of predictability in Newtonian dynamics, Proc. Roy. Soc. London A407, 35-50
12. Meyers R. A.,ed. 2009 Encyclopedia of Complexity and Systems Science, Springer, New York.
13. Pesin Ya. B. 1977, Characteristic Lyapunov exponents and smooth ergodic theory, Russ. Math. Surv. 32:4, 55-112
14. Prigogine I. 1980, From Being to Becoming, Freeman, New York.
15. Shannon C., Weaver W. 1949, The Mathematical Theory of Communication, University of Illinois Press, Urbana, Ill.
16. Shannon, C. 1949, Communication Theory of Secrecy Systems. Bell System Technical Journal, Vol.28, Issue 4, pp 656–715.
17. Smale S. 1967, "Differentiable dynamical systems". Bulletin of the American Mathematical Society 73: 747–817.
18. Smale S. 1998, Finding a horseshoe on the beaches of Rio, Mathematical Intelligencer 20, 39-44
19. Strogatz S.1994, Non-Linear Dynamics and Chaos, Perseus, Massachusetts
20. Vivaldi F. 1987, The arithmetic of Chaos, in Chaos, Noise and Fractals, volume 3 of Malvern Phys. Ser., pages 187–199. Hilger, Bristol.
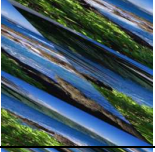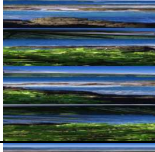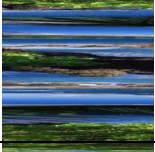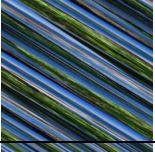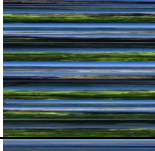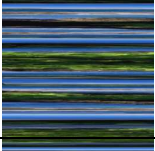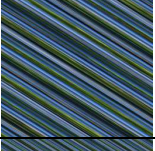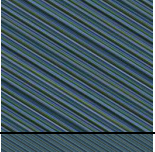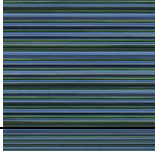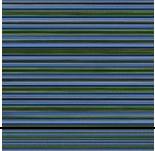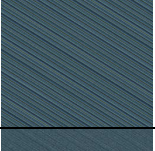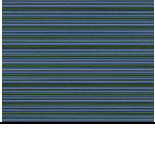
21. Xiao, D., Liao, X., Wei, P. 2009. Analysis and improvement of a chaos-based image encryption algorithm. Chaos, Solitons & Fractals, Vol. 40, Issue 5, pp 2191-2199.

Appendix A : Text encryption

Iterations	Baker Map	Horseshoe Map	Cat Map
t=0	Cryptography with chaos George Makris, Ioannis Antoniou Thessaloniki 54124 Greece.	Cryptography with chaos George Makris, Ioannis Antoniou Thessaloniki 54124 Greece.	Cryptography with chaos George Makris, Ioannis Antoniou Thessaloniki 54124 Greece.
t=1	otghr acpheiosr,g eIs TAhnetsiGkri e e5c Chryy pwtia oMsa kGrooanninoi us4a1l2o4n e .	c5e eirkGistenhA T sIe g,rsoiehpca rhgtoChryy pwtia oMsa kGrooanninoi us4a1l2o4n e .	C 4n ,ghehr iTA nIayy Gkhiet o p r e soMswt o e5oaa iGtg csnnknrehr 4ailoiio a e1.2oussrcp
t=2	,agc pehIhen eet5sc p w t iai nkoGiru2 o 4 n oetigohsrrsi G kTrAi C h r y yao ooaMnsnse4 a.1 l	n 4 o 2uriGokn iaiottwgph resi o sTrAi G k r i c 5 e esItee ngh,hCphcray yao ooaMnsnse4 a.1 l	C2ih os k he oircaw trnh uo san iIr4s a4ni ea ns r akoety y ceiG so i,p1nt geo Tg lroe 5MpGAh.
t=3	epte5hsIcwo Gti riu onh s r rkrT ryA iya.M1n sln h,eang ce a i pn k2o eot i4gs iC Gh asoe 4o oa	nls n1M.ay, hyganr e i re Arr Thsp ga2i on k4 u r inG oieostit woi cG 5k shICtpehecas oe 4o oa	Ceoieoass ah2 ,ie n tei5 pGt ysnr hMT1gn a no poG t 4 hi rsAl yrniiIuc hrs a roak.goe cke4 w o

Appendix B : Image Encryption

Iterations	Baker Map	Horseshoe Map	Cat Map
t=0			
t=1			
t=2			
t=3			
t=4			
t=5			
t=6			

Chaotic Invariants for Action Recognition

Zarine K. Manukyan

Yerevan State University. Armenia, Yerevan
E-mail: zarka88000@yahoo.co.uk

Abstract: The aim of this project is to derive a representation of the dynamical system generating the human actions directly from the experimental data. This is achieved by proposing a computational framework that uses concepts from the theory of chaotic systems to model and analyze nonlinear dynamics of human actions. The trajectories of human body joints are used as the input representation of the action.

Introduction

Our contributions include :1) investigation of the appropriateness of theory of chaotic systems for human action modeling and recognition, 2) a new set of features to characterize nonlinear dynamics of human actions, 3) experimental validation of the feasibility and potential merits of carrying out action recognition using methods from theory of chaotic systems.

Proposed Idea ...

$f(\theta_1^t, \theta_2^t, ..., \theta_N^t)$ $f(\theta_1^{t+1}, \theta_2^{t+1}, ..., \theta_N^{t+1})$ $f(\theta_1^{t+2}, \theta_2^{t+2}, ..., \theta_N^{t+2})$ $f(\theta_1^{t+3}, \theta_2^{t+3}, ..., \theta_N^{t+3})$

The evolution of the state of the dynamical system is controlled by a function that maps the values of the true state variables from one time instant to the next.
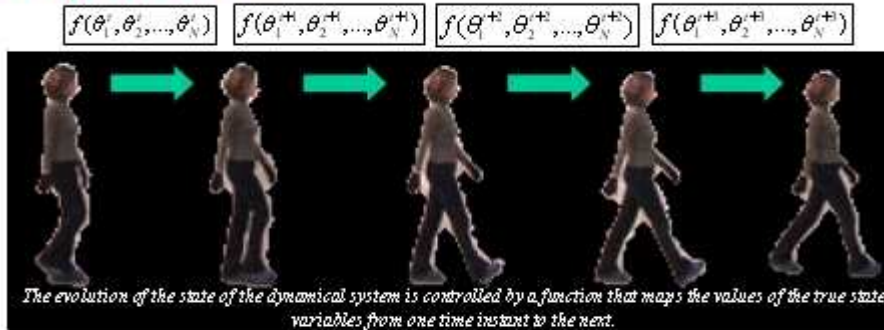
Unknown $\boxed{f}$ Function that maps current state to the next state.

$(\theta_1^t, \theta_2^t, ..., \theta_N^t)$ True State Space Variables

- We have the access to the data (trajectories of body joints) generated by the dynamical system controlling the action !

- From this data construct the phase space corresponding to the dynamical system responsible for generating the data.

- Let the data speak about the mechanisms generating the observed behavior.

Algorithmic Steps

This section describes the algorithmic steps of the proposed action recognition framework. These are: 1) Given a video of an exemplar action, obtain trajectories of reference body joints, and break each trajectory into a time series by considering each data dimension separately; 2) obtain chaotic structure of each time series by embedding it in a phase space of an appropriate dimension using the mutual information, and false nearest neighborhood algorithms; 3) apply determinism test to verify the existence of deterministic structure in the reconstructed phase space; 4) represent dynamical and metric structure of the reconstructed phase space in terms of the phase space invariants, and 5) generate global feature vector of exemplar

action by pooling invariants from all time series, and use it in a classification algorithm. Now, we describe each step of the algorithm in more detail in following subsections.
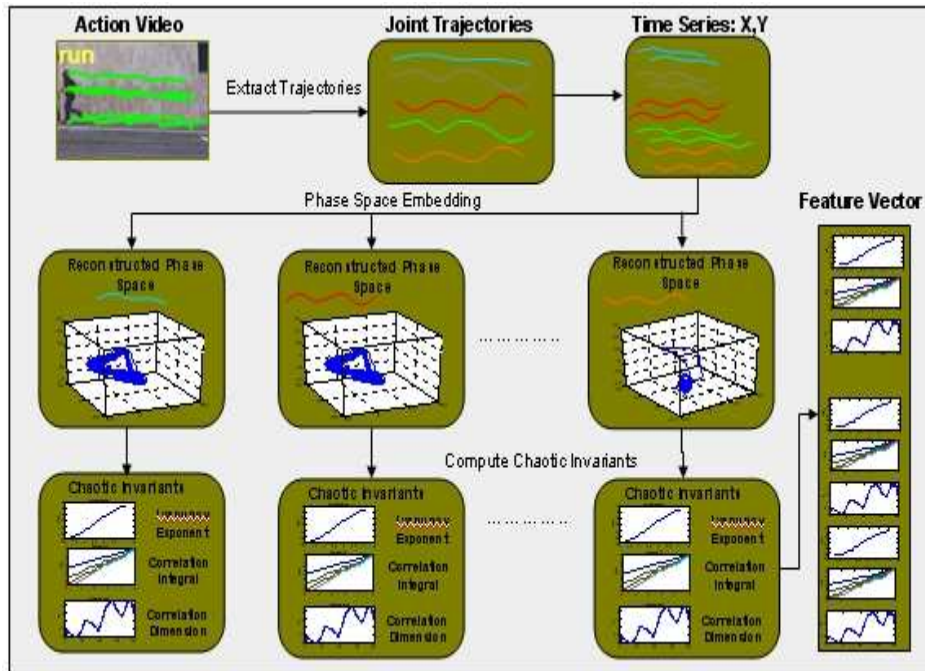
(a) The block diagram of the crowd flow segmentation and instability detection algorithm.

1) Trajectory Computation

Trajectories of six body joints (two hands, two feet, head, and belly) are used for representing an action. The trajectories are normalized with respect to the belly point, resulting in five trajectories per action. In case of the motion capture data set, each point of the trajectory in represented by a three-dimensional coordinate (x, y, z). In case of the videos, we used a semi-supervised joint detection and tracking approach for generating these trajectories. That is, first we extracted the body skeletons and their endpoints by using morphological operations on the foreground silhouettes of the actor. An initial set of trajectories is generated by joining extracted joint locations

using the spatial and motion similarity constraint.
The broken trajectories and wrong associations were corrected manually.
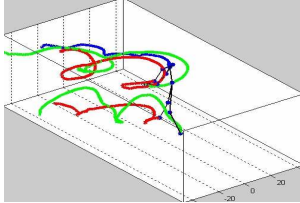
Trajectories for the ballet action from the motion capture data set.
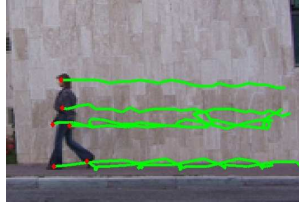
Trajectories for the walk action from the video data set.

Next, each dimension of the trajectory is treated as a separate time series. The next figure shows these time series for the walk action from the motion capture data set.
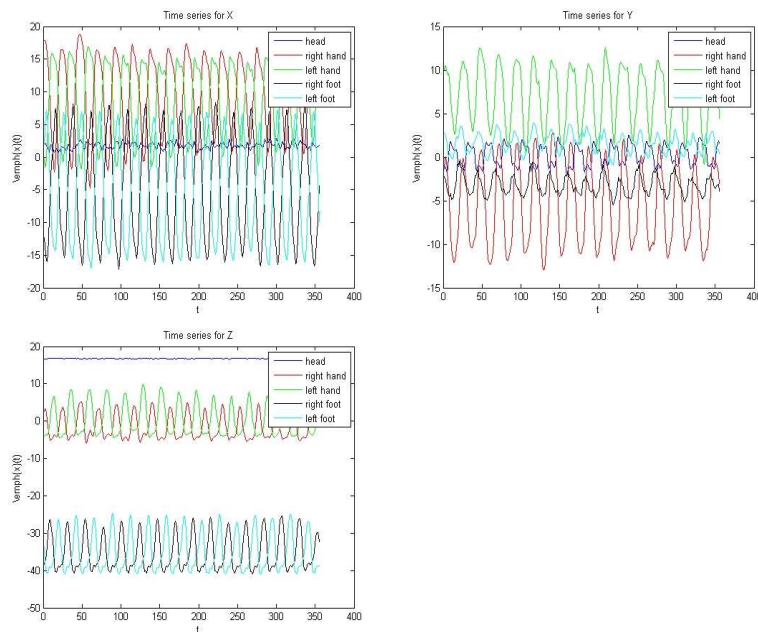
2) Phase Space Embedding

Embedding is a mapping from one dimensional space to a m-dimensional space. It is an important part of study of chaotic systems, as it allows one to study the systems for which the state space variables and the governing differential equations are unknown. The underlying idea of embedding is that all the variables of a dynamical system influence one another. Thus, every subsequent point of the given one dimensional time series results from an intricate combination of the influences of all the true state variables of the system. This observation allows us to introduce a series of substitute variables to obtain the whole m-dimensional phase space, where substitute variables carry the same information as the original variables of the system. This is pictorially described in the following figure:

Underlying Idea: All variables of the system influence each.

$$= (z_1, z_2, z_3, \ldots, z_t)$$

τ

Every point z_i of the series results from the intricate combination of influences of all the true state variables.

$(\theta_1, \theta_2, \ldots, \theta_N)$

Therefore, $z_{i+\tau}$ can be considered as a second substitute variable which carries the influence of all the true state variables during time interval τ.

$(\theta_1, \theta_2, \ldots, \theta_N)$
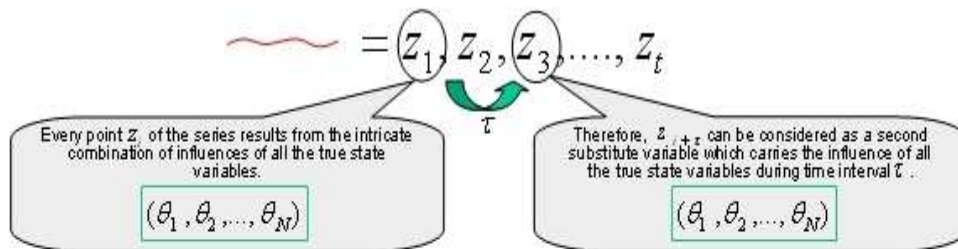
Using this reasoning, introduce a series of substitute variables and obtain the whole m-dimensional space.

Thus, for optimal m and τ, delay vectors

$$z_i, z_{i+\tau}, z_{i+2\tau} \cdots, z_{i+(m-1)\tau}$$

generates a phase space that has exactly the same properties as the original/true variables of the system.

Reconstructed phase spaces of trajectories corresponding to different body joints.
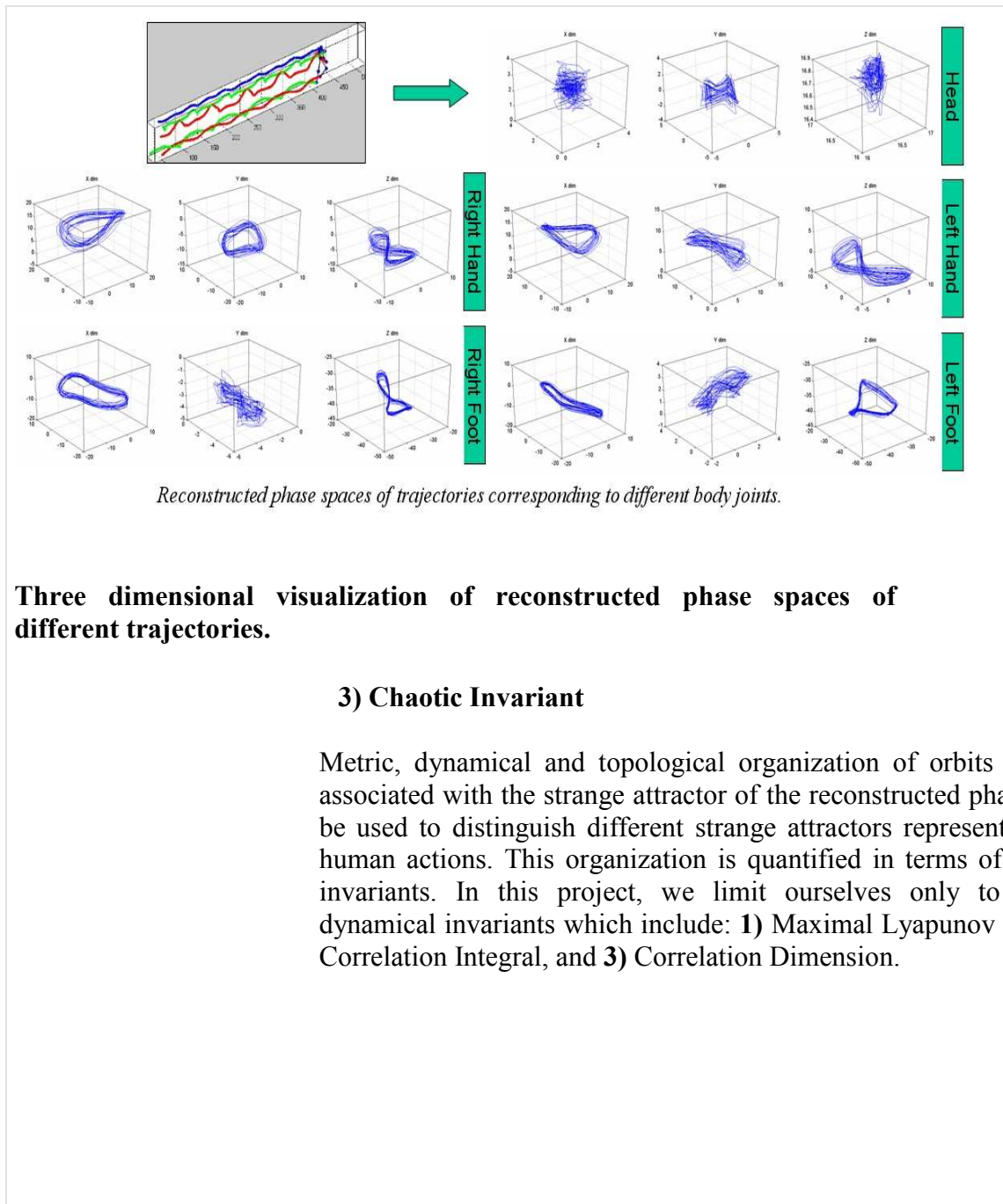
Three dimensional visualization of reconstructed phase spaces of different trajectories.

3) Chaotic Invariant

Metric, dynamical and topological organization of orbits (tr associated with the strange attractor of the reconstructed phase be used to distinguish different strange attractors representing human actions. This organization is quantified in terms of pl invariants. In this project, we limit ourselves only to m dynamical invariants which include: **1)** Maximal Lyapunov Ex Correlation Integral, and **3)** Correlation Dimension.

Maximal Lyapunov Exponent:

Lyapunov exponent is a dynamical invariant of the attra
measures the exponential divergence of the nearby trajector
phase space. If the value of maximum Lyapunov exponent is gr
zero, that means the dynamics of underlying system are chaotic
to compute maximum Lyapunov exponent of reconstructed ph
we compute select a number of reference points and their ne
points to compute the divergence.

Correlation Integral:

The correlation integral is a metric invariant, which charact
metric structure of the attractor by quantifying the density of po
phase space. It achieves this through a normalized count of pai
lying within a certain radius.

Correlation Dimension:

The correlation dimension also characterizes the metric struct
attractor. It measures the change in the density of phase s
respect to the neighborhood radius ϵ. The correlation
can be computed from the correlation integral by exploiting
law relationship.

Reference

"Knotted periodic orbits in dynamical systems I: Lorenz's equations" , ***Topology*** 22 , 47-82 (1983).

 G. B. Mindlin, X.-J. Hou, H. G. Solari, R. Gilmore, and N. B. Tufillaro proposed to use templates to characterize and classify chaotic systems:

"Classification of strange attractors by integers" , ***Phys. Rev. Lett.*** **64 , 2350-2353 (1990).**

And soon after,G. B. Mindlin, H. G. Solari, M. A. Natiello, R. Gilmore, and X.-J. Hou showed the experimental feasibility of this approach by analyzing the Belousov-Zhabotinskii reaction:

"Topological analysis of chaotic time series data from Belousov-Zhabotinski reaction" , ***J. Nonlinear Sci.*** 1 , 147-173 (1991).

 Experimental systems from various fields were characterized with topological analysis, from lasers and chemical reactions to a chaotically vibrating string (N. B. Tufillaro, P. Wyckoff, R. Brown, T. Schreiber and T.

Monte Carlo Modelling of Soliton Pulse Timing Jitter in Silicon Nanowire Waveguides

Matthew Marko[1, 2, *], Xiujian Li[2, 3], Jiangjun Zheng [2], Chee Wei Wong[2]

(1) Navy Air Warfare Center Aircraft Division (NAWCAD), Joint Base McGuire-Dix-Lakehurst, Lakehurst NJ 08733, USA
(2) Optical Nanostructures Laboratory, Columbia University in the City of New York, New York NY 10027, USA
(3) Tech-Physical Research Center, Science College, National University of Defense Technology, Changsha, Hunan 410073, China

E-mail: matthew.marko@navy.mil

Abstract: The purpose of this effort is to study changes in the amplitude noise and timing jitter of an optical pulse chain from a mode-locked laser, as it undergoes soliton propagation through a nonlinear silicon nanowire waveguide. A numerical model was developed using the Non-Linear Schrödinger Equation to model the soliton formation with two-photon absorption. The amplitude noise was modeled as a separate noise envelope, and the phase noise and timing jitter was modeled using Monte-Carlo simulations of jitter-induced phase-shifts. It was observed that while increased pulse energy will result in increased amplitude and phase noise, the presence of two-photon absorption, which attenuates optical nonlinearities in the waveguide, results in a reduction in phase noise at the output of the silicon waveguides.
Keywords: Noise, Phase Noise, Timing Jitter, Monte-Carlo, Non-Linear Schrödinger Equation, Silicon, Photonics, Soliton, Dispersion, Waveguides, Self-Phase Modulation, Kerr, Nonlinear Optics,

1. Introduction

One of the challenges that must be overcome for the practical implementation of optical data transfer is the issue of noise, particularly phase noise, amplitude noise, and timing jitter. Practical optical data communication often requires pulse repetition rates of tens of gigahertz (GHz), and therefore timing jitter on the order of femtoseconds (fs) is often necessary to ensure a low bit-rate error in the data. This paper investigates numerically the effects of soliton pulse propagation within silicon nanowire waveguides, and the effects of these nonlinearities on noise and jitter, for the purpose of applied optical data communications.

Much research has previously been conducted on the effects of optical propagation through a dispersive waveguide on the phase noise, timing jitter, and amplitude noise [1-2]. This research to date has predominantly focused on optical fibers [3], photonic crystal fibers [4], and mode-locked lasers [5]. The purpose of this paper is to investigate optical soliton propagation [6-8] through silicon nano-waveguides. Silicon waveguides are of interest to the scientific

community for their high-nonlinearities and tight optical confinement. Compared to optical fibers, silicon nano-waveguides have much smaller length scales, and offers many applications at the chip-scale level for all-optical data transfer, information manipulation, and computing.

2. Simulations
It has been previously observed that the the noise can often be attributed as a separate envelope [2,9] of much weaker intensities than the undisturbed pulse input:

$$A(z,t) = (P_0^{1/2} + a(z,t))*\exp(-j*\varphi(z)) \qquad a(z,\omega) = {}_{-\infty}\!\int^{\infty} a(z,t)*\exp(-i*\omega t)$$

With this assumption, the NLSE can be linearly separated, and a separate NLSE for the noise can be derived:

$$(j/2)*\beta_2*\omega^2*a + (j/6)*\beta_3*\omega^3*a + j*\gamma*P_0*\{a+a^*\}*\exp(-\alpha*z) = -\partial a/\partial z$$

The noise can be assumed to be an independent envelope propagating through the waveguide, and analyzed as a separate NLSE problem, propagating concurrently with the pulse.

In the time domain, $a(z,t) = a_r(z,t) + j*a_i(z,t)$, where $a_r(z,t)$ and $a_i(z,t)$ are real functions. By substituting these terms into the noise-NLS equation, one gets a simple relationship for the real and imaginary components of the noise function in the spectral domain:

$$\partial a_r(z,\omega)/\partial z = \rho * a_i(z,\omega)$$
$$\partial a_i(z,\omega)/\partial z = -\{\rho + (2*j*\gamma*P_0*\exp(-\alpha*z))\} * a_i(z,\omega)$$
$$\rho = (\beta_2*\omega^2/2) + (\beta_3*\omega^3/6)$$

Using this assumptions, with a given noise input, one can estimate the change in the power spectral density after optical soliton propagation through a given distance increment of a waveguide [9] by using the following equations:

$$\Phi(L,\omega) = \tfrac{1}{2}*\Phi(0,\omega)*\exp(-\alpha*z)*(2*|M_{11}(\omega)|^2 + |M_{12}(\omega)|^2 + |M_{21}(\omega)|^2)$$
$$M_{11}(\omega) = \cos(\delta(\omega)*L)$$
$$M_{12}(\omega) = (\rho/\delta)*\sin(\delta(\omega)*L)$$
$$M_{21}(\omega) = -(\delta/\rho)*\sin(\delta(\omega)*L)$$
$$\delta = [\rho^2 + 2*\rho*\gamma*P_0]^{\wedge 1/2}$$

Using these terms and incorporating them into the NLSE numerical simulation, an accurate prediction of the changes in the frequency noise after propagation through a silicon waveguide could be obtained.

Many NLSE simulations were conducted in order to complement the experimental silicon waveguide used in this experiment. The silicon waveguide

parameters include a length of 4.1 mm, an effective area of 250 nm by 450 nm, a Kerr coefficient of $4.4 * 10^{-18}$ m^2/W, an effective index of 2.5, a group index of 4.5, and a 2nd and 3rd order GVD of 4.5 ps^2/m and 0.01 ps^3/m, respectively. The model took into account both two-photon absorption (TPA), free-carrier absorption (FCA), and linear loss of the pulse envelope. Because the noise is assumed to be substantially weaker compared to the pulse envelope, only linear loss is applied to the noise envelope.

For the initial simulations, the wavelength was set at 2543 nm, so that there would be no effects of TPA or FCA. Simulations were run repeatedly for various input pulse energies ranging from 1 pJ to 500 pJ; these energies are far in excess of the fundamental soliton energy for the 2.3 ps hyperbolic secant pulse. As the lasers timing jitter was in excess of the pulse duration, the simulation assumed a constant noise envelope for the temporal window analyzed. It was observed that at lower input pulse powers, the noise would decrease after propagation through the waveguide, but this loss would decrease with increasing powers. After an input pulse energy of 250 pJ, it was found that the energy would in fact increase exponentially with increasing energy. This is expected, as previous work in glass photonic crystal fibers [4] has also noticed an increase in jitter from solitons not subjected to TPA.

Figure 1 – Results of NLSE simulations of noise after propagation in the silicon waveguide, with a wavelength of 2543 nm that is not subjected to the nonlinear effects of two-photon and free-carrier absorption.

The simulation was then conducted for optical pulses at 1543 nm, which are now subjected to a considerable amount of TPA at this wavelength [10,11]. It was observed numerically that for optical soliton propagation in a silicon waveguide, the noise would consistently be reduced from 1.6 to 1.4 dB; this reduction would decrease with increasing input pulse energies within the waveguide. After 1 nJ of energy, which is far more than will be practically realized experimentally, the noise decrease will plateau, and there will be little change with increasing power.
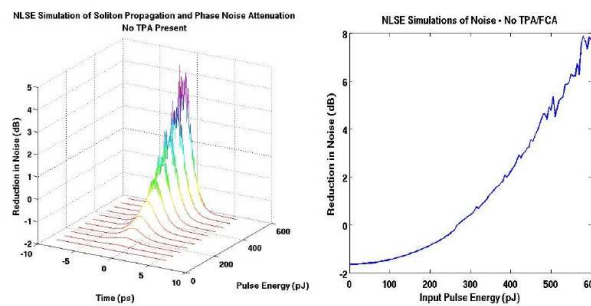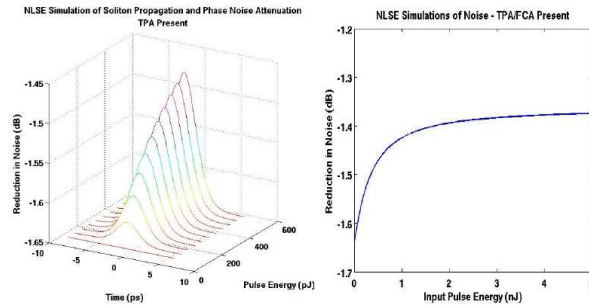
Figure 2 – Results of NLSE simulations of noise after propagation in the silicon waveguide, with a wavelength of 1543 nm that is subjected to the nonlinear effects of two-photon and free-carrier absorption.

3. Monte-Carlo Analysis of Soliton Timing Jitter

One of the challenges of performing a numerical analysis on the effects of optical soliton propagation on phase noise and timing jitter is the fact that such noise can reasonably be assumed to be random jitter. Even though most of this jitter is deterministic and repeatable, the variation of each pulse can still have a significant amount of randomness involved. Therefore, in an effort to numerically model the changes in phase noise after soliton propagation, Monte-Carlo simulations of pulse phase-shifts will be used in conjunction with the Non-Linear Schrödinger Equation (NLSE) solver.

The goal of this solver is to determine the change in timing jitter after propagation through a silicon waveguide for various energies and wavelengths. Input pulse energies from 5 pJ to 5 nJ were studied, and the wavelengths of 1550 nm and 2300 nm were analyzed. At each pulse-energy being studied, the program first solves the NLSE for a transform-limited hyperbolic secant squared pulse with no chirp; the output pulse shape and phase of the NLSE simulation will be used for comparison against a number of random trial simulations of jitter-shifted pulses. Before propagating these pulses, the same hyperbolic secant-squared input pulses are phase-shifted to represent the timing jitter. The phase shift is as follows:

Phase Shift = exp[i*(2*f*Jitter)*((2*rand)-1)]

where *f* is the frequency of the mode-locked laser (39.11 MHz), *Jitter* is the RMS of the input timing jitter (this study used 20 ps), and *rand* is a random number from zero to 1. The code is written so that the phase shift varies up to twice the specified average jitter, and can be either positive or negative.

After applying the random phase shift, the pulse was analyzed with the NLSE solver. The new output pulse phase was compared to the original non-shifted phase, the difference in phase was converted to timing jitter, and the RMS of the jitter was calculated. As Monte-Carlo simulations require many repeated random terms to be statistically significant, the simulation was repeated 1,000 times at each energy level, for a total of over 400,000 separate NLSE simulations. The raw data of the results can be seen in Figure 3, which shows the output timing jitters as a function of input pulse-energy.
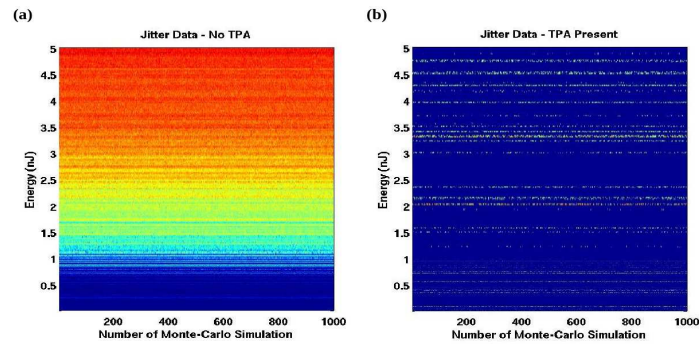
Figure 3 – Raw Data of simulations, (a) $\lambda = 2300$ nm and (b) $\lambda = 1550$ nm.

After all of the simulations were completed, in order to remove any statistical outliers, the code went through and factored out all simulations greater than 2 standard deviations away from the mean jitter. The RMS of this noise was then collected, and a final output timing jitter was given for each energy level. The data of the timing jitter as a function of energy was cleaned up of statistical outliers, and averaged out to obtain the trend of output timing jitter as a function of energy.
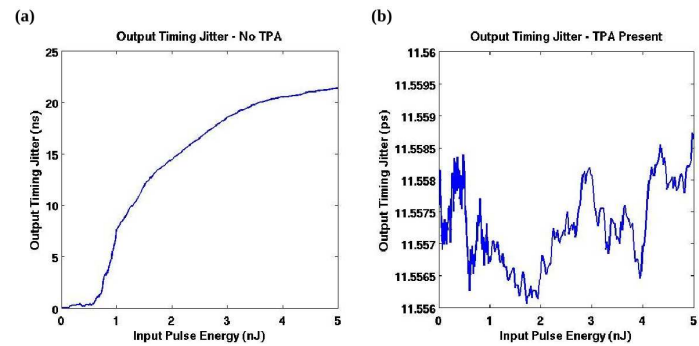
Figure 4 – Output timing jitter as a function of pulse energy, for (a) $\lambda = 2300$ nm and (b) $\lambda = 1550$ nm.

In the study of the 2300 nm pulse without TPA, the simulation clearly demonstrated the timing jitter growing exponentially with increasing pulse energy, just as the NLSE simulation of the separate noise envelope has demonstrated. In the case of the 1550 nm pulse subjected to TPA, the Monte-Carlo simulations showed the output timing jitter to consistently decrease from 20 ps RMS to 11.6 ps of RMS timing jitter. Just as observed with the study of the NLSE of the phase-noise envelope, the presence of TPA has attenuated the jitter, rather than allowed it to develop with increasing energies. It is therefore concluded, based on these two separate simulations, that soliton propagation in the presence of TPA will result in a decrease in phase noise and timing jitter.

4. Conclusion

The numerical simulations have demonstrated that an optical pulse propagating in the optical C-band within a silicon waveguide will see an attenuation of the amplitude noise and timing jitter due to the presence of the two-photon absorption. The two-photon absorption has the property of attenuating the pulse proportionally to the intensity, which acts to inhibit the self-phase modulation and thus soliton compression. If this attenuation were not present, an increase in intensity will result in an increase in nonlinear effects and thus an increase sensitivity to jitter-induced phase-shifts; for this reason high optical intensities have shown to increase the timing-jitter in the simulations of longer wavelengths not subjected to two-photon absorption. In the presence of two-photon absorption, however, less variation in the pulse phase-shifts can be expected as a result the reduction in two-photon absorption. For this reason, it is concluded that optical soliton propagation in the presence of two-photon absorption has the ability to attenuated the phase noise and timing jitter of a mode-locked optical pulse.

References

1. "Analysis of Timing Jitter for Ultrashort Soliton Communication Systems Using Perturbation Methods." Margardia Facao and Mario Ferreira, Journal of Nonlinear Mathematical Physics, 2001.

2. "Electromagnetic Noise and Quantum Optical Measurements." Hermann Haus. Springer-Verlag Berlin Heidelberg 2000.

3. "Soliton Transmission Control," A Mecozzi, Hermann Haus, et al. Optics Letters, 1 December 1991, Volume 16, Number 3

4. "Supercontinuum generation and soliton timing jitter in SF6 soft glass photonic crystal fibers." Anatoly Efimov and Antoinette Taylor, Optics Express, Volume 16, Number 8. 14 April 2008.

5. "Noise and Stability of Actively Mode-locked Fiber Lasers," PhD thesis by Matthew Edward Grein, Massachusetts Institute of Technology, June 2002.

6. "Nonlinear Fiber Optics," 4th Edition, Govind Agrawal.

7. "Temporal solitons and pulse compression in photonic crystal waveguides," P. Colman, C Husko. Nature Photonics, 21 November 2010. DOI: 10.1038/NPHOTON.2010.261

8. "Fundamentals of Photonics." 2nd Edition. Saleh, Teich.

9. Husko, De Rossi, and Wong, Effect of multi-photon absorption and free carriers on self-phase modulation in slow-light photonic crystals. Optics Letters, Vol. 36, No. 12. June 15, 2011

10. "Modeling nonlinear phase noise in differentially phase-modulated optical communication systems." Leonardo Coelho. Optics Express 3226, 2 March 2009, Volume 17, Number 5.

11. "Introduction to Solid State Physics, 8th Edition." Kittel, Charles. Wiley, 2004.

12. "Characterization of the Noise in Continuously Operating Mode-Locked Lasers," Dietrich Von der Linde. Applied Physics B 39, 201-216 (1986).

13. JitterTime Consulting LLC: http://www.jittertime.com/articles/pnsheet.shtml

A Similar Nonlinear Telegraph Problem Governed By Lamé System

Mabrouk Meflah

LAMA Kasdi Merbah University of Ouargla, Algeria
(E-mails: meflah@ymail.com)

Abstract. Introducing the Lamé operator in the telegraph equation, we obtain theoretically a similar nonlinear system. In this work we are interested in the existence and uniqueness of function $u = u(x,t)$, $x \in \Omega$, $t \in (0,T)$ solution for the new system by the elliptic regularization method.

1 Notations and position of the problem

Let Ω an open bounded domain of $\mathbb{R}^n$, with regular boundary Γ.We denot by Q the cylinder $\mathbb{R}^n_x \times \mathbb{R}_t : Q = \Omega \times \,]0,T[$, with boundary Σ. L designe Lamé system define by $\mu\Delta + (\lambda + \mu)\nabla div$; λ and μ are constants Lamé with $\lambda + \mu \geq 0$. and h, f are functions, .We look for the existence and uniqueness of a function $u = u(x,t)$, $x \in \Omega$, $t \in]0,T[$, solution of the problem (P).

$$(P)\begin{cases} u'' + u' + u - Lu + |u'|^{p-2}\,u' = f & \text{in } Q & 1.1.1 \\ \qquad\qquad u = 0 \text{ on } \Sigma & & 1.1.2 \\ \quad u(x,0) = u(x,T) & x \in \Omega & 1.1.3 \\ \quad u'(x,0) = u'(x,T) & x \in \Omega & 1.1.4 \end{cases} \qquad (1.1)$$

2 Existence of the solution

Theorem 1. *Assume that Ω is bounded open of $\mathbb{R}^n$ are given f,with $f \in L^q(Q)$ .Then there exists a function $u = w_0 + w$ satisfying (P)*

$$w_0 \in H^1_0(\Omega) + W^{2,q}(\Omega) \cap W^{1,q}_0(\Omega) \qquad (1.2)$$

$$w \in L^2\left(0,T;H^1_0(\Omega)\right), \qquad (1.3)$$

$$w' \in L^p(Q) \qquad (1.4)$$

we use an approach due to G.Prodi [10] we have

$$\begin{cases} \qquad u = w_0 + w \\ w_0 \text{ independent of } t \\ \qquad \int_0^T wdt = 0 \end{cases} \qquad (1.5)$$

We introduce the Prodi idia (1.5) in (1.1.1) we having

$$u'' + u' + u - Lu + |u'|^{P-2} u' - f = f + Lu_0 \qquad (1.6)$$

We consider the derivative of (1.6) we obtain

$$\frac{d}{dt}\left(u'' + u' + u - Lu + |u'|^{P-2} u'\right) = \frac{df}{dt}. \qquad (1.7)$$

and

$$\begin{cases} \int_0^T u\,dt = 0 \\ u(T) = u(0) \\ u'(x,0) = u'(x,T) \end{cases} \qquad (1.8)$$

We deduce to (1.7)

$$u'' + u' + u - Lu + |u'|^{P-2} u' - f = h_0 \text{ with } h_0 \text{ independent of } t \qquad (1.9)$$

For resolve (1.7) and (1.8) we denotes. $A = (I-L); \beta(u') = \left(1 + |u'|^{p-2}\right)u'$ and we define the functional space V :

$$V = \begin{cases} v: \ v \in L^2(0,T,H_0^1(\Omega)); \ v' \in L^2(0,T,H_0^1(\Omega)) \cap L^p(Q); \\ v'' \in L^2(0,T,L^2(\Omega)); \int_0^T v(t)dt = 0; \ v(0) = v(T); \ v'(0) = v'(T) \end{cases} \qquad (1.10)$$

.The Banach structure of V is defined by

$$\|v\|_V = \|v\|_{L^2(0,T,H_0^1(\Omega))} + \|v'\|_{L^2(0,T,H_0^1(\Omega))} + \|v'\|_{L^P(Q)} + \|v''\|_{L^2(0,T,L^2(\Omega))}$$

We define the bilinear form:

$$b(u,v) = \int_0^T [(u'',v) + \langle Au, v' \rangle + \langle \beta(u'), v' \rangle]dt \qquad (1.11)$$

The weak formulation of (1.7)and(1.8) is to find $u \in V$ such that

$$b(u,v) = \int_0^T (f; v') \forall v \in V \qquad (1.12)$$

But $b(u,v)$ not coercive

Then we following some ideas of Lions for obtain the elliptic regularization, given $\delta > 0$ and $u, v \in V$ we define

$$\pi_\delta(u,v) = \delta \int_0^T [(u'',v'') + (u',v') + (Au',v')]ds + \int_0^T (u'' + Au + \beta(u'), v')]ds \qquad (1.13)$$

The application $v \longrightarrow \pi_\delta(u,v)$ is continuous on V so there existes an application $B_\delta \in V'$:

$$\pi_\delta \ (u, v) = (B_\delta \ (u), v) \tag{1.14}$$

The linear operator $B_\delta \ : V \longrightarrow V'$ satisfies the four properties:

B_δ is bounded in V' for all bounded set in V and is a hemicontinuous and is a strictly monotonous and is coercive

In view of these properties and as consequence of theorem of Lions [5], there existe unique a function $u_\delta \ \in V$:

$$\pi_\delta \ (u_\delta \ , v) = \int_0^T (f; v')dt \quad \forall v \in V \tag{1.15}$$

2.1   A priori estimates I.

Explicitly the elliptic regularization (1.15) and setting $v = u_\delta$ we obtain

$$\delta \int_0^T \left[|u_\delta''|^2 + \|u_\delta'\|^2 \right] dt + \int_0^T \left[|u_\delta'|^2 + (\beta(u_\delta'), u_\delta') \right] dt = \int_0^T (f, u_\delta) \, dt \tag{1.16}$$

or $\int_0^T (\beta(u'), u') \, dt = \|u'\|_{L^P(Q)}^P$ and $\int_0^T udt = 0 \Rightarrow \|u\|_{L^2(0,T,H_0^1(\Omega))} \le c \|u'\|_{L^2(0,T,H_0^1(\Omega))}$

Then

$$u_\delta' \text{ is bounded in } L^p(Q) \text{ when } \delta \to 0 \tag{1.17}$$

$$\delta \int_0^T \left[|u_\delta''|^2 + |u_\delta'|^2 + \|u_\delta'\|^2 \right] dt \le c \tag{1.18}$$

or, $\int_0^T u_\delta \, dt = 0$ we have by (1.17) and (1.18) that :we have by

$$u_\delta \text{ is bounded in } L^p(Q) \tag{1.19}$$

$$\delta \int_0^T \|u_\delta\|^2 \, dt \le c_1 \tag{1.20}$$

2.2   A priori estimates II

Intoduce in (1.15) v

$$v(t) = \int_0^T u_\delta \ (s)ds - \frac{1}{T} \int_0^T (T - s)u_\delta \ (s)ds \tag{1.21}$$

$$\begin{cases} \int_0^T vdt = 0 \ \ \forall v \in V \\ v' = u_\delta \end{cases} \tag{1.22}$$

Taking into account (1.21) in (1.15) we get

$$\delta \int_0^T [(u_\delta'', u_\delta') + (u_\delta', u_\delta) + (Au_\delta', u_\delta)]dt + \int_0^T [(u_\delta'', u_\delta) + (u_\delta', u_\delta)$$
$$+ \|u_\delta\|^2 + (\beta(u_\delta'), u_\delta')]dt = \int_0^T (f, u_\delta)\, dt$$

$$(1.23)$$

By using periodicity of u_δ, $u_\delta' \in V$, we obtain:

$$\int_0^T (u_\delta'', u_\delta')dt = \int_0^T (Au_\delta', u_\delta)dt = 0 \qquad (1.24)$$

And

$$\int_0^T (u_\delta'', u_\delta)dt = (u_\delta'(T), u_\delta(T)) - (u_\delta'(0), u_\delta(0)) - \int_0^T (u_\delta', u_\delta')dt \quad 1.25(1)$$

$$= -\int_0^T |u_\delta'|^2\, dt$$

By $(1.24), 1.)$ and (1.17) we have

$$\left| \int_0^T (u_\delta'', u_\delta)dt \right| \le c \text{ when } \delta \to 0 \qquad (1.26)$$

Also, from (1.17) and (1.19) we obtain

$$\left| \int_0^T (\beta(u_\delta'), u_\delta)dt \right| \le \|\beta(u_\delta')\|_{L^q(Q)} \|u_\delta\|_{L^p(Q)} \le c' \qquad (1.27)$$

Combining $(1.24), (1.26), (1.27)$ with (1.23) we deduce

$$\int_0^T \|u_\delta\|^2\, dt \le C \qquad (1.28)$$

2.3   Passage to the limit

From (1.17) and (1.28) that there exists a subsequence from (u_δ), such that

$$u_\delta \longrightarrow u \text{ weak in } L^2(0, T; H_0^1(\Omega)) \qquad (1.29)$$

$$u_\delta' \longrightarrow u' \text{ weak in } L^p(Q) \qquad (1.30)$$

$$\beta(u_\delta') \longrightarrow \chi \text{ weak in } L^q(Q)) \qquad (1.31)$$

Passage to the limit in (1.15) we obtain

$$\int_0^T ((-u', v'') + (Au, v') + (\chi, v'))dt = \int_0^T (f; v')dt \ \forall v \in V \qquad (1.32)$$

Use the convolution technic in (1.32) we have

$$\int_0^T (\chi, u' * \eta_\delta \ * \eta_\delta \ )dt = \int_0^T (f; u' * \eta_\delta \ * \eta_\delta \ )dt \qquad (1.33)$$

When

$$\int_0^T (\chi, u')dt = \int_0^T (f; u')dt \qquad (1.34)$$

3   Uniqueness of solution:

Theorem 2. *Under the hypotheses of the theorem of existence,we consider two solutions u_1 and u_2 of the problem (P) then $u_1 = u_2$*

Proof. We subtract the equations (1.5) corresponding to u_1 and u_2 and setting $\phi = u_1 - u_2$ we have

$$\phi'' + A\phi + \beta(u_1' \ ) - \beta(u_2' \ ) \qquad (2.1)$$

Denoting by $(\eta_\delta \ )$ the regularizing sequence a similar argument by Brézis [2] we obtain

$$\phi' * \eta_\delta \ * \eta_\delta \ = \phi * \eta_\delta' \ * \eta_\delta \qquad (2.2)$$

Hence, by using (1.2) and (1.3), we have

$$\phi = \varphi + \phi_0: \quad \phi_0 \in V \text{ and } \varphi \in L^2 \left(0, T; H_0^1 \left(\Omega\right)\right) \qquad (2.3)$$

From (2.2) we get

$$\phi' * \eta_\delta \ * \eta_\delta \ = \phi * \eta_\delta' \ * \eta_\delta \ = \varphi' * \eta_\delta \ * \eta_\delta \qquad (2.4)$$

show that

$$\int_0^T (\phi'', \phi' * \eta_\delta \ * \eta_\delta \ )dt = 0 \text{ and have sense}$$

When

$$\int_0^T \frac{d}{dt}(\phi', \phi' * \eta_\delta \ * \eta_\delta \ )dt = \int_0^T (\phi'', \phi' * \eta_\delta \ * \eta_\delta \ )dt$$

$$+ \int_0^T (\phi', \phi'' * \eta_\delta \ * \eta_\delta \ )dt = +2 \int_0^T (\phi'', \phi' * \eta_\delta \ * \eta_\delta \ )dt = 0 \qquad (2.5)$$

Therefore

$$\int_0^T (\phi'', \phi' * \eta_\delta \ * \eta_\delta \ )dt = \frac{1}{2} \int_0^T \frac{d}{dt}(\phi', \phi' * \eta_\delta \ * \eta_\delta \ )dt = 0 \qquad (2.6)$$

ϕ' and η_δ periodic then we have

$$\int_0^T (\phi, \phi' * \eta_\delta * \eta_\delta) dt = \int_0^T (\phi', \phi' * \eta_\delta * \eta_\delta) dt = \int_0^T (A\phi, \phi' * \eta_\delta * \eta_\delta) dt = 0$$
(2.7)

From $(2.1); (2.6); (2.7)$; we obtain

$$\int_0^T (\beta(u_1') - \beta(u_2'), \phi' * \eta_\delta * \eta_\delta) dt = 0 \tag{2.8}$$

Passage to the limit in (2.8) we have

$$\int_0^T (\beta(u_1') - \beta(u_2'), u_1' - u_2') dt = 0 \tag{2.9}$$

where

$$u_1' - u_2' = 0 \Rightarrow u_1' = u_2' \tag{2.10}$$

This implies that

$$\phi = u_1 - u_2 = \theta, \quad \theta \text{ independent of } t \tag{2.11}$$

But

$$(A\theta, \theta) = \int_\Omega (-L + I) \theta . \theta dx = \|\theta\|_2^2 + \mu \|\nabla\theta\|_2^2 + (\mu + \lambda) \|div\theta\|_2^2 \tag{2.12}$$

We deduce from (1.2)

$$\theta \in H_0^1(\Omega) + W^{2,q}(\Omega) \cap W_0^{1,q}(\Omega) \tag{2.13}$$

By (2.12) and (2.13) we have the uniqueness of solution.

References

1. R.A. Adams, Sobolev Spaces, Academic Press, (1976).
2. H. Brezis, Analyse fonctionnelle, théorie et applications. Masson (1983).
3. G. Duvaut, J.L. Lions, Les inéquations en mécanique et en physique. Dunod. Paris. (1972).
4. J.L. Lions, Quelques méthodes de résolution des problèmes aux limites non linéaires. Dunod. (1969).
5. Luc Tartar, Topics in non lineair analysis. Université de Paris-Sud, Publications Mathematiques d'Orsay,novembre (1978).
6. M. Meflah, Study of Nonlinear Elasticity Problem by Elliptic Regularization with Lamé System, Int. J. of Mathematical Archive-2(5), May 2011, Page 693-697, ISSN 2229-5046.

7. M. Meflah, A Nonlinear Elasticity Problem by Elliptic Regularization Technics, Int. J. Contemp. Math. Sciences, Vol 6, 2011, no. 25, 1221-1229, ISSN 1312-7586

8. M. Meflah B, Merouani, A Nonlinear Elasticity Probrned by Lamé System, Applied Mathematical Sciences, Vol.4, 2010,no. 36,1785-1796.

9. B. Merouani, M. Meflah, A. Boulaouad, The Generalized and perturbed Lamé system, Applied Mathematical Sciences Vol.2, 2008,no. 49,2425-2430..

10. F. Messelmi, B. Merouani, M. Meflah, Nonlinear thermoelasticity problem, Analele Universitatii Oradea, Fasc. Matematica,Tom XV (2008), 207-217.

11. G. Prodi, Soluzioni periodiche dell'equazione delle onde com termine dissipativo nonlineare.Rend. Sem.
Mat. Pandova, 35 (1965).

12. V. Patron, P. Perline, Méthode de la théorie mathématique de l'élasticité, Editions Mir, Moscou, 1981.

Analysis of FIPS 140-2 Test and Chaos-Based Pseudorandom Number Generator

Lequan Min, Tianyu Chen, and Hongyan Zang

Mathematics and Physics School, University of Science and Technology Beijing,
Beijing 100083 China
(E-mails: {minlequan,zhy‗lixiang}@sina.com, cty‗furmosi@sina.com)

Abstract. Pseudo random numbers are used for various purposes. Pseudo random
number generators (PRNG) are useful tools to provide pseudo random numbers.
The FIPS 140-2 test issued by the American National Institute of Standards and
Technology has been widely used for the verifications the statistical properties of
the randomness of the pseudo random numbers generated by PRNGs.

First this paper analyzes the FIPS 140-2 test. The results show that

- The required interval of the FIPS140-2 Monobit Test corresponds to the confident interval with significant level $\alpha = 0.0001(1 - \alpha)$.
- The required interval of the FIPS140-2 Pork Test corresponds to χ^2 test with significant level $\alpha = 0.0002(1 - \alpha)$.
- The required intervals of the FIPS140-2 Run Test correspond to the confident interval with significant level $\alpha = 0.00000016(1 - \alpha)$.

Second this study considers a novel chaotic map (NCP), whose prototype is the
Lorenz three-dimensional Lorenz chaotic map. A NCP -based PRNG (CPRNG) is
designed. Using the FIPS 140-2 test measures the 1000 keystreams randomly generated by the RC4 algorithm, and the 1000 keystreams generated by the CPRNG
with perturbed randomly initial conditions in a range $|\epsilon| \in [10^{-16}, 10^{-4}]$. The
results show that the statistical properties of the randomness of the sequences generated via the CPRNG and the RC4 do not have significant differences. Our results
confirm once again that suitable designed chaos-based PRNGs may generate sound
random sequences, in particular for a replacement for the one-time pad system.
Keywords: FIPS 140-2 Test, Analysis in required intervals, Chaos-based pseudorandom number generator, RC4, Randomness comparison..

1 Introduction

Pseudorandom numbers are important in applications such as simulations
of physical systems[1], in cryptography[2], in Entertainment[3], and in protecting computer systems. John von Neumann was the first contributor in
computer-based random number generators. Today algorithmic pseudorandom number generators (PRNGs) have replaced almost random number tables and hardware random number generators in practical uses.

A algorithmic PRNGs is an algorithm for generating sequences of numbers
that approximate the properties of random numbers. A poor PRNG will lead

to weak or guessable its keys, and leak the information which is prevented.
There are many designed tests for measuring the randomness quantities of
the sequences of numbers generated via PRNGs. The FIPS 140-2 test[4], the
SP800-22 test[6], the Diehard battery[5] test are popular tests to be used in
evaluating the randomness quantities of the sequence numbers deriving from
PRNGs.

Since Lorenz's influential book[7] and Li and York's pioneer paper [8],
the study of chaos has been rapidly developed. Matthews has first derived
a chaotic encryption algorithm and shown that it may be suitable for a re-
placement for the one-time pad system[9].

Lérrez et al. have considered a modified Chua's circuit generator of 5-
scroll chaotic attractor and shown that it may have a potential application
to transmit encrypted audio and image information[11]. Stojanovski and
Kocarev [10] have analyzed the application of a chaos-based PRNG. Li et
al.[12] have reported that using only 120 consecutive known plain-byres can
broken the whole secret key of a multiple one-dimensional chaotic map -
based PRNG. Yu et al[13] have introduced and analyzed a quadric polynomial
chaotic map based PRNG by the FIPS 140-2 test.

This paper analyzes the standards of the randomness criteria of the FIPS
140-2 test, introduces a novel chaotic map (NCM), designs a NCM-based
PRNG. Using the FIPS 140-2 test measures and compares the randomness
performances of the NCM-based PRNG and the RC4 algorithm – a famous
algorithm PRNG used in computer prevent.

The rest of this paper is organized as follows. Section 2 discusses the
standards of the randomness criteria of the FIPS 140-2 test. Section 3 in-
troduces the NCM, stimulates numerically its dynamic orbits, designed the
NCM-based PRNG. Section 4 compares the randomness quantities of the
NCM-based PRNG and the RC4 PRNG. Section 5 gives concluding remarks.

2   Analysis of FIPS 140-2 Test

The FIPS 140-2 Test issued by the National Institute of Standard and Tech-
nology consists of four tests: Monobit test, Poker test and long Run test.
Each test needs a single stream of 20,000 one and zero bits from keystream
generation. Any failure in the test means the sequence of stream must be
rejected. The four test are listed as for follows:

(1) Monobit test: Count the numbers N of "0" and "1" in the 20,000 bit-
stream, respectively. The test is passed if the N is fallen into the required
interval given in the second column in Table 1.
(2) Poker test: Divide a sequence of 20,000 into 5,000 consecutive 4-bit
segments. Denote $f(i)$ to be the number of each 4-bit valve i where
$0 < i < 15$. Then calculate the following:

$$N = \frac{16}{5000} \sum_{i=1}^{16} f(i)^2 - 5,000. \tag{1}$$

The test is passed if the N is fallen into the required interval given in the second column in Table 1.

(3) Run test: Run is defined as maximal sequence of consecutive bits of either all $'1'$ or all $'0'$ that is the part of a 20,000 bitstream. Count and store the run bits with ≥ 1. The test is passed if the length of each run is fallen into the required interval listed in the second column in Table 1

Table 1. The required intervals of the FIPS 140-2 Monobit Test Pork Tests and Run Test, and the calculated confident intervals of random sequences with different significant level $\alpha's$. Here MT, and PT represent the Monobit Test and the Pork Test; LR represents the length of the run of a tested sequence.

	FIPS 140-2 Standard	$\alpha = 10^{-4}$	Golomb's
	Required Interval	Confident Interval	Postulates
MT	9,725~10,275	9,725~10,275	10000
		$\alpha = 2 \times 10^{-4}$	
PT	2.16~46.17	2.41~44.26	16.01
RT	FIPS 140-2 Standard	$\alpha = 1.6 \times 10^{-7}$	Golomb's
k	Required Interval	Confident Interval	Postulates
1	2,315~2,685	2,315~2,685	2,500
2	1,114~1,386	1,119~1,381	1,250
3	527~723	532~718	625
4	240~384	247~378	313
5	103~209	110~203	156
6+	103~209	110~203	156

Golomb has proposed three postulates on the randomness that pseudo-random sequences should satisfy [14]:

1. **Balance Property**. In one period of a pseudorandom sequence, if the period p is even, then the number of ones is equal to the number of zeros otherwise they differ only by one.

2. **Run Distribution Property**. In one period of a pseudorandom sequence, the frequency of runs of length k is $\dfrac{1}{2^k}$. The numbers of the same length one run and zero run are the same.

3. **Ideal Autocorrelation Property**. The autocorrelation function $AC(k)$ has two values for a period. Explicitly:

$$AC(k) = \frac{1}{p}\sum_{i=1}^{p} s_i s_{i+k} = \begin{cases} 1 & for\ k = np \\ \dfrac{-1}{p} & otherwise \end{cases}$$

where 0's of the sequence are replace by 1's and 1's by -1's, $s_i s_j$ denote the multiplication of two bits s_i and s_j.

According to Golomb's postulates (1) and (2), the idea values of the N's of the Monobit test and the Run test should be those listed in the 4th column in Table 1.

1. **Monobit test analysis**: Let $\epsilon = \epsilon_1 \epsilon_2 \cdots \epsilon_n$ be an one and zero bit sequence where n is the length of the bit string. Denote $X_i = 2\epsilon_i - 1$, then $S_n = X_1 + X_2 + \cdots X_n = 2(\epsilon_1 + \epsilon_2 + \cdots + \epsilon_n) - n$ If ϵ is a sequence of independent identically distributed Bernoulli random variables, then[6]

$$\frac{S_n}{\sqrt{n}} \sim N(0,1)$$

   where $N(0,1)$ is a standard normal distribution.
   The confident interval of $S'_n = \epsilon_1 + \epsilon_2 + \cdots \epsilon_n$ with significant level α is given by

$$\frac{n}{2} - \frac{\sqrt{n}}{2} Z_{\frac{\alpha}{2}} \leq S'_n \leq \frac{n}{2} + \frac{\sqrt{n}}{2} Z_{\frac{\alpha}{2}}$$

   where $Z_{\frac{\alpha}{2}}$ (Matlab command $norminv(1 - \alpha/2)$) is the inverse of the normal cumulative distribution function. In the case $n = 20,000$ and $\alpha = 0.0001$, the calculated result is given in the third column in Table 1 which is the same as the required interval given by the FIPS 140-2 test.

2. **Run test analysis**. Pick up the the runs of length k from the an one and zero bitstream and construct a new bit stream. Replace each one run of length k by 1, and zero run of length k by 0. Then we obtain an one and zero bit sequence $\epsilon' = \epsilon'_1 \epsilon'_2 \cdots \epsilon'_{n'}$ where n' is the length of the new bit string. Assume ϵ' is a sequence of independent identically distributed Bernoulli random variables, then similar to the analysis in the case of the Monobit test, we obtain

$$\frac{S_{n'}}{\sqrt{n'}} \sim N(0,1)$$

   The confident interval of $S'_{n'} = \epsilon'_1 + \epsilon'_2 + \cdots \epsilon'_{n'}$ with significant level α is given by

$$\frac{n'}{2} - \frac{\sqrt{n'}}{2} Z_{\frac{\alpha}{2}} \leq S'_{n'} \leq \frac{n'}{2} + \frac{\sqrt{n'}}{2} Z_{\frac{\alpha}{2}}$$

   For an idea 20,000 one and zero bit pseudorandom stream, the length n' of a bit sequence ϵ' generated via the runs of length k should equal to $10000/2^k$. Let $\alpha = 1.6 \times 10^{-7}$, the calculated confident intervals are listed in the third column in Table 1 which are almost the same as the required intervals given by the FIPS 140-2 test.

3. **Poker test analysis**. Assume the the 4-bit segments are distributed independently and identically. Then the statistic quality

$$N = \frac{16}{5000} \sum_{i=1}^{16} f(i)^2 - 5,000$$

$$= \sum_{i=1}^{16} \frac{5000}{1/16} (\frac{f(i)}{5000} - \frac{1}{16})^2$$

obeys χ^2 distribution. Hence the confident interval of the statistic quality of N with significant level α is given by

$$\chi^2_{1-\frac{\alpha}{2}}(15) \le N \le \chi^2_{\frac{\alpha}{2}}(15),$$

where $\chi^2_\alpha(15)$ (Matlab command chi2inv(α,15)) is the inverse of the χ^2 cumulative distribution function with free degree 15.

Let $\alpha = 0.0002$. The calculated confirmation interval is given in Table 1 which is similar to the one given by the FIPS 140-2 test.

3 New Chaotic Map and Pseudorandom Number Generator

we consider a novel chaotic map (NCP), whose prototype is the Lorenz three-dimensional Lorenz chaotic map [15].

$$\begin{cases} X(n+1) = k_1 X(n)Y(n) - k_2 Z(n) - k_3 X(n) \\ Y(n+1) = k_4 X(n) - k_5 Y(n) \\ Z(n+1) = k_6 Y(n) - k_7 Z(n) \end{cases}$$

where

$$k_1 = 1 - 10^{-6}, k_2 = 1 + 10^{-6}, k_3 = 2 \times 10^{-6},$$
$$k_4 = 1 + 10^{-6}, k_5 = 3 \times 10^{-6}, k_6 = 1 - 10^{-6}, k_7 = 10^{-6}.$$

The
Lyapunov exponents of the NCM are $[\lambda_1, \lambda_2, \lambda_3] = [+0.0824, 0, -0.0824]$. If select an initial condition $[X_0, Y_0, Z_0] = [0.5 \ 0.5 \ -1]$, The numerical simulations of the orbits of the NCM display are given in Fig. 1. Observe that the dynamic patterns are similar to those of the 3D Lorenz map[7].
Let
$$K_n = \sqrt{3}X(n) + \sqrt{5}Y(n) + \sqrt{2}Z(n), n = 1, 2, \cdots, N;$$

$$Min(K) = \min_{1 \le n \le N} K_n, Max(K) = \max_{1 \le n \le N} K_n.$$
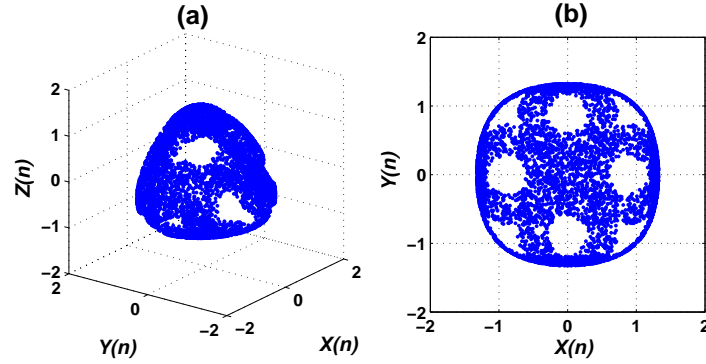
Fig. 1. Orbits of the first 5000 iterations: (a) $X(n), Y(n), Z(n)$, and (b) $X(n)$ and $Y(n)$.

Define a transformation T by

$$T(K_n) = mod\left(round\left(\frac{255\sqrt{2} \times 10^5(K_n - Min(K))}{Max(K) - Min(K)}\right), 256\right), n = 1, 2, \cdots, N.$$

Transferring $T(K_n)$ into binary codes, we obtain a binary sequence

$$s(k) = binary(T(K_n)), n = 1, 2, \cdots, N. \qquad (2)$$

Hence, we construct a chaos-based pseudorandom number generator (CPNG).

4 FIPS 140-2 test

The RC4 was designed by Ron Rivest of RSA Security in 1987, and widely used in popular protocols such as Secure Sockets. Now we use the FIPS 140-2 test to test the 1000 keystreams randomly generated by the RC4, and the 1000 keystreams generated by the CPNG with an initial condition $[X(0), Y(0), Z(0)] = [0.5, 0.5, -1]$ perturbed randomly in a range $|\epsilon| \in [10^{-16}, 10^{-4}]$. The results are shown in Table 2. It follows that the statistical properties of the randomness of the sequences generated via the CPNG and the RC4 do not have significant differences.

Matlab commands for implement the RC4 algorithms are listed as follows.

```
L=8; K=randint(1,2^L,[0 2^L-1]);S=[0:2^L-1]; j=0;
for i=1:2^L
j=mod(j+S(i)+K(i),2^L);
Sk=S(j+1); S(j+1)=S(i); S(i)=Sk;
end
l=1; C=zeros(1,20000/8+10); j=0;i=0; k=1;
```

```
for l=1:20000/8+10; i=mod(i+1,2^L); j=mod(j+S(i+1),2^L);
Sk=S(j+1); S(j+1)=S(i+1); S(i+1)=Sk;
C(k)=S(mod(S(j+1)+S(i+1),2^L)+1);
k=k+1;
end
```

Table 2. The confident intervals of the FIPS 140-2 tested values of 1000 key streams generated by the RC4 and the CPNG respectively. The significant level. $\alpha = 0.00001$

Test item	bits $\{0,1\}$	Golomb's Postulates	RC4 Confident Interval	CPNG Confident Interval
MT	0	10000	$9992.2 \sim 10012$	$9990.1 \sim 10010$
	1	10000	$9988 \sim 10008$	$9989.6 \sim 10009$
PT	–	16.01	$14.408 \sim 15.899$	$13.373 \sim 13.914$
LT	0	< 26	$13.443 \sim 13.971$	$13.405 \sim 13.913$
	1	< 26	$13.340 \sim 13.872$	$13.328 \sim 13.823$
LR			Run Test	
1	0	2500	$2493.6 \sim 2506.9$	$2492.0 \sim 2504.9$
	1	2500	$2493.7 \sim 2506.6$	$2489.9 \sim 2503.3$
2	0	1250	$1244.9 \sim 1253.8$	$1244.7 \sim 1253.9$
	1	1250	$1242.6 \sim 1251.3$	$1243.6 \sim 1252.2$
3	0	625	$621.46 \sim 628$	$622.10 \sim 628.60$
	1	625	$622.44 \sim 629.25$	$622.96 \sim 629.31$
4	0	313	$310.09 \sim 314.68$	$309.92 \sim 314.56$
	1	313	$311.27 \sim 315.74$	$310.29 \sim 314.83$
5	0	156	$154.8 \sim 158.21$	$154.18 \sim 157.44$
	1	156	$154.79 \sim 158.2$	$154.66 \sim 158.14$
6^+	0	156	$154.29 \sim 157.64$	$155.32 \sim 158.56$
	1	156	$154.54 \sim 157.93$	$155.28 \sim 158.67$

5   Concluding Remarks

Based on the Golomb's postulates for the randomness of pure pseudorandom sequences, this paper analyzes the required intervals of the statistic quantities of three tests given in the FIPS 140-2. The results show that the required intervals for different tests do not have the same significant levels.

This study introduces a perturbed 3D Lorenze discrete map. This map The Lyapunov exponents and the dynamic orbits of the map are both similar to those of the 3D Lorenz map.

This paper constructs a chaos-based PRNG which has 7 key parameters. This feature of the PRNG may make it have large key space. Comparing the results of the FIPS 140-2 test for the RC4 PRNG and our chaos-based

PRNG shows that statistical properties of the randomness of the sequences generated via the our PRNG and the RC4 PRNG do not have significant differences.

Our results confirm once again that suitable designed chaos-based PNGs may generate sound random sequences, in particular for a replacement for the one-time pad system[9]. Further research along this line is promising.

Acknowledgements

References

1. K. Binder, and D. W. Heermann, *Monte Carlo Simulation in Statistical Physics: An Introduction* (4th edition). 2002. Springer.
2. N. Ferguson, B. Schneier, and T. Kohno, *Cryptography Engineering: Design Principles and Practical Applications.*, 2010. Wiley Publishing.
3. S. Wegenkittl, Gambling tests for pseudorandom number generator, *Mathematics and Computers in Simulation*, 55: 281-288, 2001.
4. NIST, *FIPS PUB 140-2, security requirements for cryptographic modules.* 2001.
5. G. Marsaglia, http://www.stat.fsu.edu/pub/diehard/, 1996 [2012-03-30].
6. R. Rukhin, J. Soto, J. Nechvatal et al., *A statistical test suite for random and pseudorandom number generator for cryptographic applications*, page 64, NIST Special Publication, 2001.
7. E. N. Lorenz, Deterministic nonperiodic flow, *J. of Atmospheric Sciences*, Vol. 20(2): 2130–148, 1963.
8. T. Y. Li and J. A. York, Period three implies chaos, *American Mathematical Monthly*, 82(10): 481–485, 1975.
9. R. A. J. Matthews, On the derivation of a chaotic encryption algorithm, *Cryptologia*, XIII(1): 29–42, 1989.
10. T. Stojanovski and L. Kocarev01, Choas-based random number generators-part I: analysis, *IEEE Transaction on Circuitts and Systems-I: Fundamental Theory and Applications*, 48(3): 281–288, 2001.
11. L. Gámez-Guzmán, C. Cruz-Hernández, R.M. Lérrez et al., Synchronization of Chua's circuits with multi-scroll attractors Application to communication, *Commum Nonlinear Sci Numer Simulat*, 14: 2765–2775, 2009.
12. C. Li, S. Li, G. Alvarez et al., Cryptanalysis of a chaotic block cipher with external key and its improved version, *Chaos Solitons & Fractals*, 37: 299–307, 2008.
13. X. Yu, L. Min, and T. Chen, Chaos criterion on some quadric polynomial maps and design for chaotic pseudorandom number generator. *In Proc. of the 2011 Sewventh Int. Conf. on Nutural Computation*(26-28 July 2011, Shaghai, China), Vol.3: 1399–1402, 2011.
14. S. W. Golomb, *Shift Register Sequences.* Revised edition, CA: Aegean Park, 1982. Laguna Hills.
15. J. C. Sprott, *Chaos and Time-Sries Analysis*, page 427, Oxford. 2003. Oxford University Press.

A Multi-Input Multi-Output Delayed Feedback Controller for Stabilizing Periodic Solutions of the Lorenz System

Soraia Moradi[1,2], Ali Khaki Sedigh[1] and Nastaran Vasegh[1,3]

[1] Advanced Process Automation and Control (APAC) Research Group, K. N. Toosi University of Technology, Tehran, Iran

[2] Automation and Control Institute (ACIN), Vienna University of Technology, Vienna, Austria (E-mail: e1126740@student.tuwien.ac.at)

[3] Department of Electrical Engineering and Computer, Shahid Rajaee Teacher Training University, Lavizan, Tehran, Iran

Abstract. In this paper the idea of harmonic balance method is used in a new framework to analyze and predict the periodic solutions of the Lorenz system. An analytic equation has been derived for these predicted limit cycles for the first time. The proposed method is fairly straightforward avoiding complicated calculations. A multi-input multi-output Delayed Feedback Controller (DFC) is designed and implemented for stabilizing unstable periodic solutions of the Lorenz system. All previous works done on stabilization of periodic solutions of this system, using a simple DFC (without adding a new dynamic to the system) were unsuccessful. Choosing an appropriate signal to use in the delayed feedback loop and an appropriate point for introducing the control signal are very important tasks in DFC implementation. Considering these facts, we overcome the mentioned problem by choosing the third state variable of the Lorenz system that to our knowledge has not been used before, in the delayed feedback loop and introducing the control signal to the system in a different point from previous works. Our proposed controller is also able to stabilize the equilibrium points (EPs) of the system. The stability analysis is also done.

Keywords: Lorenz system, delay feedback control, harmonic balance.

1 Introduction

DFC is an efficient method of chaos control, which stabilizes Unstable Periodic Orbits (UPO) embedded in a chaotic attractor. In 1994 researchers found out that DFC is not able to stabilize systems with odd number of Floquet exponents. In other words, they thought it is impossible to stabilize any UPOs with odd-number of real characteristic multipliers greater than unity [1–3]. So they tried to overcome this limitation. In [4] authors used an expanded DFC. In [5] it was shown that this stable controller can not overcome all the DFCs limitations. Since they thought these limitations were due to the odd number of positive Floquet exponents, in later studies, researchers tried to solve this problem by adding an unstable term to change the total number of real-positive Floquet exponent to an even number [6,7]. Another

method was using some different values of delay in the feedback to increase the controllers degrees of freedom [8,9].

Variety of methods were suggested to eliminate this problem till 2007, but in[10] it was shown that, this limitation that scientists were trying to overcome for more than fifteen years did not exist at all and theoretical analysis and simulations confirmed this fact too [11]. One of the systems that was thought it can not be stabilized with the use of the DFC, due to the "odd-number limitation" was the Lorenz system. Several studies were done to avoid this limitation (see [7,12,13]. In all these studies, it was tried to avoid the limitation by introducing an unstable degree of freedom in a feedback loop to change the number of unstable torsion-free modes to an even number and the control signal was just applied to one of the state variables (the second one).

In this paper we use a simple DFC to stabilize an unstable periodic solution of the Lorenz system. The key idea of our work is using the third state variable of the Lorenz system in the control loop and introducing the controller to both the second and the third state equations (see Eq.1). The next section is devoted to the open loop analysis of the system. Using the Harmonic Balance (HB) idea, the analytical predicted periodic solutions of the system have been derived and their stability features have been studied. In section 3 an analysis is done to predict the chaotic dynamics and finally in section 4, a MIMO DFC is used to stabilize an unstable periodic solution of the system. Also it has shown that this control structure can be used for stabilization of the EPs of the system.

2   The open loop analysis

Consider the following classical Lorenz chaotic system

$$
\begin{cases}
\dot{x} = -\sigma x + \sigma y \\
\dot{y} = \rho x - y - zx \\
\dot{z} = -\mu z + xy
\end{cases}
\tag{1}
$$

The Lorenz equations have three parameters σ, μ and ρ. To simplify matters, most researchers have kept $\sigma = 10$ and $\mu = 8/3$ while varying ρ. As shown in [14] by assuming $f = x$ the system equations can be rewritten in the following form

$$
\begin{cases}
\frac{1}{\sigma} + (1 + \frac{1}{\sigma})\dot{f} + (1 - \rho) + fz = 0 \\
\dot{z} = -\mu z + f(\frac{1}{\sigma}\dot{f} + f)
\end{cases}
\tag{2}
$$

Eq.2 puts in evidence the feedback structure of the system, as shown in Fig.1 where a linear subsystem is connected to a nonlinear one. Due to the existence of the dynamical term $1/(s+\mu)$ in the nonlinear subsystem of Fig.1, it may be difficult to use the general approach originally proposed by Tesi
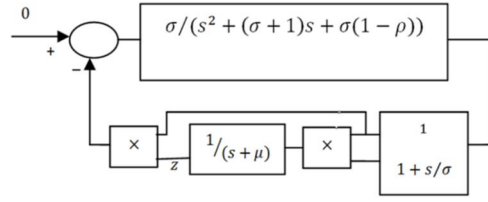
Fig. 1. The feedback structure of the Lorenz system.

and Genesio in 1992 to find the periodic solutions of the system. So in this paper we use the idea of the well-known HB method in the following simple manner.

2.1 Periodic solutions

At the first step, it is assumed that these steady solutions can be approximated as

$$x = A + B \cos \omega t \tag{3}$$

Substituting Eq.3 in the first state equation of Eq.1 results in

$$y = \frac{1}{\sigma}\dot{x} + x = A + B \cos(\omega t) - \frac{1}{\sigma}B\omega \sin(\omega t) \tag{4}$$

Then by substituting Eq.3 and Eq.4 in the third state equation of Eq.1, eliminating the second harmonics which appear, and ignoring the transient solution, we conclude the steady solution of z as

$$z = \frac{3}{80}(10A^2 + 5B^2 + \frac{8AB(160 + 3\omega^2)\cos(\omega t)}{64 + 9\omega^2} + \frac{416AB\omega \sin(\omega t)}{64 + 9\omega^2}) \tag{5}$$

After substituting Eq.3 and Eq.5 in the second state equation of Eq.1 and doing similar calculations, we obtain an expression for y that should be equal to Eq.4. Equalizing the related coefficients results in the following three equations for A^2, B^2 and ω^2 in terms of ρ

$$A^2 = \frac{-2}{1561512117}(527280000\sqrt{3}\rho m - 3845514915\rho + 4056000\sqrt{3}m^3$$
$$- 12168000\sqrt{3}\rho^2 m + 106221667541 - 9892726305\sqrt{3}m) \tag{6}$$

$$B^2 = \frac{4}{425866941}(21884475789 - 2258100\sqrt{3}m^3 + 4498028807\sqrt{3}m$$
$$- 319929891\rho - 293553000\sqrt{3}\rho m + 6774300\sqrt{3}\rho^2 m) \tag{7}$$

$$\omega^2 = \frac{40}{201}(-1113 + 39\rho + 13\sqrt{3}m) \tag{8}$$

where $m = \sqrt{2123 - 130\rho + 3\rho^2}$. The solution of the problem is possible, when the terms A^2, B^2 and ω^2 are real and positive. Therefore, we can derive the domain of parameter space where there are admissible solutions. The domain of existence is

$$7.7693 \leq \rho \leq 24.7368 \tag{9}$$

The obtained results on periodic solutions (Predicted Limit Cycles) are approximate, due to the first harmonic analysis carried out on the system. The reliability of a PLC is based on a strong attenuation (filtering hypothesis) of the higher frequency components 2ω, 3ω ,$\cdots$ along the loop.

2.2 Stability analysis

The system EPs are: $C^{\pm} = (\pm\sqrt{(\mu(\rho - 1))}, \pm\sqrt{(\mu(\rho - 1))}, \rho - 1)$ that exist for $\rho > 1$ and $C^0 = (0, 0, 0)$. In this region C^0 is a saddle and $C^{\pm}$ are symmetric stable fixed points. For $0 < \rho \leq 1$ there exist just C^0 which is a stable node. We use the Loeb criterion to check the stability features of PLCs. according to this criteria, in case the PLC be stable, the following inequality will be true[14]:

$$\frac{\Delta\omega}{\Delta B} = \frac{\delta\omega/\delta\rho}{\delta B/\delta\rho} \leq 0 \tag{10}$$

That is true in our case for $\rho \geq 15.1$.

3 The chaotic dynamic prediction

In this section the famous phenomenon of Homoclinic Orbit (HO) which is one of the main routes to chaos in the most dynamic systems has been analyzed and an approximate region of parameter space is derived in which this phenomenon may occur. As stated in [15], the HO conditions includes the existence of a stable PLC and a saddle type EP (different from that generating the PLC) and the interaction between PLC and EP as $B \geq |E - A|$, where E denotes the mentioned saddle EP and is equal to zero in the Lorenz case. This inequality is valid for $7.77 \leq \rho \leq 15.06$. Considering the regions of PLC existence (Eq.9), PLC stabilization ($\rho \geq 15.1$) and the region in which the interaction condition is satisfied ($7.77 \leq \rho \leq 15.06$), we predict that the HO phenomenon may occur at some values around $\rho = 15$. Therefore the Lorenz system may show chaotic behaviors. Numerical solutions show that Homoclinic bifurcation occurs at $\rho = 13.962$ which is near the predicted value.

4 Chaos control

It is obvious that this system exhibits a chaotic behavior in some regions of its parameter space, for example at $\rho = 24.5$. Whereas the efforts for stabilization of this system with the use of a SISO DFC have not been successful
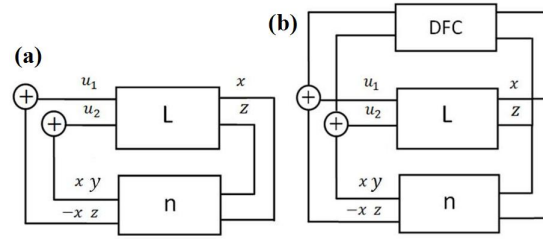
Fig. 2. (a) MIMO Lure form of the Lorenz system. (b) The closed loop system.

up to now, in this paper we consider the system as a MIMO system with the Lure form shown in Fig.2a; which L and n denote respectively the dual-input dual-output linear and nonlinear parts of the system.

$$n = \begin{bmatrix} -zx \\ xy \end{bmatrix} \tag{11}$$

$$L : \begin{cases} \begin{bmatrix} \dot{x} \\ \dot{y} \\ \dot{z} \end{bmatrix} = \begin{bmatrix} -\sigma & \sigma & 0 \\ \rho & -1 & 0 \\ 0 & 0 & -\mu \end{bmatrix} \begin{bmatrix} x \\ y \\ z \end{bmatrix} + \begin{bmatrix} 0 & 0 \\ 1 & 0 \\ 0 & 1 \end{bmatrix} \begin{bmatrix} u_1 \\ u_2 \end{bmatrix} \\ \begin{bmatrix} y_1 \\ y_2 \end{bmatrix} = \begin{bmatrix} 1 & 0 & 0 \\ 0 & 0 & 1 \end{bmatrix} \begin{bmatrix} x \\ y \\ z \end{bmatrix} \end{cases}$$

$$\implies L(s) = \begin{bmatrix} \frac{\sigma}{s^2+(1+\sigma)s+\sigma(1-\rho)} & 0 \\ 0 & \frac{1}{s+\mu} \end{bmatrix} \tag{12}$$

The goal is to design a MIMO DFC to stabilize an unstable periodic solution of the system. The closed loop system is shown in Fig.2b. So the MIMO DFC will be in the following form

$$\underline{U} = \begin{bmatrix} k_{11} & k_{12} \\ k_{21} & k_{22} \end{bmatrix} \begin{bmatrix} x(t-\tau) - x(t) \\ z(t-\tau) - z(t) \end{bmatrix} \tag{13}$$

The aim is to determine the gain matrix and delay (τ) of the controller, so that the closed loop system has a periodic response in the form of Eq.3 for ($\rho = 24.5$). For simplicity we consider a simple case that is in the following form

$$\underline{U} = \begin{bmatrix} u_1 \\ u_2 \end{bmatrix} = \begin{bmatrix} 0 & k \\ 0 & k \end{bmatrix} \begin{bmatrix} x(t-\tau) - x(t) \\ z(t-\tau) - z(t) \end{bmatrix} \tag{14}$$

So our suggested closed loop system is as follows

$$\begin{cases} \dot{x} = -\sigma x + \sigma y \\ \dot{y} = \rho x - y - zx + k(z(t-\tau) - z(t)) \\ \dot{z} = -\mu z + xy + k(z(t-\tau) - z(t)) \end{cases} \tag{15}$$
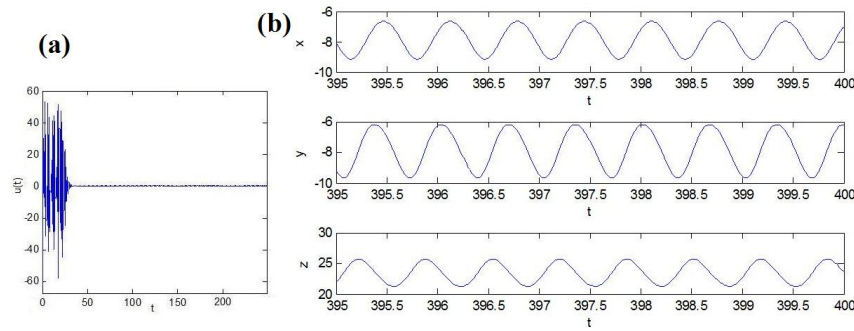
Fig. 3. (a) Control signal tends to zero. (b) The steady state periodic responses of the closed loop system.

τ coincides with the period of the desired periodic solution of the closed loop system. In case stabilization be successful, the control signal will vanish and there will not be any power dissipation in the feedback loop. So by setting $\tau = 2\pi/\omega$ and using the approximation $e^{-\tau s} \approx 1 - \tau s$, we try to determine k. Once more looking back to Eq.3, after doing some calculations similar to those of section (2.1) and substituting A, B and ω with their values at $(\rho = 24.5)$ from Eqs. 6-8 ($A = 7.8685, B = 1.0405, \omega = 9.5104$ rad/s $\Rightarrow T = 0.6607$ s), the controller's gain $k = 2.5227$ is obtained. The value obtained for delay here ($T = \tau$) is nearly equal to the value obtained for it in [7] that was 0.67 s.

Fig.3a and Fig.3b show the control signal and the steady state stable periodic responses of the closed loop system. The control signal tends to zero which means that the stabilization strategy has been successful.

Fig.4 shows a zoom view of the steady response of the first state variable of the system $(x(t))$. It illustrates that the bias A, amplitude B and period T of x are equal to those obtained from Eqs. 6-8 at $\rho = 24.5$ and confirms the accuracy of the implemented analytical approach. A noticeable point about
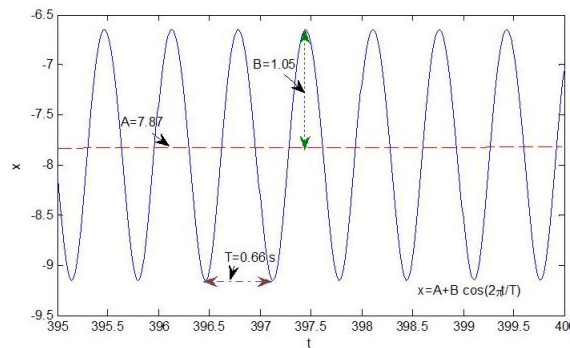
Fig. 4. The bias, amplitude and period of the state variable x.
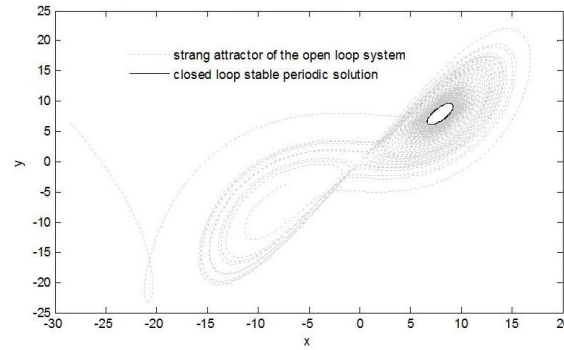
Fig. 5. Stabilizing an unstable periodic orbit embedded in the strange attractor of the open loop system.

the closed loop system is that we have stabilized one of the unstable periodic solutions of the open loop system. In other words we have selected one of the infinite number unstable periodic orbits embedded in the strange attractor and stabilized the system towards it. This fact is shown in Fig.5.

The implemented control structure can be also used for stabilizing the EPs of the Lorenz system. As shown in Fig.6, using $k = 2.5$ and $\tau = 0.8$, the closed loop system will be stabilized to C^+ with the stable eigen values $\lambda_{1,2} = -3.7987 \pm j3.84365$ and $\lambda_3 = -1.561087$.

5   Conclusion

In our paper, using straightforward calculations, the Lorenz system's periodic solutions have been analytically calculated. The results are approximate, due to the first harmonic analysis carried out on the system. The purpose of the paper is to design a DFC in order to stabilize unstable periodic solutions of
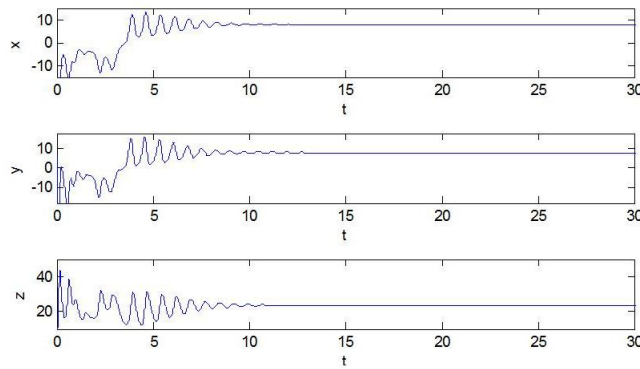
Fig. 6. Lorenz system stabilization to its EPs C^+.

the system. For $\rho = 24.5$ the open loop system shows chaotic behaviors. But the implemented MIMO DFC stabilizes an unstable periodic solution of the system at this value. The key point of our controller, which makes it able to stabilize Lorenz system, is using a different signal in the feedback loop and applying the control signal to the appropriate points. It is the first time, that a simple DFC is implemented successfully for Lorenz periodic solutions stabilization. The simulation results confirm the accuracy of the implemented analytical approach.

References

1. W. Just, T. Bernard, M. Ostheimer, E. Reibold, and H. Benner. Mechanism of time-delayed feedback control. *Physical Review Letters*, 78:203–206, 1997.
2. W. Just, E. Reibold, H. Benner, K. Kacperski, P. Fronczak, and J. Hoyst. Limits of time-delayed feedback control. *Physics Letters A*, 254:158–164, 1999.
3. H. Nakajima. On analytical properties of delayed feedback control of chaos. *Physics Letters A*, 232:207–210, 1997.
4. J. E. S. Socolar, D. W. Sukow, and D. J. Gauthier. Stabilizing unstable periodic orbits in fast dynamical systems. *Physical Review E*, 50:3245–3248, 1994.
5. H. Nakajima, and Y. Ueda. Limitation of generalized delayed feedback control. *Physica D: Nonlinear Phenomena*, 111:143–150, 1998.
6. K. Pyragas. Control of chaos via an unstable delayed feedback controller. *Physical Review Letters*, 86:2265–2268, 2001.
7. K. Pyragas, V. Pyragas, IZ Kiss, and JL Hudson. Adaptive control of unknown unstable steady states of dynamical systems. *Physical Review E*, 70:26215, 2004.
8. A. Ahlborn, and U. Parlitz. Controlling dynamical systems using multiple delay feedback control. *Physical Review E*, 72:16206, 2005.
9. A. Ahlborn, and U. Parlitz. Controlling spatiotemporal chaos using multiple delays. *Physical Review E*, 75:65202, 2007.
10. B. Fiedler, V. Flunkert, M. Georgi, P. Hövel, and E. Schöll. Refuting the odd-number limitation of time-delayed feedback control. *Physical review letters*, 98:114101, 2007.
11. W. Just, B. Fiedler, M. Georgi, V. Flunkert, P. Hövel, and E. Schöll. Beyond the odd number limitation: a bifurcation analysis of time-delayed feedback control. *Physical Review E*, 76:26210, 2007.
12. V. Pyragas, and K. Pyragas. Delayed feedback control of the Lorenz system: an analytical treatment at a subcritical Hopf bifurcation. *Physical Review E*, 73:36215, 2006.
13. K. Pyragas. Delayed feedback control of chaos. *Philosophical Transactions of the Royal Society A: Mathematical, Physical and Engineering Sciences*, 364:2309, 2006.
14. N. Vasegh, and A. Khaki Sedigh. Chaos control via TDFC in time-delayed systems: The harmonic balance approach. *Physics Letters A*, 373:354–358, 2009.
15. R. Genesio, and A. Tesi. Harmonic balance methods for the analysis of chaotic dynamics in nonlinear systems. *Automatica*, 28:531–548, 1992.

Chaos in Modified CFOA-Based Inductorless Sinusoidal Oscillators Using a Diode

Buncha Munmuangsaen and Banlue Srisuchinwong

Sirindhorn International Institute of Technology, Thammasat University
Pathum-Thani 12000, Thailand
E-mail: banlue@siit.tu.ac.th

Abstract: Two modified inductorless sinusoidal oscillators are presented as two chaotic oscillators. The active component employs a current-feedback operational amplifier (CFOA) whereas the nonlinear component employs a simple diode. Numerical and PSpice simulations are demonstrated in terms of chaotic attractors. A bifurcation diagram is also included.

Keywords: Chaos, Nonlinear circuit and system, RC oscillator.

1. Introduction

The design and development of autonomous chaotic oscillators over the past three decades have been increasing due to a variety of applications in, for example, spacecraft trajectory control, stabilization of the intensity of a laser beam, noise radars and sonar [1], synchronization [2, 3] and secure communications [4, 5, 6]. One of the best known chaotic circuits is Chua's circuit [7] as well as its variants [8, 9], using a Chua's diode. However, an active nonlinear resistor such as the Chua's diode is not recommended by [10] because it does not follow the design rules of [10]. Instead, a passive nonlinear component for chaos has been suggested using either a diode or a junction field effect transistor (JFET) [10].

A current-feedback operational amplifier (CFOA) is currently recognized as a versatile alternative to the traditional op amp for its excellent performance in high-speed and high slew-rates analog signal processing, and therefore does not suffer from the finite gain bandwidth product typically encountered in the conventional voltage op amps [11]. A chaotic oscillator has been designed using a modified CFOA-based sinusoidal oscillator with two capacitors and an inductor for a third-order chaotic system [11]. Such a chaotic oscillator has subsequently been further investigated by [12] using three capacitors. The nonlinear device of both chaotic oscillators has exploited a two-terminal nonlinear resistor formed by a JFET (J2N4338). However, chaos has not successfully found in [12] using a single diode as a nonlinear component.

In this paper, chaos in two modified CFOA-based inductorless sinusoidal oscillators is presented. The active element employs the CFOA whereas the nonlinear component employs a single diode. Chaos can be found by replacing a JFET resistor of [12] with a sub-circuit consisting of a diode and a resistor.

2. Circuit Implementation

Figures 1(a) and 1(b) show two proposed chaotic oscillators using a single diode as a nonlinear device. Both circuits are modified CFOA-based inductorless sinusoidal oscillators which almost resemble the existing circuits reported in [12], except that the JFET nonlinearity of [12] is replaced with a new sub-circuit consisting of a diode D_1 and a resistor R_3. The latter is connected to a negative DC supply.
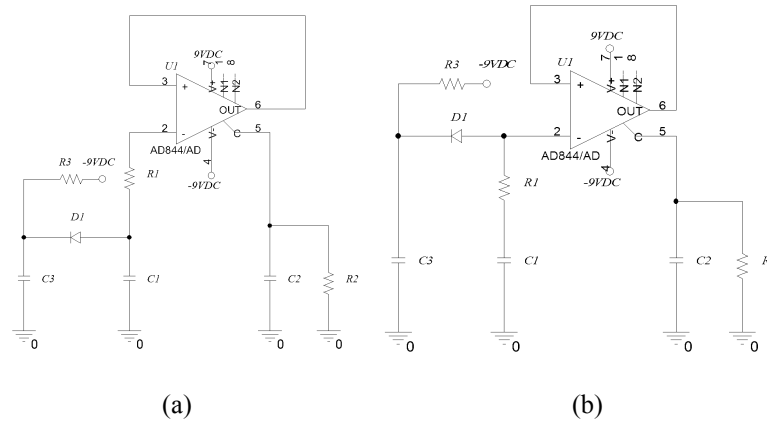
Fig. 1 Modified CFOA-based inductorless sinusoidal oscillators using a diode for : (a) the first chaotic oscillator, (b) the second chaotic oscillator.

The proposed chaotic oscillator shown in Figure 1(a) is described by a set of differential equations as follows :

$$C_1 \dot{V}_{C1} = \left(\frac{V_{C2}-V_{C1}}{R_1}\right) - I_D$$

$$C_2 \dot{V}_{C2} = \left(\frac{V_{C2}-V_{C1}}{R_1}\right) - \frac{V_{C2}}{R_2} \tag{1}$$

$$C_3 \dot{V}_{C3} = I_D - \left(\frac{V_{C3}+9}{R_3}\right)$$

where the overdot denotes a time (t) derivative. The voltages across capacitors C_1, C_2, and C_3 are V_{C1}, V_{C2}, and V_{C3}, respectively. A diode current $I_D = I_S\{exp[(V_{C1}-V_{C3})/nV_T] - 1\}$ where I_S is the reverse saturation current, n is the nonideality factor, and V_T is the thermal voltage of 25.85 mV at room temperature (300K). The proposed chaotic oscillator shown in Figure 1(b) is described by another set of differential equations as follows :

$$C_1 \overset{\&}{J}_{C1} = \frac{V_{C2} - V_{C1}}{R_1} \qquad\qquad (2)$$

$$C_2 \overset{\&}{J}_{C2} = (\frac{V_{C2} - V_{C1}}{R_1}) - (\frac{V_{C2}}{R_2}) + I_D$$

$$C_3 \overset{\&}{J}_{C3} = I_D - (\frac{V_{C3} + 9}{R_3})$$

where the diode current $I_D = I_S\{exp[(V_{C2} - V_{C3})/nV_T] - 1\}$

3. Simulation Results

The CFOA can be implemented using the commercially available AD844. The diode D_1 is 1N4001 using PSpice parameters $I_S = 14.11 \times 10^{-9}$ A and $n = 1.984$. The junction capacitance of 1N4001 is typically 15 pF and, for simplicity, may be neglected compared to the much larger values of C_1, C_2 and C_3. For a PSpice simulation, Figure 2(a) shows a circuit diagram of (*i*) a diode circuit (D_4, R_2), (*ii*) a nonlinear JFET resistor (J_1, R_4), and (*iii*) a sub-circuit consisting of a diode and resistors (D_3, R_1, R_3). Figure 2(b) shows a comparison of the three simulation results of current-voltage characteristics in (*i*), (*ii*) and (*iii*) where the currents on the vertical axis are through R_2, R_4 and R_1, respectively, and the voltage on the horizontal axis is Vs, which is swept linearly from -2V to +1V with an increment of 0.01 V. It should be noted that the current in (*i*) is always positive whereas the current in (*ii*) can be either positive or negative. This may probably be the reason why the authors in [12] could not find chaos in their proposed oscillators using only a diode in (*i*). With a new sub-circuit in (*iii*), the current in (*iii*) can be either positive or negative, as shown in Figure 2, and chaos can be quickly found without changing the connections of other components.

(a)   (b)
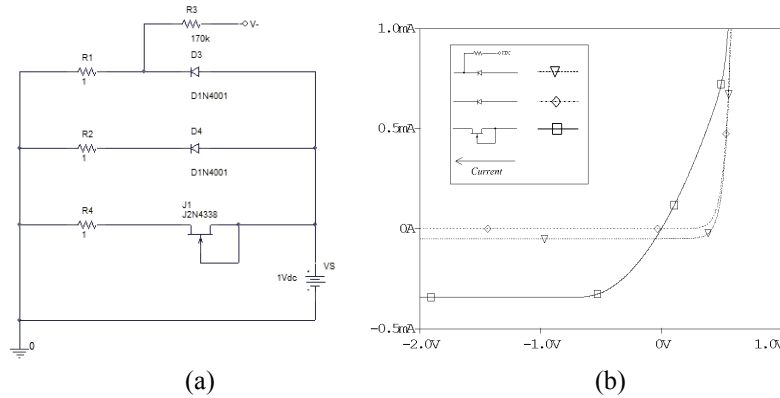
Fig. 2 (a) A circuit diagram of three circuits using (*i*) a diode circuit (D_4, R_2), (*ii*) a nonlinear JFET resistor (J_1, R_4), and (*iii*) a sub-circuit consisting of a diode and resistors (D_3, R_1, R_3), (b) A comparison of three simulation results.

Fig. 3. A numerical result of a chaotic attractor projected onto $V_{C3}-V_{C1}$ plane of equation (1).

Fig. 4. A PSpice simulation of a chaotic attractor projected onto $V_{C3}-V_{C1}$ plane of the oscillator shown in Figure 1(a).

Figure 3 shows a numerical result of a chaotic attractor projected onto a $V_{C3}-V_{C1}$ plane of equation (1) using a fourth-order Runge-Kutta integrator with a fixed step size of 0.1µs. The same values of components reported in [12] are used except R_3, i.e. $C_1 = C_2 = 10$ nF, $C_3 = 18$ nF, $R_1= 220$ Ω, $R_2 = 1.5$ kΩ, and $R_3 = 170$ kΩ. Figure 4 shows a PSpice simulation of a chaotic attractor projected onto $V_{C3}-V_{C1}$ plane of the oscillator shown in Figure 1(a) with the same values of components reported in [12] except $R_3 = 180$ kΩ. As shown in Figure 4, the PSpice simulation runs up to 30 ms with a fixed step size of 0.5 µs. The results in the first 20 % are discarded to ensure that the solution is on the attractor. Initial conditions are $(V_{C1}, V_{C2}, V_{C3})_{t=0} = (0, 0, 0)$. The numerical and PSpice results are in a similar manner.

It can be seen from Figures 1(a) and 1(b) that R_3 is connected in series with the diode D_1. This enables R_3 to control the current of D_1 in DC operation (by opening C_1, C_2, and C_2). Therefore R_3 can be exploited as a tunable bifurcation parameter. As an example, Figure 5 depicts a bifurcation diagram of the peak of V_{C3} (V_{C3}−max) of Figure 1(a) versus R_3 varied from 140 to 220 kΩ. A period-doubling route to chaos is evident. There are various periodic windows immersed in chaos.
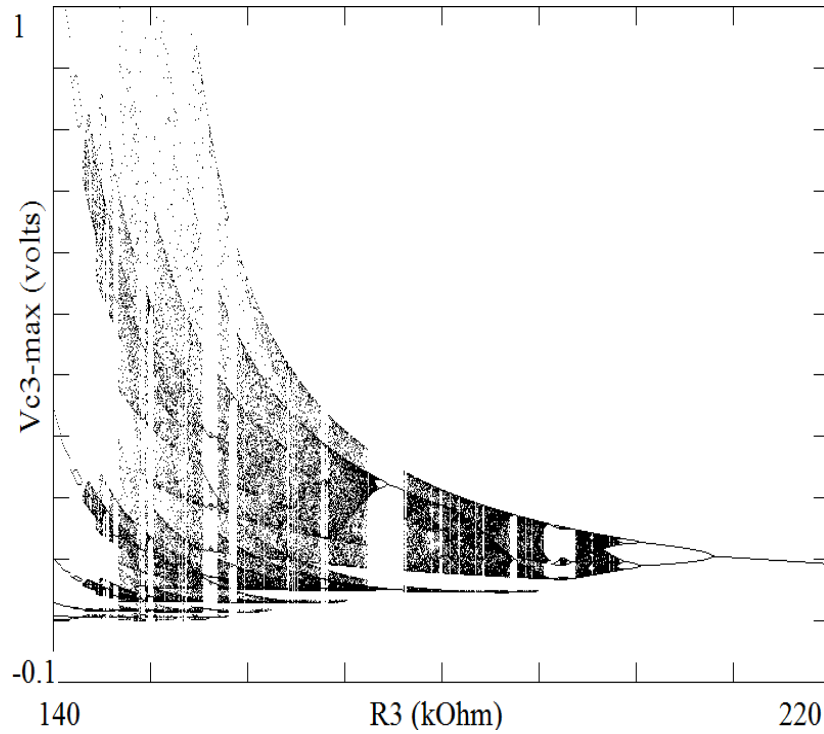
Fig. 5. A bifurcation diagram of the peak of V_{C3} of Figure 1(a).

Figure 6 shows a numerical result of a chaotic attractor projected onto a V_{C3}−V_{C2} plane of equation (2) using a fourth-order Runge-Kutta integrator with a fixed step size of 0.1μs, $C_1 = 10$ nF $C_2 = 11$ nF, $C_3 = 5$ nF, $R_1 = 220$ Ω, $R_2 = 2.7$ kΩ, and $R_3 = 220$ kΩ. Figure 7 illustrates a PSpice simulation of a chaotic attractor projected onto V_{C3}−V_{C2} plane of the oscillator shown in Figure 1(b) with the same values of components used in Figure 6. The PSpice simulation runs up to 20 ms with a fixed step size of 0.1 μs. The results in the first 20 % are discarded to ensure that the solution is on the attractor. Initial conditions are $(V_{C1}, V_{C2}, V_{C3})_{t=0} = (0, 0, 0)$.
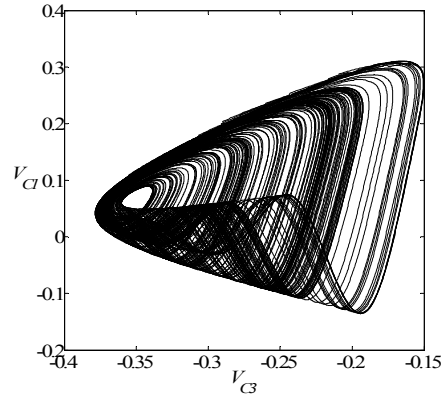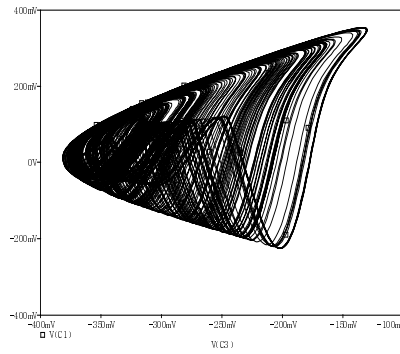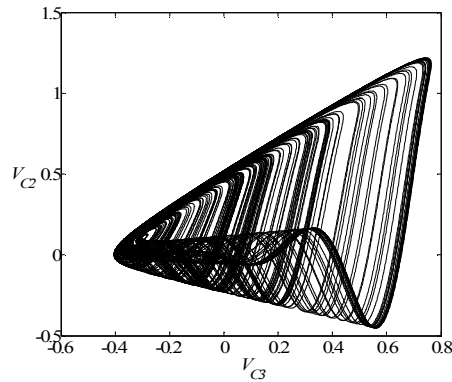
Fig. 6. A numerical result of a chaotic attractor projected onto $V_{C3}-V_{C2}$ plane of equation (2).
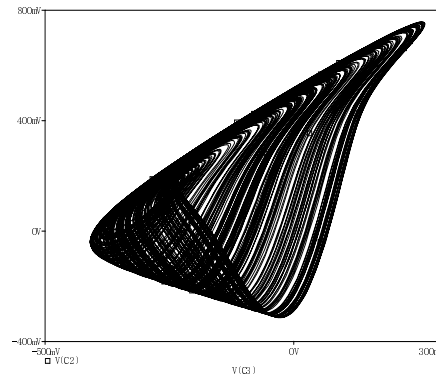
Fig. 7. A PSpice simulation of a chaotic attractor projected onto $V_{C3}-V_{C2}$ plane of the oscillator shown in Figure 1(b).

4. Conclusions

Two chaotic oscillators have been presented through the use of two modified CFOA-based inductorless sinusoidal oscillators. A CFOA has been exploited as the active component whereas a single diode has been exploited as the nonlinear component. Numerical and PSpice simulations have been demonstrated with chaotic attractors. A bifurcation diagram has been studied.

References

1. T. Kilias, K. Kelber, A. Mogel, and W. Schwarz. Electronic chaos generators−design and applications. *Int J Electron* 79: 737-753, 1995.

2. T. L. Carroll and L. M. Pecora. Synchronizing chaotic circuits. *IEEE Trans Circuits Syst* 38: 453-456, 1991.

3. B. Munmuangsaen and B. Srisuchinwong. A new Lorenz-like chaotic attractor and its synchronization. *CCDC*2009: 1508-1512, 2009.

4. K. M. Cuomo, A. V. Oppenheim and S. H. Strogatz. Synchronization of Lorenz-based chaotic circuits with applications to communications. *IEEE Trans Circuit Syst 40*: 626-633, 1993.

5. L. Kocarev, K. S. Halle, K. Eckert and L. O. Chua. Experimental demonstration of secure communications via chaotic synchronization. *Int J Bifurcat Chaos* 2: 709-713,1992.

6. B. Srisuchinwong, B. Munmuangsaen. A highly chaotic attractor for a dual-channel single-attractor, private communication system. In: C. H. Skiadas, I. Dimotikalis and C. Skiadas, Eds, *Chaos Theory: Modeling, Simulation and Applications: Selected Papers from the CHAOS2010 International Conference.* World Scientific, Singapore, pp. 399-405, 2011.

7. L. Fortuna, M. Frasca, and M. G. Xibilia. Chua's *Circuit Implementations: Yesterday, Today and Tomorrow,* World Scientific, Singapore, 2009.

8. E. Bilotta and P. Pantano. *A Gallery of Chua Attractors*, World Scientific, Singapore, 2008.

9. L. O. Chua and G. Lin. Canonical realization of Chua's circuit family. *IEEE Trans Circuits Syst* 37: 885-902, 1990.

10. A. S. Elwakil and M. P. Kennedy. A semi-systematic procedure for producing chaos from sinusoidal oscillators using diode-inductor and FET-Capacitor composites. *IEEE Trans Circuits Syst* 47: 582-590, 2000.

11. A. S. Elwakil and M. P. Kennedy. Chaotic oscillator derived from sinusoidal oscillator based on the current feedback op amp. *Analog Integ Circuits Signal Proc* 24: 239-251, 2000.

12. P. Bernát and I. Baláž. RC autonomous circuit with chaotic behaviour. *Radioengineering* 11: 1-5, 2002.

Performance Analysis of Time Hopping Ultra Wide Band System Using Chaotic vs. Conventional system

Anis Naanaa and Safya Belghith

Sys'com laboratory, National Engineering School of Tunis (ENIT), Tunisia.
(E-mail: anis_naanaa@yahoo.com, safya.belghith@enit.rnu.tn)

Abstract. This paper proposes to use chaotic modulation and coding for Time-Hopping Ultra Wide Band (TH-UWB) system with multi-path channel.

We compare the performances of chaotic systems using the Skew tent map against those of a conventional systems, as the Gold code, and demonstrate that chaotic system enhances the system performances when compared with the conventional system in terms of Bit Error Rate (BER).
We report simulation results clearly showing that the chaotic system outperforms the conventional system.

Keywords: Ultra wide band systems, Time-Hopping, Multi-path, Chaotic system, Bit error rate.

1 Introduction

Ultra-wideBand (UWB) systems is a spread-spectrum technique, that employs pulses of temporal extension of less than one nano second [1].

The sucess of UWB systems for short-range wireless communications [1,2] is due to the fact that they potentially combine reduced complexity with low power consumption, low probability-of-intercept (LPI) and immunity to multipath fading. In 2004, the IEEE 802.15.4a group presented a comprehensive study of the UWB channel over the frequency range 2-10 GHz for indoor residential, indoor office, industrial, outdoor and open outdoor environments [3].
In this work we are concerned with the indoor residential environment channel.
In Time Hopping format (TH-UWB), TH codes are used as a multiple user diversity and Pulse Position Modulation (PPM) as data [1,2].
In wireless communication system where more than one user share the same channel, the interference between users represents an additional source of noise. this may degrade the performance of the system. Thus the choice of the modulation type, the multiple access techniques and the codes allowing multiple access is crucial for the determination of system performance.
Different works have dealt with the statistical characteristics of the Multi-User Interference (MUI). In many works, the MUI has been modeled by a

random Gaussian process [1,2,4], others works tackled with the optimization of the performance by code selection [5], and thus no optimization with respect to the TH codes has been done. In the most detailed analysis [5], the authors considered the asynchronous case, multi-channel propagation such as IEEE 802.15.3a channel. They derived a criterion to find optimal codes that minimizes the variance of MUI. But, the optimization is done for only one reference user, and so even if the codes satisfied the given criterion, it is not guaranteed that the performance of the other users is optimized or even improved. In [6] we introduced a criterion named Average Collision Number (ACN) that minimize the MUI variance. It has been shown that sequences having smaller ACN allow better BER. In another work [7] we showed that, ACN criterion is unsuitable in some cases for selecting codes. Hence an improved criterion called Average of Squared Collision Number (ASCN).
Based on this criterion we study in the present paper how much chaoticity of the chaotic codes affects the performance of the considered TH-UWB system. To validate our criterion, the performance in terms of BER is computed by simulating the TH-UWB system with line-of-sight (LOS) multi-path channel in a residential environment IEEE 802.15.4a.

This paper is organized as follows. Section 2 gives a detailed description of UWB signal generations; after introducing the TH-UWB-PPM system model, we give the format of the receiver signal. In Section 3, we define the different sequences considered in this work. For chaotic sequences, the ASCN is computed versus bifurcation parameter and compared to Lyapunov exponent.

In Section 4, we define the new chaotic modulation and we validate our method by reporting simulation results showing the advantage of using ASCN and the relevance of chaotic sequences. Finally we conclude in section 5.

2   UWB signal generations

In this section, we begin by describing the TH-UWB system model and the expression of the received signal in an asynchronous TH-UWB system using the PPM modulation. Then we compute the variance of the MUI in the case of TH-code sequences when a correlating receiver is used.

2.1   TH-UWB System model

In this paper, we assume pulse position modulation for the transmitted binary symbols in both the UWB techniques. Second derivative of the Gaussian pulse was used as basic UWB pulse shape. The pulse waveform, $w(t)$ can be expressed as,

$$w(t) = (1 - 4\pi(\frac{t}{\tau})^2)\exp(-2\pi(\frac{t}{\tau})^2) \tag{1}$$

The pulse waveform $w(t)$ is assumed to be non-zero only during the interval $0 \leq t \leq T_c$, T_c is the chip duration and τ is the pulse duration. The second derivative of Gaussian pulse is shown in Figure 1.
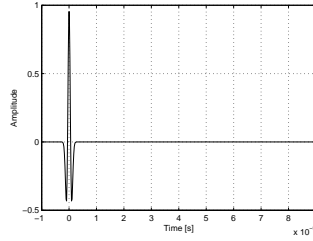
Fig. 1. The second derivative of Gaussian pulse

A typical expression of the TH-UWB transmitted signal for a user j is given by equation 2.

$$s^{(j)}(t) = \sum_{k=-\infty}^{\infty} \sum_{l=0}^{N_f-1} w(t - kT_s - lT_f - \tilde{c}_l^{(j)}T_c - d_k^{(j)}\delta) \tag{2}$$

Where T_s is the period of one bit. Every bit is conveyed by N_f frames. Each frame has a duration of T_f and is divided into N_c time slots. Each time slot has a duration of T_c. $\tilde{c}_l^{(j)}$ is the TH code sequence assigned to the user j, where $\tilde{c}_l^{(j)} \in \{0, 1, \ldots, N_c - 1\}$. The location of each pulse in each frame is defined by the code $\tilde{c}_l^{(j)}$. $d_k^{(j)} \in \{0, 1\}$ is the binary transmitted symbol at time k by user j, δ is the time shift associated with binary PPM, the pulses corresponding to bit 1 are sent δ seconds later than the pulses corresponding to bit 0. $N = N_c N_f$ presents the total processing gain of the system. The signals corresponding to bits 1 and 0 are depicted in Figure 2.
In this work, we use the IEEE 802.15.4a UWB channel model [3] in a residential area. According to this model the impulse response is [3,8],

$$h^{(j)}(t) = \sum_{m=0}^{M-1} \sum_{r=0}^{R-1} \alpha_{r,m}^{(j)} \delta(t - T_m^{(j)} - \tau_{r,m}^{(j)}) \tag{3}$$

where $\alpha_{r,m}$ is the tap weight of the r-th ray (path) in the m-th cluster, T_m is the arrival time of the m-th cluster and $\tau_{r,m}$ is the arrival time of the r-th ray in the m-th cluster. The distribution of the cluster arrival times is given by a Poisson process and the distribution of the ray arrival times is given by a mixed Poisson process [3]. The channel model which is used in the paper is for LOS scenarios in residential environments as shown in Figure 3, referred
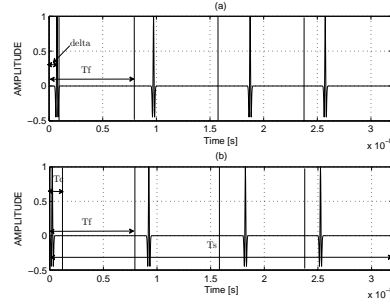
Fig. 2. A TH-UWB signal with binary PPM modulation where $N_f = 4$, $N_c = 8$ and the TH code sequence is {0 1 2 1}. (a): Bit 1, (b): Bit 0.
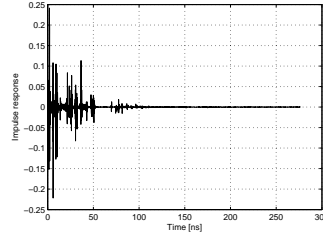
Fig. 3. Impulse response channel model 1 in residential environments.

to as CM1 [3].

If N_u is the number of active users transmitting asynchronously; the received signal is

$$r(t) = \sum_{j=1}^{N_u} \sum_{m=0}^{M-1} \sum_{r=0}^{R-1} \alpha_{r,m}^{(j)} s^{(j)}(t - T_m^{(j)} - \tau_{r,m}^{(j)}) + n(t) \tag{4}$$

2.2 Receiver Signal Processing

The output of the correlation receiver of the ith user at time h is given by:

$$s_h^{(i)} = \sum_{p=0}^{N_f-1} \int_{hT_s+pT_f+\widetilde{c}_p^{(i)}T_c+\tau_{0,0}^{(i)}+T_0^{(i)}}^{hT_s+pT_f+\widetilde{c}_p^{(i)}T_c+T_c+\tau_{0,0}^{(i)}+T_0^{(i)}} r(t)v(t-hT_s-pT_f-\widetilde{c}_p^{(i)}T_c-\tau_{0,0}^{(i)}-T_0^{(i)})dt \tag{5}$$

where $v(t)$ is the receiver's template signal defined by $v(t) = w(t+\delta) - w(t)$. From the previous equations and after variable changes, we obtain

$$s_h^{(i)} = T_U(i) + T_{ISI}(i) + T_I(i) + T_N(i) \tag{6}$$

with T_U is the useful signal, T_{ISI} is inter-symbol interference signal, T_I is the MUI and T_N is the term corresponding to the noise. For more details see

[6,7].

In [6], it has been shown that,

$$T_I(i) = E_w \sum_{j=1,j\neq i}^{N_u} \alpha^{(j)}(2d_h^{(j)} - 1)cn(i,j) \tag{7}$$

where E_w is the amplitude which controls the transmitted power, $\alpha^{(j)}$ is the tap weight of the user j, $d_h^{(j)}$ is the binary sequence, $cn(i,j)$ is the number of collision between codes $\tilde{c}^{(i)}$ and $\tilde{c}^{(j)}$. $\tilde{c}^{(j)}$ can be computed by taking into account the developed Time-Hopping Codes (DTHC) corresponding to TH codes as follows, for a given code $\tilde{c}^{(j)}$, the DTHC is a binary code of length $N_c N_f$ and is defined by

$$c_r^{(j)} = \begin{cases} 1 \; if \; r = \tilde{c}_l^{(j)} + lN_c, \;\; 0 \le l \le N_f - 1 \\ 0 \; otherwise. \end{cases} \tag{8}$$

where $r = 0 \ldots, N_c N_f - 1$. The relation between TH sequence $\tilde{c}_l^{(j)}$ and the developed code $c_r^{(j)}$ is illustrated in Figure 4.
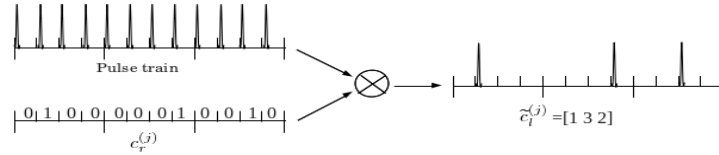
Fig. 4. Correspondence between DTHC and THC.

$$cn(i,j) = \sum_{l=0}^{N_f N_c - 1} c_l^{(i)} c_l^{(j)} \tag{9}$$

The Average Collision Number ACN of the sequence set $(\tilde{c}^{(j)})$, $j = 1, \ldots N_u$ is therefore defined by [6]:

$$ACN = \frac{1}{N_u(N_u - 1)} \sum_{i=1}^{N_u} \sum_{j=1,j\neq i}^{N_u} cn(i,j) \tag{10}$$

In [6] we have defined the ACN criterion, and we have showed that the experimental results validate the relevance of the ACN as an 'off-line' performance evaluation criterion for codes sequences. These results motivated us to use the ACN as a tool to predict the performance of code sequences.

However, we found intuitively that this criterion may in some cases be unsuitable for code selection [7]. To remedy to this drawback, we defined a new criterion called Average of Squared Collision Number ASCN which is defined as:

$$ASCN = \frac{1}{N_u(N_u - 1)} \sum_{i=1}^{N_u} \sum_{j=1, j \neq i}^{N_u} cn^2(i, j) \qquad (11)$$

This is motivated by the observation that when the collisions are regrouped on few positions the performance are significantly degraded.

3 Generation of sequence

Chaotic sequences have some properties that motivate researchers to use them in various applications: determinism, long term unpredictability and high sensitivity to initial conditions. Especially, chaotic sequences generated by one dimensional non linear transformation have been used in cryptography, watermarking, spectrum spreading systems [9].

We begin by defining chaotic and Gold sequences that will be considered in this work. Then we show the ASCN for chaotic sequence versus their bifurcation parameter. Next, we analyse how chaoticity measured by Lyapunov exponent is correlated with the ASCN.

3.1 Sequences generated by Skew tent map

Chaotic sequences are generated by the Skew tent map (STM) defined by:

$$x_{n+1} = \begin{cases} \frac{x_n}{r}, & 0 \leq x_n \leq r \\ \frac{1 - x_n}{1 - r}, & r < x_n \leq 1 \end{cases} \qquad (12)$$

The STM exhibits chaotic behavior for every value of the bifurcation parameter $r \in [0\ 1]$.
Figure 5, show the Lyapunov exponent and ASCN versus the bifurcation parameter r for STM chaotic sequences. We can see that the curve of the ASCN follow the one of Lyapunov exponent and that the greater the exponent is the smaller the ASCN. For $r = 0.5$, the STM have a best ASCN and Lyapuonv exponent. We showed numerically that the ASCN of a quantized chaotic sequence depends on the chaoticity of these sequences measured by their Lyapunov exponent.
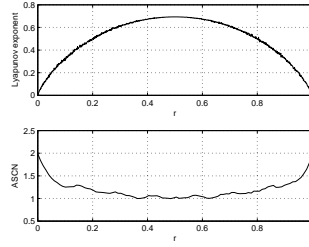
Fig. 5. Lyapunov exponent and ASCN for skew tent map.

3.2   Gold sequences

The Gold sequence based TH codes are generated as shown in [7], where we illustrate how is generated a sequence taking values in $\{0, 1, \cdots, N_c - 1 = 7\}$ and with a length $N_f \leq 29$.

In Figure 6, we represent the ASCN versus user number for $N_c = 8$; for Gold sequences considered here as a reference and STM sequence defined above; the ASCN of chaotic sequence are averaged over 100 realizations. For STM we considered the bifurcation parameter that gives the best ASCN, i.e. $r = 0.5$.
The results show that STM, have a better ASCN than Gold sequences. We can notice likewise that Gold sequences show better performance compared to the chaotic sequence when $N_u < 6$, this is because of the orthogonality of this sequences.
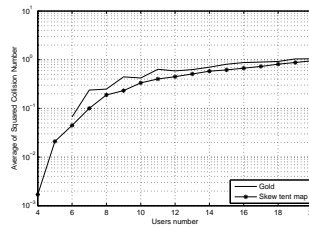
Fig. 6. ASCN versus user number for STM and Gold sequences. $N_c = 8$.

4   BER performance analysis

In our simulation, the second derivative of the Gaussian pulse is selected as UWB pulse in a residential environment CM1 channel with the correlation receiver. The simulation parameters are listed in Table 1. For simplicity, we

Table 1. Simulations parameters of TH-UWB system

Simulation parameters	acronym	Value
Chip duration	T_c	1ns
Pulse duration	τ	0.2ns
Number of chip	N_c	8
Number of path	L	10
Number of frame	N_f	4
Sampling frequency	F_s	8GHz
Number of sampling	N_e	50
Signal to Noise Ratio	SNR	10dB
Number of bits for each user	Nb	10^5
Factor for spread spectrum Gold	N	31

assume that the number of paths L is the same for all users.

To enhances the performance of the TH-UWB system we propose a chaotic modulation combined with chaotic code. The idea is to split the state space of STM and to associate a symbol to each partition. We suppose that the state space is represented by the interval $I = [0 \;\; 1]$, and we define the two sub-intervals $I_0 = [0 \;\; 0.5 - \tau[$ and $I_1 = [0.5 \;\; 1 - \tau]$, where τ is the pulse duration. According to this consideration we associate the transmitted binary sequence 0 and 1 to the sub-intervals I_0 and I_1, respectively. This process of modulation is called Chaotic Position Pulse Modulation (CPPM). A similar scheme was designed in [9].

The simulation results are shown in Figure 7, where we presented the BER of the system versus the user number for Gold, STM+PPM and STM+CPPM sequences. We can see that STM combined with CPPM modulation allow the best performance. This is due to the random effect of chaotic systems which reduce the interference between users. Moreover, Gold sequence allow the worst performance, excepted when $N_u < 10$. These results compared to the results shown in Figure 6, prove that the ASCN is a suitable criterion to select TH-codes.
For STM, we fixed the bifurcation parameters r to 0.5. This value correspond to the minimal of the ASCN (the maximal of Lyapunov exponent).
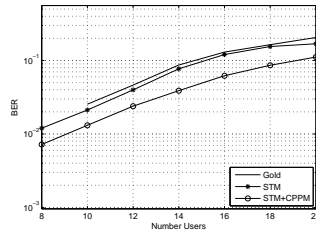
Fig. 7. BER performance evaluation of TH-UWB systems: Chaotic vs. Gold.

We can clearly see that the THC generated by the STM can get better performance than THC generated by Gold sequence. Thus, the proposed STM chaotic system considered is not only advantageous in terms of synchronization, but it can also generate TH-codes that outperform the conventional system.

5   Conclusion

In this paper, we proposed a chaotic pulse position modulation and chaotic time hopping spectrum spreading in UWB system. It has been proved that the chaotic sequences are appropriate for UWB systems with multiple access. The performance comparaison of TH-PPM-UWB system showed that chaotic sequences has better performance in term of bit error rate than Gold sequences. We specifically showed that the higher the Lyapunov exponent is the lower is the ASCN, and subsequently the better the performances.
In addition, chaotic systems enhances the quality and the security of the transmission.

References

1. M. Z. Win and R. A. Scholtz, Ultra-Wide Bandwidth Time Hopping Spread-Spectrum Impulse Radio for Wireless Multiple Access Comm, *IEEE Trans. On Comm*, vol. 48, pp. 679–691, Apr. 2000.
2. Z. X. Zhang, Time Hopping Spread-Spectrum based on Balance Gold Sequences in Ultra-Wide Band Communications, *in IEEE Shanxi kaisheng automation*, 2008.
3. A. F. Molisch, and al. *IEEE 802.15.4a channel modelfinal report,*, November 2004.
4. F. Ramirez Mireles, Error probability of ultra wideband ssma in a dense multipath environment,*in Proc. Milcom Conf*, Anaheim, CA, USA, Oct. 2002, vol. 2, pp. 1081–1084.
5. C. J. Le Martret, A. L. Deleuze and P. Ciblat, Optimal TH Codes for Multi-User Interference Mitigation in UWB Impulse Radio, *IEEE Trans On Comm*, vol. 5, No. 6, Jun. 2006.
6. A. Naanaa, Z. B. Jemaa and S. Belghith, Average Collision Number Criterion for TH-UWB Code Selection, *in Fifth ICWMC 2009*, Cannes, France, August 2009, pp. 122–127.
7. A. Naanaa, and S. Belghith, Performance enhancement of a Time hopping?pulse Position modulation Ultra-wide-band system using Guided local search, *IET Communcations*, vol. 5, pp. 2212–2220, Dec. 2011.
8. A. Saleh and R. Valenzuela, A statistical model for indoor multipath propagation,. *IEEE Journal on Select. Areas Commun*, vol. SAC-5, no. 2, pp. 128-137, Feb. 1987.

9. G.M. Maggio, N. RulLov and L. Rggiani, Pseudo chaotic time hopping for UWB impulse radio, *IEEE Trans. Circuits and Systems-I*, vol. 48, No. 12, pp. 1424–1435, Dec. 2001.

A Master equation approach to deciphering non-detailed balance systems

S. Nicholson[1] and E. Kim[2]

[1] Department of Applied Mathematics, University of Sheffield, Sheffield, S3 7RH, UK
(E-mail: `smp11sbn@sheffield.ac.uk`)
[2] Department of Applied Mathematics, University of Sheffield, Sheffield, S3 7RH, UK
(E-mail: `e.kim@sheffield.ac.uk`)

Abstract. The world is filled with complex systems whether it is the traffic patterns of city's, weather patterns, information flow in the internet, or turbulence in fusion reactors. These complex systems are not often amenable to simple analytic solutions, understanding these systems requires a new statistical method beyond traditional equilibrium theory, i.e. Boltzmann Gibbs statistics. We present a novel method for understanding complex dynamics of such systems by using the Observable Representation which has been successfully applied to complex systems in detailed balance. Specifically we generalise it to non-equilibrium systems where detailed balance does not hold, i.e. the system has non zero currents. We construct a new transition matrix by accounting for this current and compute the eigenvalues and eigenvectors. From these, we define a metric whose distance provides a useful measure of correlation among variables. This is a very general method of understanding correlation in various systems, in particular, long-range correlation, or chaotic properties. As an example we show that these distances can be utilized to control chaos in a simple dynamical system given by the logistic map.
Keywords: detailed balance, non-equilibrium, chaos, complex systems.

1 Introduction

When studying a system in nature, we often devise experiments whose goal is to understand the interactions of a set of proposed variables. The ultimate goal of these investigations is to try and discover how the variables interact to form the underlying dynamical equations which govern the system. Often though the system is so complicated that finding these unknown equations is impossible. Instead of attempting to derive the underlying functions of a system, we take a different approach. Just as the field of dynamical systems uses graphical representations of systems that are difficult or impossible to solve analytically. We use a graphical representation of the system which comes from a master equation. The distances in this representation can be used to understand the original system without having any knowledge of its underlying functions which govern the system.

This representation of a system is called the Observable Representation (OR), it was originally developed by Schulman and Gaveau to try and understand non-equilibrium phase transitions, [4], [5]. Since its inception the OR has been applied to Ising models [6], course graining [1] and the reconstruction of coordinate spaces [2] among others. Coifmann et.al. have also used an extremely similar spectral approach which has been applied to the Fokker-Planck equation [3]. This paper will outline the notation of both the detailed balance OR and our non-detailed balance extension of the OR, the NOR. We will then show how to use this approach to control chaos in a simple dynamical system given by the Logistic map. Finally we will summarize with a brief conclusion.

2   Observable Representation with detailed balance

The system which is being studied is represented by the NxN stochastic matrix of transition probabilities R_{xy}. States of the system are given by $x, y \in \mathbf{X}$, $\mathbf{X}$ is a state space of cardinality $N < \infty$. The system moves according to R_{xy}, R_{xy} is defined as,

$$R_{xy} = Pr(x \leftarrow y) = Pr[state\ at\ (t+1)\ is\ x\ |state\ at\ t\ is\ y]. \qquad (1)$$

$p_o(x)$ is a unique strictly positive stationary distribution such that $\sum_x p_o = 1$, and $R_{xy}p_o(y) = p_o(x)$. There are several requirements of R_{xy}, the two main ones are that $\sum_x R_{xy} = 1$. We also require that R_{xy} is irreducible and assume R_{xy} is diagonalizable though the ideas should carry over if R_{xy} requires a Jordan form. These lead to an eigenvalue $\lambda_o = 1$ which corresponds to the stationary probabilities $p_o(x)$. We rearrange the eigenvalues in decreasing magnitude, $1 = \lambda_o \geq |\lambda_1| \geq |\lambda_2| \geq \ldots \geq |\lambda_N|$. The eigenvectors corresponding to each eigenvalue are reordered accordingly. The left and right eigenvectors of R_{xy} are defined as,

$$A_\alpha(x)^T R_{xy} = \lambda_\alpha A_\alpha^T(y), \quad R_{xy}P_\alpha(y) = \lambda_\alpha P_\alpha(x). \qquad (2)$$

The subscript α denotes column number while the argument of the eigenvector x or y denotes the row, T is the transpose. The slowest decaying eigenfunctions of R_{xy}, will be the macroscopic "observables" which will give the averaged quantities of the system. While the faster decaying eigenvectors are the quickly fluctuating quantities of the system, which average themselves out. It follows from the form of R_{xy} that $\exists$ a left eigenvector, $A_o = 1$, s.t. $A_o^T R = A_o^T$. We normalize the eigenfunctions, A_j and P_k to form an orthonormal basis, $\langle A_j | P_k \rangle = \delta_{jk}$.

To see how the OR can be used to represent the coordinate space underlying system, we will build the basic structure of the Sierpinski fractal. This self similar fractal at its heart consists of three points or states as we will refer to them connected to form a triangle, with a smaller rotated triangle inside.

To find the coordinate space we first built an adjacency matrix $W^{N \times N}$ of the connections between the states of the system,

$$W = \begin{pmatrix} 0 & 1 & 0 & 0 & 0 & 1 \\ 1 & 0 & 1 & 1 & 0 & 1 \\ 0 & 1 & 0 & 1 & 0 & 0 \\ 0 & 1 & 1 & 0 & 1 & 1 \\ 0 & 0 & 0 & 1 & 0 & 1 \\ 1 & 1 & 0 & 1 & 1 & 0 \end{pmatrix} \tag{3}$$

Where each non zero value in W_{xy} says that the system can move from state y to state x in one time step. This is normalized so that $R_{xy} = \frac{W_{xy}}{\sum_x W_{xy}}$. Diagonalizing R_{xy} and plotting A_1, A_2 in figure (1) we recover the basic structure of the Sierpinski fractal. This process can be increased for as many layers of the fractal as one wishes. A 3-D version can also be created using the same process. This time plotting A_1, A_2 and A_3 in figure (2).
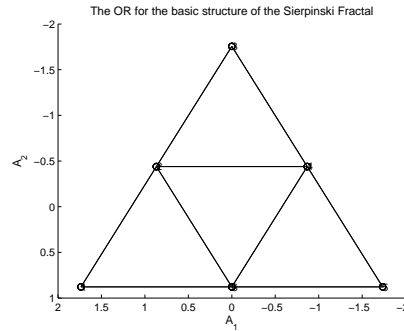
Fig. 1. Plotting the OR for the basic structure of the Sierpinski fractal. The lines have been added in to show connections.

It was shown in [2] that using the left eigenvectors, one can create a distance metric. The metric inequality is defined as,

$$\sum_x \left| \frac{R_{xi} - R_{xj}}{\sqrt{p_o(x)}} \right| \geq \sqrt{\sum_\alpha^m |\lambda_\alpha (A_\alpha(i) - A_\alpha(j))|^2}. \tag{4}$$

The right hand side is the distance in the OR called, D_{OR}. While the left hand side is a distance using R_{xy}. m is the dimension of the OR, where $m \leq N$. The inequality says that states of the system, which are related dynamically are also related in the OR. For the inequality to hold, R_{xy} must satisfy detailed balance, which is defined as,
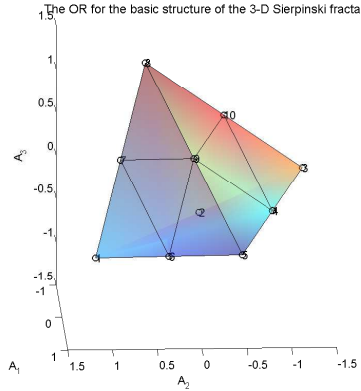
Fig. 2. Plotting the OR for the basic structure of the 3-D Sierpinski fractal. The lines have been added in to show connections.

$$J_{xy} = R_{xy}p_o(y) - R_{yx}p_o(x) = 0. \tag{5}$$

Though, even when $J_{xy} \neq 0$ the OR can often still recover the topology of the underlying coordinate space for simple systems. The derivation of the right hand side of equation (4) which represents the distance in the OR, abbreviated D_{OR}, relies on the eigenfunctions of R_{xy} having a one to one relation with a similarly symmetric matrix, S_{xy}. When $J_{xy} \neq 0$ this is not guaranteed. To recover the ability to relate distances in an OR, we define a new matrix B_{xy},

$$B_{xy} = R_{xy} - \frac{J_{xy}}{2p_o(y)}. \tag{6}$$

B_{xy} is an NxN matrix which is column wise stochastic. This is due to the fact that J_{xy} follows Kirchoff's loop rule, that the amount of current into a node is equal to the amount out. We also require B_{xy} to be irreducible. It can easily be shown that R_{xy} and B_{xy} share the same unique stationary distribution, $p_o(x)$. There is at least one eigenvalue of order unity, $\nu_o = 1$. The rest we again reorder into decreasing magnitude, $\nu_o \geq |\nu_1| \geq \ldots \geq |\nu_N|$. The right and left eigenvectors of B_{xy} are similarly defined as,

$$B_{xy}\varphi_\alpha(y) = \nu_\alpha\varphi_\alpha(x) \quad \Gamma_\alpha(x)^T B_{xy} = \nu_\alpha\Gamma_\alpha(y)^T. \tag{7}$$

There is a relationship between the matrix B_{xy} and the corresponding matrix S_{xy}, which can be shown to be symmetric even when $J_{xy} \neq 0$. The symmetry in S_{xy} is what guarantees the completeness of the eigenvectors of B_{xy}. The eigenvectors of B_{xy} and S_{xy} also share a relationship,

$$\frac{\varphi_\alpha(i)}{\sqrt{p_o(i)}} = \psi_\alpha(i), \quad \Gamma_\alpha(i)\sqrt{p_o(i)} = \psi_\alpha(i). \tag{8}$$

Using S_{xy} and the left eigenvectors of B_{ij} we can construct the non-detailed balance version of the OR, which we denote the (NOR). As was done in [2] we can also construct a distance metric where in equation (4) $\lambda_\alpha \to \nu_\alpha$ and $A_\alpha(i) \to \Gamma_\alpha(i)$. The metric which we will call D_{NOR} quantifies the relationship between the dynamical relations of a system to its macroscopic behavior when the system does not satisfy detail balance. The derivation of our metric conveniently follows just as was done in [2]. This simple extension opens up an entirely new class of systems to be studied using the NOR. As an example we will control the chaotic properties of the logistic map when its control parameter, $a = 4$.

3   Controlling chaos in the Logistic map

The Logistic map is defined as,

$$x_{n+1} = M(x_n) = ax_n(1 - x_n), \tag{9}$$

x_n is the position of a test particle in the system on iteration n, a is the control parameter which will be equal to 4 in the following. To control chaos in this system we initially track how the position of particles changes over many iterations and use this information to make, R_{xy} and B_{xy}. B_{xy} is then used to find the distances D_{NOR} between course grained points in the domain of the Logistic map. The minimum of the first off-diagonal of D_{NOR} will be the point that we perturb the system to when the Lyapunov exponents L, is greater than 0. L is defined as,

$$L = \frac{1}{n}\sum_i \log|M'(x_n)|. \tag{10}$$

We see in figure (3) that from $1 \leq n \leq 50$, $L > 0$ for all the particles. From $n > 50$ we start to perturb the system on each iteration which is $50 < n \leq 75$ until $L \leq 0$ for all particles. From approximately $n > 75$ the system is allowed to freely evolve unless $L > 0$ for a particle, then it is perturbed back to the chosen position.

4   Conclusion

In this paper we have shown a general method for deciphering the interactions of complex system when they no longer satisfy detailed balance. We have then applied this to the toy problem of stopping chaos in the Logistic map. Future work will consist of applying this method to real world system and
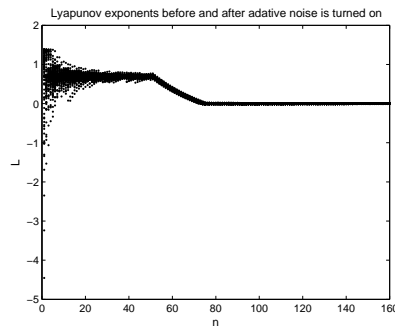
Fig. 3. The evolution of Lyapunov exponents for 100 particles in the Logistic map. we see the Lyapunov exponents become greater than zero until we begin to perturb the system at $n = 50$. Then the Lyapunov exponents approach and stay around zero.

system with more variables. We will also address questions with regards to the correct dimension of the OR and the NOR for a general system in future publications. We would like to thank Paul Mitchener, Mike Ruderman, Chris Nelson, Nabil freij and Stuart Mumford for their useful discussions.

References

1. Gaveau B and Schulman L. Multiple phases in stochastic dynamics: Geometry and probabilities. *Phys. Rev. E*, 73:,2006.
2. B. Gaveau, L. S. Schulman and L.J. Schulman. Imaging geometry through dynamics: the observable representation. *J. Phys. A*, 39:10307-10321,2006.
3. R.R Coifman, I.G. Kevrekidis, S. Lafon, M Maggioni and B Nadler. Diffusion maps, Reduction coordinates and low Dimensional Representation of Stochastic Systems.
4. B. Gaveau and L.S. Schulman. A general framework for non-equilibrium phenomena: the master equation and its formal consequences. *Physics Letters A*, 229:347-353,1997.
5. Bernard Gaveau and L.S. Schulman. Theory of nonequilibrium first-order phase transitions for stochastic dynamics. *Journal of Mathematical Physics*, 39: 1998.
6. L. Schulman. Mean-Field Spin Glass in the Observable Representation. *Physical Review Letters*, 98:257201,2007.

New aspects in approximation of a Markov chain by a solution of a stochastic differential equation

Gabriel V. Orman and Irinel Radomir

Transilvania University of Brasov, 500091 Braşov, Romania.
E-mail: `ogabriel@unitbv.ro`

Abstract. The usual class of Markov processes which we involve many times has some restrictions that it does not cover many interesting processes. We shall refer, in this paper, to some problems involving stochastic calculus, diffusion approximation and Markov processes. In this context the problem of absorbing and reflecting barriers is also discussed.
Keywords: stochastic differential equations, Markov chains, transition probabilities, Brownian motion.

1 Introduction

When a stochastic differential equation is considered if it is allowed for some randomness in some of its coefficients, it will be often obtained a so-called *stochastic differential equation* which is a more realistic mathematical model of the considered situation.

Many practical problems conduct us to the following notion: *the equation obtained by allowing randomness in the coefficients of a differential equation is called a "stochastic differential equation".*

Therefore, it is clear that any solution of a stochastic differential equation must involve some randomness. In other words one can hope to be able to say something about the probability distribution of the solutions.

In the sequel we shall refer to some aspects relating to the approximation in the study of Markov processes and Brownian motion. Such problems were developed particularly by Schuss[13], Kushner and Yin[5], Itô and McKean Jr.[3], Wasan[14].

Results on almost sure convergence of stochastic approximation processes are often proved by a separation of deterministic (pathwise) and stochastic considerations. A key problem in effective applications concerns the *amount of noise* in the observations, and this leads to variations that incorporate variance reduction methods. With the use of these methods, the algorithm becomes more effective, but also more complex. Hence, it is desirable to have robust algorithms, which are not overly sensitive to unusually large noise values.

More details and related topics can be found in Schuss[13], Kushner and Yin[5], Itô and McKean Jr.[3], Itô[4], Øksendal[6], Øksendal and Sulem[7],

Stroock[12], Orman[9], [10], Wasan[14] which are also the basis in our development.

2 Preliminaries

Definition 1. The *sample space* Ω of a random experiment is the collection of all possible outcomes. An *event A* is a subset of the sample space, that is, a set of outcomes.

Definition 2. A *probability measure* on a sample space Ω of a random experiment is a function P[·] that maps events in Ω to real numbers such that:

(*i*) P[Ω] = 1,

(*ii*) P[A] $\geq$ 0 for all events A,

(*iii*) $P\left[\bigcup_{i \in I} A_i\right] = \sum_{i \in I} P[A_i]$ where I is a finite or countable infinite set of integers and any pair of the events $A_1, A_2, A_3, \cdots$ is disjoint.

Let us consider the triplet $(\Omega, \mathcal{K}, P)$ where

- Ω is the *sample space*. Its elements are referred to as *sample points*;
- $\mathcal{K}$ is a σ-field of subsets of Ω containing Ω itself. Its elements are *events*;
- P is a *probability measure* on the measurable space $(\Omega, \mathcal{K})$.

If an event A is of the type $A = \{\omega \in \Omega \,|\, R(\omega)\}$ for some property $R(\cdot)$, (of the probability) we may write $P(R)$ for $P(A)$. An event is called a *sure event* if $P(A) = 1$ and a *null event* if $P(A) = 0$. Alternatively, $R(\cdot)$ is said to hold *a.s.* if $P(R) = 1$.

The triplet $(\Omega, \mathcal{K}, P)$ is referred to as a *probability space*.

Let now consider an experiment that is repeated n times and suppose that m ($m \leq n$) times the event B occurred. Also suppose that k times ($k \leq m$) the event A occurred, provided that B occurred. Then, the event $A \cap B$ occurred k ($k \leq n$) times, such that we have $P(A \cap B) = \frac{k}{n}$. Now $\frac{k}{n} = \frac{m}{n} \cdot \frac{k}{m} = P(B) \cdot P(A \,|\, B)$. In this way the following relation is obtained $P(A \cap B) = P(B) \cdot P(A \,|\, B)$ or

$$P(A \,|\, B) = \frac{P(A \cap B)}{P(B)}, \quad P(B) > 0. \tag{1}$$

$P(A \,|\, B)$ in (1) is called a *conditional probability* whenever $P(B) > 0$. We retain that the function

$$P_B(A) = P(A \,|\, B) \tag{2}$$

is a probability measure in B, where B is now considered as a smaller sample space.

Hence, the measure $P(A \mid B)$ is the probability of the event A provided that B occurs.

A fundamental concept of probability is the notion of random variable. A *random variable* is a function that gives a numerical value to each outcome of a random experiment. The distinction between the random variable and the experimental outcome itself can become blurry in this case, because if ω denotes an outcome, then $X(\omega) = \omega$. But we retain that the random variable is a function and the outcome is its input. The domain of the random variable is the sample space and that its range is a set of numbers.

Definition 3. Let $(\Omega, \mathcal{K}, P)$ be a probability space and let us denote by E a subset of R^n. A *random variable* X is a function from Ω into E. We refer to E as being the *state space* of the random variable.

So, a random variable encodes an experimental outcome as a number, or a vector of real numbers in the multidimensional case. When a random variable has a multidimensional state space, we emphasize that fact by calling it a *random space*.

Let (E, ξ) be a measurable space and $X : (\Omega, \mathcal{K}, P) \to (E, \xi)$ a random variable (i.e. a measurable map). The image μ of P under X is a probability measure on (E, ξ), called the *law of* X and denoted by $\mathcal{L}(X)$. The events $\{\omega \mid X(\omega) \in A\}$ for $A \in \xi$ form a sub-σ-field of $\mathcal{K}$ called the σ-field generated by X and denoted by $\sigma(X)$. More gneral, given a family X_α, $\alpha \in I$, of random variables on $(\Omega, \mathcal{K}, P)$ taking values in measurable spaces (E_α, ξ_α), $\alpha \in I$, respectively, the σ-field generated by X_α, $\alpha \in I$, denoted by $\sigma(X_\alpha, \alpha \in I)$, is the smallest sub-$\sigma$-field with respect to which they are all measurable. They may be situations where it is preferable to view $\{X_\alpha, \alpha \in I\}$ as a single random variable taking values in the product space $\prod E_\alpha$ endowed with the product σ-field $\prod \xi_\alpha$. If so, this definition reduces to the preceding one.

Two (or more) random variables are said *to agree in law* if their laws coincides. They could be defined on different probability spaces. A random variable $X(\omega)$ generates a field (σ-field) $\mathcal{K}_X$ of events generated by events of the form $\{\omega \mid X(\omega) = a\}$ where a is any number. The field consists of events which are unions of events of the form $\{\omega \mid X(\omega) = a\}$. The probability function P on the events of this field $\mathcal{K}_X$ generated by $X(\omega)$ is called the *probability distribution of* $X(\omega)$.

Suppose we have n random variable $X_1(\omega), \cdots, X_n(\omega)$ defined on a probability space. The random variables $X_1, \cdots, X_n$ *are said to be independent* if the fields (σ-fields) $\mathcal{K}_{X_1}, \cdots, \mathcal{K}_{X_n}$ generated by them are independent.

Definition 4. A *stochastic process* is a parametrized collecion of random variables

$$\{X_t\}_{t \in T}$$

defined on a probability space $(\Omega, \mathcal{K}, P)$ and assuming values in R^n.

The parameter space T may be the halfline $[0, +\infty)$, or it may also be an interval $[a, b]$, or the non-negative integers and even subsets of R^n, for $n \geq 1$.

Now, for each $t \in T$ fixed, we have a random variable $\omega \to X_t(\omega)$, $\omega \in \Omega$. On the other hand, fixing $\omega \in \Omega$, we can consider the function

$$t \to X_t(\omega), \quad t \in T \tag{3}$$

which is called a *path* of the random variable X_t. It is useful to think of t as *time* and each ω as an individual *particle* or *experiment*. Thus, $X_t(\omega)$ would represent the position (or the result) at time t of the particle (experiment) ω. In some cases it is convenient to write $X(t, \omega)$ instead of $X_t(\omega)$, such that the process can be regarded as a function of two variables $(t, \omega) \to \psi(t, \omega)$ from $T \times \Omega$ into R^n. In stochastic analysis this is often a natural point of view, because there it is crucial to have $X(t, \omega)$ jointly measurable in (t, ω).

In this paper we shall denote a stochastic process by $X(t)$.

3 Markov process and diffusion process

Definition 5. A stochastic process $X(t)$ on $[0, T]$ is called a *Markov process* if for $n = 1, 2, 3, \cdots$ and any sequences $0 \leq t_0 < t_1 < \cdots < t_n \leq T$ and $x_0, x_1, \cdots, x_n$, the following equality is satisfied:

$$P(X(t_n) < x_n \,|\, X(t_{n-1}) = x_{n-1}, X(t_{n-2}) = x_{n-2}, \cdots, X(t_0) = x_0) =$$
$$= P(X(t_n) < x_n \,|\, X(t_{n-1}) = x_{n-1}). \tag{4}$$

The equation (4) means the fact that the process $forget$ the past, provided that t_{n-1} is regarded as the present.

Let Ω_X be the state space of the random variables X_t. Take $\mathcal{K}_X$ as the σ-field of measurable subsets of Ω_X. For convenience, assume that there is a first point to the set T. The probability structure is specified in terms of an initial probability measure and a transition probability function describing how transitions take place from one time to another.

We denote by $P(t_0, A)$ a probability measure on the sets A of $\mathcal{K}_X$. This is the probability distribution at the initial time t_0. Further let the transition probability function $p(t, x; \tau, A)$, $t_0 \leq \tau < t$, $x \in \Omega_X$, $A \in \mathcal{K}_X$ be a function with the following properties:

   i $p(t, x; \tau, A)$ is a probability measure in $A \in \mathcal{K}_X$ for fixed t, x, τ;
 ii $p(t, x; \tau, A)$ is measurable in x with respect to $\mathcal{K}_X$ for fixed t, τ, A;
iii $p(t, x; \tau, A)$ satisfies the integral equation (commonly called the *Chapman-Kolmogorov equation*)

$$p(t, x; \tau, A) = \int_{\Omega_X} p(s, y; \tau, A) p(t, x; s, dy) \tag{5}$$

for any s with $t < s < \tau$.

As it is shown in the theory of stochastic processes, the transition probability function $p(t, x; \tau, A)$ is the conditional probability

$$p(t, x; \tau, A) = P[X_\tau(\omega) \in A \mid X_t(\omega) = x]. \tag{6}$$

Now the *transition distribution function*

$$F(t, x; \tau, y) = P(X_\tau(\omega) < y \mid X_t(\omega) = x) \tag{7}$$

can be obtained, corresponding to the case when in $p(t, x; \tau, A)$ we take A of the form $(-\infty, y)$. It verifies the following relation

$$F(t, x; \tau, y) = \int_R F(s, z; \tau, y) d_z F(t, x; s, z).$$

Then, the *transition density function* with respect to y is as follows

$$f(t, x; \tau, y) = \frac{\partial}{\partial y} F(t, x; \tau, y), \tag{8}$$

and verifies the equalities

$$F(t, x; \tau, y) = \int\limits_{-\infty}^{y} f(t, x; \tau, z)\, dz, \qquad \int_R f(t, x; \tau, y)\, dy = 1. \tag{9}$$

Furthermore, the Markov property (4) implies that

$$f(t, x; \tau, y) = \int_R f(s, z; \tau, y) f(t, x; s, z) dz, \qquad t < s < \tau \tag{10}$$

that is, the probability that $X(t)$ goes from x to y in the time interval $[t, T]$ is that probability that $X(\cdot)$ goes to any point z at any time s and then, *independently* of the way it reached z, it goes to y. The equality (10) is also referred to as the *Chapman-Kolmogorov equation* for Markov processes.

In certain conditions of existence, the transition density function satisfies the following two equations which are referred to as the *backward Kolmogorov equation* and respective the *forward Kolmogorov equation*

$$\frac{\partial f(t, x; \tau, y)}{\partial t} = -a(t, x) \frac{\partial f(t, x; \tau, y)}{\partial x} - \frac{1}{2} b(t, x) \frac{\partial^2 f(t, x; \tau, y)}{\partial x^2} \tag{11}$$

and

$$\frac{\partial f(t, x; \tau, y)}{\partial \tau} = -\frac{\partial}{\partial y}[a(\tau, y) f(t, x; \tau, y)] + \frac{1}{2} \frac{\partial^2}{\partial y^2}[b(\tau, y) f(t, x; \tau, y)] \tag{12}$$

where $a(t, x)$, $b(t, x)$, $a(\tau, y)$, $b(\tau, y)$ are functions satisfying some conditions to assure the existence and the uniqueness of the solution of the equations. The forward Kolmogorov equation is also referred to as the *Fokker-Planck equation*.

Definition 6. A Markov process $X(t)$ is called a *diffusion process* if the following conditions are satisfied:

  i For every $\varepsilon > 0$, t and x,

$$\lim_{\Delta t \to 0} \frac{1}{\Delta t} \int_{|y-x|>\varepsilon} F(t, x, t + \Delta t, y) dy = 0. \qquad (13)$$

  ii There exist the functions $a(t, x)$ and $b(t, x)$ such that for all $\varepsilon > 0$, t and x,

$$\lim_{\Delta t \to 0} \frac{1}{\Delta t} \int_{|y-x|\leq\varepsilon} (y - x) f(t, x, t + \Delta t, y) dy = a(t, x), \qquad (14)$$

$$\lim_{\Delta t \to 0} \frac{1}{\Delta t} \int_{|y-x|\leq\varepsilon} (y - x)^2 f(t, x, t + \Delta t, y) dy = b(t, x). \qquad (15)$$

The function $a(t, x)$ is called the *(infinitesimal) drift coefficient* of $X(t)$ and $b(t, x)$ is called the *(infinitesimal) diffusion coefficient*. The intuitive meaning of conditions (13) - (15) and of the coefficients $a(t, x)$ and $b(t, x)$ is the following. In a short time interval h, the displacement of $X(\cdot)$ from a point x at time t is given by $a(t, x)\Delta t + \delta x + 0(\Delta t)$, where $a(t, x)$ is the velocity of the medium in which a particle (whose motion is described by $X(\cdot)$) drifts, δx is the random fluctuation of the particle due to random collision or thermal fluctuation, a.s.o. Furthermore, $E \, \delta x = 0, Var \, \delta x = b(t, x)\Delta t$. That is to say $b(t, x)$ is proportional to the average energy of the fluid molecules in the neighborhood of the particle. One can observe that the following conditions imply the conditions *i* and *ii* above:

(a) For any positive number δ, as $\Delta t \to 0$

$$\frac{1}{\Delta t} E_{x,t} |X(t + \Delta t) - X(t)|^{2+\delta} \to 0$$

(b) and

$$\frac{1}{\Delta t} E_{x,t} [X(t + \Delta t) - X(t)] \to a(t, x),$$

$$\frac{1}{\Delta t} E_{x,t} [X(t + \Delta t) - X(t)]^2 \to b(t, x).$$

4   Absorbing and reflecing barriers

Let us consider that a particle located on a straight line moves along the line via random impacts occurring at times $t_1, t_2, t_3, \cdots$. The particle can be at points with integral coordinates $a, a + 1, a + 2, \cdots, b$. At points a and b there are absorbing barriers. Each impact displaces the particle to the right with

probability p and to the left with probability $q = 1 - p$ so long as the particle is not located at a barrier. If the particle is at a barrier then, it remains in the states A_1 and A_{n-1} with probability 1.

A similar example can be considered for a particle being in a random walk, when at points a and b there are reflecting barriers. The conditions remain the same as in the former case, the only difference being that if the particle is at a barrier, any impact will transfer it one unit inside the gap between the barriers.

1. Let now be the case of a Brownian motion with an absorbing barrier. The forward Kolmogorov equation (12) for a Brownian motion on $x > 0$ with an absorbing boundary at $x = 0$ is given by

$$\frac{\partial p}{\partial t} = \frac{1}{2}\frac{\partial^2 p}{\partial y^2} \quad \text{in} \quad y > 0$$

$$p(0, t, y) = 0, \quad t > 0, \quad y > 0$$

$$p(x, t, y) \to \delta(x - y) \quad \text{as} \quad t \downarrow 0, \quad x > 0, \quad y > 0.$$

The solution of such an initial boundary value problem is as follows

$$p(x, t, y) = \frac{1}{t\sqrt{2\pi}}\left[e^{-\frac{(x-y)^2}{2t^2}} - e^{-\frac{(x+y)^2}{2t^2}}\right].$$

It can be seen that by symmetry, $p(x, t, 0) = 0$. Then, it can be shown that

$$\frac{1}{t\sqrt{2\pi}}\int_{-\infty}^{+\infty} e^{-\frac{(x+y)^2}{2t^2}}\varphi(x)dx \to \varphi(-y) = 0$$

as $t \downarrow 0$ if $y > 0$. Therefore,

$$p(x, t, y) \to \delta(x - y) \quad \text{as} \quad t \downarrow 0 \quad \text{for all} \quad x > 0, y > 0.$$

2. Now let us consider the Brownian motion on $x > 0$ but with a reflection barrier at the origin.

The forward Kolmogorov equation for a Brownian motion on $x > 0$ with an absorbing boundary at $x = 0$ is given by

$$\frac{\partial p}{\partial t} = \frac{1}{2}\frac{\partial^2 p}{\partial y^2}, \quad y > 0$$

$$\left.\frac{\partial p(x, t, y)}{\partial y}\right|_{y=0} = 0$$

$$p(x, t, y) \to \delta(x - y) \quad \text{as} \quad t \downarrow 0, \quad x > 0, \quad y > 0.$$

In this case the following solution is found

$$p(x, t, y) = \frac{1}{t\sqrt{2\pi}}\left[e^{-\frac{(x-y)^2}{2t^2}} + e^{-\frac{(x+y)^2}{2t^2}}\right]$$

and the condition

$$\frac{\partial p(x,t,y)}{\partial x}\bigg|_{x=0} = 0$$

holds too.

References

1. Bharucha-Reid, A.T. Elements Of The Theory Of Markov Processes And Their Applications. Mineola, New York, 1997. Dover Publications, Inc.
2. Gnedenko, B.V. The Theory of Probability. Moskow, 1976. Mir Publisher.
3. Itô K. and McKean H.P. Jr. Diffusion Processes and their Sample Paths. Berlin Heidelberg, 1996. Springer-Verlag.
4. K. Itô. Stochastic Processes. Ole E. Barndorff-Nielsen and Ken-iti Sato, editors, 2004. Springer.
5. Kushner, H.J. and Yin, G.G. Stochastic Approximation Algorithms and Applications. New York, 1997. Springer-Verlag.
6. Øksendal, B. Stochastic Differential Equations: An Introduction with Applications, Sixth Edition. 2003. Springer-Verlag.
7. Øksendal B. and Sulem A. Applied Stochastic Control of Jump Diffusions. 2007. Springer-Verlag.
8. Orman, G.V. Lectures on *Stochastic Approximation Methods and Related Topics.* Preprint, "Gerhard Mercator" University, 2001. Duisburg, Germany.
9. Orman, G.V. Handbook of Limit Theorems and Stochastic Approximation. Brasov, 2003. "Transilvania" University Press.
10. Orman, G.V. On a Problem of Approximation of Markov Chains by a Solution of a Stochastic Differential Equation. In Christos H. Skiadas, Ioannis Dimotikalis and Charilaos Skiadas, editors, *Chaos Theory: Modeling, Simulation and Applications*, pages 30-40, 2011. World Scientific Publishing Co Pte Ltd.
11. Steele, J. M. Stochastic Calculus and Financial Applications. 2001. Springer-Verlag New York, Inc.
12. Stroock D. W. Markov Processes from K. Itô Perspective. Princeton, 2003. Princeton Univ. Press.
13. Schuss Z. Theory and Application of Stochastic Differential Equations. New York, 1980. John Wiley & Sons.
14. Wasan, M.T. Stochastic Approximation. Cambridge, 1969. Cambridge University Press.

Bifurcation and chaos in driven simple pendulum under the effect of nonlinear damping

Vinod Patidar, Anjali Sharma and **G. Purohit**

Department of Physics, Sir Padampat Singhania University
Bhatewar, Udaipur-313601, Rajsthan, INDIA
E-mail: vinod.patidar@spsu.ac.in

Abstract: In this communication, we discuss the dynamical behaviour of driven simple pendulum under the effect of nonlinear damping. We particularly consider the nonlinear damping term proportional to the power of velocity and focus our attention on how the damping exponent affects the global dynamical behaviour of the forced pendulum. We obtain analytically the threshold condition for the occurrence of homoclinic bifurcation using Melnikov technique and compare the results with the computational results. We also identify the regions of the 2D parameter space (consists of external forcing amplitude and damping coefficient) corresponding to the various types of asymptotic dynamics under linear (viscous or friction like) and nonlinear (drag like) damping. We also analyse how basin of attraction patterns corresponding to various attractors change with the introduction of nonlinear damping as well as damping strength.

Keywords: Chaos, driven pendulum, nonlinear damping, Melnikov analysis

Nonlinearity is abundant in nature. It is having an increasingly important impact on a variety of applied subjects ranging from the study of turbulence and the behavior of weather, through the investigation of electrical and mechanical oscillations in engineering systems, to the analysis of various biological, ecological and economic phenomena. The nonlinearity in the dynamical systems may exist in various forms e.g., in a mechanical system: the nonlinearity may be due to the presence of nonlinear elastic/spring elements, nonlinear damping, systems with fluids, nonlinear boundary conditions etc., in an electromagnetic system: the nonlinear resistive, inductive, capacitive elements, hysteresis properties of ferromagnetic materials, nonlinear active elements like vacuum diode, transistor etc. may be responsible for nonlinearities in the system. The oscillatory motion of driven simple pendulum has been the most investigated motion in physics as well as in various fields of science and technology. The driven simple pendulum is one of the most common examples of nonlinear systems [1] (under the large amplitude oscillations) exhibiting chaotic motion and it is also isomorphic to many nonlinear systems such as Josephson junctions and the phase-locked-loop configuration of a voltage-controlled oscillator (VCO) etc [2, 3]. It is very important to point out here that seemingly simple situation of a driven pendulum is quite complex due to fact that the parameter space is very large. Besides the amplitude and frequency of the driving force, one has to investigate the role of strength of dissipation/damping as the simultaneous consideration of supply and dissipation of energy in the oscillatory system decides the boarder of stability and instability. In addition to this the

type of dissipation/damping (whether linear or nonlinear) also plays a major role in deciding the global dynamical behavior of the oscillator [4]. During the last decade there has been a growing interest to study some of the ubiquitous nonlinear physical oscillators (e.g. forced Duffing, escape oscillator, Rayleigh-Duffing oscillator etc.) under the presence of nonlinear damping [4-8] due to the fact that the nonlinear dissipation/damping is necessary in several engineering applications such as rolling in ship dynamics [9], vibration isolators [10], drag forces in flow induced vibrations [11] etc.

The simple pendulum is essentially a nonlinear dynamical system modeled by a second order nonlinear differential equation but in many practical situations it is described by a linear differential equation due to small amplitude oscillations. Very few nonlinear systems can be solved explicitly hence one has to resort to numerical techniques to understand the dynamics of such systems.
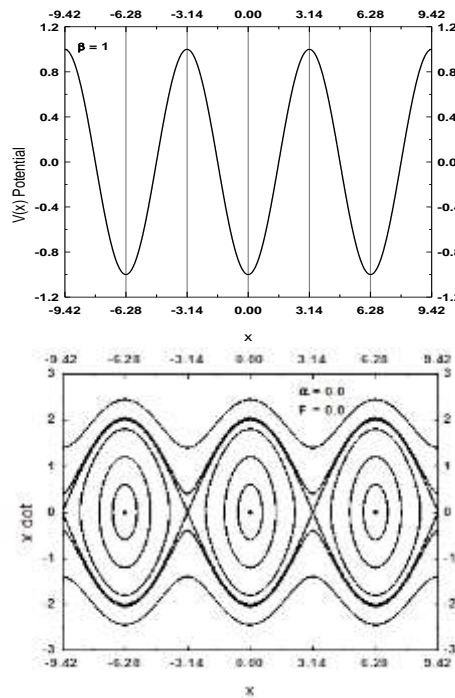
Fig. 1. The plot of $V(x) = -\beta cosx$ for $\beta = 1$, (b) phase trajectories of undamped and unforced simple pendulum

We consider the following form of generalized driven simple pendulum to understand the effect of nonlinear damping on its global dynamical behavior

$$\ddot{x} + \alpha \dot{x}|\dot{x}|^{p-1} + \beta sinx = Fcos\omega t \qquad (1)$$

Here, α is the damping coefficient, p is damping exponent, F and ω respectively are the amplitude and frequency of driving force. The unperturbed and undamped system can be written as (i.e. α=0 and F = 0)

$$\dot{x} = y$$
$$\dot{y} = -\beta sinx, \tag{2}$$

which is equivalent to the unit mass particle moving in negative cosine potential (i.e. $V(x) = -\beta cosx$, Fig. 1(a)). The unperturbed system has centers at (nπ,0) for n = 0, ±2, ±4..... and saddle points at (nπ,0) for n = ±1, ±3, ±5........ as the equilibrium points. In fig 1(b), we have depicted the phase space trajectories for the system (2) with $\beta = 1$ (i.e a unit mass particle in a cosine potential which has minima at $\pm 2n\pi$ and local maxima at $\pm(2n+1)\pi$, where n=0, 1, 2, 3 ...... as shown in Fig 1(a)).
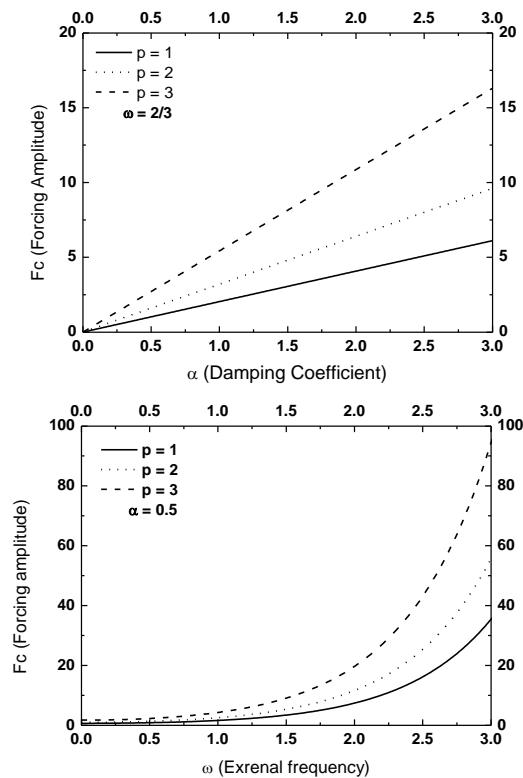
Fig. 2. Critical value of forcing amplitude F_c : (a) as a function of damping coefficient α for $\beta = 1$, $\omega = 2/3$ and p = 1, 2 and 3, (b) as a function of external frequency ω for $\beta = 1$, $\alpha = 0.5$ and p = 1, 2 and 3.
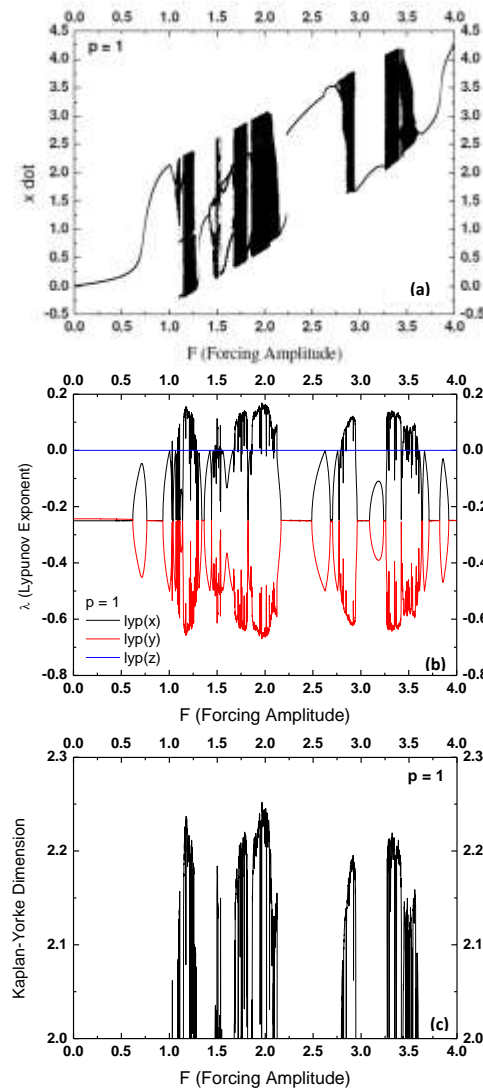
Fig. 3. Dynamical behavior of driven simple pendulum under linear/viscous damping (p = 1) as a function of forcing amplitude (F) for $\beta = 1, \omega = 2/3$ and $\alpha = 0.5$: (a) bifurcation diagram showing route to chaos, (b) all three Lyapunov exponents and (c) the Kaplan-Yorke dimension.

The solution of the unperturbed system (2) obtained by integrating it is given as

$$x_o(t) = 2sin^{-1}\left[\tanh(\sqrt{\beta}t)\right] \tag{3}$$
$$\dot{x}_o(t) = 2\sqrt{\beta}sech\left[\sqrt{\beta}t\right] \tag{4}$$
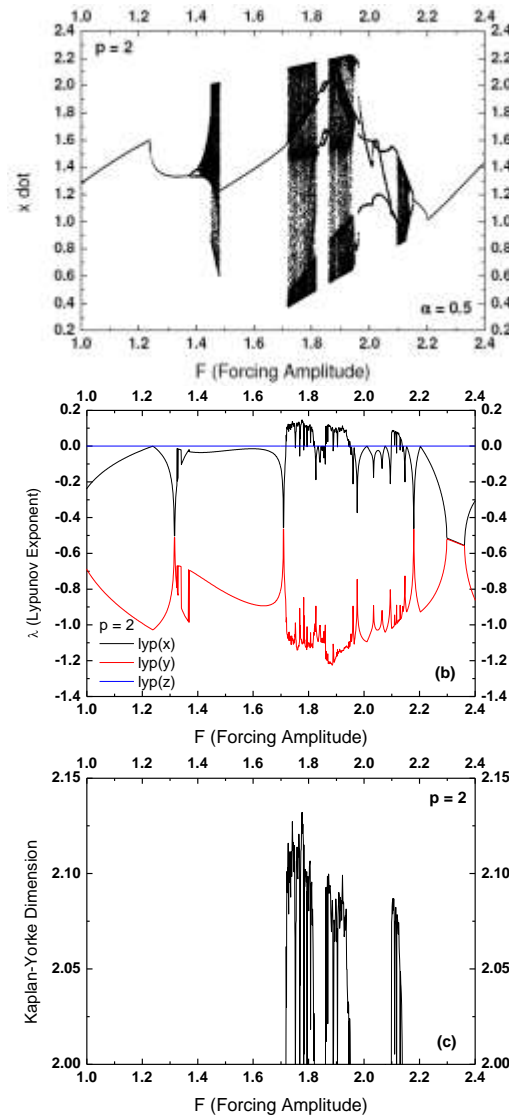
Fig. 4. Dynamical behavior of driven simple pendulum under drag like damping (p = 2) as a function of forcing amplitude (F) for $\beta = 1, \omega = 2/3$ and $\alpha = 0.5$: (a) bifurcation diagram showing route to chaos, (b) all three Lyapunov exponents and (c) the Kaplan-Yorke dimension.

Now we apply Melnikov's method [12] to obtain the homoclinic bifurcation condition in the driven simple pendulum with nonlinear damping (Eq. (1)). The Melnikov function gives the distance between the stable and unstable manifolds of a saddle point in forced systems, hence the simple zeros of the Melnikov

function give the critical value of the forcing amplitude (for a given set of other system parameters α, p, β and ω) for which the distance between stable and unstable manifolds becomes zero and a homoclinic orbit originates. The Melnikov function for the driven simple pendulum with nonlinear damping (Eq. (1)) is given by

$$M(t_o) = \int_{-\infty}^{\infty} \dot{x}_o(t - t_o)[-\alpha \dot{x}_o(t - t_o)|\dot{x}_o(t - t_o)|^{p-1} + Fcos\omega t]dt \quad (5)$$

$$M(t_o) = -\alpha \int_{-\infty}^{\infty}[\dot{x}_o(t - t_o)]^2|\dot{x}_o(t - t_o)|^{p-1}dt + F \int_{-\infty}^{\infty} \dot{x}_o(t - t_o)cos\omega t \, dt \quad (6)$$

Using Eq. (4) and then evaluating the integrals, we obtain

$$M(t_o) = -2^{p+1}\alpha\beta^{p/2}B\left(\frac{1}{2}, \frac{p+1}{2}\right) + 2\sqrt{\beta}Fcos t_o \frac{\sum_{n=0}^{\lfloor\sqrt{\beta}-1/2\rfloor}(-1)^{n+1}2\pi\sqrt{\beta}cosh\left(\frac{(2n+1)\pi\omega}{2\sqrt{\beta}}\right)}{[1+cosh(\pi\omega)]} \quad (7)$$

Here $B(\bullet,\bullet)$ and $\lfloor\bullet\rfloor$ respectively, are the Euler beta and floor functions. For a given set of parameters F, α, p, β and ω, $M(t_o)$ will vanish if a real solution can be found for t_o. Assuming that F, α, β >0, the above condition will be met if $|cos\omega t_o| \leq 1$. Hence

$$F = F_c = \frac{-2^{p-1}\alpha\beta^{\frac{p}{2}-1}B\left(\frac{1}{2}, \frac{p+1}{2}\right)[1+cosh(\omega\pi)]}{\pi\sum_{n=0}^{\lfloor\sqrt{\beta}-1/2\rfloor}(-1)^{n+1}cosh\left(\frac{(2n+1)\pi\omega}{2\sqrt{\beta}}\right)} \quad (8)$$

The above formula (Eq. 8) gives the critical value of forcing amplitude (F_c) where homoclinic orbit originates for a unit mass particle in a driven negative cosine potential. In Figure 2 we have shown the theoretical comparison of the variation of critical values of forcing amplitude (F_c): particularly in Frame (a) the variation of F_c with damping coefficient (α) for a specific choice of external forcing frequency $\omega = 2/3$ and β=1 (i.e., $F_c = \alpha(1/\pi)2^pB(1/2, (p + 1)/2)cosh(\pi/3)$) and different values of damping exponent p = 1, 2 and 3. In Frame (b) the variation of F_c with external forcing frequency (ω) for a specific choice of damping coefficient $\alpha = 0.5$ and β=1 (i.e., $F_c = (1/\pi)2^{p-1}B(1/2, (p + 1)/2)cosh(\pi\omega/2)$) and different values of damping exponent p = 1, 2 and 3 have been depicted. It is clear that F_c linearly increases with the damping coefficient (α) and for a fixed set of α and β, F_c increases with damping exponent p. However F_c increases exponentially with the external forcing frequency (ω) and for a fixed set of ω and β, F_c increases with damping exponent p. The variation of critical value of forcing amplitude (F_c) with respect to the damping exponent p in case of driven simple pendulum is opposite to the case of forced Duffing oscillator [4]. To understand the various features of the dynamical behavior of driven simple pendulum under the nonlinear damping we have done extensive numerical computation for the bifurcation diagrams, Lyapunov exponent and Kaplan Yorke dimension for various types of damping i.e. p=1 and 2. The results have been depicted in Figures 3 and 4. We observe that the number of periodic windows decreases as we increase the damping exponent (p) and the range of external forcing amplitude (F) for which chaos exists also decreases with the increment in the damping exponent (p). The Lyapunov exponent results shown in frames (b) of each figures are computed by integrating the system up to upto $t = 10^4$ with the step size $\Delta t = 10^{-2}$ and then averaged. The results of corresponding Kalpan Yorke Dimension for phase space attractor are shown in frames (c) of each

figure. The Kaplan Yorke Dimension [13] is calculated using the following relation: $D_{KY} = m + \sum_{i=1}^{m} \frac{\lambda_i}{\lambda_{m+1}}$, where D_{KY} is Kaplan Yorke Dimension and m is the largest integer for which sum of first m Lyapunov exponents is positive.

Fig. 5. Parameter space consisting of external forcing amplitude and damping coefficient corresponding to chaotic and periodic behavior in the driven simple pendulum for $\beta = 1, \omega = 2/3$ under: (a) linear/viscous damping (p = 1), (b) drag like damping (p = 2).

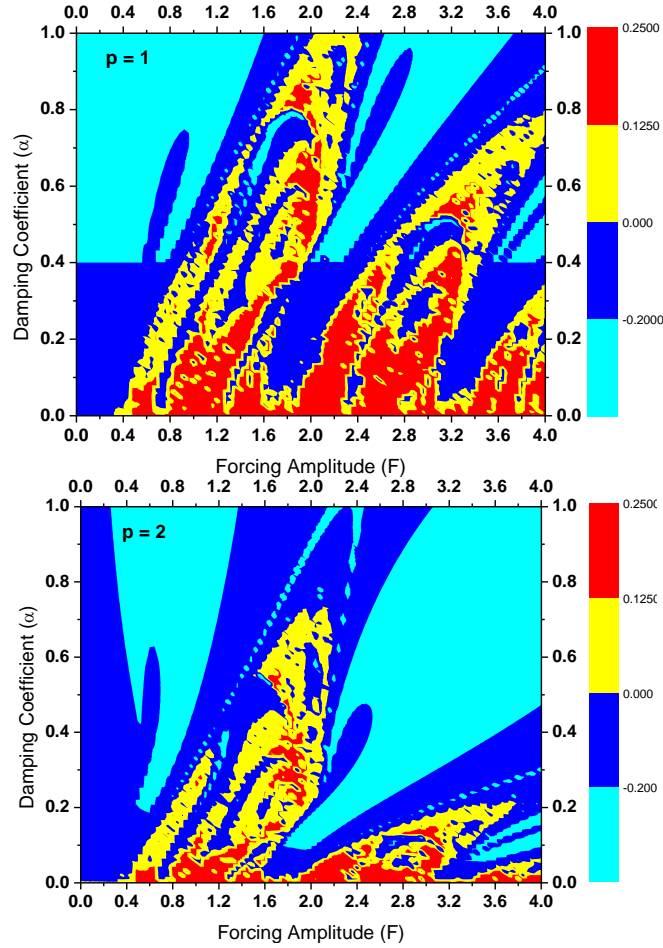We have also identified the regions of 2D parameter space consisting of external forcing amplitude and damping coefficient corresponding to chaotic and periodic behaviour for driven simple pendulum for various types of damping using extensive Lyapunov exponent calculation for $0 \leq F \leq 4.0$ and $0 \leq \alpha \leq 1.0$ with step sizes $\Delta F = 0.04$ and $\Delta \alpha = 0.01$. For the calculation of largest

Lyapunov exponent (LLE), we have integrated the system and averaged the results up to $t = 3\pi \times 10^3$ with a time step $\Delta t = 3\pi \times 10^{-3}$. The different regions of parameter space corresponding to chaotic and period behavior are shown with different colors in Figure 5. The whole parameter space region is divided into four sub-regions corresponding to different range of largest Lyapunov exponent (LLE). The periodic regions is shown by the light-blue/cyan ($LLE \leq -0.2$) and blue ($-0.2 < LLE \leq 0$) colors whereas the chaotic regions is shown by yellow ($0 < LLE \leq 0.125$) and red ($0.125 < LLE \leq 0.25$) colors. We may clearly observe that the chaos becomes less fragile i.e. the number of periodic windows decreases as we increase the damping exponent (p), which is also confirmed by corresponding bifurcation diagrams. We also observe that chaos is less global in the parameter space with the increase in the nonlinearity in the damping.

We have also calculated the percentage of the regions of parameter space corresponding to chaotic and periodic motions. The results are summarized in Table 1, which confirms that chaotic region is decreasing with the increase in damping exponent. These results are opposite in nature as compare to the case of forced Duffing oscillator [4].

Table 1: Comparison of the regions of parameter space corresponding to chaotic and periodic motions

	Colour	P=1		P=2	
Chaos	Red $0.125 \leq LLE < 0.25$	16.07%	31.67%	5.64%	14.55%
	Yellow $0 \leq LLE < 0.125$	15.60%		8.91%	
Periodic	Blue $-0.2 \leq LLE < 0$	40.32%	68.33%	44.46%	85.45%
	Light Blue $LLE < -0.2$	28.01%		40.99%	

To observe the effect of nonlinear damping on the fractalness and complexity of basin boundaries, we have computed the basin of attraction patterns for a set of initial conditions defined by $-3.14 \leq x \leq 3.14$ and $-3.14 \leq \dot{x} \leq 3.14$ with steps $\Delta x = 0.02$ and $\Delta \dot{x} = 0.02$ for p =1 and 2. In Figure 6 one such comparison is shown between the basin of attraction patterns for a period-1 attractor observed at the forcing amplitude values $F = 1.35$ and $F = 1.70$ for viscous (p=1) and drag like damping (p=2) (by fixing the other parameters at α=0.5, $\omega = 2/3$ and β=1) respectively. For the driven simple pendulum there are two stable rotary modes with average components of angular velocity either positive or negative for different basins. The phase portraits of these modes are shown in frame (a), (b), (e) and (f) of Figure 6. For drawing the basin of attractions we have considered 314×314 different initial conditions defined by $-3.14 \leq x \leq 3.14$ and $-3.14 \leq \dot{x} \leq 3.14$ with steps $\Delta x = 0.02$ and $\Delta \dot{x} = 0.02$. For each pair of initial condition we calculate the trajectory over many cycles and then average the angular velocity. To eliminate transient effect, the first 100 cycles are discarded. The two basins of attraction are distinguished by

the sign of average of angular velocity. For positive average velocity we assign
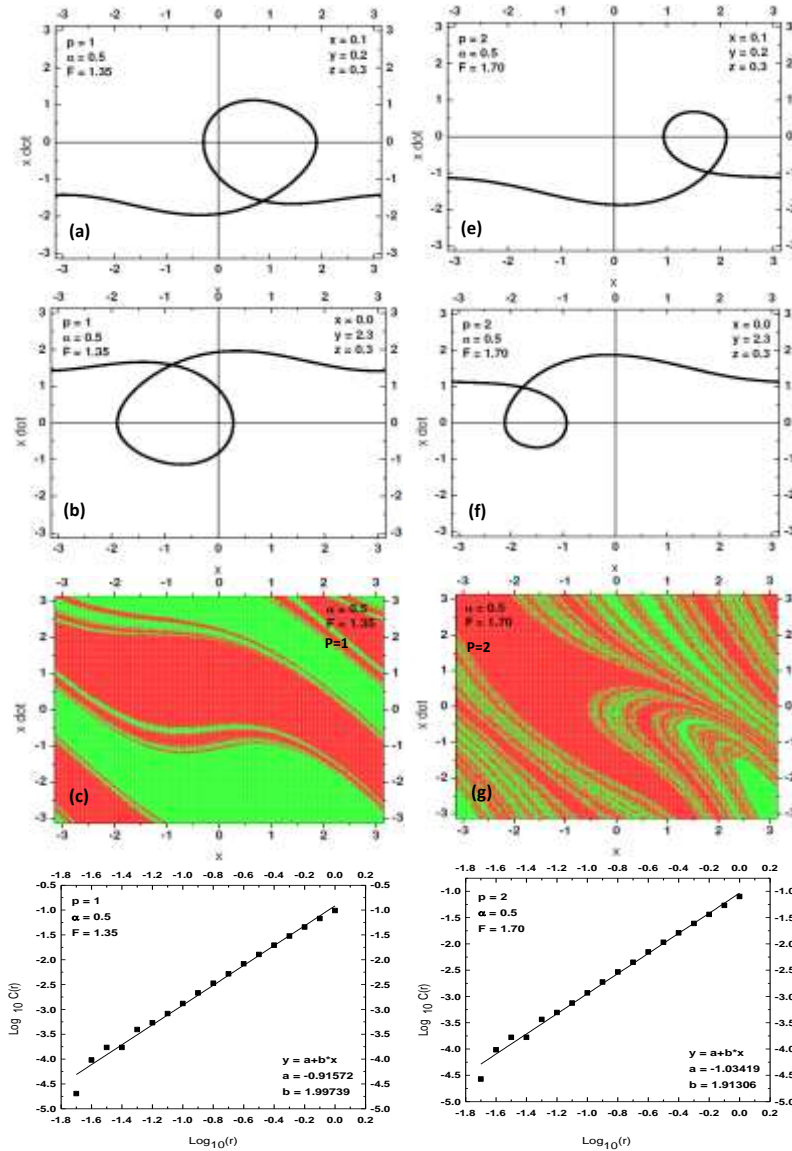the green color and for negative average velocity we assign the red color.

Fig. 6. Comparison of the basin of attraction patterns of a period-1 attractors in
driven pendulum under the linear/viscous damping (p=1) and drag like damping
(p=2) for the parameters $\beta = 1, \omega = 2/3, \alpha = 0.5 \; and \; F = 1.35$ and $\beta = 1, \omega = 2/3, \alpha = 0.5 \; and \; F = 1.70$ respectively

The results of basins of attractions patterns are shown in frame (c) and (g) of Figure 6. From the first visualization it appears that the basin of attraction patterns become more complex due to nonlinear damping. To quantify the fractalness of these basins of attraction patterns, we have also computed the correlation dimension [14] for these patterns by converting them into binary images (each points in these patterns has been considered as a pixel and the positive average velocity and negative average velocity respectively are denoted by 1 and 0). Then we calculate the correlation dimension of the object represented by all nonzero pixels. The results have been depicted in the frames (d) and (h) of Figure 6 respectively for the basin patterns shown in Frames (c) and (g) of same figure and the correlation dimension values respectively are 1.99739 and 1.91306. Hence the increase in the order of nonlinear damping does not increase the fractalness of the basin boundaries.

In conclusion, we have revisited the driven simple pendulum to observe the effect of nonlinear damping on the global dynamical behavior. Overall the effect of nonlinear damping on the dynamics of driven simple pendulum is opposite in nature as compare to the forced Duffing oscillator.

References

1. G. L. Baker and J. A. Blackbum. *The Pendulum: A case study in Physics*, Oxford University Press, Oxford, 2005.

2. B. A. Huberman, J. P. Crutchfield and N. H. Packard. Noise phenomena in Josephson junctions. *Applied Physics Letters* 37; 750-752, 1980.

3. D. D'Humeries D., M. R. Beasley, B.A. Huberman and A. Libchaber. Chaotic states and routes to chaos in the forced pendulum. *Phys. Rev. A* 26; 2383-3496, 1982.

4. A. Sharma, V. Patidar, G. Purohit and K. K. Sud. Effects of bifurcation and chaos in forced Duffing oscillator due to nonlinear damping. *CNSNS* 17; 2254-2269, 2012.

5. M. A. F. Sanjuan. The effect of nonlinear damping on the universal escape oscillator, *Int. J. Bifurcat Chaos* 9;735-744, 1999.

6. J. L. Trueba, J. Rams and M. A. F. Sanjuan. Analytical estimates of the effect of nonlinear damping in some nonlinear oscillators, *Int. J. Bifurcation and Chaos* 10; 2257-2267, 2000.

7. J. P. Baltanas, J. L. Trueba and M. A. F. Sanjuan. Energy dissipation in nonlinearly damped Duffing oscillator, *Physica D* 159;22-34, 2001.

8. M. S. Siewe, H. Cao and M. A. F. Sanjuan, Effect of nonlinear dissipation on the boundaries of basin of attraction in two-well Rayleigh-Duffing oscillators, *Chaos, Solitons and Fractals* 39; 1092-1099, 2009.

9. J. M. T. Thompson, R. C. T. Rainey and M. S. Soliman. Ship stability criteria based on chaotic transients from incursive fractals. *Philos. Trans. R. Soc. London A* 332; 149-167, 1990.

10. A. K. Mallik. *Principles of Vibrations Control,* Affiliated Publishers, New Delhi, 1990.

11. F. C. Moon. *Chaotic and Fractal Dynamics*, Wiley, New York, 1992

12. V. K. Melnikov. On the stability of the center for time periodic perturbations. *Trans Moscow Math Soc* 12; 1-56, 1963.

13. J. L. Kaplan and J. A. Yorke. Chaotic behavior of multidimensional difference equations. In: Peitgen H-O, Walther (Eds.) *Functional differential equations and approximations of fixed points, Lecture Notes in Mathematics* 730; 204-227, 1979.

14. P. Grassberger and I. Procaccia. Measuring the strangeness of the strange attractors, *Physica D* 9; 189-208, 1983.

Universality of Tsallis Non-Extensive Statistics and Fractal Dynamics for Complex Systems

G.P. Pavlos[1], M.N. Xenakis[2], L.P. Karakatsanis[1], A.C. Iliopoulos [1], A.E.G. Pavlos [3], D.V. Sarafopoulos [1]

[1]Department of Electrical and Computer Engineering, Democritus University of Thrace, 67100 Xanthi, Greece (Email: gpavlos@ee.duth.gr)
[2]German Research School for Simulation Sciences, Aachen, Germany
[3]Department of Physics, Aristotle University of Thessaloniki, 54624 Thessaloniki, Greece

Abstract: Tsallis q-extension of statistics and fractal generalization of dynamics are two faces of the same physical reality, as well as the Kernel modern complexity theory. The fractal generalization dynamics is based at the multiscale – multifractal characters of complex dynamics in the physical space-time and the complex system's dynamical phase space. Tsallis q-triplet of non-extensive statistics can be used for the experiment test of q-statistic as well as of the fractal dynamics. In this study we present indicative experimental verifications of Tsallis theory in various complex systems such as solar plasmas, (planetic magnetospheres, cosmic stars and cosmic rays), atmospheric dynamics, seismogenesis and brain dynamics.
Keywords: Tsallis non-extensive statistics, Non-equilibrium phase transition, intermittent turbulence, Self Organized Criticality, Low Dimensional Chaos, Magnetosphere, Superstorm.

1. Introduction

Physical theory today has been led into admirable experience and knowledge. Namely, at all levels of physical reality a global ordering principle is operating. Prigogine [1], Nicolis [2], Davies [3], El Naschie [4], Iovane [5], Nottale [6], Castro [7]. All classical physical theory dominates the Demokritean and Euclidean reductionistic point of view. That is, cosmos is created from elementary particles which obey to the fundamental laws, space consists of points and time from moments points or moments have zero measure. In Einstein's relativistic physical theory Democritean (elementary material particles) and Euclidian (points, space, point view) are joined into a unified physical entity that of the space time manifold. Here, geometry explains physics since the forces-fields are identified with the curvature of the space-time manifold. Although Einstein showed, with a rare genius way, the unity of universe through a mathematization and geometrization modification of the cosmos subject-matter, however he didn't escape from the reductionistic and deterministic point of view [8]. According to this concept, the observed and macroscopic reality is illusion as the only existed reality is the fundamental geometrical and objective reality of the space-time manifold in general. This is the Democritian, Parmenidian, Euclidian, Spinozian point of view.

The overthrow of the dogmatic determinism and reductionism in science started to be realized after the novel concept of Heisenberg according to which the physical magnitude properties are not objective and divided realities but operators as the dynamical states are infinite dimensional vectors. This new concept of Heisenberg led to a new theoretical status corresponding to a microscopical complexity point view of cosmos. Neuman inspired from Heisenberg's novel theory introduced non-commutatively in geometry, according to which Space does not consist of points but from "states". In addition, superstring theory forced physicists to introduce non-commutatively at the Planck scale of space-time, confirming Neuman's as well as Heisenberg's intuition. This, of course, was the initiation of an avalanche of serious of changes in the fundamentals of physical theory, corresponding to new theoretical concepts as: poly-dimensional and p-adic physics, scale relativity fractal dynamics and fractal space-time etc El Naschie [4], Khrenminov [9], Nottale [6], Castro [7], Kroger [10], Pezzaglia [11], Tarasov [12], El-Naboulsis [13], Gresson [14], Goldfain [15].

Prigogine [1] and Nicolis [2] were the principal leaders of an outstanding transition to the new epistemological ideas in the macroscopical level. Far from equilibrium they discover an admirable operation of the physical-chemical systems. That is, the discovered the possibility of long range spatiotemporal correlations development when the system lives far from equilibrium. Thus, Prigogine and Nicolis opened a new road towards to the understanding of random fields and statistics, which lead to a non-Gaussian reality. This behavior of nature is called Self-Organization. Prigogine's and Nicoli's self-organized concepts inspired one of the writers of this paper to introduce the self organization theory as basic tool to interpret the dynamics of the space plasmas dynamics [16] as well as seismogenesis [17] as a result of the self organization of Earth's manage-crust system. However Lorenz[18] had discovered the Lorenz's attractor as the weather's self organization process while other scientists had observed the self organization of fluids (e.g. dripping faucet model) or else, verifying the Feinebaum [19] mathematical scenarios to complexity includes in nonlinear maps or Ordinary Differential Equations – Partial Differential Equations [20]. However, scientists still now prefers to follow the classical theory, namely that macro-cosmos is just the result of fundamental laws which can be traced only at the microscopical level. Therefore, while the supporter of classical reductionistic theory considers the chaos and the self organization macroscopic characteristics that they ought to be the result of the fundamental Lagrangian or the fundamental Hamiltonian of nature, there is an ongoing a different perception. Namely, that macroscopic chaos and complexity not only cannot be explained by the hypothetical microscopic simplicity but they are present also in the microscopic reality.

Therefore, scientists like Nelson [21], Hooft [22], Parisi [23], Beck [24] and others used the complexity concept for the explanation of the microscopic

"simplicity", introducing theories like stochastic quantum field theory or chaotic field theory. This new perception started to appear already through the Wilsonian theories of renormalization which showed the multiscale cooperation of the physical reality [25]. At the same time, the multiscale cooperativity goes with the self similarity characters of nature that allows the renormalization process. This leads to the utilization of fractal geometry into the unification of physical theories, as the fractal geometries are characterized by the scaling property which includes the multiscale and self similar character. Scientists like Ord [26], El Naschie [4], Nottale [6] and others, will introduce the idea of fractal geometry into the geometry of space-time, negating the notion of differentiability of physical variables. The fractal geometry is connected to non-commutative geometry since at fractal objects the principle of self similarity negates the notion of the simple geometrical point just like the idea of differentiability. Therefore, the fractal geometry of space-time is leading to the fractal extension of dynamics exploiting the fractal calculus (fractal integrals-fractal derivatives) [27]. Also, the fractal structure of space-time has intrinsically a stochastic character since a presupposition for determinism is differentiability [6, 14]. Thus, in this way, statistics are unified with dynamics automatically, while the notion of probability obtains a physical substance, characterized as dynamical probabilism. The ontological character of probabilism can be the base for the scientific interpretation of self-organization and ordering principles just as Prigogine [1] had imagined, following Heisenberg's concept. From this point of view, we could say that contemporary physical theory returns to the Aristotetiles point of view as Aristotelianism includes the Newtonian and Democritian mechanistical determinism as one component of the organism like behavior of Nature [28].

Modern evolution of physical theory as it was described previously is highlighted in Tsallis q-statistics generalization of the Boltzmann-Gibbs statistics which includes the classical (Gaussian) statistics, as the $q=1$ limit of thermodynamical equilibrium. Far from equilibrium, the statistics of the dynamics follows the q-Gaussian generalization of the B-G statistics or other more generalized statistics. At the same time, Tsallis q-extension of statistics can be produced by the fractal generalization of dynamics. The traditional scientific point of view is the priority of dynamics over statistics. That is dynamics creates statistics. However for complex system their holistic behaviour does not permit easily such a simplification and division of dynamics and statistics. Tsallis $q-$ statistics and fractal or strange kinetics are two faces of the same complex and holistic (non-reductionist) reality.

Moreover, the Tsallis statistical theory including the Tsallis extension of entropy to what is known as q-entropy [29], the fractal generalization of dynamics [6, 7] and the scale extension of relativity theory C [6, 7] are the cornerstones of modern physical theory related with nonlinearity and non-integrability as well as with the non-equilibrium ordering and self organization. In the following, in section (2) we present the theoretical concepts of q-statistics and fractal dynamics, while in section (3) we present indicative experimental

verification of the Tsallis statistical theory. Finally in section (4) we present estimations of q-statistics index for various kinds of complex systems and in section (5) we summarize and discuss the results of this study.

2. Theoretical Concepts

2.1 Complexity Theory and the Cosmic Ordering Principle

The conceptual novelty of complexity theory embraces all of the physical reality from equilibrium to non-equilibrium states. This is noticed by Castro [7] as follows: *"...it is reasonable to suggest that there must be a deeper organizing principle, from small to large scales, operating in nature which might be based in the theories of complexity, non-linear dynamics and information theory which dimensions, energy and information are intricately connected." [7].* Tsallis non-extensive statistical theory [29] can be used for a comprehensive description of space plasma dynamics, as recently we became aware of the drastic change of fundamental physical theory concerning physical systems far from equilibrium.

The dynamics of complex systems is one of the most interesting and persisting modern physical problems including the hierarchy of complex and self-organized phenomena such as: intermittent turbulence, fractal structures, long range correlations, far from equilibrium phase transitions, anomalous diffusion – dissipation and strange kinetics, reduction of dimensionality etc [30-37].

More than other scientists, Prigogine, as he was deeply inspired by the arrow of time and the chemical complexity, supported the marginal point of view that the dynamical determinism of physical reality is produced by an underlying ordering process of entirely holistic and probabilistic character at every physical level. If we accept this extreme scientific concept, then we must accept also for complex systems the new point of view, that the classical kinetic is inefficient to describe sufficiently the emerging complex character as the system lives far from equilibrium. However resent evolution of the physical theory centered on non-linearity and fractality shows that the Prigogine point of view was so that much extreme as it was considered at the beginning.

After all, Tsallis $q-$ extension of statistics [29] and the fractal extension for dynamics of complex systems as it has been developed by Notalle [6], El Naschie [4], Castro [7], Tarasov [12], Zaslavsky [38], Milovanov [32], El Nabulsi [13], Cresson [14], Coldfain [15], Chen [39], and others scientists, they are the double face of a unified novel theoretical framework, and they constitute the appropriate base for the modern study of non-equilibrium dynamics as the q-statistics is related at its foundation to the underlying fractal dynamics of the non-equilibrium states.

For complex systems near equilibrium the underlying dynamics and the statistics are Gaussian as it is caused by a normal Langevin type stochastic process with a white noise Gaussian component. The normal Langevin

stochastic equation corresponds to the probabilistic description of dynamics by the well-known normal Fokker – Planck equation. For Gaussian processes only the moments-cummulants of first and second order are non-zero, while the central limit theorem inhibits the development of long range correlations and macroscopic self-organization, as any kind of fluctuation quenches out exponentially to the normal distribution. Also at equilibrium, the dynamical attractive phase space is practically infinite dimensional as the system state evolves in all dimensions according to the famous ergodic theorem of Boltzmann – Gibbs statistics. However, in Tsallis $q-$statistics even for the case of $q = 1$ (corresponding to Gaussian process) the non-extensive character permits the development of long range correlations produced by equilibrium phase transition multi-scale processes according to the Wilson RGT [40]. From this point of view, the classical mechanics (particles and fields), including also general relativity theory, as well as the quantum mechanics – quantum field theories, all of them are nothing else than a near thermodynamical equilibrium approximation of a wider theory of physical reality, characterized as complexity theory. This theory can be related with a globally acting ordering process which produces the $q-$statistics and the fractal extension of dynamics classical or quantum.

Generally, the experimental observation of a complex system presupposes non-equilibrium process of the physical system which is subjected to observation, even if the system lives thermodynamically near to equilibrium states. Also experimental observation includes discovery and ascertainment of correlations in space and time, as the spatio-temporal correlations are related or they are caused by from the statistical mean values fluctuations. The theoretical interpretation prediction of observations as spatial and temporal correlations – fluctuations is based on statistical theory which relates the microscopic underling dynamics with the macroscopic observations indentified to statistical moments and cumulants. Moreover, it is known that statistical moments and cumulants are related to the underlying dynamics by the derivatives of the partition function (Z) to the external source variables (J) [41].

From this point of view, the main problem of complexity theory is how to extend the knowledge from thermodynamical equilibrium states to the far from equilibrium physical states. The non-extensive $q-$statistics introduced by Tsallis [29] as the extension of Boltzmann – Gibbs equilibrium statistical theory is the appropriate base for the non-equilibrium extension of complexity theory. The far from equilibrium $q-$statistics can produce the q-partition function (Z_q) and the corresponding $q-$moments and cumulants, in correspondence with Boltzmann – Gibbs statistical interpretation of thermodynamics.

The miraculous consistency of physical processes at all levels of physical reality, from the macroscopic to the microscopic level, as well as the inefficiency of existing theories to produce or to predict the harmony and hierarchy of structures inside structures from the macroscopic or the microscopic level of cosmos. This completely supports or justifies such new

concepts as that indicated by Castro [7]: *"of a global ordering principle or that indicated by Prigogine, about the becoming before being at every level of physical reality."* The problem however with such beautiful concepts is how to transform them into an experimentally testified scientific theory.

The Feynman path integral formulation of quantum theory after the introduction of imaginary time transformation by the Wick rotation indicates the inner relation of quantum dynamics and statistical mechanics [42, 43]. In this direction it was developed the stochastic and chaotic quantization theory [22-24, 44], which opened the road for the introduction of the macroscopic complexity and self-organization in the region of fundamental quantum field physical theory. The unified character of macroscopic and microscopic complexity is moreover verified by the fact that the $n-$point Green functions produced by the generating functional $W(J)$ of QFT after the Wick rotation can be transformed to $n-$point correlation functions produced by the partition function $Z(J)$ of the statistical theory. This indicates in reality the self-organization process underlying the creation and interaction of elementary particles, similarly to the development of correlations in complex systems and classical random fields Parisi [23]. For this reason lattice theory describes simultaneously microscopic and macroscopic complexity [40, 42].

In this way, instead of explaining the macroscopic complexity by a fundamental physical theory such as QFT, Superstring theory, M-theory or any other kind of fundamental theory we become witnesses of the opposite fact, according to what Prigogine was imagining. That is, macroscopic self-organization process and macroscopic complexity install their kingdom in the heart of reductionism and fundamentalism of physical theory. The Renormalizable field theories with the strong vehicle of Feynman diagrams that were used for the description of high energy interactions or the statistical theory of critical phenomena and the nonlinear dynamics of plasmas [45] lose their efficiency when the complexity of the process scales up [40].

Many scientist as Chang [31], Zelenyi [30], Milovanov [32], Ruzmaikin [33], Abramenko [36], Lui[46], Pavlos[37], in their studies indicate the statistical non-extensivity as well as the multi-scale, multi-fractal and anomalous – intermittent character of fields and particles in the space plasmas and other complex systems far from equilibrium. These results verify the concept that space plasmas and other complex systems dynamics are part of the more general theory of fractal dynamics which has been developed rapidly the last years. Fractal dynamics are the modern fractal extension of physical theory in every level. On the other side the fractional generalization of modern physical theory is based on fractional calculus: fractional derivatives or integrals or fractional calculus of scalar or vector fields and fractional functional calculus [12, 39]. It is very impressive the efficiency of fractional calculus to describe complex and far from equilibrium systems which display scale-invariant properties, turbulent dissipation and long range correlations with memory

preservation, while these characteristics cannot be illustrated by using traditional analytic and differentiable functions, as well as, ordinary differential operators. Fractional calculus permits the fractal generalization of Lagrange – Hamilton theory of Maxwell equations and Magnetohydrodynamics, the Fokker – Planck equation Liouville theory and BBGKI hierarchy, or the fractal generalization of QFT and path integration theory [12-15, 39].

According to the fractal generalization of dynamics and statistics we conserve the continuity of functions but abolish their differentiable character based on the fractal calculus which is the non-differentiable generalization of differentiable calculus. At the same time the deeper physical meaning of fractal calculus is the unification of microscopic and macroscopic dynamical theory at the base of the space – time fractality [4, 6, 39, 47-49]. Also the space-time is related to the fractality – multi-fractality of the dynamical phase – space, whish can be manifested as non-equilibrium complexity and self-organization.

Moreover fractal dynamics leads to a global generalization of physical theory as it can be related with the infinite dimension Cantor space, as the microscopic essence of physical space – time, the non-commutative geometry and non-commutative Clifford manifolds and Clifford algebra, or the p-adic physics [4, 7, 13, 50, 51]. According to these new concepts introduced the last two decades at every level of physical reality we can describe in physics complex structure which cannot be reduced to underlying simple fundamental entities or underlying simple fundamental laws. Also, the non-commutative character of physical theory and geometry indicates [51, 52] that the scientific observation is nothing more than the observation of undivided complex structures in every level. Cantor was the founder of the fractal physics creating fractal sets by contraction of the homogenous real number set, while on the other side the set of real numbers can be understood as the result of the observational coarse graining [27, 50, 53]. From a philosophical point of view the mathematical forms are nothing else than self-organized complex structures of the mind-brain, in self-consistency with all the physical reality. On the other side, the generalization of Relativity theory to scale relativity by Nottale [6] or Castro [7] indicates the unification of microscopic and macroscopic dynamics through the fractal generalization of dynamics.

After all, we conjecture that the macroscopic self-organization related with the novel theory of complex dynamics, as they can be observed at far from equilibrium dynamical physical states, are the macroscopic emergence result of the microscopic complexity which can be enlarged as the system arrives at bifurcation or far from equilibrium critical points. That is, far from equilibrium the observed physical self-organization manifests the globally active ordering principle to be in priority from local interactions processes. We could conjecture that is not far from thruth the concept that local interactions themselves are nothing else than local manifestation of the holistically active ordering principle. That is what until now is known as fundamental lows is the equilibrium manifestation or approximation of the new and globally active ordering principle. This concept can be related with the fractal generalization of dynamics which is indentified with the dynamics of correlations supported by

Prigogine [1], Nicolis [2] and Balescu [54], as the generalization of Newtonian theory. This conjecture concerning the fractal unification of macroscopic and microscopic dynamics at can be strongly supported by the Tsallis nonextensive q-statistics theory which is verified almost everywhere from the microscopic to the macroscopic level [7, 29]. From this point of view it is reasonable to support that the q-statistics and the fractal generalization of space plasma dynamics is the appropriate framework for the description of their non-equilibrium complexity.

2.2 Chaotic Dynamics and Statistics

The macroscopic description of complex systems can be approximated by non-linear partial differential equations of the general type:

$$\frac{\partial \vec{U}(\vec{x},t)}{\partial t} = \vec{F}(\vec{u},\vec{\lambda}) \tag{1}$$

where u belongs to a infinite dimensional state (phase) space which is a Hilbert functional space. Among the various control parameters, the plasma Reynold number is the one which controls the quiet static or the turbulent plasma states. Generally the control parameters measure the distance from the thermodynamical equilibrium as well as the critical or bifurcation points of the system for given and fixed values, depending upon the global mathematical structure of the dynamics. As the system passes its bifurcation points a rich variety of spatio-temporal patterns with distinct topological and dynamical profiles can be emerged such as: limit cycles or torus, chaotic or strange attractors, turbulence, Vortices, percolation states and other kinds of complex spatiotemporal structures [31, 49, 55-63].

Generally chaotic solutions of the mathematical system (1) transform the deterministic form of equation (1) to a stochastic non-linear stochastic system:

$$\frac{\partial \vec{u}}{\partial t} = \vec{\Phi}(\vec{u},\vec{\lambda}) + \vec{\delta}(\vec{x},t) \tag{2}$$

where $\vec{\delta}(\vec{x},t)$ corresponds to the random force fields produced by strong chaoticity [64, 65].
   The non-linear mathematical systems (1-2) include mathematical solutions which can represent plethora of non-equilibrium physical states included in mechanical, electromagnetic or chemical and other physical systems which are study here.

The random components ($\delta(\vec{x},t)$) are related to the BBGKY hierarchy:

$$\frac{\partial f_q}{\partial t} = [H_q, f_a] + S_q, q = 1, 2, ..., N \tag{3}$$

where f_q is the $q-$particle distribution function, H_q is the $q-$th approximation of the Hamiltonian $q-$th correlations and S_q is the statistical term including correlations of higher than q-orders [45, 65].

The non-linear mathematical systems (1, 2) correspond to the new science known today as complexity science. This new science has a universal character, including an unsolved scientific and conceptual controversy which is continuously spreading in all directions of the physical reality and concerns the integrability or computability of the dynamics [66]. This universality is something supported by many scientists after the Poincare discovery of chaos and its non-integrability as is it shown in physical sciences by the work of Prigogine, Nicolis, Yankov and others [1, 2, 66] in reality. Non-linearity and chaos is the top of a hidden mountain including new physical and mathematical concepts such as fractal calculus, p-adic physical theory, non-commutative geometry, fuzzy anomalous topologies fractal space-time etc [4, 7, 12-15, 38, 39, 50-52]. These new mathematical concepts obtain their physical power when the physical system lives far from equilibrium.

After this and, by following the traditional point of view of physical science we arrive at the central conceptual problem of complexity science. That is, how is it possible that the local interactions in a spatially distributed physical system can cause long range correlations or how they can create complex spatiotemporal coherent patterns as the previous non-linear mathematical systems reveal, when they are solved arithmetically, or in situ observations reveal in space plasma systems. For non-equilibrium physical systems the above questions make us to ask how the development of complex structures and long range spatio-temporal correlations can be explained and described by local interactions of particles and fields. At a first glance the problem looks simple supposing that it can be explained by the self-consistent particle-fields classical interactions. However the existed rich phenomenology of complex non-equilibrium phenomena reveals the non-classical and strange character of the universal non-equilibrium critical dynamics [31, 35].

In the following and for the better understanding of the new concepts we follow the road of non-equilibrium statistical theory [31, 36]

The stochastic Langevin equations (11, 13, 17) can take the general form:

$$\frac{\partial u_i}{\partial t} = -\Gamma(\vec{x})\frac{\delta H}{\delta u_i(\vec{x},t)} + \Gamma(\vec{x})n_i(\vec{x},t) \qquad (4)$$

where H is the Hamiltonian of the system, $\delta H / \delta u_i$ its functional derivative, Γ is a transport coefficient and n_i are the components of a Gaussian white noise:

$$\left.\begin{array}{c} < n_i(\vec{x},t) >= 0 \\ < n_i(\vec{x},t)n_j(\vec{x}',t') >= 2\Gamma(\vec{x})\delta_{ij}\delta(\vec{x}-\vec{x}')\delta(t-t') \end{array}\right\} \qquad (5)$$

[31, 65, 67, 68]. The above stochastic Langevin Hamiltonian equation (18) can be related to a probabilistic Fokker – Planck equation [31]:

$$\frac{1}{\Gamma(\vec{x})}\frac{\partial P}{\partial t} = \frac{\delta}{\delta\vec{u}}\cdot\left(\frac{\delta H}{\delta\vec{u}}P + \frac{\delta}{\delta\vec{u}}[\Gamma(\vec{x})P]\right) \qquad (6)$$

where $P = P\left(\{u_i(\vec{x},t)\},t\right)$ is the probability distribution function of the dynamical configuration $\{u_i(\vec{x},t)\}$ of the system at time t. The solution of the Fokker – Planck equation can be obtained as a functional path integral in the state space $\{u_i(\vec{x})\}$:

$$P\left(\{u_i(\vec{x})\},t\right) \quad \int\Delta\vec{Q}\exp(-S)P_0\left(\{u_i(\vec{x})\},t_0\right) \qquad (7)$$

where $P_0\left(\{u_i(\vec{x})\},t_0\right)$ is the initial probability distribution function in the extended configuration state space and $S = i\int Ldt$ is the stochastic action of the system obtained by the time integration of it's stochastic Lagrangian (L) [31, 69]. The stationary solution of the Fokker – Planck equation corresponds to the statistical minimum of the action and corresponds to a Gaussian state:

$$P\left(\{u_i\}\right) \quad \exp\left[-(1/\Gamma)H\left(\{u_i\}\right)\right] \qquad (8)$$

The path integration in the configuration field state space corresponds to the integration of the path probability for all the possible paths which start at the configuration state $\vec{u}(\vec{x},t_0)$ of the system and arrive at the final configuration state $\vec{u}(\vec{x},t)$. Langevin and F-P equations of classical statistics include a hidden relation with Feynman path integral formulation of QM [23, 31, 42, 43]. The F-P equation can be transformed to a Schrödinger equation:

$$i\frac{d}{dt}\hat{U}\left(t,t_0\right) = \hat{H}\cdot\hat{U}\left(t,t_0\right) \qquad (9)$$

by an appropriate operator Hamiltonian extension $H\left(u(\vec{x},t)\right) \Rightarrow \hat{H}\left(\hat{u}(\vec{x},t)\right)$ of the classical function (H) where now the field (u) is an operator distribution [31, 68]. From this point of view, the classical stochasticity of the macroscopic Langevin process can be considered as caused by a macroscopic quandicity revealed by the complex system as the F-K probability distribution P satisfies the quantum relation:

$$P\left(u,t\,|\,u,t_0\right) = \left\langle u\,|\,\hat{U}(t,t_0)\,|\,u_0\right\rangle \qquad (10)$$

This generalization of classical stochastic process as a quantum process could explain the spontaneous development of long-range correlations at the macroscopic level as an enlargement of the quantum entanglement character at critical states of complex systems. This interpretation is in faithful agreement with the introduction of complexity in sub-quantum processes and the chaotic – stochastic quantization of field theory [22-24, 44], as well as with scale relativity principles [6, 7, 49] and fractal extension of dynamics [4, 12, 13-15, 39] or the older Prigogine self-organization theory [1]. Here, we can argue in addition to previous description that quantum mechanics is subject gradually to a fractal generalization [7, 12, 13-15]. The fractal generalization of QM-QFT drifts along also the tools of quantum theory into the correspondent generalization of RG theory or path integration and Feynman diagrams. This generalization implies also the generalization of statistical theory as the new road for the unification of macroscopic and microscopic complexity.

If $P\left[\vec{u}(\vec{x},t)\right]$ is the probability of the entire field path in the field state space of the distributed system, then we can extend the theory of generating function of moments and cumulants for the probabilistic description of the paths [60, 69]. The n-point field correlation functions (n-points moments) can be estimated by using the field path probability distribution and field path (functional) integration:

$$\left\langle u(\vec{x}_1,t_1)u(\vec{x}_2,t_2)...u(\vec{x}_n,t_n)\right\rangle = \int \Delta\vec{u}\, P\left[\vec{u}\left(\vec{x},t\right)\right]u(\vec{x}_1,t_1)...u(\vec{x}_n,t_n) \quad (11)$$

For Gaussian random processes which happen to be near equilibrium the $n-$th point moments with $n>2$ are zero, correspond to Markov processes while far from equilibrium it is possible non-Gaussian (with infinite nonzero moments) processes to be developed. According to Haken [69] the characteristic function (or generating function) of the probabilistic description of paths:

$$\left[u(x,t)\right] \equiv \left(u(\vec{x}_1,t_1),u(\vec{x}_2,t_2),...,u(\vec{x}_n,t_n)\right) \quad (12)$$

is given by the relation:

$$\Phi_{path}\left(j_1(t_1),j_2(t_2),...,j_n(t_n)\right) = \left\langle \exp i\sum_{i=1}^{N} j_i u(\vec{x}_i,t_i)\right\rangle_{path} \quad (13)$$

while the path cumulants $K_s(t_{a_1}...t_{a_s})$ are given by the relations:

$$\Phi_{path}\left(j_1(t_1),j_2(t_2),...,j_n(t_n)\right) = \exp\left\{\sum_{s=1}^{\infty}\frac{i^s}{s!}\sum_{a_1,...a_s=1}^{n} K_s(t_{a_1}...t_{a_s})\cdot j_{a_1}...j_{a_s}\right\} (14)$$

and the $n-$point path moments are given by the functional derivatives:

$$\left\langle u(\vec{x}_1,t_1),u(\vec{x}_2,t_2),...,u(\vec{x}_n,t_n)\right\rangle = \left(\delta^n\Phi\left(\{j_i\}\right)/\delta j_1...\delta j_n\right)t\{j_i\}=0 \quad (15)$$

For Gaussian stochastic field processes the cumulants except the first two vanish $\left(k_3=k_4=...0\right)$. For non-Gaussian processes it is possible to be

developed long range correlations as the cummulants of higher than two order are non-zero [69]. This is the deeper meaning of non-equilibrium self-organization and ordering of complex systems. The characteristic function of the dynamical stochastic field system is related to the partition functions of its statistical description, while the cumulant development and multipoint moments generation can be related with the BBGKY statistical hierarchy of the statistics as well as with the Feynman diagrams approximation of the stochastic field system [41, 70]. For dynamical systems near equilibrium only the second order cumulants is non-vanishing, while far from equilibrium field fluctuations with higher – order non-vanishing cumulants can be developed.

Finally, we can understand how the non-linear dynamics correspond to self-organized states as the high-order (infinite) non-vanishing cumulants can produce the non-integrability of the dynamics. From this point of view the linear or non-linear instabilities of classical kinetic theory are inefficient to produce the non-Gaussian, holistic (non-local) and self-organized complex character of non-equilibrium dynamics. That is, far from equilibrium complex states can be developed including long range correlations of field and particles with non-Gaussian distributions of their dynamic variables. As we show in the next section such states such states reveal the necessity of new theoretical tools for their understanding which are much different from the classical linear or non-linear approximation of kinetic theory.

2.3 Strange attractors and Self-Organization

When the dynamics is strongly nonlinear then for the far from equilibrium processes it is possible to be created strong self-organization and intensive reduction of dimensionality of the state space, by an attracting low dimensional set with parallel development of long range correlations in space and time. The attractor can be periodic (limit cycle, limit m-torus), simply chaotic (mono-fractal) or strongly chaotic with multiscale and multifractal profile as well as attractors with weak chaotic profile known as SOC states. This spectrum of distinct dynamical profiles can be obtained as distinct critical points (critical states) of the nonlinear dynamics, after successive bifurcations as the control parameters change. The fixed points can be estimated by using a far from equilibrium renormalization process as it was indicated by Chang [31].

From this point of view phase transition processes can be developed by between different critical states, when the order parameters of the system are changing. The far from equilibrium development of chaotic (weak or strong) critical states include long range correlations and multiscale internal self organization. Now, these far from equilibrium self organized states, the equilibrium BG statistics and BG entropy, are transformed and replaced by the Tsallis extension of $q-$ statistics and Tsallis entropy. The extension of renormalization group theory and critical dynamics, under the $q-$ extension of partition function, free energy and path integral approach has been also

indicated [37, 70-72]. The multifractal structure of the chaotic attractors can be described by the generalized Rényi fractal dimensions:

$$D_{\bar{q}} = \frac{1}{\bar{q}-1} \lim_{\lambda \to 0} \frac{\log \sum_{i=1}^{N\lambda} p_i^{\bar{q}}}{\log \lambda}, \tag{16}$$

where $p_i \quad \lambda^{\alpha(i)}$ is the local probability at the location (i) of the phase space, λ is the local size of phase space and $a(i)$ is the local fractal dimension of the dynamics. The Rényi $\bar{q}$ numbers (different from the $q-$index of Tsallis statistics) take values in the entire region ($-\infty, +\infty$) of real numbers. The spectrum of distinct local fractal dimensions $\alpha(i)$ is given by the estimation of the function $f(\alpha)$ [73, 74] for which the following relations hold:

$$\sum p_i^{\bar{q}} = \int d\alpha' \, p(\alpha') \lambda^{-f(\alpha')} d\alpha' \tag{17}$$

$$\tau(\bar{q}) \equiv (\bar{q}-1)D\bar{q} \overset{\overset{min}{a}}{=} \bar{q}\alpha - f(\alpha) \tag{18}$$

$$a(\bar{q}) = \frac{d[\tau(\bar{q})]}{d\bar{q}} \tag{19}$$

$$f(\alpha) = \bar{q}\alpha - \tau(\bar{q}), \tag{20}$$

The physical meaning of these magnitudes included in relations (2.15-2.18) can be obtained if we identify the multifractal attractor as a thermodynamical object, where its temperature (T), free energy (F), entropy (S) and internal energy (U) are related to the properties of the multifractal attractor as follows:

$$\left. \begin{array}{ll} \bar{q} \Rightarrow \dfrac{1}{T}, & \tau(\bar{q}) = (\bar{q}-1)D_q \Rightarrow F \\[2mm] \alpha \Rightarrow U, & f(\alpha) \Rightarrow S \end{array} \right\} \tag{21}$$

This correspondence presents the relations (2.17 -2.19) as a thermodynamical Legendre transform [75]. When $\bar{q}$ increases to infinite ($+\infty$), which means, that we freeze the system ($T_{(q=+\infty)} \to 0$), then the trajectories (fluid lines) are closing on the attractor set, causing large probability values at regions of low fractal dimension, where $\alpha = \alpha_{\min}$ and $D_{\bar{q}} = D_{-\infty}$. Oppositely, when $\bar{q}$ decreases to infinite ($-\infty$), that is we warm up the system ($T_{(q=-\infty)} \to 0$) then the trajectories are spread out at regions of high fractal dimension ($\alpha \Rightarrow \alpha_{\max}$). Also for $\bar{q}' > \bar{q}$ we have $D_{\bar{q}'} < D_{\bar{q}}$ and $D_{\bar{q}} \Rightarrow D_{+\infty}(D_{-\infty})$ for

$\alpha \Rightarrow \alpha_{min}(\alpha_{max})$ correspondingly. However, the above description presents only a weak or limited analogy between multifractal and thermodynamical objects. The real thermodynamical character of the multifractal objects and multiscale dynamics was discovered after the definition by Tsallis [29] of the $q-$entropy related with the $q-$statistics as it was summarized previously in relations (2.1-2.13).

2.4 Intermittent Turbulence

According to previous description dissipative nonlinear dynamics can produce self-organization and long range correlations in space and time. In this case we can imagine the mirroring relationship between the phase space multifractal attractor and the corresponding multifractal turbulence dissipation process of the dynamical system in the physical space. Multifractality and multiscaling interaction, chaoticity and mixing or diffusion (normal or anomalous), all of them can be manifested in both the state (phase) space and the physical (natural) space as the mirroring of the same complex dynamics. We could say that turbulence is for complexity theory, what the blackbody radiation was for quantum theory, as all previous characteristics can be observed in turbulent states. The theoretical description of turbulence in the physical space is based upon the concept of the invariance of the HD or MHD equations upon scaling transformations to the space-time variables ($\vec{X}, t$) and velocity ($\vec{U}$):

$$\vec{X}' = \lambda \vec{X}, \ \vec{U}' = \lambda^{\alpha/3}\vec{U}, t' = \lambda^{1-a/3}t \tag{22}$$

and corresponding similar scaling relations for other physical variables [45, 76]. Under these scale transformations the dissipation rate of turbulent kinetic or dynamical field energy E_n (averaged over a scale $l_n = l_o\delta_n = R_o\delta_n$) rescales as ε_n:

$$\varepsilon_n \quad \varepsilon_0(l_n \backslash l_0)^{\alpha-1} \tag{23}$$

Kolmogorov [77] assumes no intermittency as the locally averaged dissipation rate, in reality a random variable, is independent of the averaging domain. This means in the new terminology of Tsallis theory that Tsallis q-indices satisfy the relation $q = 1$ for the turbulent dynamics in the three dimensional space. That is the multifractal (intermittency) character of the HD or the MHD dynamics consists in supposing that the scaling exponent α included in relations (2.20, 2.21) takes on different values at different interwoven fractal subsets of the $d-$dimensional physical space in which the dissipation field is embedded. The exponent α and for values $a < d$ is related with the degree of singularity in the field's gradient ($\frac{\partial A(x)}{\partial x}$) in the $d-$dimensional natural

space [78]. The gradient singularities cause the anomalous diffusion in physical or in phase space of the dynamics. The total dissipation occurring in a $d-$ dimensional space of size l_n scales also with a global dimension $D_{\overline{q}}$ for powers of different order $\overline{q}$ as follows:

$$\sum_n \varepsilon_n^{\overline{q}} l_n^d \quad l_n^{(\overline{q}-1)D_{\overline{q}}} = l_n^{\tau(\overline{q})}$$ (24)

Supposing that the local fractal dimension of the set $dn(a)$ which corresponds to the density of the scaling exponents in the region $(\alpha, \alpha + d\alpha)$ is a function $f_d(a)$ according to the relation:

$$dn(\alpha) \quad \ln^{-f_d(\alpha)} da$$ (25)

where d indicates the dimension of the embedding space, then we can conclude the Legendre transformation between the mass exponent $\tau(\overline{q})$ and the multifractal spectrum $f_d(a)$:

$$\left.\begin{array}{l} f_d(a) = a\overline{q} - (\overline{q}-1)(D_{\overline{q}} - d + 1) + d - 1 \\ a = \dfrac{d}{d\overline{q}}[(\overline{q}-1)(D_{\overline{q}} - d + 1)] \end{array}\right\}$$ (26)

For linear intersections of the dissipation field, that is $d = 1$ the Legendre transformation is given as follows:

$$f(a) = a\overline{q} - \tau(\overline{q}), \quad a = \frac{d}{d\overline{q}}[(q-1)D_q] = \frac{d}{d\overline{q}}\tau(\overline{q}), \quad \overline{q} = \frac{df(a)}{da}$$ (27)

The relations (24-27) describe the multifractal and multiscale turbulent process in the physical state. The relations (16-19) describe the multifractal and multiscale process on the attracting set of the phase space. From this physical point of view, we suppose the physical identification of the magnitudes $D_{\overline{q}}, a, f(a)$ and $\tau(\overline{q})$ estimates in the physical and the corresponding phase space of the dynamics. By using experimental timeseries we can construct the function $D_{\overline{q}}$ of the generalized Rényi $d-$ dimensional space dimensions, while the relations (26) allow the calculation of the fractal exponent (a) and the corresponding multifractal spectrum $f_d(a)$. For homogeneous fractals of the turbulent dynamics the generalized dimension spectrum $D_{\overline{q}}$ is constant and equal to the fractal dimension, of the support [76]. Kolmogorov [79] supposed that $D_{\overline{q}}$ does not depend on $\overline{q}$ as the dimension of the fractal support is $D_q = 3$. In this case the multifractal spectrum consists of the single point ($a = 1$ and $f(1) = 3$). The singularities of degree (a) of the dissipated fields,

fill the physical space of dimension d with a fractal dimension $F(a)$, while the probability $P(a)da$, to find a point of singularity (a) is specified by the probability density $P(a)da \quad \ln^{d-F(a)}$. The filling space fractal dimension $F(a)$ is related with the multifractal spectrum function $f_d(a) = F(a) - (d-1)$, while according to the distribution function $\Pi_{dis}(\varepsilon_n)$ of the energy transfer rate associated with the singularity a it corresponds to the singularity probability as $\Pi_{dis}(\varepsilon_n)d\varepsilon_n = P(a)da$ [78].

Moreover the partition function $\sum_i P_i^{\overline{q}}$ of the Rényi fractal dimensions estimated by the experimental timeseries includes information for the local and global dissipation process of the turbulent dynamics as well as for the local and global dynamics of the attractor set, as it is transformed to the partition function $\sum_i P_i^q = Z_q$ of the Tsallis q-statistic theory.

2.5 Fractal generalization of dynamics

Fractal integrals and fractal derivatives are related with the fractal contraction transformation of phase space as well as contraction transformation of space time in analogy with the fractal contraction transformation of the Cantor set [27, 53]. Also, the fractal extension of dynamics includes an extension of non-Gaussian scale invariance, related to the multiscale coupling and non-equilibrium extension of the renormalization group theory [38]. Moreover Tarasov [12], Coldfain [15], Cresson [14], El-Nabulsi [13] and other scientists generalized the classical or quantum dynamics in a continuation of the original break through of El-Naschie [4], Nottale [6], Castro [7] and others concerning the fractal generalization of physical theory.

According to Tarasov [12] the fundamental theorem of Riemann – Liouville fractional calculus is the generalization of the known integer integral – derivative theorem as follows:

if
$$F(x) = {}_\alpha I_x^a f(x) \tag{28}$$

then
$$_a D_x^a F(x) = f(x) \tag{29}$$

where ${}_a I_x^a$ is the fractional Riemann – Liouville according to:

$$_a I_x^a f(x) \equiv \frac{1}{\Gamma(a)} \int_a^x \frac{f(x')dx'}{(x-x')^{1-a}} \tag{30}$$

and ${}_a D_x^a$ is the Caputo fractional derivative according to:

$$_aD_x^a F(x) = {}_aI_x^{n-a}D_x^n F(x) =$$

$$= \frac{1}{\Gamma(n-a)}\int_a^x \frac{dx'}{(x-x')^{1+a-n}}\frac{dnF(x)}{dx^n} \tag{31}$$

for $f(x)$ a real valued function defined on a closed interval $[a,b]$.

In the next we summarize the basic concepts of the fractal generalization of dynamics as well as the fractal generalization of Liouville and MHD theory following Tarasov [12]. According to previous descriptions, the far from equilibrium dynamics includes fractal or multi-fractal distribution of fields and particles, as well as spatial fractal temporal distributions. This state can be described by the fractal generalization of classical theory: Lagrange and Hamilton equations of dynamics, Liouville theory, Fokker Planck equations and Bogoliubov hierarchy equations. In general, the fractal distribution of a physical quantity (M) obeys a power law relation:

$$M_D \quad M_0 \left(\frac{R}{R_0}\right)^D \tag{32}$$

where (M_D) is the fractal mass of the physical quantity (M) in a ball of radius (R) and (D) is the distribution fractal dimension. For a fractal distribution with local density $\rho(\vec{x})$ the fractal generalization of Euclidean space integration reads as follows:

$$M_D(W) = \int_W \rho(x)dV_D \tag{33}$$

where
$$dV_D = C_3\left(D,\vec{x}\right)dV_3 \tag{34}$$

and
$$C_3\left(D,\vec{x}\right) = \frac{2^{3-D}\Gamma(3/2)}{\Gamma(D/2)}\left|\vec{x}\right|^{D-3} \tag{35}$$

Similarly the fractal generalization of surface and line Euclidean integration is obtained by using the relations:

$$dS_d = C_2\left(d,\vec{x}\right)dS_2 \tag{36}$$

$$C_2\left(d,\vec{x}\right) = \frac{2^{2-d}}{\Gamma(d/2)}\left|\vec{x}\right|^{d-2} \tag{37}$$

for the surface fractal integration and

$$dl_\gamma = C_1(\gamma,\vec{x})dl_1 \tag{38}$$

$$C_1(\gamma,\vec{x}) = \frac{2^{1-\gamma}\Gamma(1/2)}{\Gamma(\gamma/2)}\left|\vec{x}\right|^{\gamma-1} \tag{39}$$

for the line fractal integration. By using the fractal generalization of integration and the corresponding generalized Gauss's and Stoke's theorems we can

transform fractal integral laws to fractal and non-local differential laws [12] The fractional generalization of classical dynamics (Hamilton Lagrange and Liouville theory) can be obtained by the fractional generalization of phase space quantative description [12]. For this we use the fractional power of coordinates:

$$X^a = \text{sgn}(x)|x|^a \tag{40}$$

where $\text{sgn}(x)$ is equal to +1 for $x \geq 0$ and equal to -1 for $x < 0$.

The fractional measure $M_a(B)$ of a $n - $ dimension phase space region (B) is given by the equation:

$$M_a(B) = \int_B g(a) d\mu_a(q, p) \tag{41}$$

where $d\mu_a(q, p)$ is a phase space volume element:

$$d\mu_a = \Pi \frac{dq_K^a \Lambda dp_K^a}{[a\Gamma(a)]^2} \tag{42}$$

where $g(a)$ is a numerical multiplier and $dq_K^a \Lambda dp_K^a$ means the wedge product.

The fractional Hamilton's approach can be obtained by the fractal generalization of the Hamilton action principle:

$$S = \int [pq - H(t, p, q)] dt \tag{43}$$

The fractal Hamilton equations:

$$\left(\frac{dq}{at} \right)^q = \Gamma(2 - a) p^{a-1} D_p^a H \tag{44}$$

$$D_t^a p = -D_q^a H \tag{45}$$

while the fractal generalization of the Lagrange's action principle:

$$S = \int L(t, q, u) dt \tag{46}$$

Corresponds to the fractal Lagrange equations:

$$D_q^a L - \Gamma(2 - a) D_t^a \left[D_U^a L \right]_{U = \dot{q}} = 0 \tag{47}$$

Similar fractal generalization can be obtained for dissipative or non-Hamiltonian systems [12]. The fractal generalization of Liouville equation is given also as:

$$\frac{\partial \tilde{p}_N}{\partial t} = L_N \tilde{p}_N \tag{48}$$

where $\tilde{p}_N$ and L_N are the fractal generalization of probability distribution function and the Liouville operator correspondingly. The fractal generalization

of Bogoliubov hierarchy can be obtained by using the fractal Liouville equation as well as the fractal Fokker Planck hydrodynamical - magnetohydrodynamical approximations [12].

The fractal generalization of classical dynamical theory for dissipative systems includes the non-Gaussian statistics as the fractal generalization of Boltzmann – Gibbs statistics.

Finally the far from equilibrium statistical mechanics can be obtained by using the fractal extension of the path integral method. The fractional Green function of the dynamics is given by the fractal generalization of the path integral:

$$K_{\mathrm{a}}\left(x_f,t_f;x_i,t_i\right) \quad \int_{x_i}^{x_f} D[x_{\mathrm{a}}(\tau)]\exp\left[\frac{i}{h}S_{\mathrm{a}}(\gamma)\right]$$
$$\sum_{\{\gamma\}}\exp\left[\frac{i}{h}S_{\mathrm{a}}(\gamma)\right] \tag{49}$$

where K_{a} is the probability amplitude (fractal quantum mechanics) or the two point correlation function (statistical mechanics), $D[x_{\mathrm{a}}(\tau)]$ means path integration on the sum $\{\gamma\}$ of fractal paths and $S_{\mathrm{a}}(\gamma)$ is the fractal generalization of the action integral [13]:

$$S_{\mathrm{a}}[\gamma] = \frac{1}{\Gamma(\mathrm{a})}\int_{x_i}^{x_f} L\left(D_\gamma^{\mathrm{a}}q(\tau),\tau\right)(t-\tau)^{\mathrm{a}-1}d\tau \tag{50}$$

2.6 The Highlights of Tsallis Theory

As we show in the next sections of this study, everywhere in space plasmas we can ascertain the presence of Tsallis statistics. This discovery is the continuation of a more general ascertainment of Tsallis q-extensive statistics from the macroscopic to the microscopic level [29].

In our understanding the Tsallis theory, more than a generalization of thermodynamics for chaotic and complex systems, or a non-equilibrium generalization of B-G statistics, can be considered as a strong theoretical vehicle for the unification of macroscopic and microscopic physical complexity. From this point of view Tsallis statistical theory is the other side of the modern fractal generalization of dynamics while its essence is nothing else than the efficiency of self-organization and development of long range correlations of coherent structures in complex systems.

From a general philosophical aspect, the Tsallis q-extension of statistics can be identified with the activity of an ordering principle in physical reality, which cannot be exhausted with the local interactions in the physical systems, as we noticed in previous sections.

2.6.1 The non-extensive entropy (S_q)

It was for first time that Tsallis [1], inspired by multifractal analysis, conceived that the Boltzmann – Gibbs entropy:

$$S_{BG} = -K \sum p_i \ln p_i \, , \, i = 1, 2, ..., N \tag{51}$$

is inefficient to describe all the complexity of non-linear dynamical systems. The Boltzmann – Gibbs statistical theory presupposes ergodicity of the underlying dynamics in the system phase space. The complexity of dynamics which is far beyond the simple ergodic complexity, it can be described by Tsallis non-extensive statistics, based on the extended concept of q − entropy:

$$S_q = k \left(1 - \sum_{i=1}^{N} p_i^q \right) / (q - 1) \tag{52}$$

for discrete state space or

$$S_q = k \left[1 - \int \left[p(x) \right]^q dx \right] / (q - 1) \tag{53}$$

for continuous state space.
For a system of particles and fields with short range correlations inside their immediate neighborhood, the Tsallis q − entropy S_q asymptotically leads to Boltzmann – Gibbs entropy (S_{BG}) corresponding to the value of $q = 1$. For probabilistically dependent or correlated systems A, B it can be proven that:

$$\begin{aligned} S_q(A+B) &= S_q(A) + S_q(B/A) + (1-q)S_q(A)S_q(B/A) \\ &= S_q(B) + S_q(A/B) + (1-q)S_q(B)S_q(A/B) \end{aligned} \tag{54}$$

Where $S_q(A) \equiv S_q\left(\left\{ p_i^A \right\} \right), S_q(B) \equiv Sq\left(\left\{ p_i^B \right\} \right), S_q(B/A)$ and $S_q(A/B)$ are the conditional entropies of systems A, B [29]. When the systems are probabilistically independent, then relation (3.1.4) is transformed to:

$$S_q(A+B) = S_q(A) + S_q(B) + (1-q)S_q(A)S_q(B) \tag{55}$$

The dependent (independent) property corresponds to the relation:

$$p_{ij}^{A+B} \neq p_i^A p_j^B \left(p_{ij}^{A+B} = p_i^A p_j^B \right) \tag{56}$$

Comparing the Boltzmann – Gibbs (S_{BG}) and Tsallis (S_q) entropies, we conclude that for non-existence of correlations S_{BG} is extensive whereas S_q for $q \neq 1$ is non-extensive. In contrast, for global correlations, large regions of

phase – space remain unoccupied. In this case S_q is non-extensive either $q = 1$ or $q \neq 1$.

2.6.2 The $q-$ extension of statistics and Thermodynamics

Non-linearity can manifest its rich complex dynamics as the system is removed far from equilibrium. The Tsallis $q-$ extension of statistics is indicated by the non-linear differential equation $dy / dx = y^q$. The solution of this equation includes the $q-$ extension of exponential and logarithmic functions:

$$e_q^x = \left[1 + (1-q)x\right]^{1/(1-q)} \tag{57}$$

$$\ln_q x = \left(x^{1-q} - 1\right)/\left(1-q\right) \tag{58}$$

and

$$p_{opt}(x) = e_q^{-\beta_q[f(x)-F_q]} / \int dx' e_q^{-\beta_q[f(x')-F_q]} \tag{59}$$

for more general $q-$ constraints of the forms $\left\langle f(x) \right\rangle_q = F_q$. In this way, Tsallis $q-$ extension of statistical physics opened the road for the $q-$ extension of thermodynamics and general critical dynamical theory as a non-linear system lives far from thermodynamical equilibrium. For the generalization of Boltzmann-Gibbs nonequilibrium statistics to Tsallis nonequilibrium q-statistics we follow Binney [41]. In the next we present q-extended relations, which can describe the non-equilibrium fluctuations and $n-$ point correlation function (G) can be obtained by using the Tsallis partition function Z_q of the system as follows:

$$G_q^n(i_1, i_2, ..., i_n) \equiv \left\langle s_{i_1}, s_{i_2}, ..., s_{i_n} \right\rangle_q = \frac{1}{z} \frac{\partial^n Z_q}{\partial j_{i_1} \cdot \partial j_{i_2}...\partial j_{i_n}} \tag{60}$$

Where $\left\{ s_i \right\}$ are the dynamical variables and $\left\{ j_i \right\}$ their sources included in the effective – Lagrangian of the system. Correlation (Green) equations (62) describe discrete variables, the $n-$ point correlations for continuous distribution of variables (random fields) are given by the functional derivatives of the functional partition as follows:

$$G_q^n(\vec{x}_1, \vec{x}_2, ..., \vec{x}_n) \equiv \left\langle \varphi(\vec{x}_1)\varphi(\vec{x}_2)...\varphi(\vec{x}_n) \right\rangle_q = \frac{1}{Z} \frac{\delta}{\delta J(\vec{x}_1)} ... \frac{\delta}{\delta J(\vec{x}_n)} Z_q(J) \tag{61}$$

where $\varphi(\vec{x})$ are random fields of the system variables and $j(\vec{x})$ their field sources. The connected $n-$ point correlation functions G_i^n are given by:

$$G_q^n(\vec{x}_1, \vec{x}_2, ..., \vec{x}_n) \equiv \frac{\delta}{\delta J(\vec{x}_1)} ... \frac{\delta}{\delta J(\vec{x}_n)} \log Z_q(J) \qquad (62)$$

The connected $n-$point correlations correspond to correlations that are due to internal interactions defined as [41]:

$$G_q^n(\vec{x}_1, \vec{x}_2, ..., \vec{x}_n) \equiv \left\langle \varphi(\vec{x}_1)...\varphi(\vec{x}_n) \right\rangle_q - \left\langle \varphi(x_1)...\varphi(x_n) \right\rangle_q \qquad (63)$$

The probability of the microscopic dynamical configurations is given by the general relation:

$$P(conf) = e^{-\beta S_{conf}} \qquad (64)$$

where $\beta = 1/kt$ and S_{conf} is the action of the system, while the partition function Z of the system is given by the relation:

$$Z = \sum_{conf} e^{-\beta S_{conf}} \qquad (65)$$

The $q-$extension of the above statistical theory can be obtained by the $q-$partition function Z_q. The $q-$partition function is related with the meta-equilibrium distribution of the canonical ensemble which is given by the relation:

$$p_i = e_q^{-\beta q(E_i - V_q)/Z_q} \qquad (66)$$

with

$$Z_q = \sum_{conf} e_q^{-\beta q(E_i - V_q)} \qquad (67)$$

and

$$\beta_q = \beta / \sum_{conf} p_i^q \qquad (68)$$

where $\beta = 1/KT$ is the Lagrange parameter associated with the energy constraint:

$$\left\langle E \right\rangle_q \equiv \sum_{conf} p_i^q E_i / \sum_{conf} p_i^q = U_q \qquad (69)$$

The $q-$extension of thermodynamics is related with the estimation of $q-$Free energy (F_q) the $q-$expectation value of internal energy $\left(U_q\right)$ the $q-$specific heat $\left(C_q\right)$ by using the $q-$partition function:

$$F_q \equiv U_q - TS_q = -\frac{1}{\beta} \ln qZ_q \qquad (70)$$

$$U_q = \frac{\partial}{\partial \beta} \ln q Z_q, \frac{1}{T} = \frac{\partial S_q}{\partial U_q} \tag{71}$$

$$C_q \equiv T \frac{\partial \delta_q}{\partial T} = \frac{\partial U_q}{\partial T} = -T \frac{\partial^2 F_q}{\partial T^2} \tag{72}$$

2.6.3 The Tsallis $q-$ extension of statistics via the fractal extension of dynamics

At the equilibrium thermodynamical state the underlying statistical dynamics is Gaussian ($q = 1$). As the system goes far from equilibrium the underlying statistical dynamics becomes non-Gaussian ($q \neq 1$). At the first case the phase space includes ergodic motion corresponding to normal diffusion process with mean-squared jump distances proportional to the time $\langle x^2 \rangle$ t whereas far from equilibrium the phase space motion of the dynamics becomes chaotically self-organized corresponding to anomalous diffusion process with mean-squared jump distances $\langle x^2 \rangle$ t^a, with $a < 1$ for sub-diffusion and $a > 1$ for super-diffusion. The equilibrium normal-diffusion process is described by a chain equation of the Markov-type:

$$W(x_3, t_3; x_1, t_1) = \int dx_2 W(x_3, t_3; x_2, t_2) W(x_2, t_2; x_1, t_1) \tag{73}$$

where $W(x,t; x',t')$ is the probability density for the motion from the dynamical state (x', t') to the state (x, t) of the phase space. The Markov process can be related to a random differential Langevin equation with additive white noise and a corresponding Fokker – Planck probabilistic equation [38] by using the initial condition:

$$\underset{\Delta t \to 0}{W}(x, y; \Delta t) = \delta(x - y) \tag{74}$$

This relation means no memory in the Markov process and help to obtain the expansion:

$$W(x, y; \Delta t) = \delta(x - y) + a(y; \Delta t) \delta'(x - y) + \frac{1}{2} b(y; \Delta t) \delta''(x - y) \tag{75}$$

where $A(y; \Delta t)$ and $B(y; \Delta t)$ are the first and second moment of the transfer probability function $W(x, y; \Delta t)$:

$$a(y; \Delta t) = \int dx(x - y) W(x, y; \Delta t) \equiv \langle\langle \Delta y \rangle\rangle \tag{76}$$

$$b(y;\Delta t) = \int dx (x-y)^2 W(x,y;\Delta t) \equiv \left\langle\left\langle (\Delta y)^2 \right\rangle\right\rangle \tag{77}$$

By using the normalization condition:

$$\int dy W(x,y;\Delta t) = 1 \tag{78}$$

we can obtain the relation:

$$a(y;\Delta t) = -\frac{1}{2}\frac{\partial b(y;\Delta t)}{\partial y} \tag{79}$$

The Fokker – Planck equation which corresponds to the Markov process can be obtained by using the relation:

$$\frac{\partial p(x,t)}{\partial t} = \lim_{\Delta t \to 0} \frac{1}{\Delta t}\left[\int_{-\infty}^{+\infty} dy W(x,y;\Delta t) p(y,t) - p(x,t) \right] \tag{80}$$

where $p(x,t) \equiv W(x,x_0;t)$ is the probability distribution function of the state (x,t) corresponding to large time asymptotic, as follows:

$$\frac{\partial P(x,t)}{\partial t} = -\nabla_x \left(A P(x,t) \right) + \frac{1}{2}\nabla_x^2 \left(B P(x,t) \right) \tag{81}$$

where $A(x)$ is the flow coefficient:

$$A(x,t) \equiv \lim_{\Delta t \to 0} \frac{1}{\Delta t}\left\langle\left\langle \Delta x \right\rangle\right\rangle \tag{82}$$

and $B(x,t)$ is the diffusion coefficient:

$$B(\vec{x},t) \equiv \lim_{\Delta t \to 0} \frac{1}{\Delta t}\left\langle\left\langle \Delta x^2 \right\rangle\right\rangle \tag{83}$$

The Markov process is a Gaussian process as the moments $\lim_{\Delta t \to 0} \left\langle\left\langle \Delta x^m \right\rangle\right\rangle$ for $m > 2$ are zero [63]. The stationary solutions of F-P equation satisfy the extremal condition of Boltzmann – Gibbs entropy:

$$S_{BG} = -K_B \int p(x) \ln p(x) dx \tag{84}$$

corresponding to the known Gaussian distribution:

$$p(x) \quad \exp\left(-x^2 / 2\sigma^2\right) \tag{85}$$

According to Zaslavsky [38] the fractal extension of Fokker – Planck (F-P) equation can be produced by the scale invariance principle applied for the phase space of the non-equilibrium dynamics. As it was shown by Zaslavsky for strong chaos the phase space includes self similar structures of islands inside

islands dived in the stochastic sea [38]. The fractal extension of the FPK equation (FFPK) can be derived after the application of a Renormalization group of anomalous kinetics (RGK):

$$\hat{R}_K : s' = \lambda_s S , \ t' = \lambda_t t$$

where s is a spatial variable and t is the time.

Correspondingly to the Markov process equations:

$$\frac{\partial^\beta p(\xi,t)}{\partial t^\beta} \equiv \lim_{\Delta t \to 0} \frac{1}{(\Delta t)^\beta} \left[W\left(\xi,\xi_0;t+\Delta t\right) - W\left(\xi,\xi_0;t\right) \right] \tag{86}$$

$$W(\xi,n;\Delta t) = \delta(\xi-n) + A(n;\Delta t)\delta^{(\alpha)}(\xi-n) + \frac{1}{2}B(n;\Delta t)\delta^{(2a)}(\xi-n) + \dots \tag{87}$$

as the space-time variations of probability W are considered on fractal space-time variables (t,ξ) with dimensions (β, a).

For fractal dynamics $a(n;\Delta t)$, $b(n;\Delta t)$ satisfy the equations:

$$a(n;\Delta t) = \int |n-\xi|^\alpha W(\xi,n;\Delta t)d\xi \equiv \left\langle\!\left\langle |\Delta\xi|^a \right\rangle\!\right\rangle \tag{88}$$

$$b(n;\Delta t) = \int |n-\xi|^{2\alpha} W(\xi,n;\Delta t)d\xi \equiv \left\langle\!\left\langle |\Delta\xi|^{2a} \right\rangle\!\right\rangle \tag{89}$$

and the limit equations:

$$A(\xi) = \lim_{\Delta t \to 0} \frac{a(\xi;\Delta t)}{(\Delta t)^\beta} \tag{90}$$

$$B(\xi) = \lim_{\Delta t \to 0} \frac{b(\xi;\Delta t)}{(\Delta t)^\beta} \tag{91}$$

By them we can obtain the FFPK equation.

Far from equilibrium the non-linear dynamics can produce phase space topologies corresponding to various complex attractors of the dynamics. In this case the extended complexity of the dynamics corresponds to the generalized strange kinetic Langevin equation with correlated and multiplicative noise components and extended fractal Fokker – Planck - Kolmogorov equation (FFPK) [38, 80]. The $q-$extension of statistics by Tsallis can be related with the strange kinetics and the fractal extension of dynamics through the Levy process:

$$P\left(x_n,t_n;x_0t_0\right) = \int dx_1\dots dx_{N-1}P\left(x_N,t_N;x_{N-1},t_{N-1}\right)\dots P\left(x_1,t_1;x_0,t_0\right) \tag{92}$$

The Levy process can be described by the fractal F-P equation:

$$\frac{\partial^\beta P(x,t)}{\partial t^\beta} = \frac{\partial^a}{\partial(-x)^a}\left[A(x)P(x,t) \right] + \frac{\partial^{a+1}}{\partial(-x)^{a+1}}\left[B(x)P(x,t) \right] \tag{93}$$

where $\partial^{\beta}/\partial t^{\beta}$, $\partial^{a}/\partial(-x)^{a}$ and $\partial^{a+1}/\partial(-x)^{a+1}$ are the fractal time and space derivatives correspondingly [38]. The stationary solution of the F F-P equation for large x is the Levy distribution $P(x)$ $x^{-(1+\gamma)}$. The Levy distribution coincides with the Tsallis $q-$ extended optimum distribution (3.2.4) for $q=(3+\gamma)/(1+\gamma)$. The fractal extension of dynamics takes into account non-local effects caused by the topological heterogeneity and fractality of the self-organized phase – space. Also the fractal geometry and the complex topology of the phase – space introduce memory in the complex dynamics which can be manifested as creation of long range correlations, while, oppositely, in Markov process we have complete absence of memory.

In general, the fractal extension of dynamics as it was done until now from Zaslavsky, Tarasov and other scientists indicate the internal consistency of Tsallis $q-$ statistics as the non-equilibrium extension of B-G statistics with the fractal extension of classical and quantum dynamics. Concerning the space plasmas the fractal character of their dynamics has been indicated also by many scientists. Indicatively, we refer the fractal properties of sunspots and their formation by fractal aggregates as it was shown by Zelenyi and Milovanov [30, 32], the anomalous diffusion and intermittent turbulence of the solar convection and photospheric motion shown by Ruzmakin et al. [33], the multi-fractal and multi-scale character of space plasmas indicated by Lui [46] and Pavlos et al. [37].

Finally we must notice the fact that the fractal extension of dynamics identifies the fractal distribution of a physical magnitude in space and time according to the scaling relation $M(R)$ R^{a} with the fractional integration as an integration in a fractal space [12]. From this point of view it could be possible to conclude the novel concept that the non-equilibrium $q-$ extension of statistics and the fractal extension of dynamics are related with the fractal space and time themselves [6, 39, 80].

2.6.4 Fractal acceleration and fractal energy dissipation

The problem of kinetic or magnetic energy dissipation in fluid and plasmas as well as the bursty acceleration processes of particles at flares, magnetospheric plasma sheet and other regions of space plasmas is an old and yet resisting problem of fluids or space plasma science.

Normal Gaussian diffusion process described by the Fokker – Planck equation is unable to explain either the intermittent turbulence in fluids or the bursty character of energetic particle acceleration following the bursty development of inductive electric fields after turbulent magnetic flux change in plasmas [81]. However the fractal extension of dynamics and Tsallis extension of statistics

indicate the possibility for a mechanism of fractal dissipation and fractal acceleration process in fluids and plasmas.

According to Tsallis statistics and fractal dynamics the super-diffusion process:

$$\left\langle R^2 \right\rangle \quad t^\gamma \tag{94}$$

with $\gamma > 1$ ($\gamma = 1$ for normal diffusion) can be developed at systems far from equilibrium. Such process is known as intermittent turbulence or as anomalous diffusion which can be caused by Levy flight process included in fractal dynamics and fractal Fokker – Planck Kolmogorov equation (FFPK). The solution of FFPK equation [38] corresponds to double (temporal, spatial) fractal characteristic function:

$$P(k,t) = \exp\left(-constxt^\beta \left|k\right| a\right) \tag{95}$$

Where $P(k,t)$ is the Fourier transform of asymptotic distribution function:

$$P(\xi,t) \quad constxt^\beta / \xi^{1+\alpha}, \ (\xi \to \infty) \tag{96}$$

This distribution is scale invariant with mean displacement:

$$\left\langle \left|\xi\right|^\alpha \right\rangle \quad constxt^\beta, \ (t \to \infty) \tag{97}$$

According to this description, the flights of multi-scale and multi-fractal profile can explain the intermittent turbulence of fluids, the bursty character of magnetic energy dissipation and the bursty character of induced electric fields and charged particle acceleration in space plasmas as well as the non-Gaussian dynamics of brain-heart dynamics. The fractal motion of charged particles across the fractal and intermittent topologies of magnetic – electric fields is the essence of strange kinetic [38, 80]. Strange kinetics permits the development of local sources with spatial fractal – intermittent condensation of induced electric-magnetic fields in brain, heart and plasmas parallely with fractal – intermittent dissipation of magnetic field energy in plasmas and fractal acceleration of charged particles. Such kinds of strange accelerators in plasmas can be understood by using the Zaslavsky studies for Hamiltonian chaos in anomalous multi-fractal and multi-scale topologies of phase space [38]. Generally the anomalous topology of phase space and fractional Hamiltonian dynamics correspond to dissipative non-Hamiltonian dynamics in the usual phase space [12]. The most important character of fractal kinetics is the wandering of the dynamical state through the gaps of cantori which creates effective barriers for diffusion and long range Levy flights in trapping regions of the phase space. Similar Levy flights processes can be developed by the fractal dynamics and intermittent turbulence of the complex systems.

In this theoretical framework it is expected the existence of Tsallis non extensive entropy and q-statistics in non-equilibrium distributed complex systems as, fluids, plasmas or brain and heart systems which are studied in the next section of this work. The fractal dynamics corresponding to the non-extensive Tsallis $q-$ statistical character of the probability distributions in the

distributed complex systems indicate the development of a self-organized and globally correlated parts of active regions in the distributed dynamics. This character can be related also with deterministic low dimensional chaotic profile of the active regions according to Pavlos et al. [37,].

3. Theoretical expectations through Tsallis statistical theory and fractal dynamics

Tsallis $q-$statistics as well as the non-equilibrium fractal dynamics indicate the multi-scale, multi-fractal chaotic and holistic dynamics of space plasmas. Before we present experimental verification of the theoretical concepts described in previous studies as concerns space plasmas in this section we summarize the most significant theoretical expectations.

3.1 The $q-$triplet of Tsallis

The non-extensive statistical theory is based mathematically on the nonlinear equation:

$$\frac{dy}{dx} = y^q \text{ , } (y(0) = 1, q \in \Re)$$

(98)

with solution the $q-$exponential function defined previously in equation (2.2). The solution of this equation can be realized in three distinct ways included in the $q-$triplet of Tsallis: ($q_{sen}, q_{stat}, q_{rel}$). These quantities characterize three physical processes which are summarized here, while the $q-$triplet values characterize the attractor set of the dynamics in the phase space of the dynamics and they can change when the dynamics of the system is attracted to another attractor set of the phase space. The equation (2.36) for $q = 1$ corresponds to the case of equilibrium Gaussian Boltzmann-Gibbs (BG) world [35, 36]. In this case of equilibrium BG world the $q-$triplet of Tsallis is simplified to ($q_{sen} = 1, q_{stat} = 1, q_{rel} = 1$).

a. The q_{stat} index and the non-extensive physical states

According to [35, 36] the long range correlated metaequilibrium non-extensive physical process can be described by the nonlinear differential equation:

$$\frac{d(p_i Z_{stat})}{dE_i} = -\beta q_{stat}(p_i Z_{stat})^{q_{stat}}$$

(99)

The solution of this equation corresponds to the probability distribution:

$$p_i = e_{q_{stat}}^{-\beta_{stat} E_i} / Z_{q_{stat}}$$

(100)

where $\beta_{q_{stat}} = \dfrac{1}{KT_{stat}}$, $Z_{stat} = \displaystyle\sum_j e^{-\beta_{q_{stat}} E_j}$.

Then the probability distribution function is given by the relations:

$$p_i \propto \left[1 - (1-q)\beta_{q_{stat}} E_i \right]^{1/1-q_{stat}} \tag{101}$$

for discrete energy states $\{E_i\}$ by the relation:

$$p(x) \propto \left[1 - (1-q)\beta_{q_{stat}} x^2 \right]^{1/1-q_{stat}} \tag{102}$$

for continuous X states $\{X\}$, where the values of the magnitude X correspond to the state points of the phase space.

The above distributions functions (2.46, 2.47) correspond to the attracting stationary solution of the extended (anomalous) diffusion equation related with the nonlinear dynamics of system [36]. The stationary solutions $P(x)$ describe the probabilistic character of the dynamics on the attractor set of the phase space. The non-equilibrium dynamics can be evolved on distinct attractor sets depending upon the control parameters values, while the q_{stat} exponent can change as the attractor set of the dynamics changes.

b. The q_{sen} index and the entropy production process

The entropy production process is related to the general profile of the attractor set of the dynamics. The profile of the attractor can be described by its multifractality as well as by its sensitivity to initial conditions. The sensitivity to initial conditions can be described as follows:

$$\frac{d\xi}{d\tau} = \lambda_1 \xi + (\lambda_q - \lambda_1)\xi^q \tag{103}$$

where ξ describes the deviation of trajectories in the phase space by the relation: $\xi \equiv \lim_{\Delta(x)\to 0}\{\Delta x(t) \setminus \Delta x(0)\}$ and $\Delta x(t)$ is the distance of neighboring trajectories [82]. The solution of equation (2.41) is given by:

$$\xi = \left[1 - \frac{\lambda q_{sen}}{\lambda_1} + \frac{\lambda q_{sen}}{\lambda_1} e^{(1-q_{sen})\lambda_1 t} \right]^{\frac{1}{1-q}} \tag{104}$$

The q_{sen} exponent can be also related with the multifractal profile of the attractor set by the relation:

$$\frac{1}{q_{sen}} = \frac{1}{a_{min}} - \frac{1}{a_{max}} \tag{105}$$

where $a_{min}(a_{max})$ corresponds to the zero points of the multifractal exponent spectrum $f(a)$ [36, 79, 82]. That is $f(a_{min}) = f(a_{max}) = 0$.

The deviations of neighboring trajectories as well as the multifractal character of the dynamical attractor set in the system phase space are related to the chaotic phenomenon of entropy production according to Kolmogorov – Sinai entropy production theory and the Pesin theorem [36]. The $q -$ entropy production is summarized in the equation:

$$K_q \equiv \lim_{t \to \infty} \lim_{W \to \infty} \lim_{N \to \infty} \frac{<S_q>(t)}{t}. \qquad (106)$$

The entropy production (dS_q/t) is identified with K_q, as W are the number of non-overlapping little windows in phase space and N the state points in the windows according to the relation $\sum_{i=1}^{W} N_i = N$. The S_q entropy is estimated by the probabilities $P_i(t) \equiv N_i(t)/N$. According to Tsallis the entropy production K_q is finite only for $q = q_{sen}$ [36, 82].

c. The q_{rel} index and the relaxation process

The thermodynamical fluctuation – dissipation theory [63] is based on the Einstein original diffusion theory (Brownian motion theory). Diffusion process is the physical mechanism for extremization of entropy. If ΔS denote the deviation of entropy from its equilibrium value S_0, then the probability of the proposed fluctuation that may occur is given by:

$$P \quad \exp(\Delta s/k). \qquad (107)$$

The Einstein – Smoluchowski theory of Brownian motion was extended to the general Fokker – Planck diffusion theory of non-equilibrium processes. The potential of Fokker – Planck equation may include many metaequilibrium stationary states near or far away from the basic thermodynamical equilibrium state. Macroscopically, the relaxation to the equilibrium stationary state can be described by the form of general equation as follows:

$$\frac{d\Omega}{d\tau} \quad -\frac{1}{\tau}\Omega, \qquad (108)$$

where $\Omega(t) \equiv [O(t) - O(\infty)]/[O(0) - O(\infty)]$ describes the relaxation of the macroscopic observable $O(t)$ relaxing towards its stationary state value. The non-extensive generalization of fluctuation – dissipation theory is related to the general correlated anomalous diffusion processes [36]. Now, the equilibrium relaxation process (2.46) is transformed to the metaequilibrium non-extensive relaxation process:

$$\frac{d\Omega}{dt} = -\frac{1}{T_{q_{rel}}}\Omega^{q_{rel}}$$ (109)

the solution of this equation is given by:

$$\Omega(t) \quad e_{q_{rel}}^{-t/\tau_{rel}}$$ (110)

The autocorrelation function $C(t)$ or the mutual information $I(t)$ can be used

as candidate observables $\Omega(t)$ for the estimation of q_{rel}. However, in contrast
to the linear profile of the correlation function, the mutual information includes
the non linearity of the underlying dynamics and it is proposed as a more
faithful index of the relaxation process and the estimation of the Tsallis
exponent q_{rel}.

3.2 Measures of Multifractal Intermittence Turbulence

In the following, we follow Arimitsu and Arimitsu [78] for the theoretical
estimation of significant quantitative relations which can also be estimated
experimentally. The probability singularity distribution $P(a)$ can be estimated
as extremizing the Tsallis entropy functional S_q. According to Arimitsu and
Arimitsu [78] the extremizing probability density function $P(a)$ is given as a
$q-$ exponential function:

$$P(a) = Z_q^{-1}[1-(1-q)\frac{(a-a_0)^2}{2X/\ln 2}]^{\frac{1}{1-q}}$$ (111)

where the partition function Z_q is given by the relation:

$$Z_q = \sqrt{2X/[(1-q)\ln 2]}\ B(1/2, 2/1-q),$$ (112)

and $B(a,b)$ is the Beta function. The partition function Z_q as well as the
quantities X and q can be estimated by using the following equations:

$$\left.\begin{aligned}\sqrt{2X} &= \left[\sqrt{a_0^2+(1-q)^2}-(1-q)\right]/\sqrt{b}\\ b &= (1-2^{-(1-q)})/[(1-q)\ln_2]\end{aligned}\right\}$$ (113)

We can conclude for the exponent's spectrum $f(a)$ by using the
relation $P(a) \approx \ln^{d-F(a)}$ as follows:

$$f(a) = D_0 + \log_2[1-(1-q)\frac{(a-a_o)^2}{2X/\ln 2}]/(1-q)^{-1} \qquad (114)$$

where a_0 corresponds to the $q-$ expectation (mean) value of a through the relation:

$$< (a-a_0)^2 >_q = (\int daP(a)^q (a-a_0)^q)/\int daP(a)^q \qquad (115)$$

while the $q-$ expectation value a_0 corresponds to the maximum of the function $f(a)$ as $df(a)/da\,|\,a_0 = 0$. For the Gaussian dynamics ($q \to 1$) we have mono-fractal spectrum $f(a_0) = D_0$. The mass exponent $\tau(\overline{q})$ can be also estimated by using the inverse Legendre transformation: $\tau(\overline{q}) = a\overline{q} - f(a)$ (relations 2.24 – 2.25) and the relation (2.29) as follows:

$$\tau(\overline{q}) = \overline{q}a_0 - 1 - \frac{2X\overline{q}^2}{1+\sqrt{C_{\overline{q}}}} - \frac{1}{1-q}[1-\log_2(1+\sqrt{C_{\overline{q}}})], \qquad (116)$$

Where $C_{\overline{q}} = 1 + 2\overline{q}^2(1-q)X\ln 2$.

The relation between a and q can be found by solving the Legendre transformation equation $\overline{q} = df(a)/da$. Also if we use the equation (2.29) we can obtain the relation:

$$a_{\overline{q}} - a_0 = (1-\sqrt{C_{\overline{q}}})/[\overline{q}(1-q)\ln 2] \qquad (117)$$

The $q-$ index is related to the scaling transformations (2.20) of the multifractal nature of turbulence according to the relation $q = 1 - a$. Arimitsu and Arimitsu [78] estimated the $q-$ index by analyzing the fully developed turbulence state in terms of Tsallis statistics as follows:

$$\frac{1}{1-q} = \frac{1}{a_-} - \frac{1}{a_+} \qquad (118)$$

where $a_{\pm}$ satisfy the equation $f(a_{\pm}) = 0$ of the multifractal exponents spectrum $f(a)$. This relation can be used for the estimation of $q_{sen}-$ index included in the Tsallis $q-$ triplet (see next section).

The above analysis based at the extremization of Tsallis entropy can be also used for the theoretical estimation of the structure functions scaling exponent spectrum $J(p)$ of the $S_p(\tau)$, where $p = 1, 2, 3, 4, ...$ The structure functions were first introduced by Kolmogorov [79] defined as statistical moments of the field increments:

$$S_p(\overrightarrow{r}) = <|u(\vec{x}+\vec{d}) - u(\vec{x})|^p> = <|\delta u_n|^p> \qquad (119)$$

$$S_p(\vec{r}) = <| u(\vec{x} + \Delta\vec{x}) - u(\vec{x}) |^p > \qquad (120)$$

After discretization of $\Delta\vec{x}$ displacement the above relation can be identified to:

$$Sp(l^n) = <| \delta u_n |^p > \qquad (121)$$

The field values $u(\vec{x})$ can be related with the energy dissipation values ε_n by the general relation $\varepsilon_n = (\delta u_n)^3 / l^n$ in order to obtain the structure functions as follows:

$$S_p(l^n) = <(\varepsilon_n / \varepsilon_0)^p> = <\delta_n^{p(a-1)}> = \delta_n^{j(p)} \qquad (122)$$

where the averaging processes $<...>$ is defined by using the probability function $P(a)da$ as $<...> = \int da(...)P(a)$. By this, the scaling exponent $J(p)$ of the structure functions is given by the relation:

$$J(p) = 1 + \tau(\bar{q} = \frac{p}{3}) \qquad (123)$$

By following Arimitsu [78] the relation (2.30) leads to the theoretical prediction of $J(p)$ after extremization of Tsallis entropy as follows:

$$J(p) = \frac{a_0 p}{3} - \frac{2Xp^2}{q(1+\sqrt{C_{p/3}})} - \frac{1}{1-q}[1 - \log_2(1 + \sqrt{C_{p/3}})] \qquad (124)$$

The first term $a_0 p / 3$ corresponds to the original of known Kolmogorov theory (K41) according to which the dissipation of field energy ε_n is identified with the mean value ε_0 according to the Gaussian self-similar homogeneous turbulence dissipation concept, while $a_0 = 1$ according to the previous analysis for homogeneous turbulence. According to this concept the multifractal spectrum consists of a single point. The next terms after the first in the relation (2.39) correspond to the multifractal structure of intermittence turbulence indicating that the turbulent state is not homogeneous across spatial scales. That is, there is a greater spatial concentration of turbulent activity at smaller than at larger scales. According to Abramenko [36] the intermittent multifractal (inhomogeneous) turbulence is indicated by the general scaling exponent $J(p)$ of the structure functions according to the relation:

$$J(p) = \frac{p}{3} + T^{(u)}(p) + T^{(F)}(p), \qquad (125)$$

where the $T^{(u)}(p)$ term is related with the dissipation of kinetic energy and the $T^{(F)}(p)$ term is related to other forms of field's energy dissipation as the magnetic energy at MHD turbulence [36, 83] .

The scaling exponent spectrum $J(p)$ can be also used for the estimation of the intermittency exponent μ according to the relation:

$$S(2) \equiv\; < \varepsilon^2 / \varepsilon > \quad \delta_n^\mu = \delta_n^{J(2)} \tag{127}$$

from which we conclude that $\mu = J(2)$. The intermittency turbulence correction to the law $P(f) \quad f^{-5/3}$ of the energy spectrum of Kolmogorov's theory is given by using the intermittency exponent:

$$P(f) \quad f^{-(5/3+\mu)} \tag{128}$$

The previous theoretical description can be used for the theoretical interpretation of the experimentally estimated structure function, as well as for relating physically the results of data analysis with Tsallis statistical theory, as it is described in the next sections.

4. Comparison of theory with the observations

4.1 The Tsallis q-statistics

  The traditional scientific point of view is the priority of dynamics over statistics. That is dynamics creates statistics. However for complex system their holistic behaviour does not permit easily such a simplification and division of dynamics and statistics. Tsallis $q-$statistics and fractal or strange kinetics are two faces of the same complex and holistic (non-reductionist) reality. As Tsallis statistics is an extension of B-G statistics, we can support that the thermic and the dynamical character of a complex system is the manifestation of the same physical process which creates extremized thermic states (extremization of Tsallis entropy), as well as dynamically ordered states. From this point of view the Feynman path integral formulation of physical theory [84] indicates the indivisible thermic and dynamical character of physical reality. After this general investment in the following, we present evidence of Tsallis non-extensive $q-$statistics for space plasmas. The Tsallis statistics in relation with fractal and chaotic dynamics of space plasmas will be presented in a short coming series of publications.

In next sections we present estimations of Tsallis statistics for various kinds of space plasma's systems. The q_{stat} Tsallis index was estimated by using the observed Probability Distribution Functions (PDF) according to the Tsallis q-exponential distribution:

$$PDF\left[\Delta Z\right] \equiv A_q \left[1 + \left(q-1\right)\beta_q\left(\Delta Z\right)^2\right]^{\frac{1}{1-q}}, \tag{129}$$

where the coefficients A_q, β_q denote the normalization constants and $q \equiv q_{stat}$ is the entropic or non-extensivity factor ($q_{stat} \leq 3$) related to the size of the tail

in the distributions. Our statistical analysis is based on the algorithm described in [56]. We construct the $PDF\left[\Delta Z\right]$ which is associated to the first difference $\Delta Z = Z_{n+1} - Z_n$ of the experimental sunspot time series, while the ΔZ range is subdivided into little ``cells'' (data binning process) of width δz, centered at z_i so that one can assess the frequency of $\varDelta z$-values that fall within each cell/bin. The selection of the cell-size δz is a crucial step of the algorithmic process and its equivalent to solving the binning problem: a proper initialization of the bins/cells can speed up the statistical analysis of the data set and lead to a convergence of the algorithmic process towards the exact solution. The resultant histogram is being properly normalized and the estimated q-value corresponds to the best linear fitting to the graph $\ln_q(p(z_i))\ vs\ z_i^2$. Our algorithm estimates for each $\delta_q = 0,01$ step the linear adjustment on the graph under scrutiny (in this case the $\ln_q(p(z_i))\ vs\ z_i^2$ graph) by evaluating the associated correlation coefficient *(CC)*, while the best linear fit is considered to be the one maximizing the correlation coefficient. The obtained q_{stat}, corresponding to the best linear adjustment is then being used to compute the following equation:

$$G_q(\beta, z) = \frac{\sqrt{\beta}}{C_q} e_q^{-\beta z^2}$$

(130)

where $C_q = \sqrt{\pi} \cdot \Gamma(\frac{3-q}{2(q-1)}) / \sqrt{q-1} \cdot \Gamma(\frac{1}{q-1})$, $1 < q < 3$ for different β-values. Moreover, we select the β-value minimizing the $\sum_i [G_{q_{sstat}}(\beta, z_i) - p(z_i)]^2$, as proposed again in [56].

In the following we present the estimation of Tsallis statistics q_{stat} for various cases of space plasma system. Especially, we study the $q-$statistics for the following space plasma complex systems: I Magnetospheric system, II Solar Wind (magnetic cloud), III Solar activity, IV Cosmic stars, IIV Cosmic Rays.

4.2 Cardiac Dynamics

For the study of the q-statistics we used measurements from the cardiac and especially the heart rate variability timeseries which includes a multivariate data set recorded from a patient in the sleep laboratory of the Beth Israel Hospital in Boston, Massachusetts. The heart rate was determined by measuring the time between the QRS complexes in the electrocardiogram, taking the

inverse, and then converting this to an evenly sampled record by interpolation. They were converted from 250 Hz to 2 Hz data by averaging over a 0.08 second window at the times of the heart rate samples.

Figure 1a presents the experimental time series, while Fig.1b presents the q-Gaussian functions G_q, corresponding to the time series under scrunity. The q-Gaussian function presents the best fitting of the experimental distribution function $P(z)$ estimated for the value $q_{stat} = 1.26 \pm 0.1$ for the stationary heart variability time series. The q-value was estimated by the linear correlation fitting between $\ln_q P(z_i)$ and $(z_i)^2$, shown in fig. 1c, were $P(z)$ corresponds to the experimental distribution functions, according to the description in section 4.1. The fact that the heart's variability observations obey to non-extensive Tsallis with a $q -$ values higher than the Gaussian case ($q = 1$) permit to conclude for the heart's variability dynamics case the existence of q-statistics .
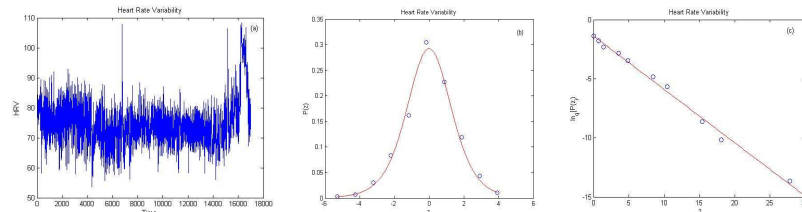
Figure 1: (a) Time series of heart rate variability **(b)** PDF $P(z_i)$ vs. z_i q Guassian function that fits $P(z_i)$ for the heart rate variability **(c)** Linear Correlation between $\ln_q P(z_i)$ and $(z_i)^2$ where q = 1.26 ± 0.10 for the heart rate variability.

4.3 Brain Epilepsy Dynamics

In this section we present the q-statistics obtained from real EEG timeseries from epileptic patients during seizure attack. Each EEG timeseries consisting of 3.750 points. The width of the timeseries is ranging from -1,000 Volt to 1,000 Volt.

In Figure 2a the experimental time series during the epilepsy is presented. The q-value was found to be $q_{stat} = 1.64 \pm 0.14$. The results of the q-statistics analysis are shown in Figure 2b and Figure 2c.
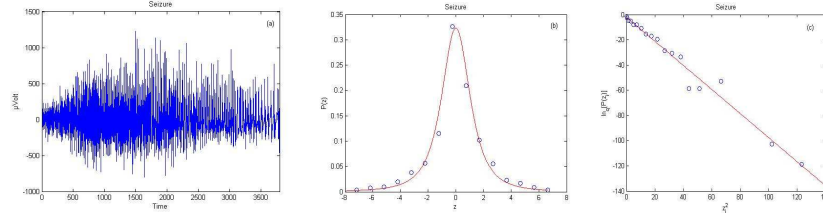
Figure 2: (a) Time series of seizure state **(b)** PDF $P(z_i)$ vs. z_i q Guassian function that fits $P(z_i)$ for the seizure state **(c)** Linear Correlation between $\ln_q P(z_i)$ and $(z_i)^2$ where $q = 1.63 \pm 0.14$ for the seizure state.

4.4 Eartquakes Dynamics

In this sub-section we present the q-statistics of the experimental data from earthquakes in the region of whole Greece with magnitude greater from 4 and time period 1964-2004. The data set was found from the National Observatory of Athens (NOA).

In Figure 3a the time series of Interevent Times is presented, while the corresponding q-value is shown in Figure 3b and was found to be $q_{stat} = 2.28 \pm 0.12$. In Figure 3d we present the experimental time series of Magnitude data. The q-statistics for this case are presented in Figure 3e. The corresponding q-value was found to be $q_{stat} = 1.77 \pm 0.09$. The results reveal clearly non-Gaussian statistics for the earthquake Interevent Times and Magnitude data. The results showed the existence of q-statistics and the non-Gaussianity of the data sets.

4.5 Atmospheric Dynamics

In this sub-section we study the q-statistics for the air temperature and rain fall experimental data sets from the weather station 20046 Polar GMO in E.T. Krenkelja for the period 1/1/1960 – 31/12/1960. In Figure 4(a,d) the experimental time series from temperature and rainfall correspondingly are presented and in the Figure 4(b,c,e,f) the results of the q-statistics analysis are shown. The estimated q-values were found to be for the temperature data set and for the rainfall data set. In both cases we observed clearly non Gaussian statistics.
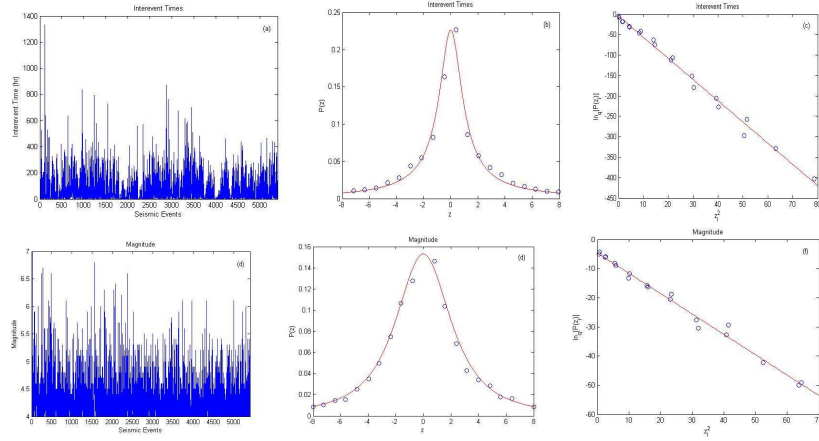
Figure 3: (a) Time series of Interevent Times **(b)** PDF $P(z_i)$ vs. z_i q Guassian function that fits $P(z_i)$ for the Interevent Times **(c)** Linear Correlation between $\ln_q P(z_i)$ and $(z_i)^2$ where q = 2.28 ± 0.12 for the Interevent Times **(d)** Time series of Magnitude **(e)** PDF $P(z_i)$ vs. z_i q Gaussian function that fits $P(z_i)$ for the Magnitude **(f)** Linear Correlation between $\ln_q P(z_i)$ and $(z_i)^2$ where q = 1.77 ± 0.09 for the Magnitude.
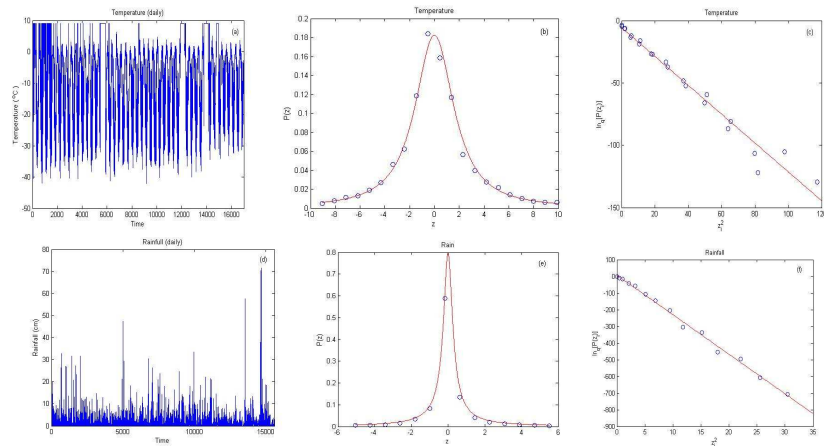

Figure 4: (a) Time series of Temperature **(b)** PDF $P(z_i)$ vs. z_i q Guassian function that fits $P(z_i)$ for the Temperature **(c)** Linear Correlation between $\ln_q P(z_i)$ and $(z_i)^2$ where q = 1.89 ± 0.08 for the Temperature **(d)** Time series of Rainfall **(e)** PDF $P(z_i)$ vs. z_i q Gaussian function that fits $P(z_i)$ for the Rainfall **(f)** Linear Correlation between $\ln_q P(z_i)$ and $(z_i)^2$ where q = 2.21 ± 0.06 for the Rainfall.

4.6 Magnetospheric Magneto Hydro Dynamics (MHD) Dynamics

The estimation of V_x, B_z Tsallis statistics during the substorm period is presented in fig.5(a-f). Fig. 2(a,d) shows the experimental time series corresponding to spacecraft observations of bulk plasma flows V_x and magnetic field B_z component. Fig. 2(b,e) presents the estimated q-values for the V_x plasma velocity time series and for the magnetic field B_z component time series. The q-values of the signals under scrutiny were found to be $q_{stat} = 1.98 \pm 0.06$ for the V_x plasma velocity time series and $q_{stat} = 2.05 \pm 0.04$ for the magnetic field B_z component. The fact that the magnetic field and plasma flow observations obey to non-extensive Tsallis with $q-$ values much higher than the Gaussian case ($q = 1$) permit to conclude for magnetospheric plasma the existence of non-equilibrium MHD anomalous diffusion process.
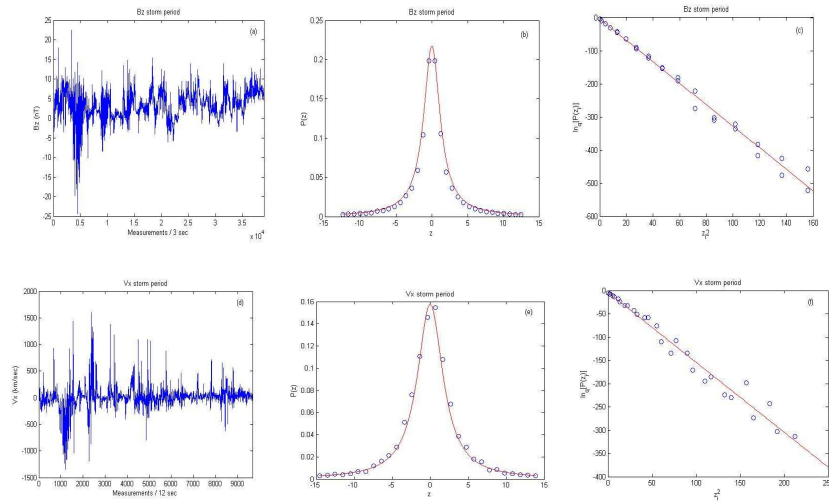

Figure 5: (a) Time series of Bz storm period **(b)** PDF $P(z_i)$ vs. z_i q Gaussian function that fits $P(z_i)$ for the Bz storm period **(c)** Linear Correlation between $\ln_q P(z_i)$ and $(z_i)^2$ where q = 2.05 ± 0.04 for the Bz storm period **(d)** Time series of Vx storm period **(e)** PDF $P(z_i)$ vs. z_i q Guassian function that fits $P(z_i)$ for the Vx storm period **(f)** Linear Correlation between $\ln_q P(z_i)$ and $(z_i)^2$ where q = 1.98 ± 0.06 for the Vx storm period.

4.7 Magnetospheric Fractal Accelerator of Charged Particles

Already Tsallis theory has been used for the study of magnetospheric energetic particles non-Gaussian by Voros [61] and Leubner [62]. In the following we study the q-statistics of magnetospheric energetic particle during a strong substorm period. We used the data set from the GEOTAIL/EPIC experiment during the period from 12:00 UT to 21:00 UT of 8/2/1997 and from 12:00 UT of 9/2/1997 to 12:00 UT of 10/2/1997. The Tsallis statistics estimated for the magnetospheric electric field and the magnetospheric particles $\left(e^-, p^+ \right)$ during the storm period is shown in Fig. 6(a-i). Fig. 6(a,d,g) present the spacecraft observations of the magnetospheric electric field E_y component and the magnetospheric electrons $\left(e^- \right)$ and protons $\left(p^+ \right)$. The corresponding Tsallis q-statistics was found to correspond to the q-values: $q_{stat} = 2.49 \pm 0.07$ for the E_y electric field component, $q_{stat} = 2.15 \pm 0.07$ for the energetic electrons and $q_{stat} = 2.49 \pm 0.05$ for the energetic protons. These values reveal clearly non-Gaussian dynamics for the mechanism of electric field development and electrons-protons acceleration during the magnetospheric storm period.
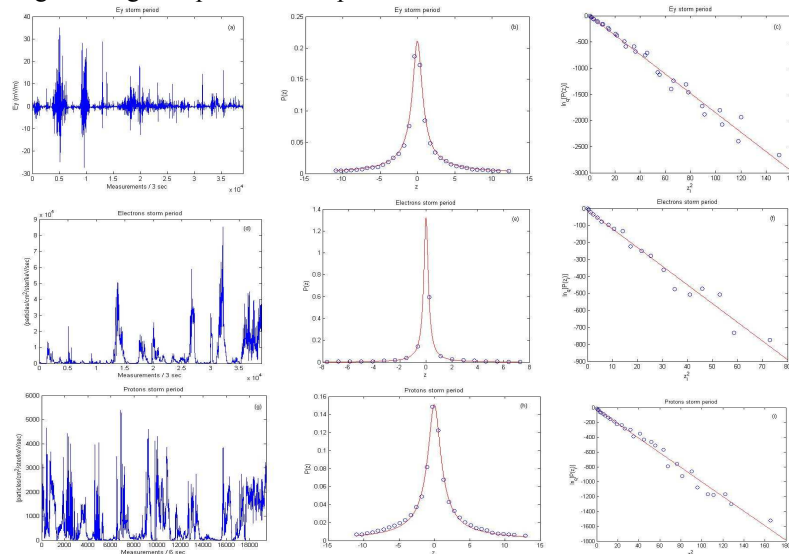

Figure 6: (a) Time series of Ey storm period **(b)** PDF P(z_i) vs. z_i q Guassian function that fits P(z_i) for the Ey storm period **(c)** Linear Correlation between $\ln_q P(z_i)$ and $(z_i)^2$ where q = 2.49 ± 0.07 for the Ey storm period **(d)** Time series of electrons storm period **(e)** PDF P(z_i) vs. z_i q Gaussian function that fits P(z_i) for the electrons storm period **(f)** Linear Correlation between $\ln_q P(z_i)$ and $(z_i)^2$ where q = 2.15 ± 0.07 for the electrons storm period time series **(g)** Time series of protons storm period **(h)** PDF P(z_i) vs. z_i q Gaussian function that fits P(z_i)

for the protons storm period **(i)** Linear Correlation between $\ln_q P(z_i)$ and $(z_i)^2$ where q = 2.49 ± 0.05 for the protons storm period.

4.8 Solar Wind Magnetic Cloud

From the spacecraft ACE, magnetic field experiment (MAG) we take raw data and focus on the Bz magnetic field component with a sampling rate 3 sec. Tha data correspond to sub-storm period with time zone from 07:27 UT, 20/11/2001 until 03:00 UT, 21/11/2003.

Magnetic clouds are a possible manifestation of a Coronal Mass Ejection (CME) and they represent on third of ejectra observed by satellites. Magnetic cloud behave like a magnetosphere moving through the solar wind. Carbone et al. [58], de Wit [63] estimated non-Gaussian turbulence profile of solar wind. Bourlaga and Vinas [55] estimated the q-statistics of solar wind at the q-value $q_{stat} = 1.75 \pm 0.06$. Fig. 7 presents the q-statistics estimated in the magnetic cloud solar plasma for the z-component B_Z of the magnetic field. The B_Z time series is shown in Fig. 7a. The q-statistics for B_Z component is shown at Fig. 7(b,c), while the q-value was found to be $q_{stat} = 2.02 \pm 0.04$. This value is higher than the value $q_{stat} = 1.75$ estimated from Bourlaga and Vinas [55] at 40 AU.
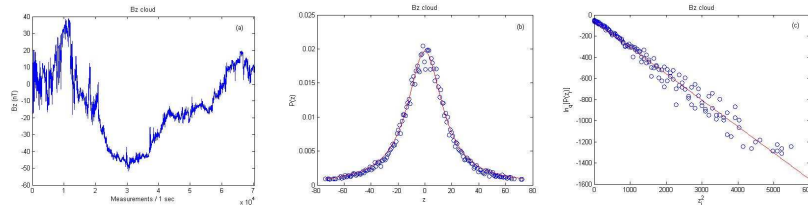

Figure 7: (a) Time series of Bz cloud **(b)** PDF $P(z_i)$ vs. z_i q Gaussian function that fits $P(z_i)$ for the Bz cloud **(c)** Linear Correlation between $\ln_q P(z_i)$ and $(z_i)^2$ where q = 2.02 ± 0.04 for the Bz cloud.

4.9 Solar Activity: Sun Spot-Flares Dynamics

In this sub-section we present the q-statistics of the sunspot and solar flares complex systems by using data of Wolf number and daily Flare Index. Especially, we use the Wolf number, known as the international sunspot number measures the number of sunspots and group of sunspots on the surface of the sun computed by the formula: (10)*R=k*(10g+s)* where: *s* is the number of individual spots, *g* is the number of sunspot groups and *k* is a factor that varies with location known as the observatory factor. We analyse a period of 184 years. Moreover we analyse the daily Flare Index of the solar activity that was determined using the final grouped solar flares obtained by NGDC (National Geophysical Data Center). It is calculated for each flare using the

formula: $Q = (i * t)$, where "i" is the importance coefficient of the flare and "t" is the duration of the flare in minutes. To obtain final daily values, the daily sums of the index for the total surface are divided by the total time of observation of that day. The data covers time period from 1/1/1996 to 31/12/2007.
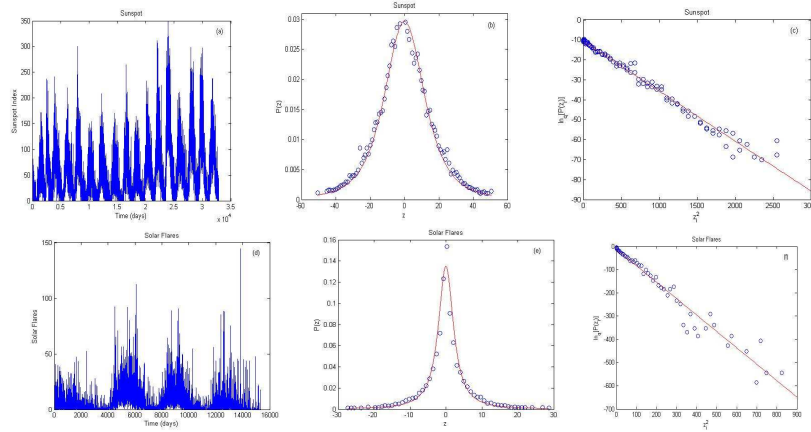

Figure 8: **(a)** Time series of Sunspot Index concerning the period of 184 years **(b)** PDF P(z_i) vs. z_i q Guassian function that fits P(z_i) for the Sunspot Index **(c)** Linear Correlation between $\ln_q$P(z_i) and $(z_i)^2$ where q = 1.53 ± 0.04 for the Sunspot Index **(d)** Time series of Solar Flares concerning the period of 184 years **(e)** PDF P(z_i) vs. z_i q Guassian function that fits P(z_i) for the Solar Flares **(f)** Linear Correlation between $\ln_q$P(z_i) and $(z_i)^2$ where q = 1.90 ± 0.05 for the Solar Flares.

Although solar flares dynamics is coupled to the sunspot dynamics. Karakatsanis and Pavlos [64] and Karakatsanis et al. [64] have shown that the dynamics of solar flares can be discriminated from the sunspot dynamics. Fig. 8 presents the estimation of q-statistics of sunspot index shown in fig. 8(b,c) and the q-statistics of solar flares signal shown in fig. 8(e,g). The q-values for the sunspot index and the solar flares time series were found to be $q_{stat} = 1.53 \pm 0.04$ and $q_{stat} = 1.90 \pm 0.05$ correspondingly. We clearly observe non-Gaussian statistics for both cases but the non-Gaussianity of solar flares was found much stronger than the sunspot index.

4.10 Solar Flares Fractal Accelerator

At solar flare regions the dissipated magnetic energy creates strong electric fields according to the theoretical concepts. The bursty character of the electric field creates burst of solar energetic particles through a mechanism of solar

flare fractal acceleration. According to theoretical concept presented in previous section the fractal acceleration of energetic particles can be concluded by the Tsallis q-extension of statistics for non-equilibrium complex states. In the following we present significants verification of this theoretical prediction of Tsallis theory by study the q-statistics of energetic particle acceleration. Finally we analyze energetic particles from spacecraft ACE – experiment EPAM and time zone 1997 day 226 to 2006 day 178 and protons (0.5 – 4) MeV with period 20/6/1986 – 31/5/2006, spacecraft GOES, hourly averaged data. Figure 9 presents the estimation of the solar protons - electrons q-statistics. The q-values for solar energetic protons and electrons time series were found to be $q_{stat} = 2.31 \pm 0.13$ and $q_{stat} = 2.13 \pm 0.06$ correspondingly. Also in this case we clearly observe non-Gaussian statistics for both cases.
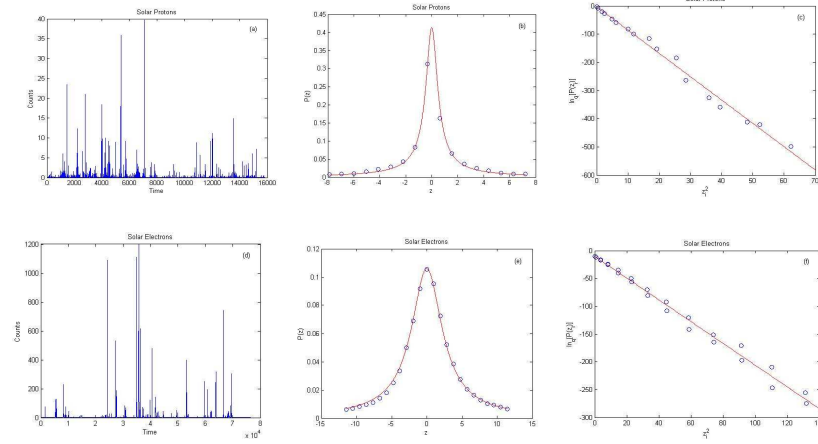

Figure 9: (a) Time series of Solar proton **(b)** PDF $P(z_i)$ vs. z_i q Guassian function that fits $P(z_i)$ for the Solar proton data **(c)** Linear Correlation between $\ln_q P(z_i)$ and $(z_i)^2$ where $q = 2.31 \pm 0.13$ for the Solar proton **(d)** Time series of Solar electrons **(e)** PDF $P(z_i)$ vs. z_i q Guassian function that fits $P(z_i)$ for the Solar electrons **(f)** Linear Correlation between $\ln_q P(z_i)$ and $(z_i)^2$ where $q = 2.13 \pm 0.06$ for the Solar electrons.

4.11 Cosmic Stars

In the following we study the q-statistics for cosmic star brightness. For this we used a set of measurements of the light curve (time variation of the intensity) of the variable white dwarf star PG1159-035 during March 1989. It was recorded by the Whole Earth Telescope (a coordinated group of telescopes distributed around the earth that permits the continuous observation of an astronomical object) and submitted by James Dixson and Don Winget of the Department of Astronomy and the McDonald Observatory of the University of Texas at Austin. The telescope is described in an article in The Astrophysical Journal (361), p. 309-317 (1990), and the measurements on PG1159-035 will be described in an article scheduled for the September 1 issue of the Astrophysical

Journal. The observations were made of PG1159-035 and a non-variable comparison star. A polynomial was fit to the light curve of the comparison star, and then this polynomial was used to normalize the PG1159-035 signal to remove changes due to varying extinction (light absorption) and differing telescope properties.

Figure 10 shows the estimation of q-statistics for the cosmic stars PG-1159-035. The q-values for the star PG-1159-035 time series was found to be $q_{stat} = 1.64 \pm 0.03$. We clearly observe non-Gaussian statistics.
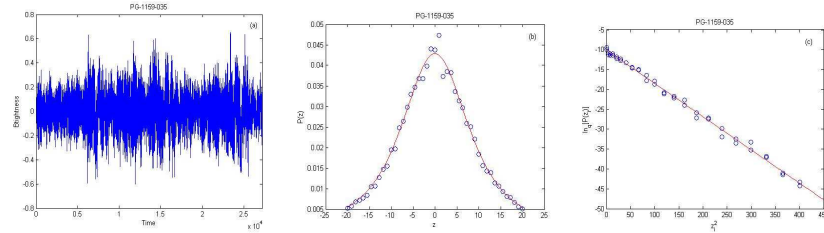

Figure 10: (a) Time series of cosmic star PG-1159-035 **(b)** PDF $P(z_i)$ vs. z_i q Guassian function that fits $P(z_i)$ for the cosmic star PG-1159-035 **(c)** Linear Correlation between $\ln_q P(z_i)$ and $(z_i)^2$ where q = 1.64 ± 0.03 for the cosmic star PG-1159-035.

4.12 Cosmic Rays

In this sub-section we study the q-statistics for the cosmic ray (carbon) data set. For this we used the data from the Cosmic Ray Isotope Spectrometer (CRIS) on the Advanced Composition Explorer (ACE) spacecraft and especially the carbon element (56-74 Mev) in hourly time period and time zone duration from 2000 – 2011.The cosmic rays data set is presented in Fig.11a, while the q-statistics is presented in Fig.11[b,c]. The estimated q_{stat} value was found to he $q_{stat} = 1.44 \pm 0.05$. This resulted reveals clearly non-Gaussian statistics for the cosmic rays data.
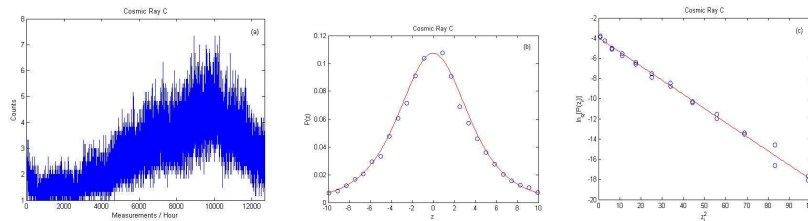

Figure 11: (a) Time series of cosmic ray Carbon **(b)** PDF $P(z_i)$ vs. z_i q Guassian function that fits $P(z_i)$ for the cosmic ray Carbon **(c)** Linear Correlation between $\ln_q P(z_i)$ and $(z_i)^2$ where q = 1.44 ± 0.05 for the cosmic ray Carbon.

System	q_stat
Cardiac (hrv)	1.26 ± 0.10
Brain (seizure)	1.63 ± 0.14
Seismic (Interevent)	2.28 ± 0.12
Seismic (Magnitude)	1.77 ± 0.09
Atmosphere (Temperature)	1.89 ± 0.08
Atmosphere (Rainfall)	2.21 ± 0.06
Magnetosphere (Bz storm)	2.05 ± 0.04
Magnetosphere (Vx storm)	1.98 ± 0.06
Magnetosphere (Ey storm)	2.49 ± 0.07
Magnetosphere (Electrons storm)	2.15 ± 0.07
Magnetosphere (Protons storm)	2.49 ± 0.05
Solar Wind (Bz cloud)	2.02 ± 0.04
Solar (Sunspot Index)	1.53 ± 0.04
Solar (Flares Index)	1.8700
Solar (Protons)	2.31 ± 0.13
Solar (Electrons)	2.13 ± 0.06
Cosmic Stars (Brigthness)	1.64 ± 0.03
Cosmic Ray (C)	1.44 ± 0.05

TABLE 1: This table includes the estimated qstat indeces for the brain and heart activity, the Magnetospheric dynamics (Bz, Vx, Ey, electron, protons time series), solar wind magnetic cloud, sunspot-solar flare time series, cosmic stars and cosmic rays

5. Summary and Discussion

In this study we presented novel theoretical concepts (sections 2-3) and novel experimental results (section 4) concerning the non-equilibrium distributed dynamics of various kinds of complex systems as : brain and heart activity, seismic and atmospheric dynamics as well as space plasmas dynamics corresponding to planetic magnetospheres, solar wind, solar corona, solar convection zone, cosmic stars and cosmic rays. In all of these cases the statistics was found to be non-Gaussian as the q-statistics index was estimated to be larger than the value q=1 which corresponds to Gaussian dynamics. The values of qstat index for the systems which were studied are presented in table 1. This experimental result constitutes strong evidence for the universality of non-equilibrium complex or strange dynamics as it was presented in section 2

of this study. As for the theory in the theoretical description of this study we have shown the theoretical coupling of Tsallis non-extensive statistical theory and the non-equilibrium fractal dynamics. That is has been shown also the internal correlation of the Tsallis q-extension of Boltzmann-Gibbs statistics with modern fractal generalization of dynamics. Our theoretical descriptions showed the possibility of the experimental testing of Tsallis statistics and fractal dynamics through the Tsallis q-triplet as well as the structure functions exponent spectrum. Moreover at this study we have tested the theoretical concepts only through the q-statistics index of Tsallis non extensive theory, the tests of the entire q-triplet and the structure functions exponent spectrum are going to be presented in a short coming paper [37].

Finally the theoretical concepts and the experimental results of this study clearly indicate the faithful character of the universality of Tsallis q-statistics and fractal dynamics in a plenty of different physical systems. In this way we can indicate faithfully that the Tsallis q-entropy theory as well as the fractal dynamics constitutes the new basis for a novel unification of the complexity physical theory.

References

1. Prigozine I., (1977), Time, structure and fluctuations, Nobel Lecture.; Prigozine I., (1996), El fin de las certitumbres, Editions Odile Jakob

2. Nicolis, G. & Prigogine, I. [1971], Fluctuations in nonequilibrium systems" Proc. Nat. Acad. Sci. 68x, p. 2102.; Nicolis, G. & Prigogine, I. [1977], Self-organization in nonequilibrium systems: From dissipative structures to order through uctuations", Willey, New York.; Nicolis, G. [1979] "Irreversible thermodynamics", Rep. Prog. Phys., 42, p. 225.; Nicolis, G. [1986] "Dissipative Systems", Rep. Prog. Phys., 49, p. 873.; Nicolis, G. [1989] "Physics of Far-From-Equilibrium Systems and Selforganisation", in Davies, Cambridge University Press.; Nicolis, G. & Prigogine, I. [1989] "Exploring Complexity: An Introduction", eds. Freeman, W.H., San Francisco.

3. Davies, P., The cosmic blueprint, Unwin Paperbacks, 1987.

4. El Naschie, M.S. [1998] "Superstrings, Knots, and Noncommutative Geometry in E(in_nity) Space", Int. Journal of Theoretical Physics, 37, p. 2935.; El Naschie, M.S. [2004] "A review of E in_nity theory and the mass spectrum of high energy particle physics", Chaos, Solitons & Fractals, 19, p. 209-236.; El Naschie, M.S. [2005] "Einstein's dream and fractal geometry", Chaos, Solitons & Fractals, 24, p. 1.; El Naschie, M.S. [2006] "Elementary prerequisites for E-in_nity (Recommended background readings in nonlinear dynamics, geometry and topology)", Chaos, Solitons & Fractals, 30, p. 579.

5. Iovane, G., Cantorian spacetime and Hilbert space: Part I – Foundations, Chaos, Solitons and Fractals, 28, 857-878, 2006.; Iovane, G., Cantorian spacetime and Hilbert space: Part II – Relevant consequences, Chaos, Solitons and Fractals, 29, 1-22, 2006.

6. Nottale, L. [1993] "Fractal Space-Time and Micro-physics", Towards a Theory of Scale Relativity, eds. World Scientific.; Nottale, L. [1994] "Scale Relativity, Fractal Space-time and Quantum Mechanics", Chaos, Solitons & Fractals, 4, p. 361.;

Nottale, L. [1996] "Scale Relativity and Fractal Space-Time: Applications to Quantum Physics, Cosmology and Chaotic Systems", Chaos, Solitons & Fractals, 7, p. 877.; Nottale L., The Theory of Scale Relativity: Non-Differentiable Geometry and Fractal Space-Time, Aip Conference Proceedings 2004, 718(20), p.68-95.; Nottale L., (2006), Fractal space – time, non – differentiable and scale relativity, Invited contribution for the Jubilee of Benoit mandelbrot.

7. Castro, C. [2005] ", On non-extensive statistics, chaos and fractal strings", Physica A 347, p. 184.

8. Bohr, N., Dialectica 1, 312, 1948.

9. Khrenninov, A., Classical and Quantum Mechanics of Information Spaces with Applications to Cognitive, Physhological, Social, and Anomalous Phenomena, Foundations of Physics, 29 (7), 1999.

10. Kroger, H., Why are probabilistic laws governing quantum mechanics and neurobiology?, Chaos, Solitons and Fractals, 25, 815-834, 2005.

11. Pezzaglia, W.W., Dimensionally Democratic Calculus and Principles of Polydimensional Physics, arxiv: gr-qc/9912025v1, 1999.

12. Tarasov, V.E., Fractional Liouville and BBGKI Equations, Journal of Physics: Conferences Series 7, 17-33, 2005.; Tarasov, V.E., Electromagnetic Fields on fractals, Modern Physics Letters, A 21, 1587-1600, 2006.; Tarasov, V.E., Fractional Variations for dynamical systems: Hamilton and Lagrange approaches, J. of Phys. A: Math. Gen., 39, 8409-8425, 2006.; Tarasov, V.E., Fractional vector calculus and fractional Maxwell's equations, Annals of Physics, 323, 2756-2778, 2008.

13. El-Nabulsi, A.R., A Fractional Approach to Nonconservative Lagrangian Dynamical Systems, FIZIKA A, 14, 289-298, 2005.; El-Nabulsi, A.R., Necessary optimality conditions for fractional action-like integrals of variational calculus with Riemann-Liouville derivatives of order (α, β), Math. Meth. Appl. Sci., 30, 1931-1939, 2007.; El-Nabulsi, A.R., Fractional dynamics, fractional weak bosons masses and physics beyond the standard model, Chaos, Solitons and Fractals, 41, 2262-2270, 2009.; El-Nabulsi, A.R., Fractional action-like variational problems in holonomic, non-holonomic and semi-holonomic constrained and dissipative dynamical systems, Chaos, Solitons and Fractals, 42, 52-61, 2009.

14. Cresson, J., Non-differentiable variational principles, J. Math. Anal. Appl., 307, 48-64, 2005.; Cresson, J. and Greff, I., Non-differentiable embedding of Lagrangian systems and partial differential equations, J. Math. Anal. Appl., 384, 626-646, 2011.

15. Goldfain, E., Fractional dynamics, Cantorian space-time and the gauge hierarchy problem, Chaos, Solitons and Fractals, 22, 513-520, 2004.; Goldfain, E., Complex Dynamics and the High-energy Regime of Quantum Field Theory, Int. J. of Nonlinear Sciences and Numerical Simulation, 6(3), 223-234, 2005.; Goldfain, E., Chaotic Dynamics of the Renormalization Group Flow and Standard Model Parameters, Int. J. of Nonlinear Science, 3, 170-180, 2007.; Goldfain, E., Fractional dynamics and the TeV regime of field theory, Communications in Nonlinear Science and Numerical Simulation, 13, 666-676, 2008.

16. Pavlos, G.P., Sarris, E.T., Paschalidis, N., The growth rate and location of the acceleration of energetic particles inside the plasma sheet, *Planetary and Space Science*, Vol. 37, issue 5, pp. 503-516, May 1989.; Pavlos, G.P., Sarris, E.T., Encounter with a source of energetic particles inside the plasma sheet, *Annales Geophysicae*, Vol. 7, pp. 531-539, October 1989.; Pavlos, G.P., Kyriakou, G.A., Rigas, A.G., Liatsis, P., Trochoutsos, P.C., Tsonis, A.A., Evidence for strange

attractor structures in space plasmas, *Annales Geophysicae*, Vol. 10, No. 5, pp. 309-322, May 1992.; Pavlos, G.P., Dialettis, D., Kyriakou, G.A., Sarris, E.T., A preliminary low-dimensional Chaotic Analysis of the solar Cycle, *Annales Geophysicae*, Vol. 10, No. 10, pp. 759-762, October 1992.; Pavlos, G.P., Rigas, A.G., Dialettis, D., Sarris, E.T., Karakatsanis, L.P., Tsonis T.T., Evidence for chaotic dynamics in the outer solar plasma and the earth magnetosphere, *Chaotic Dynamics: Theory and Practice*, NATO ASI Series B: Physics, Vol. 298, pp. 327-339, November 1992.; Pavlos, G.P., Karakatsanis, L.P., Latousakis, I., Dialettis, D., Papaioannou, G., Chaotic analysis of a time series composed by seismic events recorded in Japan, *International Journal of Bifurcation and Chaos*, Vol. 4, issue 1, pp. 87-98, February 1994.; Pavlos, G.P., Diamantidis, D., Adamopoulos, A., Rigas, A.G., Daglis, I.A., Sarris, E.T., Chaos and magnetospheric dynamics, *Nonlinear Processes in Geophysics*, Vol. 1, No. 2/3, pp. 124-135, 1994.; Pavlos, G.P., Athanasiou, M., Kugiumtzis, D., Hatzigeorgiu, N., Rigas, A.G., Sarris, E.T., Nonlinear analysis of Magnetospheric data, Part I. Geometric characteristics of the AE index time series and comparison with nonlinear surrogate data, *Nonlinear Processes in Geophysics*, Vol. 6, No. 1, pp. 51-65, 1999a.; Pavlos, G.P., Kugiumtzis, D., Athanasiou, M., Hatzigeorgiu, N., Diamantidis, D., Sarris, E.T., Nonlinear analysis of Magnetospheric data, Part II. Dynamical characteristics of the AE index time series and comparison with nonlinear surrogate data, *Nonlinear Processes in Geophysics*, Vol. 6, No. 2, pp. 79-98, 1999b.; Pavlos, G.P., Athanasiou, M., Diamantidis, D., Rigas, A.G., Sarris, E.T., Comments and new results about the magnetospheric chaos hypothesis, *Nonlinear Processes in Geophysics*, Vol. 6, No. 2, pp. 99-127, 1999c.

17. Iliopoulos, A., Pavlos, G. & Athanasiu, M. [2008], Spatiotemporal Chaos into the Hellenic Seismogenesis: Evidence for a Global Strange Attractor, Nonlin. Phenom. Complex Sys. 11(2), p. 274.; Iliopoulos, A. & Pavlos, G. [2010], Global Low Dimensional Seismic Chaos in the Hellenic Region," Intern. J. Bifurc. Chaos 20(7), p. 2071.

18. Sparrow, C., The Lorenz Equations, Bifurcations, Chaos and Strange Attractors, Springer, 1982.

19. Quantitative Universality for a Class of Nonlinear Transformations, Journal of Statistical Physics, 19, 25-52, 1978.

20. Libchaber, A., Experimental Study of Hydrodynamic Instabilites. Rayleigh-Bernard Experiment: Helium in a Small Box, Nonlinear Phenomena at Phase Transitions and Instabilities, eds. Riste, T., 259, Plenum, 1982.

21. Nelson, E. [1966], Derivation of the Schrodinger equation from Newtonian mechanics, Phys. Rev., 150, p. 1079.; Nelson, E. [1985], Quantum Fluctuations, Princeton University Press, New York.

22. Hooft, G.T. [1999] "Quantum gravity as a dissipative deterministic system", Class. Quantum Grav., 16, p. 3263-3279.; Hooft, G.T. [2001a] "Determinism and Dissipation in Quantum Gravity", Basics and highlights in fundamental physics: proceedings of the International School of Subnuclear Physics, 37, p. 397.; Hooft, G.T. [2001b] "How Does God Play Dice?(Pre) Determinism at the Planck Scale", An Essay in Honor of John S. Bell, arXiv:hep-th/0104219.

23. Parisi G. And Ramanurti S., Statistical Field Theory, Physics Today, vol. 41, issue 12, p. 110, 1988.

24. Beck, C. [1991] "Higher correlation functions of chaotic dynamical systems-a graph theoretical approach", Nonlinearity, 4, p. 1131.; Beck C. and Schlogl F. (1993), Thermodynamics of chaotic systems an introduction, Cambridge University Press.; Beck C., (1994), From the Perron-Frobenius equation to the Fokker-Planck equation, Journal of Statistical Physics, 79, 5-6, 875-894; Beck, C. [1995] "Chaotic quantization of field theories", Nonlinearity, 8, p. 423.; Beck, C. [2001] "Dynamical Foundations of Nonextensive Statistical Mechanics", Phys. Rev. Let., 87, p. 1806011.; Beck, C. [2002] "Nonextensive methods in turbulence and particle physics", Physica A, 305, p. 209.

25. Jensen, R.V., Functional Integral Approach to Classical Statistical Dynamics, Journal of Statistical Physics, 25(2), 183, 1981.

26. Ord, G.N. [1983], Fractal space-time: a geometric analogue of relativistic quantum mechanics, J. Phys. A: Math. Gen., 16, p. 1869.

27. Nigmatullin RR, (1991), Fractional integral and its physical interpretation, Theoretical and Mathematical Physics, 90, 3, 242-251.

28. Aristotle, The Physics, eds. Wicksteed, P.H. and Cornford, F.M., books I-IV, Loeb Classical Library, 1957.

29. Tsallis C., (1988), Possible generalization of Boltzmann-Gibbs statistics, Journal of Statistical Physics, 52,1-2, 479-487.; Tsallis C., (2001), Nonextensive statistical mechanics and thermodynamics: Historical Background and present status, Springer, S.Abe and Y. Okamoto (Eds.):LNP 560, 3-98.; Tsallis C. (2004), Nonextensive statistical mechanics: construction and physical interpretation, Nonextensive entropy – interdisciplinary applications Ed. Murray GM and Tsallis C., Oxford Univ. Press, 1-53; Tsallis C. (2009), Introduction to Non-extensive Statistical Mechanics, Springer.

30. Zelenyi, L. M. & Milovanov, A. V., Fractal Properties of Sunspots, Soviet Astronomy Letters, 17, p. 425, 1991.; b) Zelenyi, L. M. & Milovanov, A. V., Fractal topology and strange kinetics: from percolation theory to problems in cosmic electrodynamics, Pysics-Uspekhi, 47(8), 749-788, 2004.; Zelenyi, L.M., Malova, H.V., Artemyev, A.V., Popov, V.Yu. and Petrukovich, A.A., Thin Current Sheets in Collisionless Plasma: Equilibrium structure, Plasma Instabilities, and Particle Acceleration, Plasma Physics Reports, 37(2), 118-160, 2011.

31. Chang, T., VVedensky, D.D. and Nicoll, J.F., Differential Renormalization-Group Generators for Static and Dynamic Critical Phenomena, Physics Reports, 217(6), 279-360, 1992. Chang, T. [1992] "Low-Dimensional Behavior and Symmetry Braking of Stochastic Systems near Criticality Can these Effects be observed in Space and in the Laboratory", IEEE, 20(6), p. 691-694.; Chang, T., Self-Organized Criticality, multi-fractal spectra, sporadic localized reconnections and intermittent turbulence in the magnetotail, Physics of Plasmas, 6, (1999), 4137.; Chang et al, (2004), Complexity induced anisotropic bimodal intermittent turbulence in space plasmas, Phys. Plasmas 11, 1287.; Chang, T., Tam, S.W.Y., Wu, C-C, & Consolini, G [2003] "Complexity, Forced and/or Self-Organized Criticality, and Topological Phase Transitions in Space Plasmas", Space Sci. Rev., 107, p. 425-445.; Chang, T., Tam, S.W.Y. and Wu, C.-C., Complexity induced anisotropic bimodal intermittent turbulence in space plasmas, Physics of Plasmas, 11(4), 1287, 2004.; Chang, T., Tam, S.W.Y. and Wu, C.-C., Complexity and intermittent turbulence in space plasmas, (eds.) Sharma, A.S. and Kaw, P.K., Nonequilibrium Phenomena in Plasmas, 23-50, 2005.

32. Milovanov, A.V. and Zelenyi, L.M., Functional background of the Tsallis entropy: "coarse-grained" systems and "kappa" distribution functions, Nonlinear Processes in Geophysics, 7, 211-221, 2000.; Milovanov, A.V. and Rasmusse, J.J., Fractional generalization of the Ginzburg-Landaou equation: an unconventional approach to critical phenomena in complex media, Physics Letters A377, 75-80, 2005.; Milovanov, A.V., Dynamic Polarization random walk model and fishbone-like instability for self-organized critical systems, New Journal of Physics, 13, 043034, 2011.

33. Ruzmaikin A.A. (1985), Solar Phys. 100, 125-140.; Ruzmakin AA et al, (1996), Spectral Properties of Solar Convection and Diffusion, ApJ, 471, 1022.

34. Sharma, A.S., Baker, D.N. and Borovsky, J.E., Nonequilibrium phenomena in the magnetosphere, (eds.) Sharma, A.S. and Kaw, P.K., Nonequilibrium Phenomena in Plasmas, 3-22, 2005.; Sharma, A.S., Ukhorski, A.Y. and Sitnov, M.I., Global and multiscale phenomena of the magnetosphere, (eds.) Sharma, A.S. and Kaw, P.K., Nonequilibrium Phenomena in Plasmas, 117-144, 2005.

35. Consolini, G. et al., Multifractal Structure of Auroral Electrojet Index Data, Phys. Rev. Lett. 76, 4082–4085, 1996.; Consolini, G., [1997] "Sandpile cellular automata and magnetospheric dynamics", 8th GIFCO Conference: Cosmic physics in the year 2000, p. 123 - 126.; Consolini G., and Chang T., Magnetic Field Topology and Criticality in Geotail Dynamics: Relevance to Substorm Phenomena, Space Sc. Rev., 95, 309-321, 2001.; Consolini G. et al., On the magnetic field fluctuations during magnetospheric tail current disruption: A statistical approach, J. Geoph. Research, 110, A07202, 2005.

36. Abramenko, V.I., Solar MHD turbulence in regions with various levels of flare activity, Astronomy Reports, Volume 46, Number 2, 161-171, 2002.

37. Pavlos G.P., et al., First and second order non-equilibrium phase transition and evidence for non-extensive Tsallis statistics in Earth's magnetosphere, Physica A, 390, 2819-2839, 2011.; Pavlos, G.P., Karakatsanis, L.P. and Xenakis, M.N., Tsallis non-extensive statistics, intermittent turbulence, SOC and chaos in the solar plasma. Part one: Sunspot dynamics, Submitted for Publications, http://arxiv.org/abs/1201.6498, 2012.; Pavlos, G.P., Karakatsanis, L.P. and Xenakis, M.N., Sarafopoulos, D. and Pavlos, E.G., Tsallis Statistics and Magnetospheric Self-organization, Physica A, 393, 3069-3080, 2012.

38. Zaslavsky, G.M., Renormalization group theory of anomalous transport in systems with Hamiltoniasn chaos, Chaos 4(1), 25, 1994.; Zaslavsky, G.M., Fractional kinetc equation for Hamiltonian chaos, Physics D 76, 110-122, 1994.; Zaslavsky, G.M., Chaotic dynamics and the origin of statistical laws, American Institute of Physics, S-0031-9228-9908-030-8, 1999.; Zaslavsky, G.M., Chaos, fractional kinetics, and anomalous transport, Physics Reports, 371, 461–580, 2002.

39. Chen W., (2006), Time – space fabric underlying anomalous diffusion, Chaos, Solitons & Fractals, 28 (4), 923–929.

40. Wilson, K.G., The renormalization group: Critical phenomena and the Kondo problem, Reviews of Modern Physics, 47(4), 773, 1975.; Wilson, K.G., The renormalization group and critical phenomena, Reviews of Modern Physics, 55(3), 583, 1983.

41. Binney, J.J., et al., The Theory of Critical Phenomena An introduction to the Renormalization Group, Oxford University Press, 1992.

42. Kogut, J.B., An introduction to lattice gauge theory and spin systems, /review of Modern Physics, 51(4), 659, 1979.

43. Ivancevic, V. and Ivancevic, T.T., Complex Nonlinearity, Chaos, Phase Transitions, Topology Change and Path Integrals, Springer, 2008.

44. Biro, T., Muller, B. & Matinyan, S. [2004] "Chaotic Quantization: Maybe the Lord plays dice, after all?", Lecture Notes in Physics, 633, p. 164.

45. Krommes J.A., Systematic statistical theories of plasma turbulence and intermittency: current status and future prospects, Physics Reports 283, 5-48, 1997.; Krommes J.A., Fundamental statistical descriptions of plasma turbulence in magnetic fields, Physics Reports, 360, 1-352, 2002.

46. Lui A.T.Y., Multiscale phenomena in the near-Earth magnetosphere, Journal of Atmospheric and Solar-Terrestial Physics, 64, 125-143, 2002.

47. Svozil, K. and Zeilinger, A., Dimension of space-time, International Journal of Modern Physics A, Volume 1(4), 971-990, 1986.

48. Antoniadis I, (1998), Fractal geometry of quantum space-time at large scales, Physics Letters B, 444, 284-292.

49. Agop, M. et al., El Naschies's $\varepsilon^{(\infty)}$ space-time, hydrodynamics model of scale relativity theory and some applications, Chaos, Solitons and Fractals, 34, 1704-1723, 2007.

50. Altaisky, M.V. and Sidharth, B.G., p-Adic Physics Below and Above Planck Scales, Chaos, Solitons and Fractals, 10, 167-176, 1999.

51. Lizzi, F., The structure of Spacetime and Noncommutative Geometry, http://arxiv.org/abs/0811.0268, 2002.

52. Majid, S., Quantum groups and noncommutative geometry, Journal of Mathematical Physics, 41(6), 3892, 2000.

53. Ren, F.Y., Liang, J.R., Wang, X.T. and Qio, W.Y., Integrals and derivatives on net fractals, Chaos, Solitons and Fractals, 16, 107-117, 2003

54. Balescu R, (1975), Equilibrium and non-equilibrium statistical mechanicsm, A Wiley Inter. Publ.

55. Burlaga, L.F. and Vinas, A.F., Triangle for the entropic index q of non-extensive statistical mechanics observed by Voyager 1 in the distant heliosphere, Physica A, 356, 375-384, 2005.

56. Ferri G.L., Reynoso Savio M.F., Plastino A., "Tsallis q-triplet and the ozone layer", Physica A, 389, p. 1829-1833, 2010.

57. Temam, R., Infinite-Dimensional Dynamical Systems in Mechanics and Physics, Springer, 1988.

58. Carbone, V., Veltri, P. and Bruno, R., Solar wind low-frequency magnetohydrodynamic turbulence: extended self-similarity and scaling laws, Nonlinear Process in Geophysics, 3, 247-261, 1996.

59. Kovas, A.L. [1994] "Nonlinear Dynamics of Spatio-Temporal Processes in Complex Systems", Mathl. Comput. Modelling, 19, p. 47.

60. Mikhailov, A.S. and Loskutov, A.Yu., Foundations of Synergetic II Complex Patterns, Springer, 1991.

61. Voros, Z., On multifractality of high-latitude geomagnetic fluctuations, Ann. Geophysicae, 18, 1273-1282, 2000.; Voros, Z. et al., Multi-scale magnetic field intermittence in the plasma sheet, Annales Geophysicae, 21, 1995, 2003.; Voros, Z.

et al., Magnetic turbulence in the plasma sheet, Journal of Geophysical Research, 109, A11215, 2004.

62. Leubner, M.P. and Voros, Z., A nonextensive entropy approach to solar wind turbulence, The Astrophysical Journal, 618, 547-555, 2005.; Leubner, M.P. and Voros, Z., A nonextensive entropy path to probability distributions in solar wind turbulence, Nonlinear Processes in Geophysics, 12, 171-180, 2005.

63. Dudok de Wit, T. and Krasnosel'skikh, V.V., Non-Gaussian statistics in space plasma turbulence: fractal properties and pitfalls, Nonlinear Processes in Geophysics, 3, 262-273, 1996.

64. Karakatsanis, L.P. & Pavlos, G.P. [2008] "Self Organized Criticality and Chaos into the Solar Activity", Nonlinear Phenomena in Complex Systems, 11(2), p. 280-284; Karakatsanis, L.P., Pavlos, G.P., Iliopoulos, A.C., Tsoutsouras, V.G. & Pavlos E.G. [2011] "Evidence for Coexistence of SOC, Intermittent Turbulence and Low-Dimensional Chaos Processes in Solar Flare Dynamics", Modern Challenges in nonlinear plasma physics: A Festschrift Honoring the Career of Dennis Papadopoulos, AIP, 1320, p.55-64.

65. Born, M., Natural Philosophy of Cause and Chance, Oxford University Press, 1948.

66. YankovVV, (1997), Three rules of nonlinear physics, Physics Reports, 283, 147-160.

67. Hohenberg, P.C. and Halperin, B.I., Theory of dynamics critical phenomena, Reviews of Modern Physics, 49(3), 435, 1977.; Hohenberg, P.C. & Shraiman, B.I. [1989] "Chaotic behavior of an extended system", Physica D, 37, p. 109-115.

68. Elderfield, D., On the resolution of ordering ambiguities associated with the path integral representation of stochastic process, J. Phys. A: Math. Gen., 18, L767-L771, 1985.

69. Haken, H. [1983] Synergetics: Introduction and Advanced Topics, Springer.

70. Kubo R. et al, (1998), Statistical Physics II: Non equilibrium statistical mechanics, Springer.

71. Lenzi et al, (2000), Statistical mechanics based on Renyi entropy, Physica A, 280 (3–4), 337–345.

72. Robledo A., (2004), Unifying laws in multidisciplinary power-law phenomena: fixed –point universality and nonextensive entropy, Nonextensive entropy – interdisciplinary applications Ed. Murray GM and Tsallis C., Oxford Univ. Press, 63-77.

73. Halsey et al, (1986), Fractal measures and their singularities: the characterization of strange sets, Physical Review A, 33,2, 1141 – 1151.

74. Theiler J., Estimating fractal dimension, JOSA A, Vol. 7, Issue 6, pp. 1055-1073, 1990.

75. Paladin G. and Vulpiani A., (1987), Anomalous scaling laws in multifractal objects, Physics report, 156,4, 147 – 225.

76. Meneveau C. and K.R. Sreenivasan, The multifractal spectrum of the dissipation field in turbulent flows, Nuclear Physics B (Proc. Suppl.) 2 (1987) 49-76.; Meneveau C. and Sreenivasan KR, (1991), The multifractal spectrum of the dissipation field in turbulent flows, Nuclear Physics B,2, 49-76.

77. Umarov S. et al. (2007), A generalization of the central limit theorem concistent with non-extensive statistical mechanics, arxiv: cond-mat/0603593v4.

78. Arimitsu T. and N Arimitsu, Tsallis statistics and fully developed turbulence, (2000), J. Phys. A: Math. Gen. 33 L235 doi:10.1088/0305-4470/33/27/101.; Arimitsu T and Arimitsu A, (2001), Analysis of turbulence by statistics based on generalized entropies, Physica A, 295, 177 – 194.

79. Kolmogorov A., The Local Structure of Turbulence in Incompressible Viscous Fluid for Very Large Reynolds' Numbers, Doklady Akademiia Nauk SSSR, vol.30, p.301-305, 1941.

80. Shlesinger, M.F., Zaslavsky, G.M. and Klafter, J., Strange kinetics, Nature, 363, 31, 1993.

81. Moore, R.L., La Rosa, T.N. and Orwing, L.E., The wall of recconection-driven magnetohydrodynamics turbulence in a large solar flare, The Astrophysical Journal, 438, 985-996, 1995.

82. Rempel, E.L. and Chian A.C.-L., Space plasma dynamics: Alfven intermittent chaos, Advances in Space Research, 35, 951-960, 2005.

83. Marsch E. and Tu CY, (1997), Intermittency, non-Gaussian statistics and fractal scaling of MHD fluctuations in the solar wind, Nonlinear Processes in Geophysics 4, 2,101-124.

84. Feynman, R.P., Statistical Mechanics A set of lectures, The Benjamin/Cummings Publishing Company, INC., 1972.

Philip Glass' *Façades* — a Case Study on the Complexity of Music Scores

Pedro Pestana[1] and Dinis Pestana[2]

[1] CEAUL — Centro de Estatística e Aplicações da Universidade de Lisboa
Portuguese Catholic University – School of the Arts, CITAR, Porto, and
Lusíada University, Lisboa, Portugal
(E-mail: `pedro.duarte.pestana@gmail.com`)

[2] CEAUL — Centro de Estatística e Aplicações da Universidade de Lisboa
CFCUL — Centro de Filosofia das Ciências da Universidade de Lisboa
(E-mail: `dinis.pestana@fc.ul.pt`)

Abstract. Assimilating similar music bars with the axial-diagonal self-affine cartoons as defined by Mandelbrot [4], [5] to construct very general multi-fractals, we use one page of a score of Philip Glass' *Glassworks* to define the transition matrix of an order 1 Markov chain to simulate surrogates of the same piece, to investigate whether in this minimalist setting we obtain (i) an exact reproduction of the original, or (ii) something that though different sounds pleasantly.
Keywords: superposition of fractals, multifractals, complexity, self-affine cartoons and self-affine bars.

1   Introduction

Schröder[9], p. 109, boldly presents the key ideas of Birkhoff's *theory of aesthetic value*: an aesthetic creation is pleasing and interesting when it is neither too regular and predictable like a boring brown noise with a frequency dependence f^{-2}, nor a pack of too many surprises like an unpredictable white noise with a frequency dependence f^{-0}.
Multifractal measures — for an early overview of the field cf. Evertsz and Mandelbrot [2] — is a candidate tool to analyze the complexity of musical scores, since a single similarity exponent characterizing a monofractal set is hardly appropriate to render the rich complexity of even minimalist compositions.
Philip Glass' *Façades*, whose interpertrations range from strings, piano, flute/saxophone and oboe to piano and flute (or even an initial 42s section fingerpicked in guitar) is used as a case study on the appropriateness of multifractal tools in the description of musical complexity.

This is a first essay on using such tools, and we shall limit ourselves to assimilate the musical notion of bar (or measure) with the "cartoons" used by Mandelbrot [5], namely chapter N1, or chapter E6 in [4], analyzing bars 19–39 (page 14 of the score of *Glassworks*).

The idea of achieving aesthetic value blending harmoniously repetition with innovation and contrast — in Platzer [8] definition of the classical

rondo, for instance, a principal theme (sometimes called the "refrain") alternates with one or more contrasting themes, generally called "episodes," but also occasionally referred to as "digressions" or "couplets" — will be further discussed on an appendix of the full version of this note, where Platzner's specialist description of the rondo is contrasted to the "amateur" — but nevertheless more eloquent — description in Sorti and Monaldi's *Imprimatur*. Proust's lyrical description of the *"petite phrase de Vinteul"*, and Poe's *The Philosophy of Composition* where he expresses the essentil role of the refrain (limited to the word "nevermore" in his masterpiece The Raven, that nevertheless has some dose of consonance with the name of the dead Leonore, and whose component *never* is phonetically the reversion of "raven"

2 Façades

Although *Façades* first appeared on Philip Glass' album *Glassworks*, it was conceived as part of the soundtrack to Godfrey Reggio's *Koyaanisqatsi*, see `http://www.youtube.com/watch?v=vz_R2y1oAzw&feature=related` or `http://www.youtube.com/watch?v=GQsoMIGuPD8` for the stream introducing a similar musical theme. Originally scored for an orchestral string section and two saxophones, it is often performed using two flutes instead of saxophones, or scored for 2 soprano sax, viola, cello; synthesizer doubles va/vc. In fact, as Patrick Gary observed in *MusicWeb International*, "Philip Glass is a composer whose body of work readily lends itself to re-orchestration. In fact, many of his early works were written with intentionally vague orchestrations to allow for greater ease in performance."

Some comments by Philip Glass himself:

"Although I quite liked the way it turned out, it was not used for the film and ended up on my 1982 album for CBS, *Glassworks*. It also has become a staple of the live performances of the Philip Glass Ensemble and was included in Glasspieces, the production put on at the New York City Ballet in the spring of 1990, choreographed by Jerome Robbins." — more precisely, it is Part 5 of *Glassworks*, for more information cf. the appendix on *The IBM Glass Engine*.

"GLASSWORKS was intended to introduce my music to a more general audience than had been familiar with it up to then."

"I'm very pleased with it, the way it's received in performance. The pieces seem to have an emotional quality that everyone responds to, and they work very well as performance pieces."

On the appraisal published in *Gramophone Magazine*, the reviewer wrote "the Glass works gathered together on Glassworks make an excellent introduction to the sharp, hard sonorities, densely packed, slowly changing patterns and seemingly unstoppable linear flow of this important aspect of contemporary music." — we cannot adhere to the expression *"linear flow"*, that certainly is written to convey the more general idea of smoothness.

Musical scores are available from www.ChesterNovello.com, that stores interesting information on Glass achievements and works at `http://www.chesternovello.com/default.aspx?TabId=2431&State_2905=2&composerId_2905=540.`

3 Self-Affine Cartoons, Self-Affine Bars

One of the pathways described by Mandelbrot [4], [5] is via diagonal-axial self-affine cartoons, cf. for instance figures N1-6 and N1-7, pp. 33–34 in [4]. This inspired us to assimilate the idea of self-affine cartoons and of self-affine bars (measures).

Observe however that in any practical human made artifact, or in other practical applications, an important difference does exist: while in the construction of multifractals infinite iteration is conceived, in practical applications a rather limited number of iterations is mandatory, and hence some stopping rule has to be defined, see Pestana and Aleixo [6] and Aleixo *et al.* [1] on stuttering Cantor sets.

For instance, looking at bars 19–39 from page 14 of the score of *Glassworks*, reproduced in the left and "exploded" in the right of Fig. 3 below
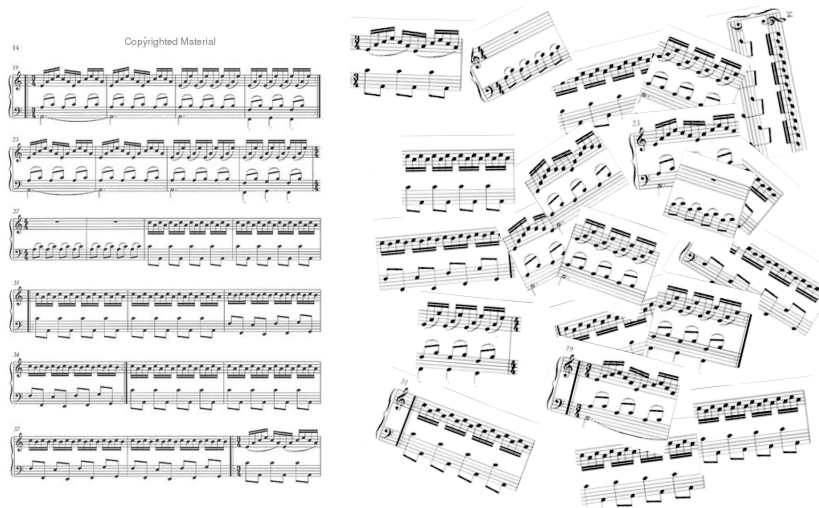
Fig. 1. Page 14 of the score of *Glassworks*, and an "exploded" view of the 21 bars # 19–39.

we observe that there exist in it only six types of bars, cf. Fig. 3, types 1 and 2, and 4 and 5 being obviously very similar.

Fig. 2. Bar types in the 21 bars 19–39 in page 14 of the score of *Glassworks*.

The description of this piece of the score can obviously be rendered very simply as the sequence of bar types $\{1 - 1 - 1 - 2 - 1 - 1 - 1 - 2 - 3 - 3 - 4 - 4 - 4 - 4 - 5 - 5 - 4 - 4 - 5 - 5 - 6\}$.

In this preliminary investigation, we decided to assess the probability of recomposing this 21 bars piece using the bar types identified in Fig. 3 together with an order 1 Markov chain defined by the initial state

$$\begin{bmatrix} 1 \\ 0 \\ 0 \\ 0 \\ 0 \\ 0 \end{bmatrix}$$

and transition matrix

	Type 1	Type 2	Type 3	Type 4	Type 5	Type 6
Type 1	$\frac{2}{3}$	$\frac{1}{3}$	0	0	0	0
Type 2	$\frac{1}{2}$	0	$\frac{1}{2}$	0	0	0
Type 3	0	0	$\frac{1}{2}$	$\frac{1}{2}$	0	0
Type 4	0	0	0	$\frac{2}{3}$	$\frac{1}{3}$	0
Type 5	0	0	0	$\frac{1}{4}$	$\frac{1}{2}$	$\frac{1}{4}$

(this of course can generate sequences with less than 21 bars, in case a transition from state 5 to state 6 effectively does occur at a discrete time less than 20). The assessment has been made generating 10,000 sequences

$\{1 - 1 - 1 - 2 - 1 - 1 - 1 - 2 - 3 - 3 - 4 - 4 - 4 - 4 - 5 - 5 - 4 - 4 - 5 - 5 - 6\}$

$\{1 - 1 - 2 - 2 - 2 - 1 - 1 - 2 - 3 - 3 - 4 - 4 - 4 - 4 - 5 - 5 - 4 - 4 - 5 - 5 - 6\}$

$\{1 - 1 - 1 - 2 - 1 - 1 - 1 - 2 - 2 - 3 - 4 - 4 - 4 - 4 - 5 - 5 - 4 - 4 - 5 - 5 - 6\}$

$\{1 - 1 - 1 - 2 - 1 - 1 - 1 - 2 - 3 - 3 - 4 - 4 - 4 - 4 - 5 - 5 - 4 - 4 - 5 - 5 - 6\}$

$\{1 - 1 - 1 - 2 - 2 - 1 - 1 - 2 - 3 - 3 - 4 - 4 - 4 - 4 - 5 - 5 - 4 - 5 - 6 - \ - \ \}$

$\{1-1-1-2-1-1-1-2-3-3-4-4-4-4-5-5-4-4-5-5-6\}$

$\{1-1-1-2-1-1-1-2-3-3-4-4-4-4-5-5-4-4-5-5-6\}$

$\{1-1-1-2-1-1-1-2-3-3-4-4-4-4-5-5-4-4-5-5-6\}$

...

Alternatively, we also generated sequences using as transition matrix

$$Type\ 1 \mid Type\ 2 \mid Type\ 3 \mid Type\ 4 \mid Type\ 5 \mid Type\ 6$$

Type 1	$\frac{2}{3}$	$\frac{1}{3}$	0	0	0	0
Type 2	$\frac{1}{2}$	0	$\frac{1}{2}$	0	0	0
Type 3	0	0	$\frac{1}{2}$	$\frac{1}{2}$	0	0
Type 4	0	0	0	$\frac{2}{3}$	$\frac{1}{3}$	0
Type 5	0	0	0	$\frac{1}{4}$	$\frac{1}{2}$	$\frac{1}{4}$
Type 6	$\frac{1}{6}$	$\frac{1}{6}$	$\frac{1}{6}$	$\frac{1}{6}$	$\frac{1}{6}$	$\frac{1}{6}$

and also with discrete uniformly distributed initial state

$$\begin{bmatrix} \frac{1}{6} \\ \frac{1}{6} \\ \frac{1}{6} \\ \frac{1}{6} \\ \frac{1}{6} \\ \frac{1}{6} \end{bmatrix}$$

Other sensible variations are under investigation, as well as a comparison with more linear and iterative procedures to generate musical scores, as for instance the Lindenmayer systems described in Pestana [7].

4   Conclusions

The proportion of 21 bars scores randomly generated as described that are strictly coincidental with Glass' original — that will be revealed at *Chaos 2012* — is rather less than we had expected in such minimalist setting.

Deeper results may indeed be obtained using higher order Markov chains, assimilating tied pairs of bars or tied triplets of bars with digrammas and

trigrammas as used in mathematical linguistics and its applications to encryption.

We also observe that a large proportion of the random scores produced using the transition matrix so roughly defined is rather pleasing. Romantism brought in a respect for the artist and the idea of inspiration that tends to convince us that any modification of an inspired masterpiece cannot but spoil it. On his authoritative *Le Mythe de Rimbaud*, Etiemble [3] reports that in many occasions he recited *Le Bateau Ivre* purposely interchanging lines and blocks of the poem — with no complains from none of the many specialists that fiercely claim that not a single word can be changed in this immortal "chef-d'oeuvre"...

In fact, a subjective evaluation, using our own taste, is that 96.3% of the sequences of 21 bars randomly generated using the transition matrix are reasonably pleasant.

5   Appendix A: The IBM Glass Engine

The IBM Glass Engine enables deep navigation of the music of Philip Glass. Personal interests, associations, and impulses guide the listener through an expanding selection of over sixty Glass works.

The glass engine was developed at the IBM T.J. Watson Research Center in 2001. You can download it from Phip Glass page `http://www.philipglass.com/music/compositions/facades.php`.
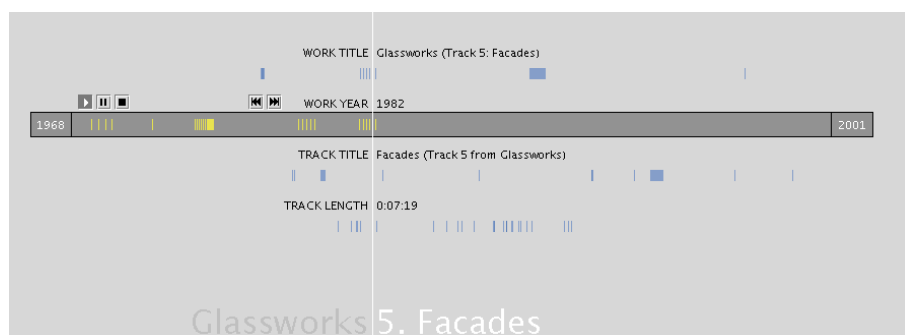
Fig. 3. glassengine — locating the track *Façades*.

The answers to two of the Frequently Asked Questions deserve to be recorded:

Q: Who decided how to assign the subjective values (such as JOY) to the tracks? Was this done by a computer?
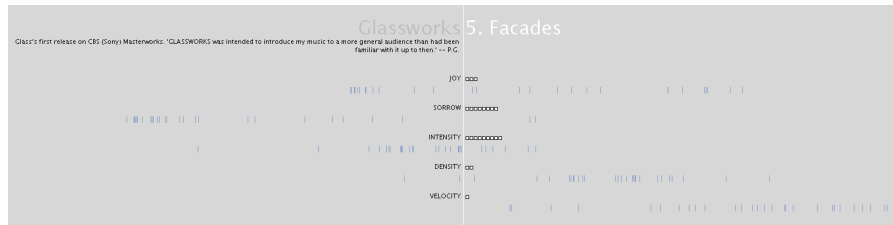
Fig. 4. glassengine — assignement of Joy, Sorrow, Intensity, Density and Velocity to the track *Façades*.

A: These values were assigned by Philip Glass's longtime producer and sound designer, Kurt Munkacsi, while eating several pounds of chocolate chip cookies.

Q: How is it possible for a track to have high amounts of both joy and sorrow?

A: Music can contain two conflicting emotions. Really.

6   Appendix B: Koyaanisqatsi

Koyaanisqatsi, Life Out Balance, 1982, directed by Godfrey Reggio, music by Philip Glass, "is the first film of the QATSI trilogy. The title is a Hopi Indian word meaning 'life out of balance'. Created between 1975 and 1982, the film is an apocalyptic vision of the collision of two different worlds — urban life and technology versus the environment. [...] *Koyaanisqatsi* attempts to reveal the beauty of the beast!".

Aside from the MGM release presented by Francis Ford Coppola, (Credits: Music: Philip Glass. Philip Glass Music: Produced & Recorded by Kurt Munkacsi. Conducted by Michael Riesman), you may be interested in *KOYAANISQATSI — Godfrey Reggio — making of*, retrieved in `http://www.youtube.com/watch?v=_Mr26_m5rGQ`.

`http://www.youtube.com/watch?v=GQsoMIGuPD8` is Part 1/9 uploaded by schipflingerfred in youtube (some other parts have been blocked on copyright infringement rights). Other *url* addresses where parts of the movie can be watched:

```
http://www.youtube.com/watch?v=Me7QaFMcQ9A&feature=relmfu,
http://www.youtube.com/watch?v=DlFg1MgATu4&feature=related,
http://www.youtube.com/watch?v=-iNJ8u4ewD8&feature=relmfu,
http://www.youtube.com/watch?v=M27874iHwpg&feature=relmfu.
```

For more information, cf. also the section `http://www.philipglass.com/music/films/koyaanisqatsi.php` in Philip Glass' webpage.

7 Appendix C: Repetition and Innovation in the Philosophy of Music Composition

(Platzner's and a layman description of the musical structure of the form *rondo* to be developed in the full length paper.)

References

1. Aleixo, S., Brilhante, M. F., and Pestana, D., General stuttering Beta(p; q) Cantor-like random sets. ISI 2011, 58th Session of the International Statistical Institute, 2011.
2. Ervertsz, C. J. G., and Mandelbrot, B., Multifractal Measures. In H.-O. Peitgen, H. Jürgens, and D. Saupe. *Chaos and Fractals: New Frontiers of Science*, Springer Verlag, New York, 1993, 921–969.
3. Etiemble, *Le Mythe de Rimbaud — L'Année du centenaire*, Gallimard, Paris, 1961.
4. Mandelbrot, B., *Fractals and Scaling in Finance; Discontinuity, Concentration, Risk*, Springer, New York, 1997.
5. Mandelbrot, B., *Multifractals and 1/f Noise; Wild Self-Affinity in Physics*, Springer, New York, 1999.
6. Pestana, D., and Aleixo, S. (2011). Stuttering Cantor-Like Random Sets, In Luzar-Stiffler, V., Jarec, I. and Bekic, Z. (eds.), Proceedings of the ITI 2010, 32nd International Conference on Information Technology Interfaces, 29-34.
7. Pestana, P., Lindenmayer Systems and the Harmony of Fractals, *Chaotic Modeling and Simulation* (CMSIM) 1: 91–99, 2012
8. Platzer, F., *Abrégé de Musique*, Ellipses, Paris, 2011.
9. M. Schroeder. *Fractals, Chaos, Power Laws: Minutes from an Infinite Paradise*, Dover, New York, 2009.
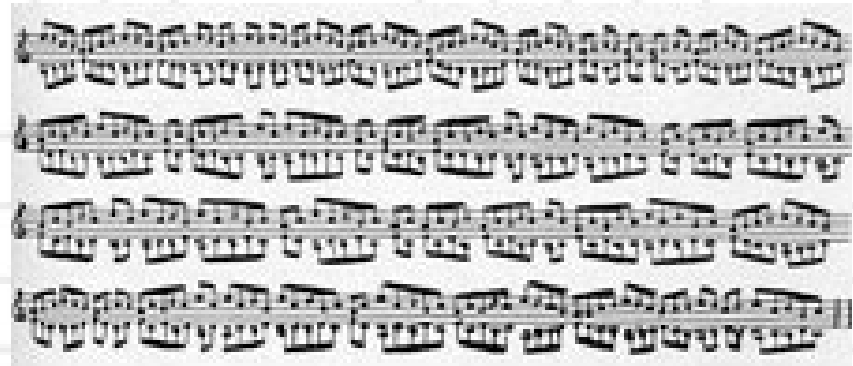
Control and Synchronization of Fractional–Order Differential Equations of Phase–Locked Loop

Viet–Thanh Pham[1], Mattia Frasca[1], Riccardo Caponetto[1], Thang Manh Hoang[2], and Luigi Fortuna[1]

[1] Dipartimento di Ingegneria Elettrica Elettronica e Informatica, Università degli Studi di Catania, 95125 Catania, Italy
(E-mail: `mfrasca@diees.unict.it`)
[2] School of Electronics and Telecommunications, Hanoi University of Science and Technology, Hanoi, Vietnam
(E-mail: `hmt@mail.hut.edu.vn`)

Abstract. Previous published researches on chaos, controlling and synchronization in phased–locked loops focused only on integer–order phase–locked loops. In this paper, we study control and synchronization of phase–locked loop systems based on fractional–order differential equations. Stability analyses of commensurate fractional–order linear system are utilized to control chaotic behaviour exhibited by fractional–order differential equation–based phase–locked loop. Furthermore, chaos synchronization is obtained by employing the nonlinear state observer method. Finally, numerical simulations verify the effectiveness and applicability of our approaches.
Keywords: Fractional–order equation, Phase–locked loop, Chaos control, Chaos synchronization.

1 Introduction

Fractional calculus was introduced in the early 17th century and has been applied to describe various real systems such as transmission lines, electrical noises, dielectric polarization and heat transfer phenomena Arena *et al.*[1]. Recently, there are amount of efforts to discover the chaos of fractional–order systems. Specifically, chaotic features have been proofed in fractional–order Lorenz system, fractional–order Chua's system, fractional–order Duffing's oscillator, fractional–order Genesio–Tesi system and fractional–order Lotka–Volterra system Caponetto *et al.*[2]. Moreover, the synchronization and controlling fractional–order chaotic systems are the topics which received more attention because of their practical applications. Li et al. implemented synchronization of fractional Lorentz system, Chen system and Chua circuit by the aid of controller and driving signals Li and Yan[3]. Matouk[4] proposed the feedback control and synchronization of a fractional–order modified Van der Pol–Duffing circuit using fractional Routh–Hurwitz conditions.

Phase–locked loop (PLL) plays a vital role in communication and control systems Gardner[5] where applications of PLL include clock synchronization,

469

carrier recovery, frequency or phase modulation and demodulation, frequency synthesis, and PLL controlled motors. Generally, PLL works in the locked range in which average frequency of the voltage controlled oscillator (VCO) exactly equal to the average frequency of the input signal. However, chaotic behaviours of PLLs have been observed and studied with second–order loop filter Endo and Chua[6] under certain conditions. In order to control undesirable chaos effects in PLLs, Zhao *et al.*[7] represented the state observer to design a non–linear feedback controller for second–order non–autonomous PLL. Experimental synchronization of two PLLs driven by a common chaotic signal derived from a master PLL was also observed Endo and Chua[6] if the detuning of the VCO free-running frequencies was not large. Even through, a fractional–order differential equation–based phase–locked loop is still not considered. There is an expectation that fractional–order differential equation–based phase–locked loop (FOPLL), which processes key features of classical PLL, will have important potential applications in such areas as communications and control. Motivated by this expectation, in this work, we introduce a new model of the FOPLL and propose control and synchronization methods for it.

This paper is organized as follows. In the next Section, we review the fractional calculus and the stability of the fractional–order systems. The model of FOPLL will be given in Section 3. After explaining chaos controlling for FOPLL in Section 4, the synchronization between two FOPLLs is described in Section 5. Finally, Section 6 draws some concluding remarks.

2   Fractional calculus review

The fractional–order differentiator can be denoted by a general fundamental operator $_aD_t^\alpha$ as a generalization of the differential and integral operators Caponetto *et al.*[2], which is defined as follows

$$_aD_t^\alpha = \begin{cases} \frac{\mathrm{d}^\alpha}{\mathrm{d}t^\alpha} & R(\alpha) > 0, \\ 1 & R(\alpha) = 0, \\ \int\limits_a^t (\mathrm{d}\tau)^{-\alpha} & R(\alpha) < 0, \end{cases}$$

where a is the initial value, in addition, α is the fractional order which can also be complex, and $R(\alpha)$ is the real part of the fractional order. The commonly used definition of fractional derivative is Grunwald-Letnikov definition which is described as the following form

$$_aD_t^\alpha f(t) = \lim_{h \to 0} \frac{1}{h^\alpha} \sum_{j=0}^{[(t-a)/h]} (-1)^j \binom{\alpha}{j} f(t - jh),$$

where [.] means the integer part. Other way to study fractional–order function is applied the Laplace transform of fractional derivative as

$$L\left\{{}_0D_t^\alpha f(t)\right\} = s^\alpha F(s).$$

The commensurate fractional–order linear time–invariant system can be presented by the state–space model

$$\begin{cases} {}_0D_t^\alpha \mathbf{x}(t) = \mathbf{A}\mathbf{x}(t) + \mathbf{B}\mathbf{u}(t), \\ \mathbf{y}(t) = \mathbf{C}\mathbf{x}(t), \end{cases}$$

where $\mathbf{x} \in R^n$, $\mathbf{u} \in R^r$ and $\mathbf{y} \in R^p$ are the state, input and output vectors of the system and $\mathbf{A} \in R^{n\times n}$, $\mathbf{B} \in R^{n\times r}$, $\mathbf{C} \in R^{p\times n}$. According to Matignon[8], the system is stable if it satisfies the condition:

$$|\arg(\text{eig}(\mathbf{A}))| > \alpha\frac{\pi}{2}, \tag{1}$$

where $0 < \alpha < 1$ and $\text{eig}(\mathbf{A})$ is the eigenvalues of matrix $\mathbf{A}$.

On the other hand, the commensurate fractional order nonlinear system could be described by

$$_0D_t^\alpha \mathbf{x} = \mathbf{f}(\mathbf{x}),$$

where $0 < \alpha < 1$ and $\mathbf{x} \in R^n$. The equilibrium points of system are asymptotically stable Tavazoei and Haeri[9] if the following condition is satisfied:

$$|\arg(\text{eig}(\mathbf{J}))| = |\arg(\lambda_i)| > \alpha\frac{\pi}{2}, \tag{2}$$

where λ_i are the eigenvalues of the Jacobian matrix $\mathbf{J}$, which is evaluated at the equilibrium points.

3 Mathematical model of fractional–order differential equation–based phase–locked loop

The model of one conventional phase–locked loop is considered firstly. The PLL contains three main components: a phase detector (PD), a loop filter (LF) and a VCO as shown in Fig. 1. PD compares the phase of input signal against the phase of VCO and creates the control voltage which is applied to VCO to change the VCO frequency. As the result, the average phase of the VCO tracks the average phase of input. To analyse the dynamical features of PLL, its model in term of phase is presented as in Fig. 2.

In Fig. 2, θ_i and θ_o denote the input and output phase, respectively; while $\phi = \theta_i - \theta_o$ is the phase error. There, PD is a mixer and LF is a first order filter with the transfer function
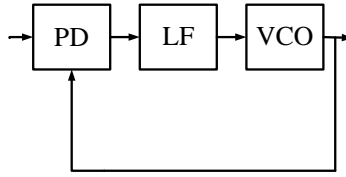
$$F_{LPF}(s) = \frac{1}{1 + \tau s},$$

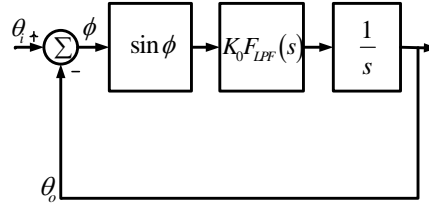**Fig. 1.** Block diagram of the typical phase–locked loop.

Fig. 2. Phase model of the typical phase–locked loop.

where τ is time constant and s is an operator denoting $\frac{d}{dt}$. The differential equation that characterizes the PLL can be written as

$$\frac{d^2\phi}{dt^2} + \beta\frac{d\phi}{dt} + \sin\phi = \beta\sigma + \beta M \sin(\Omega t) + M\Omega \cos(\Omega t),$$

where β, σ, Ω, M are normalized natural frequency, normalized frequency detuning, normalized modulation frequency and normalized maximum frequency derivation, respectively. Let $x_1 = \phi$ and $x_2 = \dot\phi$, the previous equation has the following form:

$$\begin{cases} \dot{x}_1 = x_2 \\ \dot{x}_2 = -\beta x_2 - \sin x_1 + \beta\sigma + \beta M \sin(\Omega t) + M\Omega \cos(\Omega t). \end{cases}$$

The variation of Lyapunov exponents Wolf *et al.*[10] when the parameter β changes in the range $[0.05, 0.4]$ is given in Fig. 3. For the parameter value $\beta = 0.056$, integer–order PLL is chaotic since the Lyapunov exponent is positive. By replacing integer–order derivatives in above equation by fractional–order ones, the fractional–order differential equation–based PLL is introduced as

$$\begin{cases} {}_0D_t^\alpha x_1 = x_2 \\ {}_0D_t^\alpha x_2 = -\beta x_2 - \sin x_1 + \beta\sigma + \beta M \sin(\Omega t) + M\Omega \cos(\Omega t), \end{cases} \quad (3)$$

where α is the derivative order. We found the presence of chaos in fractional–order PLL equation by observing the largest Lyapunov exponent (see Fig. 3). When $\alpha = 0.98$, $\beta = 0.056$, $\sigma = 0.2$, $M = 0.8$, $\Omega = 0.7$ the fractional–order differential equation–based phase–locked loop exhibits chaos behaviour. The phase portrait and time response are illustrated in Figs. 4, 5. It is notable that there are some similarities between two kinds of phase–locked loops in dynamical behaviour (Fig. 3) as well as tracking range (Fig. 6).
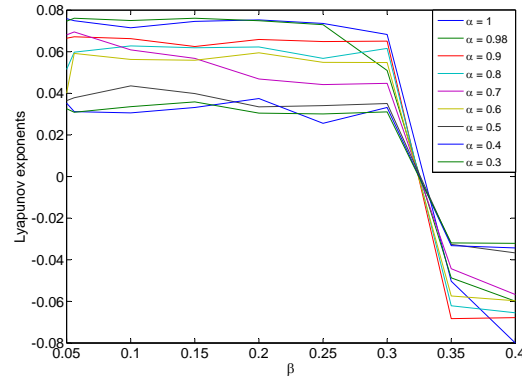
Fig. 3. Largest Lyapunov exponents according to β and σ of the typical integer–order phase–locked loop and the phase–locked loops based on fractional–order differential equation when $M = 0.8$, $\Omega = 0.7$.
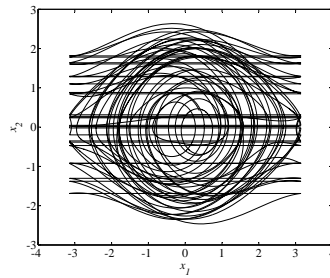

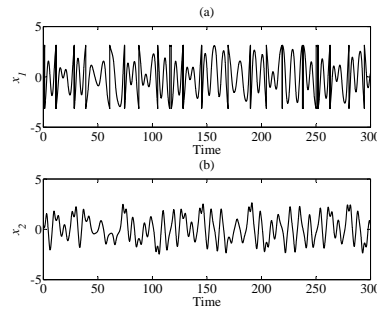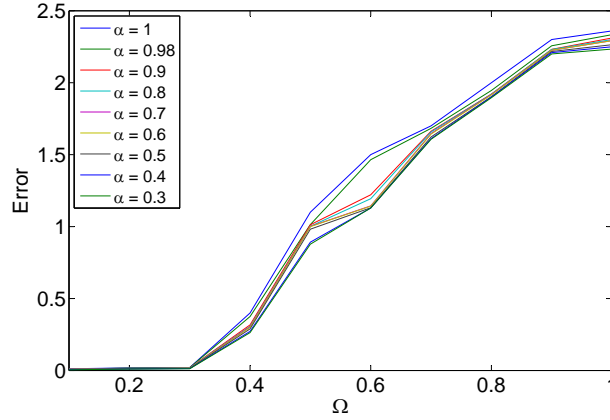**Fig. 4.** Chaotic attractor in FOPLL with $\alpha = 0.98$.

Fig. 5. Chaotic time domain representations of FOPLL with $\alpha = 0.98$: (a) x_1, (b) x_2.

4   Chaos control in fractional–order differential equation–based phase–locked loop

Control chaos is a progress to manage the unexpected performances in diverse areas of research such as biology, physiology, fluid mechanics, electron-

Fig. 6. Tracking errors of the typical integer–order phase–locked loop and the phase–locked loops based on fractional–order differential equation versus the derivative order α.

ics, chemical engineering, and so on [11]. The study of chaos control in this Section provides the designer one tool to develop applications involving FO-PLL without undesired chaos. Specifically, FOPLL (3) could be rewritten in the matrix form as follows

$$_0D_t^\alpha \mathbf{x} = \mathbf{Ax} + \mathbf{Bf}(\mathbf{x}) + \mathbf{u},$$

where $\mathbf{A} = \begin{bmatrix} 0 & 1 \\ 0 & -\beta \end{bmatrix}$, $\mathbf{B} = \begin{bmatrix} 0 & 0 \\ 0 & -1 \end{bmatrix}$, $\mathbf{f}(\mathbf{x}) = \begin{bmatrix} 0 \\ \sin x_1 \end{bmatrix}$, $\mathbf{x} = \begin{bmatrix} x_1 \\ x_2 \end{bmatrix}$, and $\mathbf{u} = \begin{bmatrix} 0 \\ \beta\sigma + \beta M \sin(\Omega t) + M\Omega \cos(\Omega t) \end{bmatrix}$. To control chaos, one addition control term $\mathbf{u}_c$ is applied in FOPLL. Hence, the controlled FOPLL system can be obtained as

$$_0D_t^\alpha \mathbf{x} = \mathbf{Ax} + \mathbf{Bf}(\mathbf{x}) + \mathbf{u} + \mathbf{u}_c.$$

There, by combining the feedback control method Schöll and Schuster[11] and condition (2), $\mathbf{u}_c$ is selected as

$$\mathbf{u}_c = \begin{bmatrix} 0 \\ k(x_1 + x_2) - \beta\sigma - \beta M \sin(\Omega t) - M\Omega \cos(\Omega t) \end{bmatrix}.$$

Therefore, the controlled FOPLL system has the reduced form

$$_0D_t^\alpha \mathbf{x} = \mathbf{g}(\mathbf{x}), \tag{4}$$

in which

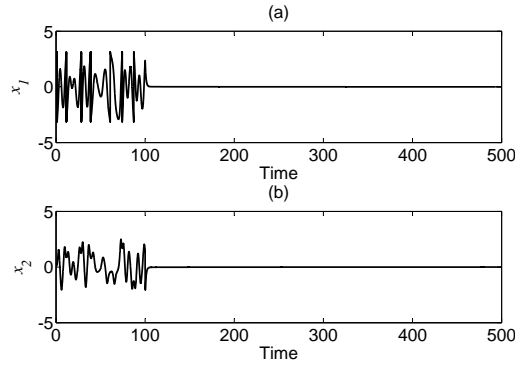$$\mathbf{g}(\mathbf{x}) = \begin{bmatrix} x_2 \\ -\sin x_1 + kx_1 + (k - \beta)x_2 \end{bmatrix}.$$

Fig. 7. Times series plots of the controlled FOPLL (a) $x_1(t)$, (b) $x_2(t)$. Controller is turned on at $t = 100$.

The Jacobian matrix of (4) is given by

$$\mathbf{J} = \begin{bmatrix} 0 & 1 \\ k - \cos x_1 & k - \beta \end{bmatrix}. \tag{5}$$

Replacing equilibrium points of system (4) $\mathbf{x}^* = \begin{bmatrix} x_1^* & x_2^* \end{bmatrix} = \begin{bmatrix} 0 & 0 \end{bmatrix}$ into the Jacobian matrix, we have

$$\mathbf{J}\,|_{\mathbf{x}=\mathbf{x}^*} = \begin{bmatrix} 0 & 1 \\ k - 1 & k - \beta \end{bmatrix}. \tag{6}$$

The eigenvalues λ_i of $\mathbf{J}\,|_{\mathbf{x}=\mathbf{x}^*}$ are the solutions to the equation

$$\det\left(\mathbf{J}\,|_{\mathbf{x}=\mathbf{x}^*} - \lambda\mathbf{I}\right) = 0. \tag{7}$$

By choosing the parameter k such that the condition (2) satisfies, equilibrium points of FOPLL (4) are asymptotically stable. To illustrate the effectiveness of the proposed controlling approach, numerical simulation is implemented with the chosen parameter $k = -16$, which makes (7) has two separated negative real solutions. Simulation results of chaos control are displayed in Fig. 7. Obviously, after applying the controlling process, FOPLL works in locked region where phase and frequency errors equal zeros.

5 Synchronization of chaos in fractional–order differential equation–based phase–locked loops

Synchronization in chaotic systems has received amount of attention because of practical application such as secure chaotic communication. As reporting in Section 3, FOPLL can be chaotic; hence, the synchronization in two FOPLL systems can derive the secure communication systems. In this Section,
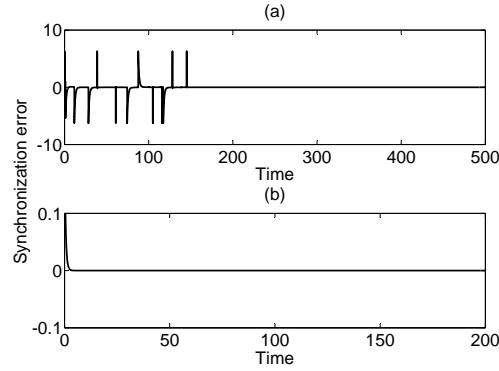
Fig. 8. Synchronization behaviour of two FOPLLs (a) $x_{1m} - x_{1s}$, (b) $x_{2m} - x_{2s}$.

the synchronous scheme between two FOPLLs, named master and slave system Boccaletti[12] is demonstrated. This synchronous scheme is based on the nonlinear state observer. Similar to the previous Section, the master is defined as

$$_0D_t^\alpha \mathbf{x}_m = \mathbf{A}\mathbf{x}_m + \mathbf{B}\mathbf{f}(\mathbf{x}_m) + \mathbf{u},$$

where $\mathbf{x}_m = \begin{bmatrix} x_{1m} \\ x_{2m} \end{bmatrix}$, $\mathbf{f}(\mathbf{x}_m) = \begin{bmatrix} 0 \\ \sin x_{1m} \end{bmatrix}$. While the slave system is built as follows

$$_0D_t^\alpha \mathbf{x}_s = \mathbf{A}\mathbf{x}_s + \mathbf{B}\mathbf{f}(\mathbf{x}_m) + \mathbf{u} + \mathbf{K}\mathbf{e},$$

where $\mathbf{x}_s = \begin{bmatrix} x_{1s} \\ x_{2s} \end{bmatrix}$, $\mathbf{K} \in R^{2\times 2}$ is the feedback gain matrix and $\mathbf{e} = \begin{bmatrix} e_1 \\ e_2 \end{bmatrix} = \begin{bmatrix} x_{1m} - x_{1s} \\ x_{2m} - x_{2s} \end{bmatrix}$ is the synchronization error. The dynamical synchronization error of system could be written as

$$_0D_t^\alpha \mathbf{e} = {}_0D_t^\alpha \mathbf{x}_m - {}_0D_t^\alpha \mathbf{x}_s = (\mathbf{A} - \mathbf{K})\mathbf{e}. \tag{8}$$

The synchronization occurs when $\mathbf{K}$ is chosen appropriately such that

$$\lim_{t\to\infty} \|\mathbf{x}_m - \mathbf{x}_s\| = \lim_{t\to\infty} \|\mathbf{e}\| = 0.$$

It is clear to see that (8) is the fractional–order linear time–invariant system; hence, the condition (1) could be applied to find matrix $\mathbf{K}$. There, $\mathbf{K}$ is achieved as

$$\mathbf{K} = \begin{bmatrix} 1 & 1 \\ 0 & 2 - \beta \end{bmatrix},$$

which makes $|\arg(\mathrm{eig}(\mathbf{A} - \mathbf{K}))| > \alpha\frac{\pi}{2}$ by the eigenvalues $\mathrm{eig}(\mathbf{A} - \mathbf{K}) = \begin{bmatrix} -1 & -2 \end{bmatrix}$. Simulation results in Fig. 8 show the feasibility of the proposed synchronization scheme.

6   Conclusion

We have introduced a novel model of fractional–order differential equations of phase–locked loops. Some principal characteristics of FOPLL, such as phase tracking and chaos, are investigated. The control of chaotic behaviour in FOPLL is implemented in order to guarantee the precision on phase tracking in practice. Moreover, synchronization scheme based on nonlinear state observer is performed. We have also obtained the simulation results which fixed with theoretical analyses. In our future researches on this subject, the discovery of the novel features and promising applications of the FOPLL will be estimated.

Acknowledgement

References

1. P. Arena, R. Caponetto, L. Fortuna, and D. Porto. *Nonlinear noninteger order circuits and systems: An introduction*, Singapore, 2000. World Scientific.
2. R. Caponetto, G. Dongola, and L. Fortuna. *Fractional order systems: Modeling and control application*, Singapore, 2010. World Scientific.
3. C. Li, and J. Yan. The synchronization of three fractional differential systems. *Chaos, Solitons & Fractals*, 32:751–757, 2007.
4. A. Matouk. Chaos, feedback control and synchronization of a fractional-order modified autonomous Van der Pol-Duffing circuit. *Comm. Nonl. Sci. Num. Sim.*, 16:975–986, 2011.
5. F. M. Gardner. *Phaselock techniques*, 2005. Wiley-Interscience.
6. T. Endo and L. O. Chua. Synchronization of chaos in phase-locked loops. *IEEE Trans. Circuits Systems*, 38:1580–1588, 1991.
7. Y.–B. Zhao, D.–Q. Wei, and X.–S. Luo. Study on chaos control of second-order non-autonomous phase-locked loop based on state observer. *Chaos, Solitons & Fractals*, 39:1817–1822, 2009.
8. D. Matignon. Stability results for fractional differential equations with applications to control processing. *Proceedings Comp. Eng. Sys. Appl.*, 963–968, 1996.
9. M. S. Tavazoei and M. Haeri. A necessary condition for double scroll attractor existence in fractional–order systems. *Physic Letters A*, 367:102-113, 2007.
10. A. Wolf, J. B. Swift, H. L. Swinney, and J. A. Vastano. Determining Lyapunov exponents from a time series. *Physica D*, 16:285-317, 1985.
11. E. Schöll and H. Schuster. *Handbook of chaos control*, 2008. Wiley-VCH.
12. S. Boccaletti, J. Kurths, D. L. Valladares, G. Osipov, and C. Zhou. The synchronization of chaotic systems. *Physic Reports*, 366:1-101, 2002.

Chaos in Compound Anti-Symmetric-Case Piecewise-Linear Delay Differential Equations

Phocharavidh Phuphatana and Banlue Srisuchinwong

Sirindhorn International Institute of Technology, Thammasat University,
Pathum-Thani, Thailand 12000
E-mail: phocharavidh.pp@gmail.com, banlue@siit.tu.ac.th

Abstract: An existing anti-symmetric-case piecewise-linear delay differential equation (DDE) has exhibited chaos at a delay time $\tau = 3$ using an odd term $f_a = f_1$ for $a = 1$. Three new compound anti-symmetric-case piecewise-linear DDEs are presented. Each DDE exhibits chaos using $\tau < 3$. The first compound DDE is a combination of two odd terms f_1 and f_3 where $a = 1$ and 3, and $1.70 < \tau < 2.10$. The second compound DDE is a combination of two even terms f_2 and f_4 where $a = 2$ and 4, and $1.50 < \tau < 1.90$. Finally, the third compound DDE is a combination of two odd terms f_1 and f_3, and an even term f_2 where $a = 1$, 2, and 3, and $1.05 < \tau < 1.27$. Not only can the higher value of 'a' reduce the value of τ for chaos, but the more combination of terms f_a also can. The reduction in τ enables simple implementation of a LC network in the delay unit.
Keywords: chaos, delay differential equation; reduced-delay

1. Introduction

Since the discovery of the eminent Lorenz chaotic attractor in 1963 [1], studies of chaotic behavior in nonlinear systems have attracted great attention due to a variety of applications in science and technology, e.g. chaos-based secure communications [2], [3], [4]. Time-delay systems can exhibit chaos with a relatively simple model involving a value of the dynamical variable at one or more times in the past [5]. They have an infinite-dimensional state space with a large value of positive Lyapunov exponents and are good candidates for highly secure communications. In general, a first-order time-delay system is described by a delay differential equation (DDE) of the form.

$$\dot{x}(t) = f[x(t), x_\tau] \tag{1}$$

where the overdot denotes a time (t) derivative, $x_\tau = x(t-\tau)$ is the value of x at an earlier time ($t-\tau$), and τ is a delay time, i.e. $\tau \leq t$.

One of the earliest and most widely studied DDE is the Mackey-Glass equation [6], as shown in (2), proposed to model the production of white blood cells. The equation exhibits chaos with parameters such as $a = 0.2$, $b = 0.1$, $c = 10$, and $\tau = 23$. Other examples of DDEs exhibiting chaos include Ikeda DDE [7] and sinusoidal DDE [5].

$$\dot{x} = \frac{ax_\tau}{1 + x_\tau^c} + bx, \tag{2}$$

Recently, chaos in an anti-symmetric-case piecewise-linear DDE has been reported [5], as shown in (3).

$$\bar{x} = |x_\tau + 1| - |x_\tau - 1| - x_\tau \tag{3}$$

for $\tau = 3$. The largest Lyapunov exponent $\lambda = 0.0909$. Such a system is especially amenable to implementation with electronic circuits [8]. A delay unit may be implemented using an LC network [9]. As the size of the LC network is proportional to the value of the delay time τ, a reduction of τ in (3) is preferable.

In this paper, three new compound anti-symmetric-case piecewise-linear DDEs are presented. Each DDE exhibits chaos using delay time $\tau < 3$. Such a reduction of the delay time in the DDEs enables simple implementation of the LC network in the delay unit.

2. Compound Anti-Symmetric-Case Piecewise-Linear DDEs

For simplicity, the right hand side of (3) can be modified as a general function f_a as shown in (4)

$$f_a = |x_\tau + a| - |x_\tau - a| - x_\tau \tag{4}$$

where the parameter 'a' is an integer. Equation (3) is therefore represented by an odd term f_1 as $a = 1$. Three new compound anti-symmetric-case piecewise-linear DDEs are proposed. The first compound DDE is a combination of two odd terms f_1 and f_3 where $a = 1$ and 3, as shown in (5). The second compound DDE is a combination of two even terms f_2 and f_4 where $a = 2$ and 4, as shown in (6). Finally, the third compound DDE is a combination of two odd terms f_1 and f_3, and an even term f_2 where $a = 1, 2,$ and 3, as shown in (7).

$$\begin{aligned} \bar{x}_1 &= f_1 + f_3 \\ &= |x_\tau + 1| - |x_\tau - 1| + |x_\tau + 3| - |x_\tau - 3| - 2x_\tau \end{aligned} \tag{5}$$

$$\begin{aligned} \bar{x}_2 &= f_2 + f_4 \\ &= |x_\tau + 2| - |x_\tau - 2| + |x_\tau + 4| - |x_\tau - 4| - 2x_\tau \end{aligned} \tag{6}$$

$$\begin{aligned} \bar{x}_3 &= f_1 + f_2 + f_3 \\ &= |x_\tau + 1| - |x_\tau - 1| + |x_\tau + 2| - |x_\tau - 2| + |x_\tau + 3| - |x_\tau - 3| - 3x_\tau \end{aligned} \tag{7}$$

3. Numerical Results

For the first compound DDE shown in (5), Figures 1, 2 and 3 visualize numerical results of a chaotic waveform, a chaotic attractor, and a bifurcation diagram, respectively, using $\tau = 2.07$. The largest Lyapunov exponent is $\lambda = 0.3112$.
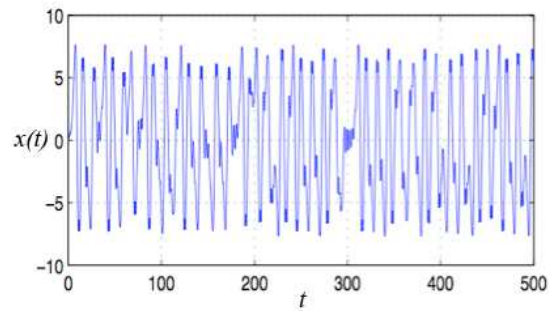

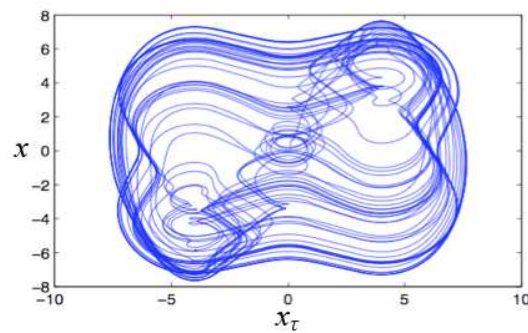Fig. 1. A chaotic waveform of (5) with $\tau = 2.07$.

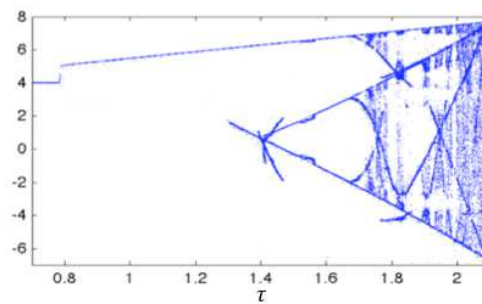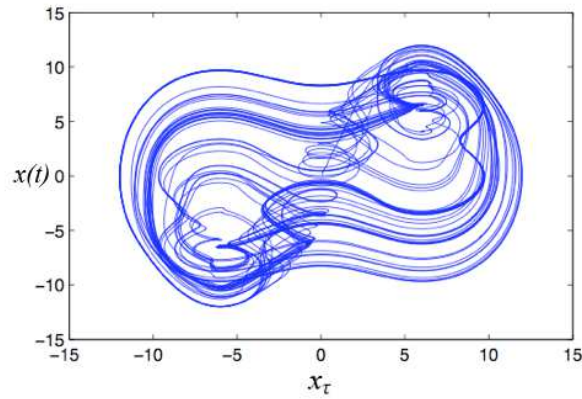Fig. 2. A chaotic attractor of (5) with $\tau = 2.07$.

Fig. 3. A bifurcation diagram of (5).

For the second compound DDE shown in (6), Figures 4 and 5 illustrate numerical results of a chaotic attractor and a bifurcation diagram, respectively. (6), using $\tau = 1.75$. The largest Lyapunov exponent is $\lambda = 0.1174$.

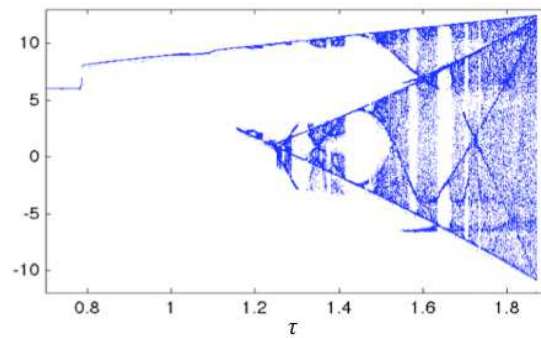Fig. 4. A chaotic attractor of (6) with $\tau = 1.75$.

Fig. 5. A bifurcation diagram of (6).

For the third compound DDE shown in (7), Figures 6 and 7 depict numerical results of a chaotic attractor and a bifurcation diagram, respectively, using $\tau = 1.20$. The largest Lyapunov exponent is $\lambda = 0.2823$.
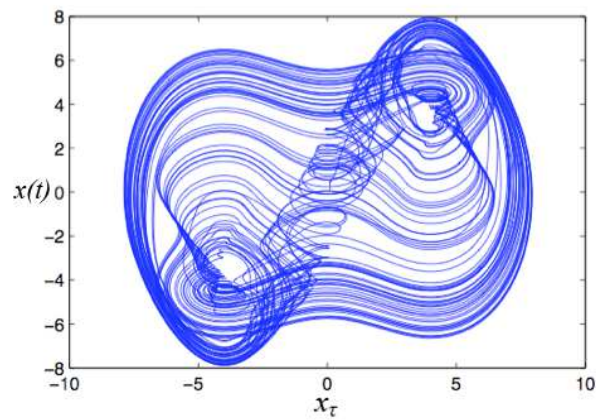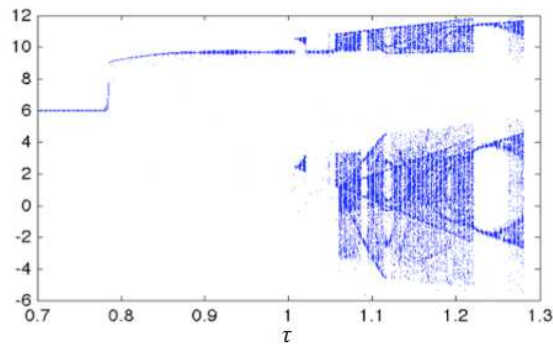
Fig. 6. A chaotic attractor of (7) with τ = 1.20.

Fig. 7. A bifurcation diagram of (7).

Table 1 summarizes ranges of delay time τ of equations (5), (6), and (7), for which chaos occurs. There are various periodic windows immersed in chaos. It can be notice from Table 1 that not only can the higher value of the parameter 'a' of f_a reduce the value of the time delay τ for chaos, but the more combination of terms f_a also can.

Table 1: Summaries of Ranges of τ For Chaos

Equations	Ranges of τ
$\dot{x}_1 = f_1 + f_3$	$1.70 < \tau < 2.10$
$\dot{x}_2 = f_2 + f_4$	$1.50 < \tau < 1.90$
$\dot{x}_3 = f_1 + f_2 + f_3$	$1.05 < \tau < 1.27$

3. Conclusions

Three new compound anti-symmetric-case piecewise-linear DDEs have been presented. The first combines two odd terms f_1 and f_3 and chaos occurs for $1.70 \angle \tau \angle 2.10$. The second combines two even terms f_2 and f_4 and chaos occurs for $1.50 \angle \tau \angle 1.90$. Finally, the third combines three terms f_1, f_2 and f_3 and chaos occurs for $1.05 \angle \tau \angle 1.27$. Chaos occurs using less delay time τ than that of the existing approach. The reduction in delay time enables the reduction in size of the LC network of the delay unit.

References

1. E. N. Lorenz. Deterministic nonperiodic flow, *J. Atmos. Sci.*, vol. 20, 130-141, 1963.

2. K. M. Cuomo, A. V. Oppenheim and S. H. Strogatz. Synchronization of Lorenz-based chaotic circuits with applications to communications, *IEEE Trans. Cir. Sys.*, vol. 40, no. 10, 626-633, 1993.

3. L. Kocarev, K. S. Halle, K. Eckert and L. O. Chua. Experimental demonstration of secure communications via chaotic synchronization, *Int. J. Bifurcat Chaos*, vol. 2, no. 3, 709-713, 1992.

4. B. Srisuchinwong, B. Munmuangsaen. A highly chaotic attractor for a dual-channel single-attractor, private communication system. In: Christos H. Skiadas, Ioannis Dimotikalis, and Charilaos Skiadas *Chaos Theory: Modeling, Simulation and Applications*. World Scientific, pp 399–405, 2011.

5. J. C. Sprott. Time-Delay Systems. In: J. C. Sprott *Elegant Chaos*. World Scientific, pp 221–232, 2010.

6. M. Mackey and L. Glass. Oscillation and chaos in physiological control systems, *Science 197*, 287-289, 1977.

7. K. Ikeda. Multiple-valued stationary state and its instability of the transmitted light by a ring cavity system, *J. Opt. Commun. 30*, 257-261, 1979.

8. U. an der Heiden, and M. C. Mackey. The dynamics of production and destruction: Analytic insight into complex behavior, *J. Math. Biol. 16*, 75-101, 1982.

9. A. Namajūnas, K. Pyragas, and A. Tamaševičius. An electronic analog of the Mackey-Glass system, *Physics Letters A*, vol. 201, 42-46, 1995.

Double power law behavior in everyday phenomena

Carla M.A. Pinto[1], A. Mendes Lopes[2], and J.A. Tenreiro Machado[3]

[1] ISEP-Institute of Engineering of Polytechnic of Porto
and Center of Mathematics of the University of Porto
Rua Dr António Bernardino de Almeida, 431
4200-072 Porto, Portugal
(Email: `cpinto@fc.up.pt`)
[2] UISPA, IDMEC - Polo FEUP
Faculty of Engineering
University of Porto
Rua Dr. Roberto Frias,
4200-465 Porto, Portugal
(Email: `aml@fe.up.pt`)
[3] Department of Electrical Engineering
ISEP-Institute of Engineering of Polytechnic of Porto
Rua Dr António Bernardino de Almeida, 431
4200-072 Porto, Portugal
(Email: `jtm@isep.ipp.pt`)

Abstract. We study similar statistical properties observed in distinct real world data. In particular, we focus on the power law (PL) distribution. We find that some data is well fitted by a single PL distribution whereas other phenomena force the use of two distinct PLs. This behavior is similar in, a priori, unrelated phenomena, such as catastrophes (terrorism, earthquakes) and variables associated to man-made systems, such as distribution of the number of words in texts or of the number of hits received by websites.
Keywords: power law, double power law, real world phenomena.

1 Introduction

Pareto [13] and Zipf [19] laws are examples of Power law (PL) distributions. These distributions are characterized by heavy tails and were first studied in 1896 by Pareto [13]. Pareto observed that the relative number of individuals with an annual income larger than a certain value x was proportional to a power of x. The later can be expressed mathematically by the expression (1).

$$F(x) = P(X \geq x) = \frac{C}{\alpha - 1} x^{-(\alpha - 1)} \tag{1}$$

where $\alpha > 0$, $C > 0$, and $F(x)$ is the complementary cumulative distribution function of the income x. In the text, we will consider $\tilde{\alpha} = \alpha - 1$ and $\tilde{C} = \frac{C}{\tilde{\alpha}}$. Zipf law is a special case of the Pareto law with exponent $\tilde{\alpha} = 1$.

Variable x in equation (1) has been used to describe quantities in a wide variety of real data. Namely, x may represent the number of: (i) individuals in a population of a city [2,19,6], (ii) articles' citations [11], (iii) hits in web-pages [1], (iv) victims in wars, terrorist attacks, or earthquakes [7,16,4], (v) words in texts [5,19], and several other phenomena [12,10]. In the literature interesting reviews on on PL behavior and applications can be found [9,18,14].

Application of PL behavior in natural or human-made phenomena usually comes with a log-log plot, where the axes represent the size of an event and its frequency. The log-log plot is asymptotically a straight line with negative slope.

The paper is organized as follows. In Section 2, we review literature concerning distinct phenomena where PL behavior has been fitted. In Section 3, we present a numerical analysis of real data where PL and double PL behavior is observed. Finally, in Section 4, we state the main conclusions and discuss future research directions.

2 Real events

PL behavior has been used to model the number of casualties in natural and human-made phenomena, such as earthquakes, tornados, terrorist attacks and wars. Understanding patterns of the number of casualties in these events may help to organize rescue operations. [7,16,4]. Other applications of PL behavior, with less impact in terms of human lives, are city and forest fires, words' frequency in texts, or the number of hits in webpages. In what concerns the study of city and forest-fire distributions, results may help to take measures beforehand in view of possible hazards, thus saving natural resources and animal and human lives.

We observe a common underneath behavior considering the number of casualties and the frequency of natural and human-made disasters. Large casualties are less frequent and are associated with low frequency phenomena. Two world wars are two examples of this type. Other wars, not so harmful in terms of preserving human lives [15], are more frequent. Analogously for earthquakes, the frequency of occurrence of terrific earthquakes, that cause a large number of victims, is much lower than that of smaller earthquakes with few casualties [7].

Johnson *et al* [8] studied war and global terrorism patterns, and developed a theory for explaining their similar dynamical evolution. The later was invariant to underlying ideologies, motivations and the terrain in which they operated. They considered each insurgent force as a generic, self-organizing system, which evolved dynamically through the continual coalescence and fragmentation of its constituent groups. Researchers have used wars in Iraq and Afghanistan, and long-term guerrilla war in Colombia, as examples. On global terrorism, attacks to London, Madrid, and New York (September 11) were main choices. Results obtained showed a PL behavior for Iraq, Colombia

and Afghanistan, with coefficient value (close to) $\tilde{\alpha} = 2.5$. This value of the coefficient equalized the coefficient value characterizing non-G7 terrorism. In 2007, Clauset *et al* [3] plotted a log-log chart for the frequency versus the severity of terrorist attacks, since 1968, and found a straight line, denoting PL behavior.

In 2003, Song *et al* [17] studied fire distribution in Chinese and Swiss cities. The authors computed the frequency loss and the rank-size plots and verified validity of a PL in both cases. The frequency loss was the frequency of fires with loss L, that is, fire loss L converted into Chinese Yuan. The rank was computed by sorting city fires from large to small, and considering the largest with rank 1. The PL distribution was invariant for scale and time, meaning that fire distribution is common for different places and times.

3   Application to real data

PLs are present in many natural and man-made systems and, for certain cases, a single PL distribution holds over the entire data range. As an example, Figure 1 represents the rank/frequency log-log plot of the largest private American companies, with respect to their annual revenue, in the year 1997, according to Forbes (`http://www.forbes.com/`). The data was collected, sorted and ranked, and then the normalization of the values was carried out. That is, the data (x-axis) was divided by the highest annual revenue, and the rank (y-axis) was divided by the rank of the smallest company. A PL was adjusted to the data using a least squares algorithm. As can be seen in Figure 1, a PL behavior distribution with parameters $(\tilde{C}, \tilde{\alpha}) = (0.0031, 1.3004)$ holds over the entire range of the companies' annual revenue.

In other real applications, different PLs, characterized by distinct parameters, may also be observed. In the sequel, several cases of such behavior are illustrated.

Figure 2 shows the cumulative distribution function of the size of forest fires in Portugal, over the year 2001. The adopted measure for size is the total burned area. Only fires greater than 100 ha in total burned area are considered. The data is available on the Portuguese National Forest Authority (AFN) website (`http://www.afn.min-agricultura.pt/`). For this case, two distinct PLs with parameters $(\tilde{C}_1, \tilde{\alpha}_1) = (0.0383, 0.9232)$ and $(\tilde{C}_2, \tilde{\alpha}_2) = (0.0065, 2.4665)$ fit the data. The change in the behavior occurs at the relative value of 0.35, approximately.

Figure 3 represents the severity of tornadoes in the USA, during 2003. The total number of human victims (killed and injured) directly related to a given occurrence is used to quantify its severity. The data is available at the U.S. National Oceanic and Atmospheric Administration (`http://www.noaa.gov/`), National Weather Service, Storm Prediction Center website (`http://www.spc.noaa.gov/`). The chart reveals a dual PL behavior with parameters $(\tilde{C}_1, \tilde{\alpha}_1) = (0.0413, 0.5804)$, $(\tilde{C}_2, \tilde{\alpha}_2) = (0.0100, 1.2374)$.
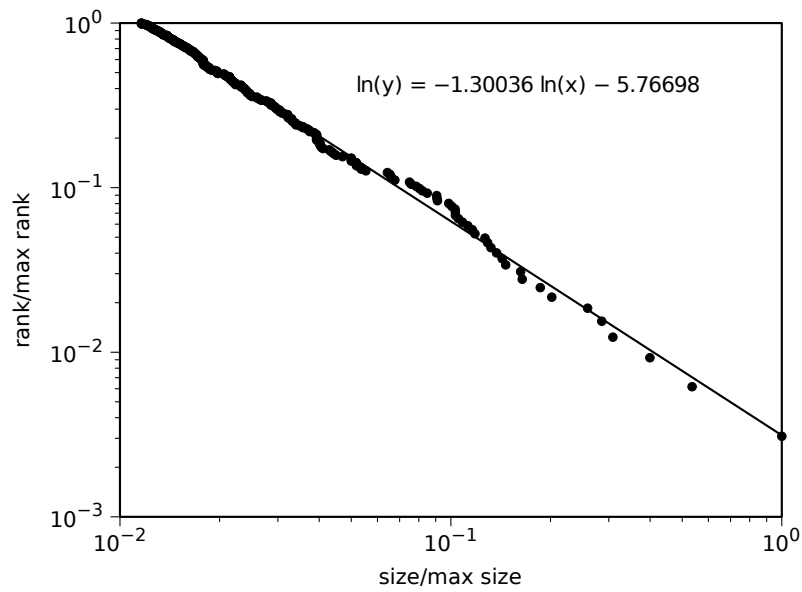
Fig. 1. Rank/frequency log-log plot of the size of the largest American companies in 1997.
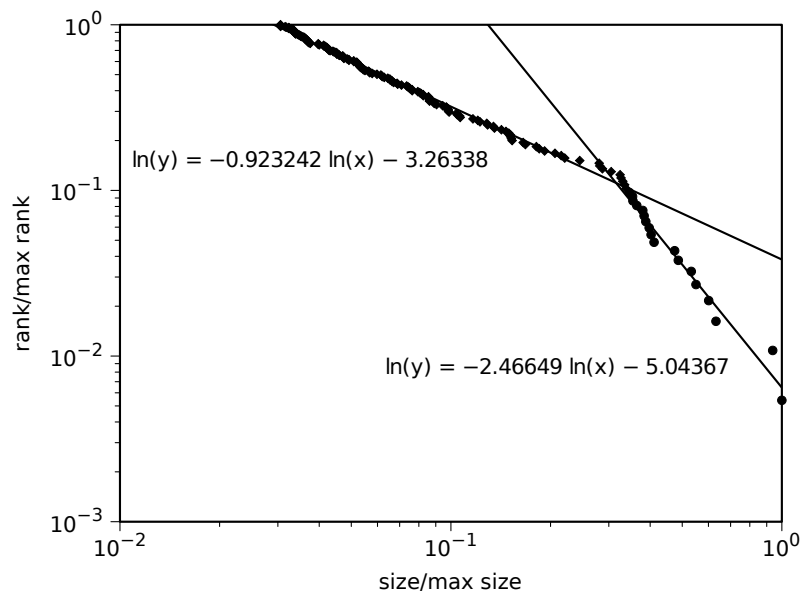

Fig. 2. Rank/frequency log-log plot of a system presenting dual PL behaviour: size of forest fires in Portugal, year 2001.
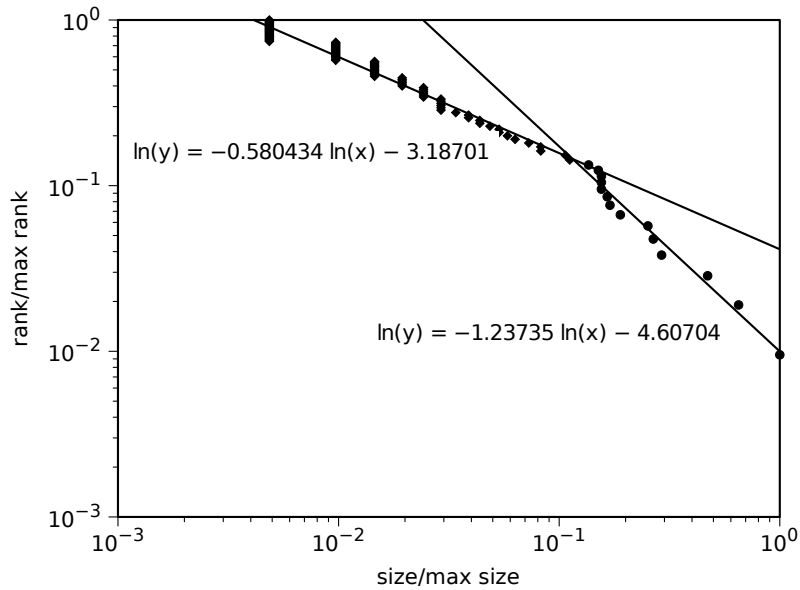
Fig. 3. Rank/frequency log-log plot of a system presenting dual PL behaviour: severity of tornadoes in the USA in 2003.

For the finale, we remark that several examples of real world phenomena, where a double PL behavior is observed, were presented. Future work will focus on possible explanation for this peculiarity seen in distinct phenomena, that are described by PLs.

4   Conclusion

In this paper, we focused on PL distributions as models of sets of real data. We presented examples of data that was well fitted by a single straight line and examples that were best described by two distinct PL distributions. The reason behind this type of behavior in distinct and not related phenomena is still to be found.

Acknowledgments

References

1. L. A. Adamic and B. A. Huberman. The nature of markets in the World Wide Web. *Quarterly Journal of Electronic Commerce*, 1:512, 2000.
2. F. Auerbach. Das Gesetz der Belvolkerungskoncentration. *Petermanns Geographische Mitteilungen*, 59:74–76, 1913.
3. A. Clauset, M. Young, K.S. Gleditsch. On the Frequency of Severe Terrorist Events. *Journal of Conflict Resolution*, 51: 58–87, 2007.
4. D.R. Davis, D.E. Weinstein. Bones, bombs, and break points: The geography of economic activity. *The American Economic Review*, 92:1269–1289, 2002.
5. J.B. Estoup. *Gammes Stenographiques*. Institut de France, 1916.
6. X. Gabaix. Zipf's Law and the Growth of Cities. *American Economic Review Papers and Proceedings*, LXXXIX:129–132, 1999.
7. B. Gutenberg, R. F. Richter. Frequency of earthquakes in california. *Bulletin of the Seismological Society of America*, 34:185–188, 1944.
8. N.F. Johnson, M. Spagat, J.A. Restrepo, O. Becerra, J.C. Bohorquez, N. Suarez, E. M. Restrepo, R. Zarama. Universal patterns underlying ongoing wars and terrorism. *arXiv:physics/0605035v1*, 2006.
9. W. Li. References on Zipf's law. `http://www.nslij-genetics.org/wli/zipf/`
10. W. Lin, Y. Yang. Zipf's Law in Importance of Genes for Cancer Classification Using Microarray Data. *J. Theor. Biol.* **219** (2002) 539-551.
11. A.J. Lotka. The frequency distribution of scientific productivity. *J Washington Acad Sci*, 16: 317–324, 1926.
12. R.N. Mantegna, H.E. Stanley. The scaling behavior of an economic index. *Nature* **376** (1995) 46–49.
13. V. Pareto. *Cours d'Economie Politique*, Geneva, Switzerland, 1896. Droz.
14. C.M.A. Pinto, A.M. Lopes, and J.A. Tenreiro Machado. A review of power laws in real life phenomena. *Communications in Nonlinear Science and Numerical Simulations*, accepted for publication, January 2012.
15. L.F. Richardson. *Statistics of Deadly Quarrels*. Chicago, 1960. Quadrangle Books.
16. D. C. Roberts, D. L. Turcotte. Fractality and selforganized criticality of wars. *Fractals*, 6: 351–357, 1998.
17. W.G. Song, H.P. Zhang, T. Chen, W.C. Fan. Power-law distribution of city fires. *Fire Safety Journal*, 38: 453–465, 2003.
18. D. Sornette. *Critical Phenomena in Natural Sciences*, chapter 14. Heidelberg, 2nd edition, 2003. Springer.
19. G. Zipf. *Human Behavior and the Priciple of Least Effort*. Cambridge, MA, 1949. Addison-Wesley.

New vortex invariants in magneto-hydrodynamics and a related helicity theorem

Anatoliy K. Prykarpatsky[1] and Denis Blackmore[2]

[1] The Ivan Franko State Pedagogical University, Drohobych, Lviv region, Ukraine
(E-mail: `pryk.anat@ua.fm`)
[2] The NJIT, University Heights, Newark, 07102, NJ USA
(E-mail: `deblac@m.njit.edu`)

Long ago it was stated [7,5] that quantum vortices in superfluid helium can be studied either as open lines with their ends terminating on free surfaces of walls of the container or as closed curves. Nowadays the closed vortices are treated as topological objects equivalent to circles. The existence of structures such as knotted and linked vertex lines in the turbulent phase is almost obvious [12] and has forced researchers to develop new mathematical tools for their detailed investigation. In this proposed direction Z. Peradzyński [8] proved a new version of the Helicity theorem, based on differential-geometric methods applied to the description of the collective motion in the incompressible superfluid. The Peradzyński helicity theorem describes in a unique way, both the superfluid equations and the related helicity invariants, which are, in the conservative case, very important for studying the topological structure of vortices.

By reanalyzing the Peradzyński helicity theorem within the modern symplectic theory of differential-geometric structures on manifolds, we propose a new unified proof and give a magneto-hydrodynamic generalization of this theorem for the case of an incompressible superfluid flow. As a by-product, in the conservative case we construct a sequence of nontrivial helicity type conservation laws, which play a crucial role in studying the stability problem of a superfluid under suitable boundary conditions.

1   Symplectic and symmetry analysis

We consider a quasi-neutral superfluid contained in a domain $M \subset \mathbf{R}^3$ and interacting with a "frozen" magnetic field $B : M \longrightarrow \mathbf{E}^3$, where $\mathbf{E}^3 := (\mathbf{R}^3, < ., . >)$ is the standard three-dimensional Euclidean vector space with the scalar $< ., . >$ and vector "$\times$" products. The magnetic field is considered to be source-less and to satisfy the condition $B = \nabla \times A$, where $A : M \longrightarrow \mathbf{E}^3$ is some magnetic field potential. The corresponding electric field $E : M \longrightarrow \mathbf{E}^3$, related with the magnetic potential, satisfies the necessary superconductivity conditions

$$E + u \times B = 0, \qquad \partial E/\partial t = \nabla \times B, \qquad (1)$$

where $u : M \longrightarrow T(M)$ is the superfluid velocity.

Let ∂M denote the boundary of the domain M. The boundary conditions $\langle n, u \rangle|_{\partial M} = 0$ and $\langle n, B \rangle|_{\partial M} = 0$ are imposed on the superfluid flow, where $n \in T^*(M)$ is the vector normal to the boundary ∂M, considered to be almost everywhere smooth.

Then adiabatic magneto-hydrodynamics (MHD) quasi-neutral superfluid motion can be described, using (1), by the following system of evolution equations:

$$\partial u / \partial t = -\langle u, \nabla \rangle u - \rho^{-1} \nabla P + \rho^{-1} (\nabla \times B) \times B,$$

$$\partial \rho / \partial t = -\langle \nabla, \rho u \rangle, \qquad \partial \eta / \partial t = -\langle u, \nabla \eta \rangle, \qquad \partial B / \partial t = \nabla \times (u \times B), \tag{2}$$

where $\rho : M \longrightarrow \mathbf{R}_+$ is the superfluid density, $P : M \longrightarrow \mathbf{E}^3$ is the internal pressure and $\eta : M \longrightarrow \mathbf{R}$ is the specific superfluid entropy. The latter is related to the internal MHD superfluid specific energy function $e = e(\rho, \eta)$ owing to the first law of thermodynamics:

$$T \, d\eta = de(\rho, \eta) - P \rho^{-2} d\rho, \tag{3}$$

where $T = T(\rho, \eta)$ is the internal absolute temperature in the superfluid. The system of evolution equations (2) conserves the total energy

$$H := \int_M \left[\frac{1}{2\rho} |\mu|^2 + \rho e(\rho, \eta) + \frac{1}{2} |B|^2 \right] d^3 x, \tag{4}$$

called the Hamiltonian, since the dynamical system (2) is a Hamiltonian system on the functional manifold $\mathcal{M} := C^\infty(M; T^*(M) \times \mathbf{R}^2 \times \mathbf{E}^3)$ with respect to the following [4] Poisson bracket:

$$\{f, g\} := \int_M \left\{ \langle \mu, [\frac{\delta f}{\delta \mu}, \frac{\delta g}{\delta \mu}]_c \rangle + \rho \left(\langle \frac{\delta g}{\delta \mu}, \nabla \frac{\delta f}{\delta \rho} \rangle - \langle \frac{\delta f}{\delta \mu}, \nabla \frac{\delta g}{\delta \rho} \rangle \right) \right.$$

$$+ \eta \langle \nabla, (\frac{\delta g}{\delta \mu} \frac{\delta f}{\delta \eta} - \frac{\delta f}{\delta \mu} \frac{\delta g}{\delta \eta}) \rangle + \langle B, [\frac{\delta g}{\delta \mu}, \frac{\delta f}{\delta B}]_c \rangle \tag{5}$$

$$\left. + \langle \frac{\delta f}{\delta B}, \langle B, \nabla \rangle \frac{\delta g}{\delta \mu} \rangle - \langle \frac{\delta g}{\delta B}, \langle B, \nabla \rangle \frac{\delta f}{\delta \mu} \rangle \right\} dx,$$

where we denoted by $\mu := \rho u \in T^*(M)$ the specific momentum of the superfluid motion and by $[., .]_c$ the canonical Lie bracket of variational gradient vector fields:

$$[\frac{\delta f}{\delta \mu}, \frac{\delta g}{\delta \mu}]_c := \langle \frac{\delta f}{\delta \mu}, \nabla \rangle \frac{\delta g}{\delta \mu} - \langle \frac{\delta g}{\delta \mu}, \nabla \rangle \frac{\delta f}{\delta \mu} \tag{6}$$

for any smooth functionals $f, g \in \mathcal{D}(M)$ on the functional space $\mathcal{M}$. Moreover, as was shown in [4], the Poisson bracket (5) is, in reality, the canonical Lie–Poisson bracket on the dual space to the Lie algebra $\mathcal{G}$ of the semidirect product of vector fields on M and the direct sum of functions, densities and differential one-forms on M. Namely, the specific momentum $\mu = \rho u \in T^*(M)$ is dual to vector fields, ρ is dual to functions, η is dual

492

to densities and B is dual to the space of two-forms on M. Thus, the set of evolution equations (2) can be equivalently recast as follows:

$$\partial u/\partial t = \{H, u\}, \qquad \partial \rho/\partial t = \{H, \rho\},$$
$$\partial \eta/\partial t = \{H, \eta\}, \qquad \partial B/\partial t = \{H, B\}. \tag{7}$$

The Poisson bracket (5) can be rewritten for any $f, g \in \mathcal{D}(M)$ as

$$\{f, g\} = (Df, \vartheta\, Dg), \tag{8}$$

with $Df := \left(\frac{\delta f}{\delta \mu}, \frac{\delta f}{\delta \rho}, \frac{\delta f}{\delta \eta}, \frac{\delta f}{\delta B}\right) \in T^*(\mathcal{M})$ and $\vartheta : T^*(\mathcal{M}) \longrightarrow T(\mathcal{M})$, being the corresponding (modulo the Casimir functionals of bracket (5)) invertible [3] co-symplectic operator, satisfying the standard [10,2] properties

$$\vartheta^* = -\vartheta, \qquad \delta(\delta w, \wedge\, \vartheta^{-1}\delta w) = 0, \tag{9}$$

where the differential variation complex condition $\delta^2 = 0$ is assumed, the differential variation vector $\delta w := (\delta\mu, \delta\rho, \delta\eta, \delta B) \in T^*(\mathcal{M})$ and the symbol "$*$" denotes the conjugate mapping with respect to the standard bilinear convolution $(.,.)$ of the spaces $T^*(\mathcal{M})$ and $T(\mathcal{M})$. Note here that the second condition of (9) is equivalent [2,10] to the fact that the Poisson bracket (5) satisfies the Jacobi commutation condition. Thus, one can define the closed generalized variational differential two-form on $\mathcal{M}$

$$\omega^{(2)} := (\delta w, \wedge \vartheta^{-1}\, \delta w), \tag{10}$$

which provides the symplectic structure on the functional factor manifold $\mathcal{M}$ (modulo the Casimir functionals of bracket (5)). Owing now to the commutation property

$$[\partial/\partial t + L_u, L_v] = 0, \tag{11}$$

equivalent to the subgroup $\mathcal{D}_t$ and $\mathcal{D}_\tau$ commuting for any suitable $t, \tau \in \mathbf{R}$, from the invariance condition

$$\partial\rho/\partial\tau = 0, \tag{12}$$

we deduce that the quantities

$$\gamma_n := L_v^n \gamma \tag{13}$$

for all $n \in \mathbf{Z}_+$ are invariants of the MHD superfluid flow (2) if the density $\gamma \in \Lambda^3(M)$ is also an invariant on M.

We construct the following new functionals on the functional manifold $\mathcal{M}$

$$\tilde{H}_n := \int_M \tilde{\gamma}_n \, d^3x = \int_M \rho L_v^n (\rho^{-1}\langle B, A\rangle) \, d^3x \tag{14}$$

for all $n \in \mathbf{Z}_+$, which are invariants of our MHD superfluid dynamical system (2). In particular, when $n = 0$ we obtain the well-known [4] magnetic helicity invariant

$$\tilde{H}_0 = \int_M \langle A, \nabla \times A \rangle \, d^3x, \tag{15}$$

which exists independently of boundary conditions, imposed on the MHD superfluid flow equations (2).

The result obtained above can be formulated as the following theorem.

Theorem 1. *The functionals (14), where the Lie derivative L_v is taken along the magnetic vector field $v = \rho^{-1}B$, are global invariants of the system of compressible MHD superfluid and superconductive equations (2).*

Below we proceed to a symmetry analysis of the incompressible superfluid dynamical system and construct the related local and global new helicity invariants. The case of superfluid hydrodynamical flows [9] is of great interest for many applications owing to the very nontrivial dynamical properties of so-called vorticity structures appearing in the motion.

2 The incompressible superfluid: symmetry analysis and conservation laws

The helicity theorem result of [8], where the kinematic helicity invariant

$$H_0 := \int_M \langle u, \nabla \times u \rangle \, d^3x \tag{16}$$

was derived, employed differential-geometric tools in Minkowski space in the case of an incompressible superfluid in the absence of a magnetic field ($B = 0$). We shall now describe its general dynamical symmetry nature. The governing equations are

$$\partial u / \partial t = -\langle u, \nabla \rangle u + \rho^{-1}\nabla P, \qquad \partial \rho / \partial t + \langle u, \nabla \rho \rangle = 0, \qquad \langle \nabla, u \rangle = 0, \tag{17}$$

where the density conservation properties

$$(\partial / \partial t + L_u)\rho = 0, \qquad (\partial / \partial t + L_u)d^3x = 0 \tag{18}$$

hold for all suitable $t \in \mathbf{R}$. Define now the vorticity vector $\xi := \nabla \times u$ and find from (17) that it satisfies the vorticity flow equation

$$\partial \xi / \partial t = \nabla \times (u \times \xi). \tag{19}$$

Actually, the first equation of (17) can be rewritten as

$$\partial u / \partial t = u \times (\nabla \times u) - \rho^{-1}\nabla P - \frac{1}{2}\nabla |u|^2. \tag{20}$$

Then, applying the operation "$\nabla \times \cdot$" to (20), one easily obtains the vorticity equation (19). Moreover, equation (19) can be recast in the equivalent form

$$\partial \xi / \partial t + \langle u, \nabla \rangle \xi = \langle \xi, \nabla \rangle u, \tag{21}$$

which allows a new dynamical symmetry interpretation. Now, define $\beta^{(1)} \in \Lambda^1(M)$ as the one–form

$$\beta^{(1)} := \langle u, dx \rangle \tag{22}$$

and readily conclude that

$$(\partial / \partial t + L_u)\beta^{(1)} = -\rho^{-1}dP + \frac{1}{2}d|u|^2 = d(\rho^{-1}P + \frac{1}{2}|u|^2). \tag{23}$$

We have shown that the following generalized functionals

$$H_n := \int_M \rho L_v^n(u \times \xi) \, d^3x \tag{24}$$

for all $n \in \mathbf{Z}_+$ are new helicity invariants for (17). Notice here that all of the constraints imposed above on the vorticity vector $\xi = \nabla \times u$ are automatically satisfied if the condition $supp \, \xi \cap \partial M = \emptyset$ holds. The result obtained can be summarized as follows.

Theorem 2. *Assume that an incompressible superfluid, governed by the set of equations (17) in a domain $M \subset \mathbf{E}^3$, possesses the vorticity vector $\xi = \nabla \times u$, which satisfies the boundary constraints $L_{\rho^{-1}\xi}^n \xi|_{\partial M}$ for all $n \in \mathbf{Z}_+$. Then all of the functionals (24) are generalized helicity invariants of (17).*

The results obtained above allow some interesting modifications. To present them in detail, observe that equality (23) can be rewritten as

$$(\partial / \partial t + L_u)\beta^{(1)} - dh = (\partial / \partial t + L_u)\tilde{\beta}^{(1)} = 0, \tag{25}$$

where, by definition,

$$h := \rho^{-1}P + \frac{1}{2}|u|^2, \qquad \tilde{\beta}^{(1)} := \langle u - \nabla\varphi, dx \rangle, \tag{26}$$

and the scalar function $\varphi : M \longrightarrow \mathbf{R}$ is chosen in such a way that

$$(\partial / \partial t + L_u)\varphi = \nabla h. \tag{27}$$

Then, obviously, one obtains the additional equation

$$(\partial / \partial t + L_u)d\tilde{\beta}^{(1)} = 0, \tag{28}$$

following from the commutation property $[d, \partial / \partial t + L_u] = 0$. Then, we see that the density $\tilde{\lambda} := \tilde{\beta}^{(1)} \wedge d\tilde{\beta}^{(1)} \in \Lambda^3(M)$ satisfies the condition

$$(\partial / \partial t + L_u)\tilde{\mu} = 0, \tag{29}$$

for all $t \in \mathbf{R}$. A similar result holds for densities $\tilde{\lambda}_n := L_v^n \tilde{\lambda} \in \Lambda^3(M)$, $n \in \mathbf{Z}_+$; namely,

$$(\partial/\partial t + L_u)\tilde{\lambda}_n = 0, \tag{30}$$

owing to the commutation property (11). Therefore, the following functionals on the corresponding functional manifold $\mathcal{M}$ are invariants of the superfluid flow (2):

$$\Upsilon_n := \int_M \tilde{\lambda}_n = \int_{D_t} \rho L_{\rho^{-1}\xi}^n \langle (u - \nabla\varphi), \xi \rangle \, d^3x \tag{31}$$

for all $n \in \mathbf{Z}_+$ and an arbitrary domain $D_t \subset M$, independent of boundary conditions, imposed on the vorticity vector $\xi = \nabla \times u$ on ∂M. Notice here that only the invariants (31) strongly depend on the function $\varphi : M \longrightarrow \mathbf{R}$, implicitly depending on the velocity vector $u \in T(M)$. It should be mentioned here that the practical importance of the constructed invariants (31) remains to be fully clarified.

3 Conclusions

The symplectic and symmetry analysis of compressible MHD super-fluids developed above, appears to be an effective approach for constructing the related helicity type conservation laws, which are generally important for practical applications. In particular, these conserved quantities play a decisive role [4,1] when studying the stability of MHD superfluid flows under special boundary conditions. Some of the results in this direction can also be obtained making use of group-theoretical and topological tools developed in [1,13,11], where the importance of the basic group of diffeomorphisms $Diff(M)$ of a manifold $M \subset \mathbf{R}^3$ and its differential-geometric characteristics were shown in considerable detail.

Acknowledgments

References

1. Arnold V.I. and Khesin B.A. Topological methods in hydrodynamics. Springer, NY, 1998.
2. Abraham R. and Marsden J. Foundations of mechanics. Cummings Publ., NY, 1978.

3. Holm D. and Kupershmidt B. Poisson structures of superfluids. Phys. Lett., 91A (1982), pp. 425–430.
4. Holm D., Marsden J., Ratiu T. and Weinstein A. Nonlinear stability of fluid and plasma equilibria. Physics Reports, 123/(1 and 2) (1985), pp. 1–116.
5. Moffat H.K. The degree of knottedness of tangled vortex lines. Journal of Fluid Mechanics, 35/1 (1969), pp. 117–129.
6. Owczarek R. Topological defects in superfluid Helium. Int. J. Theor. Phys., 30/12 (1991), pp. 1605–1612.
7. Owczarek R. Frames and fermionic excitations of vortices in superfluid Helium. J. Phys: Condens. Matter, 5 (1993), pp. 8793–8798.
8. Peradzyński Z. Helicity theorem and vertex lines in superfluid ^{4}He. Int. J. Theor. Phys., 29/11 (1990), pp. 1277–1284.
9. Putterman S.J. Superfluid Hydrodynamics, North Holland, Amsterdam, 1974.
10. Prykarpatsky A. and Mykytiuk I. Algebraic integrability of nonlinear dynamical systems on manifolds: classical and quantum aspects. Kluwer Academic Publishers, the Netherlands, 1998.
11. Prykarpatsky A. and Zagrodziński J. Dynamical aspects of Josephson type media, Ann. of Inst. H. Poincaré, Phys. Theorique, 70/5 (1999), pp. 497–524.
12. Schwarz K.W. Physical Rev. B, 38 (1988), pp. 2398–2417.
13. Troshkin O.V. Nontraditional methods in mathematical hydrodynamics. Transl. Math. Monogr., AMS, Providence, v.114, 1995.